

1-1-1978

## **Solid state extrusion of high density polyethylene and nylons 11 and 12: the process and physical properties of extrudates.**

William George Perkins  
*University of Massachusetts Amherst*

Follow this and additional works at: [https://scholarworks.umass.edu/dissertations\\_1](https://scholarworks.umass.edu/dissertations_1)

---

### **Recommended Citation**

Perkins, William George, "Solid state extrusion of high density polyethylene and nylons 11 and 12: the process and physical properties of extrudates." (1978). *Doctoral Dissertations 1896 - February 2014*. 633.  
<https://doi.org/10.7275/5s0c-sh36> [https://scholarworks.umass.edu/dissertations\\_1/633](https://scholarworks.umass.edu/dissertations_1/633)

This Open Access Dissertation is brought to you for free and open access by ScholarWorks@UMass Amherst. It has been accepted for inclusion in Doctoral Dissertations 1896 - February 2014 by an authorized administrator of ScholarWorks@UMass Amherst. For more information, please contact [scholarworks@library.umass.edu](mailto:scholarworks@library.umass.edu).



SOLID STATE EXTRUSION OF HIGH DENSITY POLYETHYLENE  
AND NYLONS 11 AND 12; THE PROCESS AND PHYSICAL  
PROPERTIES OF EXTRUDATES

A Dissertation Presented

By .

William G. Perkins

Submitted to the Graduate School of the  
University of Massachusetts in partial fulfillment  
of the requirements for the degree of

DOCTOR OF PHILOSOPHY

. May 1978

Polymer Science and Engineering

(c) William George Perkins 1978

All Rights Reserved



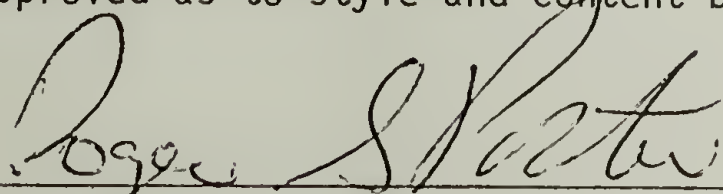
SOLID STATE EXTRUSION OF HIGH DENSITY POLYETHYLENE  
AND NYLONS 11 AND 12; THE PROCESS AND PHYSICAL  
PROPERTIES OF EXTRUDATES

A Dissertation Presented

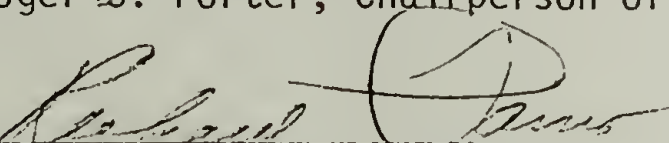
By

William G. Perkins

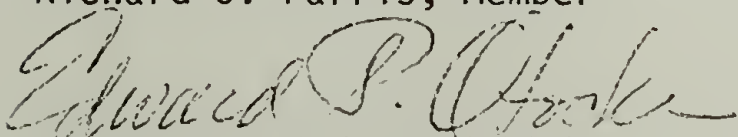
Approved as to style and content by



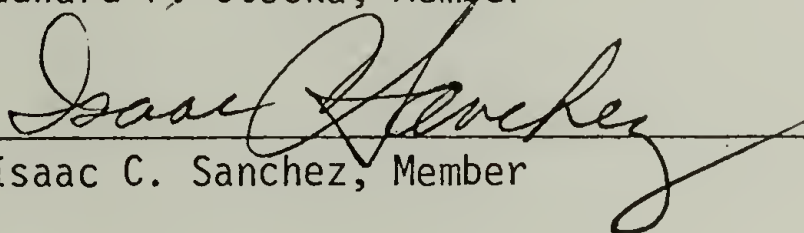
Roger S. Porter, Chairperson of Committee




Richard J. Farris, Member



Edward P. Otocka, Member



Isaac C. Sanchez, Member



William J. MacKnight, Department Head  
Polymer Science and Engineering

## DEDICATION

To my parents, Tom and Mary,  
for their tireless support throughout  
my extended college career  
and

To Nina and Jessie-Lee,  
who constitute the next step.

## ACKNOWLEDGMENT

I wish to thank my advisor, Dr. Roger S. Porter, for his patience, encouragement, and advice during this research program. I have benefited particularly from his editorial expertise, ability to approach a problem from many angles, and willingness to arrange meetings with outside scientists for in-depth discussions on particular problems. I am also grateful for his encouragement to present my work at national scientific meetings and for providing me with the opportunities to do so.

The other members of my committee, Dr. R. J. Farris, Dr. E. P. Otocka, and Dr. I. C. Sanchez, also deserve thanks for their part in shaping my research program and giving advice on research and thesis proposals. Their time and assistance is acknowledged with gratitude.

Another member of my committee, Dr. F. P. Price, sadly passed away during my tenure here. His help during the early phases of my program was important in getting off to a good start in my research and will not be forgotten.

Some other people who were of immense help during my stay here include Bob Cembrola, who provided x-ray photographs, and Paul Gilmore, who prepared SEM photographs. Also, Ms. Sophia Kinney, whose efficiency and expertise expedited preparation of this thesis; Ms. Eleanor Thorpe and Ms. Kathy Yurgielewicz, who helped in the preparation of many manuscripts; Mr. Chester Napikowski, whose skill in the machine shop was invaluable; and Mr. Joe DeCaro, who always kept the instruments working well despite a heavy workload and numerous frustrating occurrences.

Finally, thanks to Professor Otto Vogl for many helpful discussions, both scientific and philosophical.



## PREFACE

### Background

This thesis is an original extension of the work begun in the late sixties in this laboratory by Professor Roger S. Porter and Dr. John H. Southern, then a graduate student. They investigated the crystallization and extrusion of high density polyethylene under pressure and shear in an Instron Capillary Rheometer. Dr. Norman Weeks, another graduate student of Professor Porter, extended the work and characterized more specifically the morphology and mechanical properties of the ultra-oriented morphologies. The present work details a related but separate process for producing ultra-oriented films and fibers in the Instron Rheometer. Specific investigations described below include the solid state extrusion and characterization of high density polyethylenes and nylons 11 and 12. Solid state extrusion means processing below the crystalline melting point. My intent was to further develop prior work and develop the process of solid state extrusion while applying the new technique to other polymers.

### Outline

This thesis consists of seven chapters: An introductory chapter on the state of the art for solid state deformation of semicrystalline polymers is followed by five chapters on original experimental work. A concluding seventh chapter details additional investigations which can be done in this research area. Each chapter represents a self-contained study bound by the common idea of polymeric crystalline state extrusion and the molecular interpretation of the effects of such deformation.

The first chapter has been published in the Journal of Materials Science [12, 2355 (1977)]. It is a comprehensive review for all prior solid state deformation studies of polyethylenes and nylons. It details the processes and proposed molecular models and served as an important starting point for my investigations into solid state extrusion.

Parts of Chapter II were co-authored by Numa Capiati and Shunji Kojima. Chapter II nonetheless includes my own experimental results regarding the procedure we currently use for solid state extrusion. The specific preparation procedure described in the first section of the chapter was taken from an article co-authored by Capiati, Kojima, myself and Professor Porter and published in the Journal of Materials Science [12, 334 (1977)]. This procedure differs from that of Southern and Weeks in that crystallization is completed prior to extrusion so that extrusion is conducted entirely in the crystalline state.

Chapter III is a study of the effect of entrance angle on capillary extrusion rate, on the maximum extrusion (draw) ratio attainable, and the physical properties of the extrudates obtained. High density polyethylene was extruded through brass dies of 10, 14, 20, 30, 60, 90, 120 and 180°C. The results are presented as a function of die entrance angle for two molecular weights. This chapter will be submitted for publication.

Chapter IV deals with a material property, molecular weight, rather than a processing property. This chapter has been published in Polymer Engineering and Science [16, 200 (1976)]. It was co-authored by Numa Capiati and delves into the effect of weight average molecular weight on the physical and mechanical properties of solid state extruded high density polyethylene fibers.

The study reported in Chapter V has been accepted for publication in a symposium issue of Polymer Engineering and Science. It was presented at the American Chemical Society annual meeting in Chicago, September, 1977, and was co-authored by Professor V. T. Stannett of North Carolina State University. It involves the effect of  $\gamma$  radiation and annealing on the physical and mechanical properties of ultra-oriented high density polyethylene.

Chapter VI was presented in part at the American Physical Society March meeting in Atlanta in 1976. It will be submitted for publication. It includes data on processing characteristics and characterization of nylon 11 and nylon 12 extruded in the solid state. Activation energies of viscous flow are calculated and the effect of hydrogen bonding is discussed in terms of its effect on solid state extrusion.

The final chapter, VII, discusses possible future work in this research area including continuation of some studies initiated in this thesis. The implications of solid state deformation are far reaching as polymer scientists search for ways of more efficiently utilizing polymeric materials, now in commercial production, for engineering applications.

### Nomenclature

A comment on nomenclature is appropriate. The terms "capillary" and "die" are used throughout the text. A die would be the appropriate name for the brass or stainless steel tool having a conical entrance region and a straight capillary section of constant diameter. The two words are used

interchangeably herein. Another commonly used term is "draw ratio". This is more accurately an "extrusion ratio" and is the ratio of the cross-sectional areas of the original billet to the final extrudate. The two terms are equivalent. Earlier publications used "draw ratio" whereas our more recent studies use the term "extrusion ratio".

The terms "extended chain crystals" and "extended chains" are also used interchangeably in this text. Although the meanings may differ according to various investigators, they are here intended to refer to polymer chains greater than  $1000\text{\AA}$  in length consisting of all trans bonds. They may or may not be aggregated into macro-crystals and are considered to be a separate morphological entity distinct from folded chain crystals and from amorphous or non-crystalline regions. Extended chains, chain-extended, or extended chain crystals are seen as oriented in the extrusion direction since it is this process that caused their orientation and unfolding and thus chain extension.



## ABSTRACT

SOLID STATE EXTRUSION OF HIGH DENSITY POLYETHYLENE  
AND NYLONS 11 AND 12; THE PROCESS AND PHYSICAL  
PROPERTIES OF EXTRUDATES

May, 1978

William G. Perkins, B.S., Lowell Technological Institute  
M.S., Lowell Technological Institute  
M.S., University of Massachusetts  
Ph.D., University of Massachusetts

Directed by: Professor Roger S. Porter

Solid state deformation processes have been used to achieve polymers of high tensile moduli. The processes are based on achieving continuity for the oriented high strength covalent bonds of the polymer chain. This is accomplished by the pulling out of chain folds and the subsequent extension of the long polymer chains which run both through and between crystal lamellae. In solid state extrusion, a plug of solid polymer is forced by a ram through an orifice of smaller cross-sectional area to achieve draw. Proposed molecular models for the process generally consider the break-up of crystalline lamellae, their orientation in the deformation direction, and the pulling out of folded chains. These unfolded chains form tie-molecules between and among the disrupted lamellae. At highest deformation fibril formation is observed which involves the partially extended tie-molecules. It is these chain-extended tie-molecules which are responsible for the unusually high tensile properties for drawn semicrystalline thermoplastics in the orientation direction.

The solid state extrusion process used to produce ultra-oriented extrudates in this thesis consisted of crystallization under pressure in the Instron rheometer barrel, and subsequent extrusion through a tapered brass or stainless steel die. Extrusion was carried out at either constant (extrusion) pressure or constant (extrusion) rate. Advantages of this process over those used previously include a minimization of shear flow and maximization of elongational deformation which provides a higher efficiency for chain orientation and extension (1).

The effect of capillary die entrance angle on processing characteristics and extrudate properties is investigated using HDPE of two molecular weights. The optimum entrance angle with regard to ease of extrusion, maximum extrusion ratio (ER) obtainable, and optimum physical properties decreases with increasing polymer molecular weight. At a weight-average molecular weight ( $\bar{M}_w$ ) of 59,000, 20 - 30° appears to be the optimum angle, while at  $\bar{M}_w = 92,000$ , 14 - 20° seems best.

The effect of molecular weight on physical and mechanical properties of solid state extruded HDPE fibers has been investigated at one entrance angle (20°). It is found that percent crystallinity, linear expansion coefficient, and modulus do not change significantly with  $\bar{M}_w$ , while melting point, tensile strength, and strain to break do increase with increasing  $\bar{M}_w$ . This leads to the conclusion that the amount of extended chain crystals is invariant with molecular weight. Higher molecular weights are seen as providing a greater number of tie chains, thus giving the fiber a higher tensile strength and breaking strain.

Filaments of ultra-oriented HDPE were irradiated by a Cobalt-60 source at 10, 20, 40 and 60 megarads (MRad). Some of these samples underwent post-irradiation annealing at 128°C for one-half hour. Melting point and percent crystallinity decrease with increasing radiation dose, while birefringence and thermomechanical analysis indicate that orientation is not disrupted by irradiation. For unannealed samples, mechanical properties exhibit maxima when plotted vs. dose. For annealed samples, mechanical properties rise significantly at first then level off at higher radiation doses.

Finally, the solid state extrusion process is used with nylons 11 and 12. Nylon 11, which exhibits a high temperature (crystalline) relaxation, was found to be more readily processable than nylon 12, which shows no such transition (2). Neither nylon processed in the solid state as well as HDPE. Maximum ER's of 12 (nylon 11) and 7 (nylon 12) were obtained, while HDPE was extruded up to an ER of ~ 40. Inter-molecular hydrogen bonds are seen as acting as quasi-crosslinks and hindering the efficient unfolding, orientation and extension of nylon molecules during crystalline state extrusion.

1. N. J. Capiati, S. Kojima, W. G. Perkins and R. S. Porter, J. Mater. Sci. 12, 334 (1977).
2. S. Onogi, T. Asada, Y. Fukui and I. Tachinaka, Bull. Inst. Chem. Res., Kyoto University 52, 368 (1974).

## TABLE OF CONTENTS

PageCHAPTER I - SOLID-STATE DEFORMATION OF POLYETHYLENE AND  
NYLON AND ITS EFFECTS ON THEIR STRUCTURE  
AND MORPHOLOGY

I. Introduction	1
II. Undeformed Structure and Morphology	2
A. Polyethylene	2
1. General	2
2. Crystal Structure	3
3. Spherulitic Structure	3
4. Chain Folding and Annealing	5
5. High Pressure Crystallization	6
B. Nylon	10
1. Crystal Structure	10
2. Morphology	15
III. Effects of Deformation	21
A. Crystallinity	21
B. Structural Models	22
C. Spherulitic Deformation	30
D. Amorphous Orientation	36
E. Annealing	38
F. Mechanical Properties	40



G. Polymorphism	41
IV. Deformation Processes	44
V. Summary and Conclusions	62
References	64
Captions for Figures	78

## CHAPTER II - ON PREPARATION OF AN ULTRA-ORIENTED POLYETHYLENE MORPHOLOGY

I. Preparation Procedure	108
II. Comments on Capillary Geometry	113
III. Billet Length and Extrusion Pressure	114
IV. Pressure Effects	115
V. Possibilities of This Method	116
References	118
Captions for Figures	120

## CHAPTER III - EXTRUSION PROPERTIES OF HIGH DENSITY POLYETHYLENE AS A FUNCTION OF CAPILLARY ENTRANCE ANGLE

I. Introduction	127
II. Experimental	131
III. Results	133
A. Extrusion Rate	133
B. Deformation Intensity	134
C. Extrusion Length at Fracture	135
D. Maximum Extrusion Ratio	135
E. Birefringence	136

F. Calorimetry	138
G. Thermomechanical Analysis	138
H. Mechanical Testing	139
IV. Discussion and Conclusions	141
A. Extrusion Rate	141
B. Extrusion Length and Extrusion Ratio at Fracture	141
C. Birefringence	142
D. Calorimetry	143
E. Coefficient of Expansion	143
F. Mechanical Testing	144
G. Elastic Hysteresis	145
V. Summary	146
References	147
Captions for Figures	151

#### CHAPTER IV - THE EFFECT OF MOLECULAR WEIGHT ON THE PHYSICAL AND MECHANICAL PROPERTIES OF ULTRA-DRAWN HIGH DENSITY POLYETHYLENE

I. Introduction	173
II. Experimental	174
III. Results and Discussion	176
A. Melting Point and Degree of Crystallinity	176
B. Coefficient of Expansion	177
C. Modulus, Tensile Strength, and Strain to Break	178
IV. Conclusions	179

References	180
Captions for Figures	185
CHAPTER V - THE EFFECT OF $\gamma$ RADIATION AND ANNEALING ON ULTRA-ORIENTED POLYETHYLENE	
I. Introduction	190
II. Experimental	192
III. Results and Discussion	194
A. Unannealed Samples	194
1. Calorimetry	194
2. Birefringence	195
3. Thermomechanical Analysis (TMA)	195
4. Mechanical Testing	196
B. Annealed Samples	197
1. Calorimetry	197
2. Birefringence	197
3. Thermomechanical Analysis	198
4. Mechanical Testing	198
V. Conclusions	199
References	201
Captions for Figures	207
CHAPTER VI - SOLID STATE EXTRUSION OF NYLONS 11 AND 12; PROCESSING, MORPHOLOGY AND PROPERTIES	
I. Introduction	218

II. Experimental	219
III. Part I - Nylon 11	220
A. Introduction	220
B. Experimental Results	224
IV. Part II - Nylon 12	226
A. Introduction	226
B. Experimental Results	229
V. Discussion and Conclusions	231
A. Strain Hardening	234
B. Degradation	236
C. Plasticizers	237
References	245
Captions for Figures	251
CHAPTER VII - FUTURE WORK	
I. Flow Patterns	278
II. Capillary Length	278
III. Film Extrusion	279
IV. Nylon 6; Nylon 66	279
V. Split Billet	279
VI. Drawing	280
VII. Morphological Characterization	280
VIII. Strain Cycling	281
IX. Lubricants	281
References	283



# C H A P T E R   I

## SOLID-STATE DEFORMATION OF POLYETHYLENE AND NYLON AND ITS EFFECTS ON THEIR STRUCTURE AND MORPHOLOGY

### I. Introduction

Solid-state deformations of semicrystalline polymers can cause an efficient orientation of chains in the stress direction with a consequent large increase in mechanical properties in the orientation direction. The processing conditions for solid-state deformation vary widely with polymers. There is evidence (1,2) that the optimum temperature for such a process lies above the so-called  $\alpha$  transition temperature and below the crystalline melting point. This suggests that solid-state deformations are ideally done in a temperature range where the polymer crystals are able to plastically deform without the concomitant occurrence of covalent bond rupture.

The three major processes used in solid-state deformation of semicrystalline polymers are cold drawing, cold extrusion and hydrostatic extrusion. These will be reviewed later, after a general discussion on the effects of solid-state deformation on polymer structure. Because the most published work and thus this review deals primarily with polyethylenes and nylons, the structure and morphology of these two polymer types are discussed prior to discussion of deformation processes and the consequent products.

## II. Undeformed Structure and Morphology

Polyethylene (both high and low density) and the various aliphatic polyamides (nylons) have been studied extensively using various solid-state deformation processes. Linear (high density) polyethylene offers a simple hydrocarbon structure that is readily characterized and uncomplicated by side groups, labile substituents or strong intermolecular secondary bonding forces. Its theoretical modulus is also among the highest of any thermoplastic (3). Nylons, on the other hand, offer the promise of enhanced mechanical properties and thermal stability due to their abundant hydrogen bonding. For these reasons, many laboratories, including this one, have undertaken investigations of the solid-state deformation behavior of these two thermoplastics.

### A. Polyethylene.

#### 1. General.

Polyethylenes,  $(\text{CH}_2\text{CH}_2)_n$ , commonly have chain ends of methyl ( $-\text{CH}_3$ ) or vinyl ( $-\text{CH}=\text{CH}_2$ ) groups. Low density (branched) polyethylene ( $\rho \sim 0.91 - 0.92$ ) consists of the same chain backbone but contains about 20 - 40 short (2 to 5 carbon atoms) side chains per 1000 main chain atoms. Medium density polyethylene ( $\rho \sim 0.93 - 0.94$ ) contains fewer short side chains, whereas high density (linear) polyethylene ( $\rho \sim 0.95 - 0.96$ ) commonly has less than 10 short side chains per 1000 main chain atoms. Lesser concentrations of long-chain branching are also associated with short chain branching and their effect on intrinsic viscosity and molecular weight distribution has been investigated by Billmeyer (4),

Beasley (5), and Harris (6). Long chain branching is thought to result from radical transfer from a growing chain to a dead chain, which then grows a long branch.

Polyethylenes of higher density exhibit a sharper "neck" and a greater "natural draw ratio", terms defined in the section on Deformation Processes.

## 2. Crystal Structure.

Polyethylene exists in a planar zigzag ( $2_1$  helix) chain conformation and is normally found in an orthorhombic unit cell having dimensions of  $a = 7.40 \text{ \AA}$ ,  $b = 49.3 \text{ \AA}$ , and  $c = 2.534 \text{ \AA}$  (7). The projected C-C bond length in the chain backbone is  $1.53 \text{ \AA}$  and the C-C-C bond angle of  $112^\circ$  is slightly larger than tetrahedral. A form of isomorphism exists in polyethylene in that the unit cell dimensions (and consequently the crystal density) vary with branching (8). For example, Walter and Reding (9) found that the  $a$  axis varied from  $7.68$  to  $7.36 \text{ \AA}$ , the  $b$  axis from  $5.00$  to  $4.94 \text{ \AA}$ , and the calculated crystal density from  $0.956$  to  $1.014 \text{ g/cm}^3$  as the branching ratio,  $\text{CH}_3/1000 \text{ CH}_2$ , decreased from 80 to zero. More extreme alterations of the unit cell occur upon severe sample deformations and these will be discussed in the section on polymorphism.

## 3. Spherulitic Structure.

Polyethylene crystallizes into spherulitic macrostructures of sufficient size to scatter visible light; thus thick specimens are opaque. This scattering originates both at the boundaries and inside of the spherulites themselves (10). Polyethylene spherulites are negatively birefringent (greater refractive index in the tangential direction) with



the molecular chain axis (c axis) oriented tangentially within the spherulites. Crystal growth occurs most readily along the b axis, which lies crystallographically along the radii of the spherulites. Spherulites are composed of a radiating fibrous structure and the alternating light and dark "rings" observed in many spherulites are believed to be due to a twisting of the radiating fibrils (11-14).

Spherulite size is an important factor in determining the physical and mechanical properties of polyethylene. Early detailed studies of the crystallization kinetics of linear polyethylene were conducted by Mandelkern and Quinn (15) and by Buckser and Tung (16). They found experimentally the marked effect of temperature on crystallization rate which had earlier been predicted from theories for nucleation and growth. At greater degrees of undercooling, the spherulites are more numerous and therefore grow to a smaller size as their boundaries impinge. For crystallization nearer the melting point, fewer spherulites are nucleated, but those that are grow larger and the result (for a polyethylene of given branch content) is higher crystallinity for those specimens crystallized at lower degrees of undercooling. Low density polyethylene is commonly 50 - 60% crystalline; high density polyethylene, 65 to 90%, depending on crystallization conditions and molecular weight. Compared to most other semicrystalline polymers, polyethylene crystallizes rapidly, likely because of its regular structure, short chain repeat distance, and high chain packing density. The equilibrium melting point of a linear, high molecular weight polyethylene was shown by Mandelkern (17) to be near  $137^{\circ}\text{C}$ . However, under the common non-equilibrium conditions in conventional processing, the melting point is  $132 - 135^{\circ}\text{C}$ . Low density polyethylenes melt down to  $100^{\circ}\text{C}$ .

#### 4. Chain Folding and Annealing.

The underlying reasons for chain folding in polymers have been reviewed by Lindenmeyer (18). The driving force for folding is the lowering of conformational energy by regular (crystallographic) folding of long molecules so that van der Waals interactions come into play. Such lowering of energy by regular folding obtains only below the melting point since at temperatures above  $T_m$ , the random coil conformation is energetically favored (19). Lindenmeyer (18) goes on to state that the composition of the polymer crystal will differ from that of the melt because (1) short molecules would increase the free energy of the crystal if they were incorporated and (2) long molecules would increase the free energy of the liquid if they remain in the crystal vicinity. He thus concludes that there is a driving force for both extremely short and extremely long molecules to diffuse away from the growing crystal. These uncrystallized entities remain as disordered regions within spherulites and at spherulitic boundaries.

Annealing of polyethylene crystals generally results in longer fold periods but, in the case of crystals with lamellae thicker than  $120 \text{ \AA}$ , Keller, et al. (20), found that the fold period decreased on annealing between  $95$  and  $125^\circ\text{C}$ . They attribute this decrease in long spacing to increased molecular tilt within the crystal lamellae. At higher temperatures, these crystals, also, thicken, and a molecular reorientation (rotation around the crystallographic b axis) occurs.

During isothermal annealing, crystal thickening is usually observed to be an irreversible process, and Sanchez, et al. (21,22),



treat the phenomenon as an irreversible thermodynamic process wherein the driving force for thickening arises from the unequal free energies of the fold and lateral surfaces. Their theory provides a basis for considering the effects of time, temperature, thermal history, pressure, and liquids on the thickening rate.

In a paper discussing temperature-induced reversible changes of long spacing in oriented polyethylene, Pope and Keller (23) conclude that large temperature-reversible changes in long spacing of polymers are a consequence of partial melting of small or imperfect lamellae leading to an increase in overall periodicity. The requirement of an irregular, or imperfect, crystal lattice explains why the effect is not generally observed in single crystals.

#### 5. High Pressure Crystallization.

The crystallization of polyethylene under pressures of 2 - 6 Kbars has been investigated with regard to crystallization kinetics (24-26), morphology (24-26), and physical and mechanical properties of the resultant material (27,28). Two possible modes of formation of extended chain crystals under pressure are possible: (1) thickening with time of initially-folded chain crystals into extended chain lamellae, or (2) direct formation from a melt of extended chain crystals. Yasuniwa, et al. (24), believe both types of formation can occur. They postulate that the extended chain crystal grows rapidly and directly from the melt under pressure. When quenched to the crystallization temperature,  $T_c$ , of the folded chain crystal, folded chain lamellae begin to grow and thicken because extended chains have lower free energy under high pressure. These authors found no chain extended crystals at pressures below 2500 atm.

Kyotani and Kanetsuna (25) studied polyethylene crystallization at from 840 to 5300 atm and concluded that (1) isothermal crystallization occurs much faster under high pressure at comparable undercoolings; (2) the Avrami equation is valid for high pressure crystallization and the Avrami exponent  $n$  decreases from  $\sim 2$  at 840 atm to  $\sim 1$  at 5100 atm; (3) the surface energy of crystal nuclei appears to decrease with increasing crystallization pressure; and (4) extended chain crystals grow at a high rate, predominantly in one dimension, under high pressure. Maeda and Kanetsuna (26) crystallized polyethylene at from 220 atm up to 6000 atm and noted three pressure ranges of import. In the low range, below 2000 atm, folded chain crystals are formed; between 2000 and 3500 atm, mixed crystallization of extended and folded chain crystals takes place, while extended chain crystals become more stable and appear in larger quantity with increasing pressure; in the high-pressure region above 4700 atm, two stages of crystallization and of melting are reported, one producing "ordinary" chain extended crystals and the other leading to "highly extended chain" crystals which melt at temperatures above the crystallization and melting temperatures of the "ordinary" extended chain crystals.

Early work on pressure crystallized polyethylene was carried out by Wunderlich, et al. (27,28). They found, as did Maeda, et al. (26), ten years later, three pressure regions where folded chain, folded chain/extended chain mixtures, and extended chain crystals grow. They also reached several additional conclusions: (1) pressure decreases the amorphous volume more than the crystalline volume, (2) the crystallographic  $a$  and  $b$  axes are compressed more easily than the  $c$  axis, (3) the melting

point of the crystalline phase increases approximately  $0.02^{\circ}\text{C}/\text{atm}$ , and (4) the equilibrium maximum melting point of the polyethylene crystal is  $140 \pm 0.5^{\circ}\text{C}$ . They found that at the highest pressure investigated, 5300 atm, extended chain lamellae can be as thick as  $3\mu$  (28). Well defined kink bands were observed in the thicker extended chain lamellae. The authors suggest that either molecular weight fractionation or an end-to-end alignment of molecules and subsequent folding takes place during the growth of the extended chain lamellae. Rees and Bassett (29) investigated the effect of pressure on the crystallization of polyethylene fractions and concluded that the thickness of extended chain lamellae is a function of time, temperature, and molecular weight. They found that crystallization is qualitatively similar to that of folded chain crystals at 1 atm, giving an optimum lamellar thickness which increases with time and decreased supercooling. The authors further noted that (1) fractional crystallization is widespread, (2) isothermal thickening of lamellae during crystallization occurs, and (3) layers can anneal to thicknesses ten times their initial size.

Extended chain high density polyethylene has been reported by Lupton and Regester (30) to be stiffer and somewhat stronger than normal folded chain HDPE. They note that with molecular weights in the range for molding or extrusion, the extended chain material is inductile and brittle, while molecular weights near  $2 \times 10^6$  are still rigid but tough. The authors postulate a polymorphic transition between orthorhombic and triclinic phases at 5000 atm, determined from volume-temperature behavior. Attenburrow and Bassett (31) studied the morphology of chain extended



ultra-high molecular weight linear polyethylene after drawing five-fold. Crystallization is believed to proceed via a hexagonal high pressure phase (32) into the orthorhombic crystal. The authors note that ultra-high molecular weight chain-extended polyethylene shows some ductility in tension if low molecular weight material is removed prior to pressure treatment. Because the majority of extended chain lamellae survived the drawing process, it was postulated that melting had not occurred during drawing (up to 6.5 draw ratio). However, perhaps 20% of lamellae were disrupted while others underwent uniform shearing and, as with chain-folded polyethylene, voiding and/or crazing was observed.

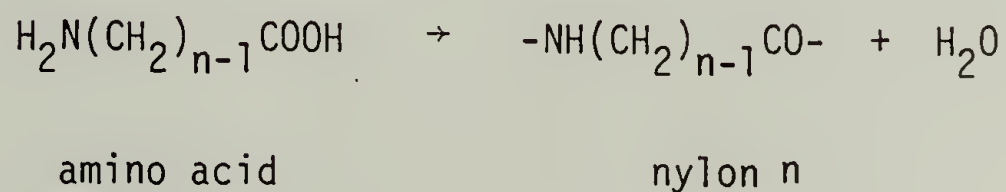
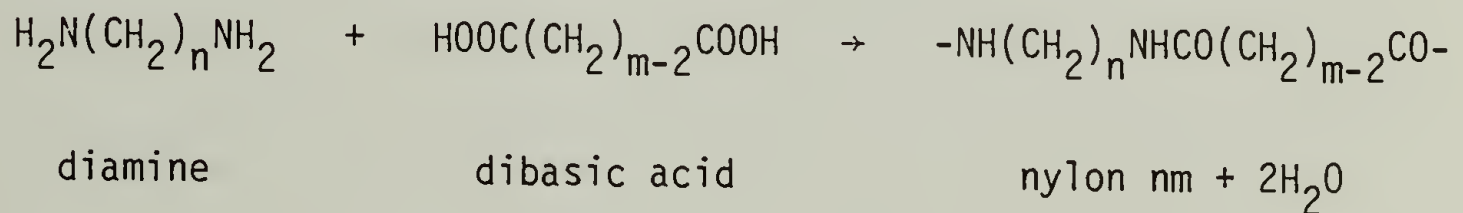
A review of polyethylene crystallization under pressure by Bassett (32) details a number of points: (1) chain-extended growth results from crystallization of a high pressure hexagonal phase, (2) the hexagonal phase incorporates gauche, as well as trans, bonds along the chain, (3) lamellar thickening occurs by a local melting and recrystallization, and (4) lamellar thickness is inversely proportional to supercooling and entropy of fusion.

This discussion of polyethylene structure and morphology represents only a minute part of the extensive associated literature. Numerous important papers have been published by A. Keller, L. Mandelkern, B. Wunderlich, E. Baer, and a host of others. General reviews of polyethylene, its technology and uses, can be found in References 8 and 10.

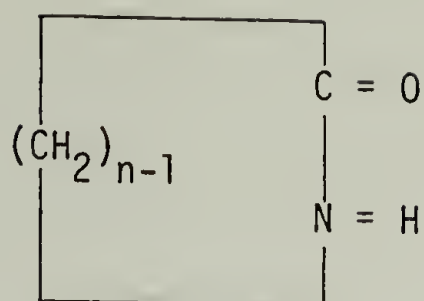
## B. Nylon.

### 1. Crystal Structure.

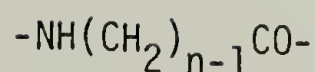
A second class of polymers which has been widely investigated with respect to solid-state extrusion is the polyamides, or nylons. By trademark definition, a nylon is any long chain, synthetic, polymeric amide which has recurring amide groups as an integral part of the main polymer chain. Nylons are synthesized in many ways. These include the condensation of diamines with diacids, the polymerization of amino acids, and the ring-opening polymerization of lactams. The varied routes to synthesis lead to many different types of nylons whose structure and properties differ widely. The various aliphatic nylons are named by a numerical system based on the number of carbon atoms in the monomer(s) from which they are synthesized. For example:







lactam



nylon n

The first number, n, indicates the number of carbon atoms in the diamine; the second, m, the number of carbons in the dibasic acid. A single number indicates the carbon number in the amino acid or lactam.

For convenience, nylons may be classified into six groups according to the number of CH<sub>2</sub> groups in the monomeric units (33):

Group A Nylons from diamines with even numbers of CH<sub>2</sub> groups and dibasic acids with even numbers of CH<sub>2</sub> groups - 66, 68, 610, 612.

Group B Nylons from diamines with even numbers of CH<sub>2</sub> groups and dibasic acids with odd numbers of CH<sub>2</sub> groups - 49, 69, 89, 109.

Group C Nylons from diamines with odd numbers of CH<sub>2</sub> groups and dibasic acids with even numbers of CH<sub>2</sub> groups - 76, 78, 710.

Group D Nylons from diamines with odd numbers of CH<sub>2</sub> groups and dibasic acids with odd numbers of CH<sub>2</sub> groups - 77, 79, 99.

Group E Nylons from ω-amino acids with even numbers of CH<sub>2</sub> groups (odd numbers in the conventional expression) - 7, 9, 11.

Group F Nylons from ω-amino acids with odd numbers of CH<sub>2</sub> groups (even numbers in the conventional expression) - 4, 6, 8, 10, 12.

Probably the most interesting and important phenomenon common to all nylons is the presence of inter- and intramolecular hydrogen bonding. They exist in both the crystalline and noncrystalline regions. Their presence and extent is responsible for many nylon characteristics. Differences in melting temperature, water sorption, tensile properties, density and solvent resistance are found among the nylons having different concentrations of amide groups in the main chain. The crystalline melting points, for example, increase with the concentration of amide groups (34-37) as shown in Figure 1. This is due to an increase in hydrogen bonding which increases the cohesive forces between adjacent molecules. Nylons with even numbers of  $\text{CH}_2$  groups have higher melting points than those with odd (Figure 1). In earlier studies it had, therefore, been suggested, on the basis of x-ray studies (38), that structures with planar zigzag chains - where hydrogen bond formation is incomplete - exist for even-odd, odd-even and odd-odd nylons (34,35,39). However, it has subsequently been shown by infrared spectroscopy that hydrogen bonding between amide groups is essentially complete in both odd and even members and that no more than 1% free NH absorption is observable at room temperature (40). This suggests that a structure must exist which deviates from the planar zigzag which allows essentially complete hydrogen bond formation. This structure has been called the  $\gamma$ -form and is the common structure for odd-even, even-odd and odd-odd nylons and sometimes occurs for even and odd nylons. The even nylons (containing odd numbers of  $\text{CH}_2$  groups) usually exhibit the  $\alpha$ - and  $\beta$ -forms for short  $\text{CH}_2$  sequences, e.g. nylon 4 and nylon 6, while the  $\gamma$ -form is found in longer sequences, as nylon 8, 10 and 12.

The  $\alpha$ -phase is comprised of planar sheets of hydrogen-bonded molecules stacked upon one another. The x-ray fiber photograph of the  $\beta$ -phase is characterized by a meridional spot and layer line streaks. It has been postulated that successive sheets in the  $\beta$ -phase are staggered "up and down" instead of always being displaced in the same direction (Figure 2). The presence of the  $\beta$ -phase cannot be reliably determined except in samples possessing a high degree of axial orientation. In the  $\gamma$ -phase, polyamide chain bonds are rotated into a puckered or pleated conformation to form strain-free hydrogen bonds (42).  $\gamma$ -phase nylons, therefore, have shorter chain repeat distances by about a constant value than those calculated for the fully-extended form. The  $\gamma$ -phase unit cells are usually pseudo-hexagonal (33).

Bunn and Garner (38) have shown that nylon 66 and 610 exist in both the  $\alpha$ - and  $\beta$ -forms. The unit cell was found to be triclinic with one chain molecule passing through it for the  $\alpha$ -form. An alternative packing of sheets (see above) gave a two molecule triclinic cell which is the  $\beta$ -form. The  $\alpha$ -form was found to be the more stable phase. Above 165-175°C the unit cell of nylon 66 changes to pseudo-hexagonal (58,59). Such polymorphism is evident in the other polyamides as subsequently discussed.

The crystal structure of nylon 6 has been investigated by several authors (33,43-48,254) on samples of various thermal and mechanical treatments. The  $\alpha$ -,  $\beta$ - and  $\gamma$ -forms have all been postulated. It has been concluded (33,43,48) that the  $\alpha$ -form is the most stable and the  $\beta$ -form can be converted to the  $\alpha$ -form by immersion in boiling water for five or six



hours (43). The shifting of the hydrogen bonds generates the different crystalline forms (48), e.g. the  $\alpha$ -form which is characterized by sheets of antiparallel chains (33,46,47) with the structures being interconvertible (47,52-57). The  $\alpha$ -form can be converted to the  $\gamma$ -form by treatment with an aqueous  $I_2$ -KI solution and an aqueous sodium thiosulfate solution, while the  $\gamma$ -form is convertible to the  $\alpha$ -form by treatment with aqueous phenol or by stretching at high temperature (47,52-57). Lindenmeyer (254) has observed stable  $\alpha$  and  $\gamma$  crystals in highly annealed nylon 6 fibers. Metastable pseudohexagonal crystals were also observed.

Recently, a method has been developed (60,61) relating quantitative structural information to wide angle x-ray diffraction results using nylon 6.

The structure of nylon 11 has been studied by various researchers (33,62-66). The unit cell is triclinic, having dimensions  $a = 4.9 \text{ \AA}$ ,  $b = 5.4 \text{ \AA}$ ,  $c = 14.9 \text{ \AA}$ ;  $\alpha = 49^\circ$ ,  $\beta = 77^\circ$ ,  $\gamma = 63^\circ$  (62). Slichter (63) found that, for nylon 66 and 610, the lateral asymmetric packing in the basal plane of the triclinic cell shifts toward hexagonal packing as the temperature is raised. A concomitant shortening of unit cell length was attributed to twisting of the chain segments during motion. Similar polymorphism has been noted in nylon 11 (64,65). Genas (64) found that, above  $70^\circ\text{C}$ , the  $a$ ,  $b$  (basal) plane of the triclinic cell assumes hexagonal packing. Onogi, et al. (65), found that quenched film of nylon 11 contains  $\gamma$  (pseudohexagonal) crystals, while film solution cast from *m*-cresol contains  $\alpha$  (triclinic) crystals. When films containing  $\gamma$  crystals were annealed above  $90^\circ\text{C}$ , they transformed into the  $\alpha$  modification.

The structure of nylon 12 has only recently been investigated (49, 50). It exhibits (50,51) the  $\gamma$ -phase (Figure 3). Northolt, et al. (49), also found that nylon 12 may exist in two different forms, depending on conditions. Melt-pressed sheet that was quenched in ice water, drawn 4.5X, and annealed at 170°C at constant length for several hours under nitrogen, revealed a hexagonal unit cell, while melt-pressed sheet that was quenched in ice water, drawn 7X, and cooled under stress to room temperature, exhibited what appeared to be a mixture of mono- and triclinic unit cell structures. Inoue and Hoshino (50) prepared their sample by drawing a nylon 12 monofilament 3.6X in boiling water then annealing it at 150°C for 10 hours. They found a monoclinic unit cell resembling the  $\gamma$ -form of the other even nylons. No transition to the  $\alpha$ -form was observed even when the sample was subjected to stretching at temperatures near 150°C or treated with aqueous phenol. It was, therefore, decided that the  $\gamma$ -form of nylon 12 is more stable than for nylon 6, nylon 8 or nylon 10. This led to the conclusion that the longer the molecular chain in the even nylons, the more the crystal shows a tendency to form the  $\gamma$ -phase. Ishikawa, et al. (51), used sheets drawn from 2.4 - 4.0X from 50 to 150°C; they also detected the  $\gamma$ -form under all test conditions.

## 2. Morphology.

Most studies of polyamide morphology have been on nylon 66 (67-74). Many aspects of its structure and behavior apply to other nylons.

Like most semicrystalline polymers, nylons normally crystallize in spherulitic forms. Under mechanical stresses or strong thermal gradients,



most crystalline polymers show a variety of non-spherulitic and oriented structures. Nylons, however, under usual processing conditions, yield spherulitic forms. Kohan (42) believes this is because the melts tend to supercool markedly. He feels that by the time crystallization begins, the stresses have reduced greatly from the initial values and the environment approaches a quiescent condition. This could also be responsible for the apparent absence of spherulites in crystalline nylon samples which have a milky appearance. The spherulites are, in fact, present and scatter visible light but are too small to be seen with a light microscope.

The many studies of nylon 66 (67,73,74,78-80) have revealed the formation of four types of spherulites under different conditions. These are:

(1) Positive Spherulites--These are spherulites having their larger refractive index in the radial direction. They grow exclusively when the melt is cooled rapidly to below  $250^{\circ}\text{C}$ . They can also grow at higher temperatures in combination with other forms. Experimental data from infrared spectroscopy (72,81), x-ray diffraction (78) and electron microscopy (79) suggest that positive spherulites are composed of fine fibrils of folded-chain ribbons. The planes of the hydrogen bonds (a axes) are directed along the radii.

(2) Negative Spherulites--These are spherulites having their larger refractive index in the tangential direction. These grow between  $250$  and  $270^{\circ}\text{C}$  and are always accompanied by spherulitic aggregates. These spherulites grow faster than positive spherulites and, as shown by x-ray (78), are highly crystalline but with little preferred orientation of the

unit cells. Infrared data (73) indicate well-developed chain folding comparable with that in single crystals. Negative spherulites seem to be composed of lamellae-type crystal units rather than the branched fibrils formed in positive spherulites.

(3) Non-birefringent Spherulites--These occur in two temperature ranges. One is around  $250^{\circ}\text{C}$ ; the other is around  $265^{\circ}\text{C}$ . No evidence of any preferred orientation of the unit cells has been found in these spherulites. It has been suggested (82) that this type of spherulite results from a mixture of positive and negative types.

(4) Spherulitic Aggregates--Found with negative spherulites but grow faster. They show evidence that the crystallographic b-axis is parallel to the radius although this orientation varies with location. They are strongly birefringent.

Starkweather and Brooks (68) investigated the effect of spherulites on the mechanical properties of nylon 66. They found that spherulite size was important in dry samples at low ( $23^{\circ}\text{C}$ ) temperatures and becomes less important with increasing moisture content and/or temperature. Dry samples with smaller spherulites show higher flexural modulus, a higher yield stress, and a lower ultimate elongation than samples with larger spherulites. As spherulite size decreases, the yield point increases (Figure 4). The yield points of spherulitic films are substantially higher than those without visible spherulites, independent of the crystallinity (67).

The rate of nylon crystallization depends partly on composition, thermal history and the presence of nucleating or plasticizing additives (42). According to Kohan, the amide concentration and molecular symmetry

are important. For a given class of nylons, the rate of crystallization will typically rise with increasing amide concentration at constant undercooling. At a given amide concentration the series with the highest degree of symmetry (e.g. even-even) will have the highest rate of crystallization. The more rapidly crystallizing nylons are generally the higher melting.

An increase in either the melt temperature or time in the melt will lower the crystallization rate. The influence is on both the induction time for crystallization and on subsequent growth rate. This implies that the melt has a memory (42).

Added agents can effectively nucleate crystallization rates and increase amounts. Such materials are commonly (1) solid near the melting point of the nylon, (2) finely divided, (3) do not agglomerate, and (4) provide polar surfaces capable of adsorbing amide groups. Effective agents include sodium phenylphosphinate, sodium isobutylphosphinate, magnesium oxide, mercuric bromide and chloride, cadmium and lead acetate, and phenolphthalein as well as silver halides and fine silicas and aluminas (84).

The infrared technique for identification of chain folds (72) indicates that folding in melt-crystallized samples of nylon 66 is the same as in single crystals prepared from solution. Samples which are initially quenched to low crystallinity show no regular folding, but regular folds are formed on annealing. Additional infrared studies (73) show that the regularity of chain folding is related to the type of spherulitic growth.



Moisture increases the rate of crystallization due to a plasticizing action which increases chain mobility (83), but in practice water is avoided because it leads to degradation and bubbles.

The change from dryness to water saturation causes a four-fold decrease in modulus of oriented nylon 66 in the machine direction at room temperature (Figure 5) while the principal mechanical relaxation, the glass transition, is shifted downward by about 70°C (71).

Moisture also has a large effect on the morphology and thus the properties of polyamides. It is believed (70) that only the disordered portions of the polymer are accessible to water. This may be due to strained, metastable, hydrogen bonds present in the chain folds and other non-crystalline regions which are disrupted and reformed in conjunction with water molecules. Although nylon is more dense than water, its density increases as water is absorbed, up to about 2.5% (70). This again is apparently due to disruption of strained hydrogen bonds which allows the hydrocarbon chain units to pack more closely, thus decreasing the volume. On the other hand, the water molecules could just be filling in intermolecular spaces in the amorphous regions. An early review of the sorption of water by polymers, including thermodynamic theories, was written by McLaren and Rowen (85). They showed how both solution theories and sorption theories are useful in predicting observed vapor pressure-water uptake relationships.

In oriented nylons, water has less effect on properties in the transverse direction than in the orientation direction. The hydrogen bonding takes place in the transverse direction between chains. One may,

therefore, surmise that many of the hydrogen bonds, presumably those in the more-ordered (crystalline) regions, are little affected by the absorbed water.

One last aspect of nylon morphology is the effect of high crystallization pressures. Gogolewski and Pennings (86,87) studied the crystallization of nylon 6 from the melt under elevated pressures. Although the effect of water content was not systematically investigated, they noted no difference in high pressure crystallization behavior between samples exposed to laboratory humidity and samples kept in a vacuum desiccator over  $P_2O_5$ . Some other results were: (1) Caprolactam (monomer) molecules stabilize the chain folds and therefore diminish the effect of pressure, (2) a pressure of 5 Kbars is necessary for chain-extended nylon 6 molecules to form (~ 3 Kbars is sufficient to form extended chain polyethylene), and (3) the melting point of nylon 6 crystallized for 320 hours at  $315^{\circ}C$  and 8 Kbars was  $256^{\circ}C$  ( $41^{\circ}$  above chain-folded nylon 6) and the authors believe it would increase further if more caprolactam had been removed from the system. A one stage process for the development of extended chain crystals of nylon 6 was postulated from the results of these investigations.

The process of solid state deformation involves a permanent conformational change of polymer molecules as contrasted with the temporary translation of chains occurring in melt processing. This change, in some cases, alters the basic unit cell structure, and, in virtually all cases, significantly alters the physical and mechanical properties of the deformed polymer. For semicrystalline polymers, the solid state processing should take place under conditions where the polymer crystals will plastically



deform without rupturing. This usually means that the deformation will optimally be done at or above the so-called  $\alpha$  (crystal-crystal) transition temperature at relatively slow rates. The changes undergone by polymer crystals and associated amorphous regions are described in the following section.

### III. Effects of Deformation

#### A. Crystallinity.

Fiber-forming polymers, as a rule, can be partially crystallized. Most are initially partly crystalline with the crystallinity being increased by deformation. The increase depends on the shape and arrangement of the macromolecules. Crystallites form, mainly, due to intermolecular bonding originating from the mutual attraction forces among macromolecule groups (88). The magnitude of these forces depends on the amount and strength of the active groups and on the ability of such groups to approach each other. The greater the forces arising between the groups in neighboring molecules, the more groups available, the more regular their disposition along the chain, and the closer to one another these macromolecules can get, the stronger are the intermolecular bonds, resulting in more facile polymer crystallization (88).

Orientation involves molecular arrangements in both crystalline and in amorphous regions. The higher the orientation, the more mutually parallel are the molecules, and the smaller is the average angle formed by them with the fiber axis. The process of axial orientation increases crystallinity by both orienting the molecules and by bringing them closer

together, enabling crystallites to form from formerly amorphous regions. As with polyethylene (89,92), a slight increase in crystallinity with drawing is generally observed. In one case for polyethylene (90), a decrease in crystallinity was observed for annealed film at low draw ratios and a subsequent increase on further drawing. The initial decrease was reportedly due to two phenomena: (1) the crystals of a fiber structure exhibit larger paracrystalline disorder (91) and (2) the decrease of long period, due to the destruction of spherulites preceding fibril formation, increases the surface-to-volume ratio and hence reduces the density.

For nylon 6 (93), fiber crystallinity was shown to increase 27% on drawing 375% (3.75X). Stretching took place in air at  $40 \text{ cm-min}^{-1}$  at  $20^{\circ}\text{C}$  and 60% RH. A corresponding increase in crystallite size (both parallel and perpendicular to the drawing direction) was also noted. Upon further stretching to 4.5X, both percent crystallinity and crystallite size (in both directions) diminished. This was reportedly due to the emergence of high stresses at the greatest draw ratios, causing the destruction of some crystalline regions with imperfect or partially disturbed lattices. Prevorsek and Sharma (94) found that the drawing of nylon 6 caused little effect on crystallite size in the direction of orientation, while the crystallite width decreased with draw.

#### B. Structural Models.

Prevorsek (95,96), et al., proposed that drawn nylon 6 is composed of microfibrils having dense crystalline parts and less dense "non-crystalline" parts, surrounded by a matrix of intermediate density.

They further concluded that the microfibrils slip past one another during stretching, on the basis of three experimental facts (95): (1) The longitudinal structure of the microfibril (amorphous and crystalline lengths) remains essentially unchanged. (2) The microfibril thinning exceeds that of the fiber. (3) The spacing between the microfibrils increases. The authors feel that in the drawing process the microfibrils are sheared with respect to each other and the matter removed from the surfaces of the microfibrils forms an interfibrillar phase whose density is similar to the average density of the microfibril. Consistent with these results, a model was proposed (95) where the microfibrils are embedded in a paracrystalline matrix (Figure 6). According to Prevorsek, this differs from the model proposed by Peterlin (97-100) and others (101,102) who worked mostly with polyethylene, which assumes that the strongest element of the fiber is the microfibril. This microfibril consists of highly oriented folded-chain crystals which are connected by many tie molecules within the amorphous layers separating the crystals (Figure 7). These authors (97-102) attribute the increase in fiber strength with increasing draw ratio primarily to the increase in the number of tie molecules which allegedly increases the strength (103).

Prevorsek, et al. (95,96), however, conclude that the microfibril structure and thus its strength remains essentially unchanged during drawing. They feel that the increase in strength on drawing must be attributed to the transformation of the (weak) microfibrils into a strong, highly-ordered, non-crystalline intermicrofibrillar phase. Their analysis of molecular dependence of fiber strength suggests that this intermicrofibrillar phase consists of highly extended polymer chains (104), and



that this is responsible for fiber properties such as strength, modulus, and diffusion of small molecules into the fiber. The relatively weak microfibrils are thought to be mainly responsible for the dimensional stability of the fiber. This description is known as the "Swiss-Cheese" model (95).

Actually, the Peterlin and Prevorsek models are quite similar since Peterlin also postulates that some of the tie molecules run laterally between microfibrils and are subsequently extended as the microfibrils initially slide past one another (100). Therefore, the strength of his model derives from these interfibrillar tie molecules, as well as from the intrafibrillar tie molecules (see Figure 7). According to Peterlin (89), the folded chains in the microfibrils are responsible for the periodicity observed from x-ray diffraction, while the partially-extended tie molecules provide the strength. He proposes (105) that the stress concentration on the tie molecules varies throughout the sample due to length variations. Therefore, the most highly strained chains become taut and fail long before the sample breaks. As these strained chains rupture, sample weakening proceeds until, finally, microcracks develop and lead to final fracture of the fiber. This microcrack phenomenon is indeed observed during the tensile testing of many polymers including both high density polyethylene and nylon 12 fibers studied in this laboratory.

The basis for the Peterlin model for polyethylene is a two-step deformation process (106): destruction of the original microspherulitic structure and deformation of a new fiber structure. Tilting and slipping



of lamellae initiates the first mechanism, and the resultant folded-chain blocks are incorporated into well-aligned microfibrils which are held together by tie molecules. Although destruction of the spherulitic morphology is nearly completed at a draw ratio of about 10, tie molecule content increases up to a draw ratio of about 20 (107) due to a pulling out of molecules from the folded-chain blocks. Plots of modulus vs. draw ratio (107) show a steep increase in modulus from DR:10 to DR:20 supporting this contention.

Fracture of drawn semicrystalline polymers is seen (108) as originating at point vacancy defects caused by the ends of microfibrils incorporated into the microfibrillar superlattice. Cracks then propagate radially and axially from these defects. Because axial crack growth involves the rupturing of fewer tie molecules, it is likely to be favored, causing the fibrous fracture surface commonly seen in stress-strain curves of such materials (109). Peterlin (110) postulates that sliding of the fibrils during stretching does not affect the morphology of the microfibrils but rather heals the aforementioned point vacancy defects. This causes a more perfect lateral contact between fibrils and results in a steadily increasing resistance to plastic deformation. He notes (109) that over long molecular distances, van der Waals forces will effectively act to retard plastic deformation (once the fibrous structure is formed) of microfibrils and cause the observed strain hardening effect as well as increase the elastic modulus and breaking stress as the draw ratio increases. Peterlin (111) also notes that the fracture surface of drawn nylon 6 is not fibrillar and surmises that the

lateral cohesion of the microfibrils in polyamides, being much stronger than in polyethylene, makes it easier for the crack to grow radially than axially although longitudinal microcracks are observed at high magnification. Peterlin further proposes that necking and post-neck deformation are separate processes for polyamides. A two-stage drawing process is indeed the method employed by Barham and Keller (112) for producing highly drawn nylon 66 [and also by Clark and Scott for polyoxymethylene (2)]. Another aspect of polyamide deformation is the important role of interfibrillar tie molecules, formed by shear displacement of microfibrils, which may have a greater effect on the mechanical properties of the drawn structure than the originally prevailing intrafibrillar tie molecules. Finally, Peterlin (111) postulates that drawing of polymers with a liquid crystal structure yields a highly aligned fibrous structure with very few chain folds and an exceptionally-high tensile modulus and strength. However, the small fraction of axially oriented tie molecules prevents the modulus from approaching that of a perfect crystal.

Takayanagi and Kajiyama (113) propose a model for drawn, crystalline polymers wherein the dominant mechanism of deformation at lower temperatures is the breakdown of lamellar crystals into mosaic blocks. They propose that the  $\alpha$  relaxation in bulk crystallized polyethylene can be separated into an  $\alpha_2$  absorption, associated with shear deformation of lamellar crystals, and an  $\alpha_1$  absorption, corresponding to molecular motions in the region of intermosaic blocks. The latter is presumed to contain tie molecules much as in the Peterlin model. Also consistent with

Peterlin (106), Takayanagi and Kajiyama believe that the mosaic blocks are not locally melted during deformation. These authors also investigated the effect of uniaxial compression on a highly-oriented solid-state extrudate. Kink bands were visible and small angle x-ray scattering (SAXS) measurements indicated a thinning of lamellae crystals, caused by tilting ( $\alpha_2$  mechanism), in the kink bands. By using wide angle x-ray scattering (WAXS) to correlate the tilting of molecular chains in the crystal and the alignment of crystallites in the ripple\*, the authors concluded that the deformation was achieved by both the  $\alpha_1$  and  $\alpha_2$  mechanisms. They further postulate that the relative contribution of the  $\alpha_1$  or  $\alpha_2$  mechanisms to the total deformation depends on temperature.

Another model considers essentially complete crystallization but with many vacancies and dislocations within the lattice. This model was proposed for nylons 66 and 610 in an early work by Zaukelies (114). The theory was based on observations of crystallographic kinking on compression of nylon samples. Such kinking allegedly involves crystalline slip. This slip is seen as beginning at screw and edge dislocations as well as at vacancies resulting from chain ends and chain folds within the (paracrystalline) lattice. Zaukelies supported his theory with density, WAXS, and diffusion phenomena. This general idea of paracrystalline structure for semicrystalline polymers has been detailed and supported by Hosemann in a lengthy review (115), with his original ideas published in 1950 (116). Hosemann envisions a paracrystalline superstructure incorporating aspects of both the fringed micelle and folded chain theories. Kinks, jogs,

\* A lamellar laminate indicating crystallite alignment; essentially parallel to the edge of the kink band.



caterpillars, and other specific conformations which are found in polyethylene (117,118,119) are seen as distorting the crystal lattice and breaking down long range order. Behavior of polyethylene subjected to irradiation, nitric acid etching, annealing, and stretching, as well as x-ray diffraction and NMR have been offered in support of the theory.

Point, et al. (120), investigated the effects of rolling deformation on nylon 11 by SAXS and WAXS. They concluded that the deformation of both superlattice and subcell can be accounted for by a sliding displacement along consecutive hydrogen bonded planes. They postulate a model wherein the sample consists of parallel arrays of crystalline and amorphous layers which are thought to deform equally, while the number of lamellae in a stack remains constant.

Deformation by rolling of nylon 11 was also carried out by Gezovich and Geil (121) who found that the chain axes gradually tilt toward the rolling direction. As deformation increased, WAXS reflections broaden indicating a partial breakup of crystallites. Thus, the state of nylon 11 at high deformations was shown to be many small crystallites with a high degree of orientation.

A review by Bowden and Young (122) encompasses the broad array of crystalline polymer deformation processes occurring at modest strains. These authors note that polymer crystals can deform plastically by slip, twinning, and by martensitic (shear) transformations, and that slip produces the largest plastic strains. They show that slip in the chain direction can be either "fine", where the crystal surface normal rotates with respect to the chain direction, or "coarse" (interfibrillar) slip



wherein the crystal surface normal remains parallel to the chain axis and lamellae are sheared with respect to one another, see Figure 8. Two other modes of polymer crystal deformation recounted are transverse slip and twinning. Transverse slip involves the sliding of molecules over each other perpendicular to the molecular axis. Twinning is a rotation of the crystal lattice (to a greater extent than by slip) and commonly occurs in polyethylene deformation and, to a lesser extent, in the nylons. The authors (122) also review deformations of the amorphous phase of semi-crystalline polymers. Three important modes are listed as: (1) Inter-lamellar slip, wherein lamellar crystals are sheared parallel to each other with the amorphous phase undergoing shear, (2) Interlamellar separation, involving a stretching of the amorphous phase between lamellae, and (3) Stack rotation, which assumes that lamellae are free to rotate under stresses and are surrounded by amorphous material which distorts under deformation.

Keller and coworkers (123) have developed a structural model based on their observations of self-hardening of linear polyethylene fibers. They found that highly drawn samples, held at fixed length, relax at elevated temperatures with a concomitant decrease in modulus. However, when held for long times at room temperature, the modulus (and density) increased substantially. The authors propose a model wherein needle crystals are aligned in an amorphous matrix. During heating, stressed tie molecules detach from the needle crystals and subsequently recrystallize in the usual chain-folded manner. However, the fibrous (needle) crystals determine their (folded chain crystals) orientation analogously

to shish-kebob and row-nucleated structures. This model explains the observed drop in modulus, the persistence of x-ray orientations, the increase in lamellar content, and the absence of large contractions in subsequent reheating of these "aged" fibers. The self-hardening is explained in their model by a stiffening of the matrix (123).

### C. Spherulitic Deformation.

In order to fully investigate the effects of solid state deformation on semicrystalline polymers, one must examine what happens to the spherulitic structure during deformation. Hay and Keller (124) published a lengthy review of spherulitic deformation, using polarized light microscopy, x-ray diffraction, and electron microscopy and using high density polyethylene film as starting material. They noted two types of spherulitic deformation during tensile drawing: (1) homogeneous and (2) inhomogeneous. In homogeneous deformation, all parts of a given spherulite extend simultaneously and in proportion. In inhomogeneous deformation, the spherulites and/or regions between them, yield selectively in areas that draw out fully, the rest of the microstructure remaining unaltered. Further stretching occurs by the drawn-out regions spreading at the expense of unaltered regions. Most observed cases, they submit, are intermediate between the two types. These authors (124) also note that often the deformation within a spherulite is greater than that in the material between spherulites, reflecting a weakness within the spherulites themselves. Some other observations were: (1) the formation of cracks parallel to the draw direction, with the resulting fibril widths corresponding to the deformed spherulite widths; (2) that spherulite deformations

are not affine; (3) that crystallite and spherulite deformation are related but not simply; (4) the greater the deformation, the greater the c-axis alignment; and (5) chain-folding occurs even in highly drawn structures (124). Many other authors (125-131) have studied the deformation of spherulites in terms of the microstructure. Among these, Stein, in particular, has pioneered in the development of experimental methods (132-136). Working mostly with low density polyethylene, he has found (137) that, although the overall spherulite length on stretching may parallel the change in sample dimensions, the microdeformation may not. Often, the spherulite is found to deform more near its equator than elsewhere (124, 138). This gives rise to a density depletion in this part of the spherulite, possibly associated with the formation and propagation of microvoids between separating lamellae (137). Such deformation processes are also rate dependent, i.e. a finite time is required for crystal orientational changes. Thus, if a polymer is stretched at a high rate, so that crystal orientation lags behind strain, large strains will concentrate on inter-crystalline tie chains, and tend to make the polymer brittle. However, if the polymer is stretched slowly, the strain will be more evenly distributed over the sample, due to conformational changes, which then may deform in a more ductile manner. The rate of structural response and the resulting mechanical properties depend upon the size, perfection, and organization of the crystalline and amorphous regions (137).

Samuels has also performed numerous investigations of spherulite deformation (139). Working mostly with isotactic polypropylene, he used small angle light scattering (SALS) to follow spherulite deformation and



and orientation (140,141). Isotropic light scattering equations were extended to include the anisotropy of polarizability and the change in shape of the spherulite deformed under uniaxial tension (140). By relating the molecular orientation of the crystalline region (the crystalline orientation function,  $f_c$ ) to the gross sample deformation, the spherulites were shown to be deformed affinely (140). In addition, quantitative information about the size of the original, undeformed spherulites and the deformed spherulites was gained by SALS. Results from spherulitic isotactic polypropylene films drawn at  $110^{\circ}$  may be summarized (139): (1) all films contained negatively birefringent spherulites with the a axis of the lamellae parallel to the radial direction; (2) along the radii aligned parallel to the extension direction, disruption and realignment of the lamellae occur in the inner regions of the spherulite whereas little or no change occurs in the outer regions; (3) the lamellae aligned along radii in the region of the spherulite transverse to the deformation direction undergo two processes: (a) lamellar slip leading to c axis orientation and (b) separation of lamellae. This increasing c axis orientation continues until the lamellae become fully aligned, at which point crystal cleavage begins. In this highly extended state, the substructure is no longer spherulitic but fibrillar. To accommodate further extension, the lamellae cleave and break off in blocks and the helical axis of the non-crystalline molecules becomes more oriented in the deformation direction (139). Similar films drawn at  $135^{\circ}\text{C}$  behave in a like manner, except that the lamellae are larger, more perfect, and thus less deformable, and the non-crystalline molecules are more mobile. This leads to diminished internal disruption



within the spherulite during extension, since relaxation processes occurring within the non-crystalline region result in deformation processes that are non-orienting in character (139).

Other investigations involving isotactic polypropylene fibers and poly(ethylene terephthalate) yarns are detailed in Reference 139.

The spherulitic deformation of nylon 66 has been investigated by Crystal and Hanson (142) using optical microscopy, electron microscopy, and small angle x-ray scattering. They found that spherulites elongated into football shapes along the draw direction when drawn 4X. This indicates that spherulite deformation is symmetric about a central axis parallel to the draw direction. Sample density also decreased upon cold drawing. This is consistent with Stein's contention (137) that microvoids are formed by non-uniform spherulitic deformation, the fibrils of impinging spherulites run together and intertwined over a width of 0.5 - 0.8 microns, forming a diffuse boundary containing fibrils from multiple spherulites. (2) The spherulite elongation was less than one-half the sample elongation, indicating that the spherulites slipped with respect to each other, and (3) the fibrils parallel to the draw apparently became thinner, while those perpendicular to the draw became thicker. Fibrils at intermediate orientations were bent toward the draw direction.

A study of the deformation of nylon 6 spherulites under uniaxial stretching was done by Matsuo, et al. (143). X-ray diffraction and SALS were used. The model proposed was similar to that for the deformation of low density polyethylene (144). The spherulitic deformation is accepted as occurring in two steps: (1) "instantaneous" deformation of the

spherulite, associated with orientation of lamellar axes and untwisting of crystal lamellae, and (2) re-orientation of crystallites within the oriented lamellae after a time lag, as shown by Stein and co-workers. The authors (144) propose a model wherein the uniaxial deformation of polyethylene spherulites are discussed on the basis of an orientation distribution function of crystallites within the crystal lamellae, taken to be a function of lamella orientation. Eight parameters are listed for describing four different types of crystallite orientation within the lamellae. Three parameters are believed sufficient, in principle, to describe spherulite deformation. These parameters are related to (1) the transition in crystal orientation from (a) b axis, oriented parallel to lamella axis, to (b) rotation of the crystallite around its own a axis, and to (c) unfolding of folded chain crystals; (2) the fraction of crystallites that have random orientation within the lamellae; and (3) the fraction of crystallites that have orientation from unfolding rather than from rotation about the a axis. With regard to nylon 6 spherulitic deformation, Matsuo, et al. (143), list eleven parameters; the five most important describe the re-orientation of nylon 6 crystallites within the orienting lamellae in such fashion that their molecular (b) axes orient in the stretching direction. Problems arose on calculating molecular polarizability of the surrounding medium in which the crystallite scattering elements are embedded, because of a considerable contribution from hydrogen bonds.

Haas and MacRae studied biaxial deformation of high density polyethylene (145) and poly-1-butene (146) films and observed that fracture

initiated at the spherulite centers whereas deformation was localized at both the spherulite centers and at the boundary intersections. They surmised that the individual lamellae in the spherulites were under radial tension with this mode of deformation, and, because of "branching" of lamellae, there are fewer lamellae available to carry the force approaching the spherulite center, thereby resulting in a stress concentration at the nucleus. This phenomenon was observed in both polyethylene and poly-1-butene, although the latter was observed to deform affinely, while the former deformed locally, i.e. "necked". Such behavior was attributed to possibly more intercrystalline links in poly-1-butene. When spherulitic films were crystallized with large amounts of rejected material or large voids along the (spherulitic) boundaries, cracks formed and propagated from these areas.

Subsequently, Olf and Peterlin (147) investigated the crazing of smectic and monoclinic polypropylene at liquid nitrogen temperatures. They noted that the crazes induced in the smectic polypropylene were similar to those found in glassy amorphous polymers and concluded that the small spherulites had no influence on craze propagation, either due to their small size or to highly disordered crystals. In monoclinic polypropylene, crazing occurred along spherulite diameters roughly transverse to the stress direction. The crazes run between stacked lamellae, possibly because of a separation along the amorphous surface layers between successive lamellae (147). The presence of a condensed gas plasticized the amorphous material, reducing the work needed for formation of new surface and facilitating craze nucleation and propagation.



#### D. Amorphous Orientation.

Another question concerning the deformation of semi-crystalline polymers is whether or not the amorphous regions become oriented. From the fringed micelle theory, it has been concluded that these regions would have to be aligned in the draw direction much as the crystals (88) but when chain folding is considered, the problem becomes more complex, and, above  $T_g$ , segmental motion could dissipate amorphous orientation. Still, it is hard to imagine complete amorphous disorientation, when crystallites are known to be highly oriented. On the other hand, total amorphous orientation is also hard to envision, when one considers chain folds and unstretched tie molecules as part of the amorphous contribution. Amorphous orientation has been found in drawn polyethylene by polarized infrared spectroscopy (148). This orientation is said to increase the content of the lower energy trans conformations and facilitate a better chain packing which increases the density (149). Chappel (150) studied crystalline and amorphous orientation in nylon 66 fibers by means of dichroism and birefringence. He found that the orientation of crystalline regions exceeded that of the amorphous regions at all stages of drawing and most noticeably in the early stages. Stein and Norris (151) also found this to be true with polyethylene and found that at high extension ratios amorphous orientation reached a limit. Chappel, on the other hand, found that the amorphous orientation in nylon 66 showed no sign of reaching a limit up to the maximum extension realizable, although the rate of increase with extension ratio did decrease slightly at the highest extensions (150). This is shown in Figure 9 where  $f_a$  and  $f_c$  are the orientation.



functions of the amorphous and crystalline regions and  $f_u$  is the birefringence orientation factor;  $C$  is a constant including the dichroic ratio of a perfectly oriented filament.

Samuels (139) used birefringence and sonic modulus techniques to measure amorphous orientation of stretched isotactic polypropylene films. They found that the amorphous orientation function,  $f_{am}$ , increased up to the highest extension investigated of 800%. He also found that tenacity and modulus correlate well with amorphous orientation. Data indicated that shrinkage, as relaxation of non-crystalline chains, occurred via a common mechanism for all semicrystalline polymers below the melting point.

Nylon 610 has been cold-extruded by Yemni and Boyd (152). They measured dielectric relaxation of both oriented and unoriented specimens in order to determine amorphous orientation. They found, with oriented specimens, that the intensity of the parallel dielectric loss factor was nearly zero, but the perpendicular loss was also reduced compared to the unoriented nylon 610. The other relaxation parameters (loss width and location) were nearly unaffected. They surmise that since the amide dipole is nearly perpendicular to the chain axis, orientation of the amorphous domains would result in very low loss in the parallel direction, while the perpendicular loss should be greater than in the unoriented case. However, because the dipole directions alternate in the extended conformation, a considerable degree of chain alignment parallel to the draw direction would cause the observed decrease in the perpendicular loss (152). These results are attributed to considerable amorphous phase orientation. Birefringence studies on isotactic polypropylene (153) and polyethylene (134) have also shown orientation of the amorphous component.

Peterlin (108) has shown that annealing of highly drawn crystalline polymers heals crystal defects but reduces drastically the number of tie molecules. As a consequence of the loss of taut tie molecules, the amorphous orientation disappears to the same extent as does the microfibrillar structure.

In summary, from the aforementioned studies it appears that the amorphous regions of drawn semicrystalline polymers are at least partially oriented. However, the extent of amorphous orientation and its relation to the extent of draw varies among polymers as may be expected. Likely variables include composition, molecular weight, temperature, original morphology preparation conditions, and extent of draw and annealing.

#### E. Annealing.

Post-drawing annealing is a prime variable. On annealing cold-drawn polyethylene at or above  $118^{\circ}\text{C}$ , rapid relaxation occurs, manifesting itself in a long period increase for the crystal lamellae, an increase in density (crystallinity), and an increase in the heat content of the amorphous component to the value of completely relaxed chains (89). Peterlin asserts this is all due to an entropic restoring force acting on strained, uncrystallized tie molecules which are given mobility by the high temperature. In the case of long period growth, the driving force is said to be the reduction of surface energy which reduces the crystal surface-to-volume ratio (21,154). Relaxation of tie molecules increases the intramolecular energy (89). In summary, Peterlin suggests that annealing smoothes out the fold surfaces, heals crystal defects, and relaxes the highly strained

tie molecules. This is consistent with the increase in small angle scattering intensity (155) due to an increase in density difference between lamellae and the (amorphous) intermediate regions.

Dismore and Statton (156) investigated the effects of annealing on oriented nylon 66 fibers using x-ray diffraction, NMR, density measurements, and tensile testing. Their results show that on heating to 160-255°C under zero tension, some of the molecules change from elongated to folded conformation. They also noted, on heating below the melting point, an increase in percent crystallinity and a larger proportion of fluid-like segments. They attribute the latter to an increase in defect concentration with annealing. Sonic modulus also decreased with annealing temperature from 160 to 250°C, as shown in Figure 10. The increased mobility may be attributed to disorientation of the amorphous phase. Annealing did not appreciably reduce crystal orientation but did lower the strength (Figure 11) and elongation to break, likely due to fewer tie molecules carrying the load (156). Unmelted, albeit annealed, intermolecular bonds appeared to prevent overall crystal deorientation.

Another study of annealing effects of drawn nylon 66 was performed by Beresford and Beven (157). They investigated the consequences of annealing by wide- and small-angle x-ray diffraction. Consistent with others (155,156,158), they noted increases in both long period and small angle scattering intensity. As a result of their observations, a model for the structure of drawn polyamide fibers was proposed which consists of chain-folded molecules aggregated into ordered states which vary between the extremes of discrete lamellar regions with a few tie molecules and



regions in which the molecules are so irregularly folded and arranged that individual lamellae are no longer distinguishable (157) (see Figure 12).

Mead and Porter (159) studied the effects of annealing on a highly-oriented linear polyethylene morphology containing ~ 15% extended chains (160). They found that annealing between 126 and 132°C split the melting endotherm into two peaks at 132 and 139°C, the latter was the melting point of the unannealed (fiber) sample, while the former (132°C) was the melting temperature of the unoriented starting material. This and other results were consistent with the thermal instability associated with the anisotropy of the surface free energies of their highly-oriented crystalline fibers of HDPE.

#### F. Mechanical Properties.

The effect of drawing on the dynamic mechanical properties of nylon 66 has been investigated by several authors (161-164). Dumbleton and Murayama (104) found several interesting results. They noted that the tensile storage modulus ( $E'$ ) curves for samples parallel and perpendicular to the stretch direction (drawn 3X) do not cross (with  $E'$  parallel always greater than  $E'$  perpendicular) in agreement with the work of Takayanagi, et al. (165), on cold-drawn polypropylene and polyethylene (Figure 13). The latter curves were found to cross when the (PE and PP) samples were annealed (Figure 14). At a draw ratio of 4.5X, Dumbleton and Murayama discovered that the nylon 66 curves do cross. They attribute this to annealing during drawing. These authors also noted other effects: (1) The crossing of the  $E'$  curves, for suitably treated samples, may be taken as evidence that the



$\alpha$  transition\* corresponds to the glass transition in nylon 66. (2) As the draw ratio increases,  $E'$  increases and the maximum in  $E''$  (loss modulus) occurs at higher temperatures. The latter is usually indicative of increased crystallinity and/or a more closely packed morphology (162). (3) There was no effect of annealing on the temperature of  $\alpha$  up to the maximum temperature studied of  $240^{\circ}\text{C}$ . These authors (161) conclude that nylon 66 is probably a paracrystalline structure and that the  $\alpha$  transition ( $T_g$ ) may be a multiple transition.

Murayama and Silverman (162) studied the effects of molecular weight on the dynamic mechanical properties of nylon 66 film and fiber. They found that the  $\alpha$  transition (glass transition) moved to higher temperatures ( $88$  to  $120^{\circ}\text{C}$ ) with increasing viscosity-average molecular weight ( $\bar{M}_v$ ) from  $45,000$  to  $120,000$  for the film, and a shift from  $110$  to  $123^{\circ}\text{C}$  with an increase in  $\bar{M}_v$  from  $35,000$  to  $52,000$  for the fiber. These authors concede that the  $\alpha$  peak of high molecular weight nylon 66 may be affected by formation of additional interlamellar connections, as pointed out by Miyagi and Wunderlich (166).

#### G. Polymorphism.

Many cases of polymorphic transformations during polyethylene deformation have been reported (167-174). Seto, et al. (167), first cold drew then laterally compressed samples of high density polyethylene and noticed changes

\*This  $\alpha$  transition for nylon 66 is the glass transition, not to be confused with the (crystalline)  $\alpha$  transition generally associated with semicrystalline polymers.

in texture of both the orthorhombic and monoclinic crystals formed. They attribute the textural changes to three possible deformations: (1) twinning and slip of crystal planes, (2) phase transformation (orthorhombic to monoclinic), and (3) slip at the grain boundaries (crystallite boundaries). Earlier investigations had revealed stress-induced transformations from an orthorhombic to a pseudo-hexagonal (168), triclinic (169,170) or monoclinic (171) unit cell. Kiho, et al. (171), reported that either twinning or a phase transformation occurs as a function of stretching. These authors also noted that the monoclinic x-ray reflections disappeared when deformed single crystals were allowed to relax (175). They further showed that the monoclinic cell is unstable above  $110^{\circ}\text{C}$  (176). In agreement, Seto, et al. (167), found that the monoclinic form either reverted to the orthorhombic form, or twinned, or underwent both processes upon removal of a compressive stress. They attributed this to restoring forces caused by elastically-distorted amorphous regions between crystallites.

More recent results (173,174) present an in-depth discussion of twinning and phase transformation modes in crystalline polyethylene and describe the procedure used for predicting such processes. Bevis and Crellin (174) surmise that the martensitic transformation to the monoclinic cell results from simple shear deformation of the orthorhombic cell. Young and Bowden (173) deformed oriented high density polyethylene by shear perpendicular to the chain direction and examined the results by WAXS. They concluded that (1) the initial orientation relationship between the monoclinic and orthorhombic forms of polyethylene corresponds closely to the  $T1_2$  martensitic transformation mode of Bevis and Crellin (174),

(2) the orientation of the monoclinic cell may change by slip during deformation or by twinning, on unloading [as did Seto, et al. (167)], (3) during a general deformation both [001] slip and the martensitic transformation should be activated, (4) (100) [010] transverse slip takes place when (100) is oriented at about  $45^{\circ}$  to the compression direction, and (5) (110) twinning is observed both during deformation and on unloading specimens. No evidence for (310) twinning was found.

Some studies have been made of the effect of drawing on polymorphic (crystal-crystal) transitions in nylon 6 (48,158,177). Miyasaka and Makishima (177) treated nylon 6 multifilament yarns with aqueous iodine. In agreement with Bradbury (46), the new crystal structure was found by x-ray to be approximately the hexagonal  $\gamma$ -phase. The  $\gamma$ -phase is known to be stable to thermal (annealing) treatment (41). When the treated sample was stressed in the chain direction  $\geq 3.5 \times 10^3 \text{ kg cm}^2$ , a crystal reversion was found to occur (back) to the  $\alpha$ -phase. This  $\alpha$ -phase remains unchanged when heated for one minute at  $100^{\circ}\text{C}$  in water without tension.

In the  $\gamma$ -phase the chains are twisted about amide groups. When stretched, they assume the planar zigzag conformation characteristic of the  $\alpha$ -phase. For hydrogen bonding to be complete in this new form ( $\alpha$ ), the adjacent chains must be antiparallel, as proposed by Arimoto (47), Bradbury (46), and Holmes, et al. (178) (Figure 15).

Sakaoku, et al. (158), found that nylon 6 fibers drawn greater than 4X and nylon 6 fibers annealed at  $215^{\circ}\text{C}$ , originally in the  $\beta$ -phase, were converted in large part to the  $\alpha$ -phase. Such an effect had been noted



previously (179,180). These  $\alpha$ -phase crystals are shown to be more stable and increase their long period less on annealing (158).

In somewhat related work, changes in the hydrogen bonded structure of nylons above and below  $T_g$  were investigated. Northolt (252), working with quenched nylon 11 film drawn 4X, found biaxial orientation with samples drawn below the glass transition temperature ( $60^{\circ}\text{C}$ ) while uniaxial orientation prevailed when drawing took place above  $T_g$ . Identical behavior was found with nylon 66, while only uniaxial orientation of crystallites was observed when nylon 12 was drawn at temperatures both below and above  $T_g$  ( $42^{\circ}\text{C}$ ). Northolt attributed the orientation behavior to the nature of the hydrogen bonding in nylons 11, 12, and 66. Based on an idea by Gordon (253) that the glass transition in nylons is caused by disruption of hydrogen bonds in amorphous regions, Northolt postulates that for nylon 11 and nylon 66 the two dimensional (010) hydrogen bonded sheets produce biaxial orientation below  $T_g$ , while disruption of these sheets above  $T_g$  results in uniaxial crystallite orientation. In the case of nylon 12, a three-dimensional hydrogen bonded network, resulting from a hexagonal unit cell and leading to a uniaxial orientation at all drawing temperatures, is said to exist (252).

#### IV. Deformation Processes

Three basic solid-state deformation processes have been used to achieve polymers of extreme modulus and tensile strength. These are (A) cold drawing, (B) cold extrusion, and (c) hydrostatic extrusion. The methods are interrelated with each having its distinct features.



(A) Cold Drawing--Cold drawing is a process that has been widely employed with both crystalline and amorphous polymers. It is characterized by load-elongation curves having three distinct regions as shown in Figure 16. The stress first rises, almost linearly, as the specimen is stretched. Next, the curve dips as a neck forms in the sample and consequently the stress falls at first, then is nearly constant and the neck propagates as stretching is continued. The length of necked-down (smaller diameter) region thus moves along the specimen until it is all drawn. At that stage, there is a marked increase in the stress on further extension, i.e. modulus increases, because the molecules aligned on necking resist further elongation. Thus, during cold drawing, there is a strain-hardening process that comes about as a result of the orientation of the molecules as part of the necking process. This orientation strain-hardening process increases the strength in the stretching direction many fold and is responsible for the usefulness of commercial synthetic fibers which are commonly cold-drawn continuously during manufacture (184).

The "natural draw ratio" is the ratio of the length of a cold-drawn segment to the original, undrawn length. It may also be defined as the smallest uniform draw ratio which can be given to a fiber or a film when it is oriented by cold drawing rather than by uniform extension (181). The natural draw ratio for a given polymer is affected by experimental conditions (182) and polymer molecular weight (183). For amorphous polymers, cold drawing occurs most readily just below the glass transition temperature,  $T_g$ . For semicrystalline polymers, cold drawing may take place from below  $T_g$  up to near the melting point (181). Other phenomena can occur at

temperatures lower and higher than the cold drawing range (181). Such deformations, however, do not result in the same extent of molecular orientation as obtainable by cold drawing.

The principles of cold drawing have been discussed by many authors (185-191), not all of whom agree with each other. However, the basic facts seem to be that a non-uniformity (with regard to mechanical response) develops in the specimen under tensile stress, possibly due to a region of smaller cross-sectional area or because of a region of stress concentrations (190). The resultant local increase in stress causes an increase in strain, which results in a thinning at that point. Eventually the system becomes unstable, and a neck is formed. The edges of the neck deform rapidly, producing a local heating and temperature rise, and the neck thus propagates while the rest of the specimen resists deformation (191). The local heating, i.e. strain-softening in the shoulders of the neck, leads to material in the neck zone becoming much stronger and stiffer in tension.

Under ideal conditions for a particular polymer, high draw can be achieved, resulting in polymers of high moduli and tensile strengths. Among investigators who have realized such properties are Ward (183,192-195,211), Clark (2), and Keller (196), each with co-workers. Andrews and Ward (192) tested a number of processing parameters in drawing tests on a high density polyethylene. They found that the yield stress appeared to be a linearly increasing function with the logarithm of strain rate while the drawing stress, after initially increasing at about the same rate as the yield stress, subsequently dropped off (Figure 17). The natural draw

ratio was found to be independent of strain rate up to about  $5 \times 10^{-2} \text{ sec}^{-1}$ , above which it increased rapidly. The authors attribute the increase to strain softening at the shoulders of the neck, due to adiabatic heating at higher strain rates. The natural draw ratio was only slightly affected by temperature, decreasing slightly up to  $100^{\circ}\text{C}$  possibly due to annealing, then increasing as the drawing temperature was raised further. The increase was attributed to melting of low molecular weight material, leading to non-homogeneous deformation on drawing. The maximum natural draw ratio achieved in these studies was 15. Other conclusions of this work (192) were (1) the natural draw ratio decreases with increasing weight-average molecular weight and (2) Young's modulus increase monotonically with increasing natural draw ratio. Higher molecular weights presumably provide a greater number of interlamellar tie molecules (213) which impede crystal orientation, causing a lower natural draw ratio and subsequent lower Young's modulus; that is, a greater concentration of interlamellar ties supposedly increases the rate of strain hardening. Vincent (190) has shown that there is a lower limit of molecular weight for cold drawing, below which there is insufficient strain hardening to stabilize the neck.

Capaccio and Ward (183,193-195) have reported on the attainment of draw ratios to approximately 40. One study (194) concentrated on the preparation of the initial morphology. It was concluded that the sample component of highest molecular weight determines the highest tensile modulus attainable. The authors also proposed that molecular weight dependent parameters such as the extent of crystal nucleation, crystal growth, and segregation of low molecular weight material, influence the initial



morphology and thus the subsequent drawing. The maximum tensile modulus attained in this study was 69 GPa, measured at a draw ratio of 30 (194).

A further result by these authors (183) supported their contention that variations in the high molecular weight tail in the molecular weight distributions for their test polyethylene was likely the dominant feature influencing draw. Here they reported a strength greater than 0.35 GPa and a low elongation to break, ~ 3%. Capaccio and Ward (195) found that the yield stress increases with the crystallinity of the starting high density polyethylene at constant molecular weight. The yield stress also increases with molecular weight at constant temperature. They concluded that the longer molecules in the distribution can form a network superstructure due to physical crosslinking by molecular entanglements. They state that high values of  $\bar{M}_w$ , and crystallization under conditions where there are many tie molecules linking the crystalline domains, both affect the morphology in a similar manner and reduce the maximum attainable draw ratio (and subsequently the modulus) achieved under standard conditions of draw.

Clark and Scott (2) carried out cold drawing experiments on polyoxymethylene up to a draw ratio of about 20. This was achieved by a two step drawing process at elevated temperature. During the first stage, the polymer was drawn to its natural draw ratio of about 7. The second step involved subsequent drawing at a very slow rate to a draw ratio of about 20. The mechanical properties of the resultant material (tensile strength: 1.7 GPa, Young's modulus: 35 GPa) exceeded prior values for this polymer (2). A model was proposed where the chain folds act as isolated units,

existing as defects in a continuous crystal matrix as shown in Figure 18. Thus, the authors claim, while chain folds may be regions of weakness, the weakness is not magnified by aggregation of these defects into a chain folded surface to create a mechanism for stress crack propagation, reducing the ability to draw.

Barham and Keller (196) have drawn single crystal mats and spherulitic sheets of polyethylene. They concluded that a component of low molecular weight was necessary to achieve high draw ratios. High temperatures ( $\geq 75^{\circ}\text{C}$ ) of drawing and slow crystallization of the starting material were also seen as important requirements for attaining high draw. They further noted that pulling out of chain folds in the drawn fiber cannot be complete because they found a contraction on heating close to the melting point (197), a phenomenon not observed in crystals actually formed from pre-extended chains by primary crystallization. They believe that the folds remaining in drawn fibers are responsible for locked-in stresses.

Other workers have obtained high strength polypropylene (198,199) fibers by cold drawing and also polyoxymethylene, nylon 6 and poly(vinyl alcohol) (200).

(B) Cold Extrusion--Cold extrusion is a relatively recent development (1,201-206). The polymer process is analogous to that used in obtaining profiles from ductile metals (207). The process consists of forcing a solid plug of polymer, commonly by high pressure, through a die having a tapered entrance region (208). This is shown schematically in Figure 19. The resulting reduction ratio in cross-sectional area (plug to extrudate) is variously known as extrusion ratio, deformation

ratio, draw ratio, or degree of processing. The process imparts an elongational deformation to polymer molecules (214) which results in remarkable physical and tensile properties (92,204,205,209-212). This solid state extrusion process has been applied to high density polyethylene (1,201-206,208,212,222), low density polyethylene (212), polypropylene (1,212,215,222), nylon 66 (206,212), nylon 6 (213,215,222) and also poly(phenyleneoxide), polyoxymethylene, polytetrafluoroethylene and poly(vinyl chloride) (212). Recently, nylons 11 and 12 have also been solid state extruded in this laboratory.

The success of this process depends on the deformation taking place under conditions where polymer crystals are readily deformed. This may well correspond to conditions above the so-called  $\alpha$  transition temperature of the particular polymer. This transition defines a lower temperature for the region (the crystalline melting point is the upper boundary) wherein crystals may be plastically deformed without being fractured by rupture of covalent bonds. The transition and thus the deformation range likely change with pressure. It is important to note, however, that as the melting point is approached, the polymer chains will deform ever more viscously with ever-less morphological change even though the sample more readily changes shape. Clark and Scott suggest that the  $\alpha$  transition temperature may commonly be about  $30^{\circ}$  below the melting point (2). Cold extrusion experiments conducted below this temperature must involve extremely long times for molecular rearrangement and thus very slow extrusion rates. Raising the pressure to increase the extrusion rate may only result in fractured extrudate.



Nielsen (182) investigated polyethylene and found that in unbranched, slowly cooled and annealed material, the  $\alpha$  transition temperature may be over  $100^{\circ}\text{C}$ , whereas if the polymer is branched, or if it is a copolymer, or if it is quenched from the melt, the  $\alpha$  transition is lower. As the degree of crystallinity is decreased, the magnitude of the transition also decreases. According to Nielsen (182), the  $\alpha$  transition may be correlated with crystallite size and the length of polyethylene sequences in a crystallite. He thus proposed that the transition may be related to the chain fold lengths and occurs at a temperature where the folded chains can "recrystallize" in a time comparable to the time required to make the dynamic test or deformation.

Below the  $\alpha$  transition, the crystallites are less able to deform plastically as they act more like chemical crosslinks. When deformed over a few percent, the covalent bonds, already stretched, lead to rupture, and the necessary pulling out of folded chain crystals into extended chain crystals is thus restricted. So, for attainment of high draw, an optimum temperature of drawing (and pressure for extrusion) will likely be found between the  $\alpha$  transition temperature and the polymer melting point. Takayanagi, et al. (1), found that the optimum temperature for the cold extrusion of polypropylene was  $110^{\circ}\text{C}$ , which is just the proposed  $\alpha$  transition temperature.

Many investigators are studying problems associated with cold extrusion as will be discussed. A problem encountered in cold extrusion is the appearance of cracks or crazes that occur usually at higher ( $\sim 30$ ) extrusion ratios (1,208,217). Work in this laboratory with high density polyethylene has shown that, as extrusion temperature is reduced, the fractures

occur at lower extrusion ratios, indicating that the polymer crystals are increasingly unable to plastically deform at the lower (extrusion) temperatures. Although the extrusion rate was slower at the lower temperatures, it nonetheless may have been faster than the crystal could accommodate to plastically deform. These defects, which apparently are small fractures oriented at various angles to the extrusion direction, result in oriented extrudates but with markedly reduced tensile properties. At high draw, the frequency of fracture is increased, and the extrudate eventually fails under its own weight.

The origin of extrudate fracture has been investigated with respect to polymer melts flowing through conical, converging dies (218-220). It has been concluded that fracture originates at a point where fluid elements are subjected primarily to extensional deformation, in the capillary inlet. Shaw (220) has shown that lubrication of the conical entrances forces the melt to converge at a sharp angle of the die itself, rather than establishing a more gradual convergence dictated by a balance of shear and extensional forces in the entry region (221). The lubricant was silicone vacuum grease. He proposed that lubricant can reduce shear stresses and favor extensional flow, thus generating high tensile stresses which result in extrudate fracture. Shaw concludes that die design for minimum pressure drop is inconsistent with production of unflawed extrudates because such a design invariably increases axial extension rates. Furthermore, he states that minimizing shear deformation in die design may cause higher tensile stresses for many shear sensitive fluids.

Cold extrusion involves the deformation of semicrystalline polymer. Corresponding deformation analyses for polymer melts (218-221) have nonetheless been applied in an effort to understand solid state deformation phenomena.

Benbow and Lamb (223) investigated melt fracture processes using both silicone gum and polyethylene extruded through dies of different materials. They measured the critical shear stress at which the onset of melt fracture began. Their results indicate that the critical shear stress for branched polyethylene through brass dies is higher than that for silver steel dies and shows a slight temperature dependence whereas critical stress is independent of temperature in the silver steel dies. Furthermore, the flow curves show a break in the case of the brass dies whereas no break is seen with extrusion through the silver steel dies. Other conclusions drawn from this work (223) are: (1) melt instability originates at the die wall near the entry to the die, (2) when the melt flow is unstable, slipping occurs along the die wall, (3) flow birefringence experiments suggest that the stress changes in a manner consistent with a stick-slip motion, and (4) interpretation of the onset of melt instability as being due to a breakdown of adhesion between the polymer and the die wall is supported by the known dependence of the critical shear stress on molecular properties and external conditions.

Predecki and Statton (206) point out that the use of a lubricant in cold extrusion reduced the extrusion pressures, consistent with Shaw's (220) results, but that the efficiency of the molecular orientation was reduced. It was concluded that a combination of extensional and shear deformation gives the most effective orientation and chain extension.



In this laboratory, we have found that the use of lubricants when cold-extruding polyethylene can allow attainment of higher extrusion ratios. With lubricant, extrudate clarity may be diminished, due to lubricant coated on the extrudate surface, but the physical and mechanical properties have not been significantly reduced.

The effect of die entrance angle on extrusion pressure has been investigated by several workers (213,215,224). Increasing the die entrance angle generally results in an increase in extrusion pressure. Imada and Takayanagi (224) explain this through a slip line analysis following the ideas of Hill (225). They calculated the slip lines for extrusion through a slit die and showed that, by integrating the force along the wall, the extrusion pressure can be estimated on the basis of the slip planes generated. The calculated result is an increase in extrusion pressure with increasing entrance angle as generally found experimentally. Takayanagi, et al. (215), suggest that this pressure increase with entrance angle is attributable to the change of stress, and consequently velocity distribution, especially around the capillary inlet. Predecki and Statton (206) noted that a small ( $< 10^0$ ) die angle was necessary to produce solid-state extrudates free of defects.

Smith, et al. (226), point out that cold extrusion, like hydrostatic extrusion, is limited by the pressure build-up at high extrusion ratios. They note that this is due to the pressure dependence of the yield behavior of polymers, which implies that higher yield stresses are required for deformation where there is any substantial hydrostatic component of stress. This latter fact was noted by Pae, et al. (227), in an

earlier work. This is consistent with the results of Buckley and Long (212) who found that a material of relatively high modulus, like nylon, requires a greater pressure for extrusion than a material of lower modulus, like polyethylene.

Extrusion pressures employed in the cold extrusion process range to several thousand atmospheres, depending on choices such as extrusion ratio and temperature, polymer, and use of lubricant. Nakamura, et al. (1), found that the molecular weight dependence of extrusion pressure for polypropylene was small compared with the case of melt viscosity. They propose that this indicates that the local molecular interaction is a predominant factor in solid state extrusion.

Increasing extrusion temperature was found to increase the long period of cold-extruded polyethylene (205,222) as shown in Figure 20. This can be attributed to an annealing effect wherein the extruded folded chain crystals grow on long period and the extruded extended chain crystals revert back to longer folded chain crystals (159). It could also be a consequence of the original crystals prepared at a higher temperature before extrusion. Imada and Takayanagi (224) also noted that polyethylene obtained at relatively low extrusion temperatures ( $\sim 80^{\circ}\text{C}$ ) showed elastic after-effects, such as shrinkage at elevated temperatures. However, that extruded at high temperatures (100 to  $120^{\circ}\text{C}$ ) remained dimensionally stable, even at temperatures as high as  $120^{\circ}\text{C}$ . The two temperature ranges are respectively below and above accepted values for  $T_{\alpha}$ . This implies that either (1) the extrudates obtained at the higher temperatures were substantially annealed in the extrusion process or (2) amorphous orientation

only occurs at low temperatures (below  $T_{\alpha}$ ) or (3) stable long periods were produced (at the higher temperatures) rather than shorter ones which were annealed. Another effect of increasing extrusion temperature may be a lower coefficient of friction at the polymer die interfaces resulting in lower extrusion pressure (222). Further studies in this laboratory on the effects of extrusion temperature and ratio on cold-extruded polyethylene will be published (228).

Kolbeck and Uhlmann (229) extruded high density polyethylene, polypropylene and poly(vinylidene fluoride) using a silicone or fluorocarbon lubricant on their dies. They observed what they believe to be necking of the deformed polymer within the conical entrance region of the die. (This could also result from relaxation of the compressed polymer upon the release of pressure prior to removal of the die.) Deformational heating was minimal so melting and recrystallization during extrusion were presumed not to occur. During the initial stages of deformation, the predominant flow appeared to be elongational, whereas shear flow was indicated during later stages of extrusion. The authors observed that at large die angles ( $\sim 40^{\circ}$  included) the flow was dominated by shear rather than elongational flow. Kolbeck and Uhlmann conclude from their studies that both elongation and shear deformation are important in high stress extrusion and that there are many similarities to extrusion in both the molten and crystalline state, leading them to believe that the amorphous component exerts a major influence on the extrusion of even highly crystalline polymers.



(C) Hydrostatic Extrusion--Hydrostatic extrusion is similar to cold extrusion in that a ram or plunger is used to apply the extrusion pressure. In hydrostatic extrusion, pressure is transmitted through a fluid which surrounds the polymer plug, see Figure 21. Frictional forces between the plug and container wall plus die are reduced by the presence of the pressurized lubricant. For these reasons, the pressure required for hydrostatic extrusion is lower, and the deformation approximates more closely a convergent flow (230). This process is discussed by Williams (231) and by Yoon, et al. (232), Fuchs (233), and by Alexander (234).

Hydrostatic extrusion has been predominantly applied to polyethylene (230,235-238) although Buckley and Long (212) examined also polypropylene, nylon 66, polyoxymethylene, poly(vinyl chloride), poly(phenylene oxide) and polytetrafluoroethylene. Williams (231) hydrostatically extruded polypropylene, and Bhakja and Pae (239), a polyamide.

Gibson, et al. (230), investigated the hydrostatic extrusion of high density polyethylene using castor oil as the pressure transmitting fluid and silicone vacuum grease as a die lubricant. An extrusion ratio up to about 20 was achieved. Above an extrusion ratio of ~ 10, they noted a marked increase in modulus as shown in Figure 22. This was also the point where the extrudate became transparent and the birefringence began to level off after initially increasing rapidly with extrusion ratio (Figure 23). The authors propose that the morphology transformation to the fiber structure is essentially complete when an extrusion ratio of 10 has been reached. They believe that further deformation takes place by

deformation of the fiber structure itself (107). This is consistent with the common belief that high density polyethylene has a natural draw ratio of  $\sim 11$ .

Davis (235) hydrostatically extruded high density polyethylene, using n-pentane, kerosene, oil and water as extrusion fluids. He found that coating the die with PTFE reduced a severe stick-slip problem. The billet apparently stuck to the die until sufficient excess pressure built up, then it would extrude suddenly and completely at a high rate. Extruding into a fluid-filled reservoir also reduced this problem. Davis found that practical extrusion ratios are limited by shear failure of the extrudate as it exits the die rather than by excessive extrusion pressure, as is the case for metals. He also notes that solid state extrusion may prove useful for processing polymers unamenable to traditional processing techniques. This latter idea has been borne out in this laboratory with some high-melting ( $> 300^{\circ}\text{C}$ ) aromatic polymers.

Nakayama and Kantesuna published three studies on hydrostatic extrusion of high density polyethylene (236-238). They studied the influence of die angle, extrusion temperature and the extrusion ratio of the extrusion pressure and the appearance of the extrudate (236). The included entrance angles used were  $20^{\circ}$ ,  $60^{\circ}$ ,  $90^{\circ}$  and  $120^{\circ}$  (Figure 24). They classified extrusion pressure-displacement curves into three groups: (1) highly-oriented extrudates having a smooth surface obtained by steady-state extrusion at higher temperature ( $100^{\circ}\text{C}$ ); (2) extrusion at lower temperature with a large entrance-angle die causing a stick-slip motion, which resulted in fluctuations in extrudate diameter; (3) high extrusion ratios where

drastic stick-slip effects resulted in fractured extrudate. When extrusion was carried out through a small angle die at constant pressure, a smooth transparent, unflawed extrudate was obtained.

Another study by these authors involved an evaluation of the critical extrusion pressure and rate of extrusion using a simple die with a  $20^\circ$  included entrance angle (237). A tensile testing machine, capable of sustaining a constant load on the billet, was used. Extrusions were carried out at 13 to  $120^\circ\text{C}$  and the minimum pressure required for extrusion was determined, see Figure 25. This critical pressure decreased with increasing temperature, which also had a large influence on the relationship between the extrusion pressure and extrusion rate (Figure 26).

The third study by Nakayama and Kantesuna investigated the effects of strain hardening and lubrication on extrusion pressure in hydrostatic extrusion of polyethylene (238). Extrusion ratios ( $R'_E$ ) of 3 to 9 were used. Critical extrusion pressure,  $P_0$ , i.e. minimum pressure required for extrusion, at different extrusion temperatures,  $T_E$ , was plotted against  $\ln R'_E$ . A rapid increase in the slope occurred at  $\ln R'_E + (90 - T_E^\circ\text{C}) \sim 1.8$ , which was associated with strain hardening. To investigate the strain hardening, the mean deformation resistance,  $\alpha_0$ , at each extrusion ratio was estimated by using Pugh's equation. Several liquids were used as the pressure medium to study lubrication effects. These included Molycote M-30, castor oil, glycerine, ethyl alcohol, glycerine-water and water. When the critical extrusion pressure was plotted against included die entrance angle ( $2\alpha$ ), it was found that pressure first drops (at  $\alpha = 20^\circ \rightarrow 60^\circ$ ) then rises (at  $\alpha = 60^\circ \rightarrow 120^\circ$ ) with



increasing entrance angle. This is shown in Figures 24 and 27. This result contrasts with other investigators (213,215,224) who have found that extrusion pressure increases with increasing entrance angle.

(D) Other Techniques--A process which has produced highly oriented and transparent strands for polyethylene and polypropylene has been developed by Collier, et al. (240), using a commercial extruder with specially-designed dies. The orientation is developed in the die entrance and is retained by crystallization in the die. Crystallization is reduced in the pre-die region by maintaining a temperature above the melting point of the flowing, oriented melt. The procedure has the advantage of relatively low pressures and the possibility of being a continuous process.

Baranov, et al., have utilized a process called "jet stretching" to deform and produce fibers of polyethylene (241), polypropylene (242), and nylon 6 (243). The polymer is pumped through spinnerets at high speed and subsequently drawn at high rate at elevated temperatures. Small angle polarized light scattering was used to characterize the structure as produced. The authors (243) postulate that the original (nylon 6) threads contain spherulites embedded in an amorphous glass-like matrix. They contend that stresses develop in this matrix, especially near the spherulite boundaries, and that these regions are subsequently destroyed, resulting in spherulite flattening which is reflected in the scattering patterns. At higher elongations, macrofibrils were observed in both optical micrographs and SALS patterns. Conclusions are that crystallization proceeds with the occurrence of molecular orientation which suppresses the growth of folded crystals in the direction of fiber formation.

Crystallization from a stressed melt was also carried out by Hashimoto and co-workers (244) using calendering equipment with linear polyethylenes of differing molecular weights. Hard elastic films, i.e. films which undergo a large elastic deformation on stretching along the machine direction, were produced from high molecular weight ( $\bar{M}_w = 30 - 35 \times 10^4$ ) polyethylene. The authors found that crystal lamellae were oriented with their normals parallel to the machine direction. B-axis orientation remained perpendicular to the machine direction whereas c- and a-axis orientation along the machine direction prevailed for the high and medium molecular weight polyethylenes, respectively. They noted that the proposal by Keller and Machin (245) that c- and a-axis orientation result, respectively, from crystallization under high and low shear stresses appeared to be applicable to their systems. The c-axis oriented films produced the hard elastic properties whereas the a-axis oriented films exhibited the usual yielding and necking. Hashimoto and co-workers conclude that the deformation of specimens along the machine direction involves lamellar bending and interlamellar slip, the former elastic in nature and the latter basically viscous and time-dependent. Both processes are thought to involve a plastic deformation of crystals.

T. K. Kwei, et al. (246,247), have developed a quench-rolling process for producing tough and transparent high density polyethylene film. The preparation involves simultaneous high speed quenching ( $10^4 \text{ }^\circ\text{C} - \text{sec}^{-1}$ ) and shearing ( $\sim 10^5 \text{ sec}^{-1}$ ) of a polymer melt during crystallization. Two cold, rotating metal rollers provide the shear and temperature gradient. Young's modulus, measured in the rolling direction, is  $4 \times 10^{10} \text{ dynes} - \text{cm}^2$  which is about 12 times higher than unoriented film and about twice

the modulus of film drawn at room temperature 10X. The tensile strength of  $1.04 \times 10^9$  dynes-cm<sup>2</sup> is about seven times greater than unoriented film and slightly less than the 10X film.

Further studies on stress- (or strain-) induced crystallization can be found in the March, 1975, and 1976 special symposium issues of Polymer Engineering and Science, while a review by Biggs (248) discusses processes used for attainment of ultra-high moduli. A review on "hard elastic fibers", which are semicrystalline polymers crystallized under stress and retaining both high modulus and elastic recovery, has been published by Cannon, et al. (249). This paper elaborates on the morphology, mechanical properties, and physical mechanisms of these materials, which the authors term "springy polymers".

#### V. Summary and Conclusions

Solid state deformation has been used to achieve materials with ultra-high tensile moduli by taking advantage of the high strength of covalent bonds. This is accomplished by the pulling out of chain folds and subsequent extension of the molecular chains which run both through and between crystal lamellae. The three major processes detailed herein are effective methods of aligning and extending chain molecules in order to gain from them the strength and stiffness needed for many of today's and tomorrow's structural applications. The cold drawing process has the advantage of adaptability to commercial equipment as now used to process polymer fibers. The cold extrusion technique brings another variable, pressure, into the picture, expanding the possibilities for more perfect uniaxial extension. The hydrostatic extrusion method, while in some cases



messy, allows lower pressures and virtually eliminates frictional problems between polymer and processing equipment. While fracture at high extrusion ratios is a problem in cold extrusion, voiding at high draw ratios is likewise a problem with cold drawing, and interaction between the polymer and the pressure-transmitting fluid can lead to faulty results in the hydrostatic extrusion technique.

In some respects, the three types of solid state deformation can be combined, as cold drawing can be done under hydrostatic pressure (232,250, 251) and the extrudates from both cold and hydrostatic extrusion can be drawn as they emerge from the die (231). The latter technique is presently being investigated in this laboratory and preliminary results show increased rates of extrusion as well as the possibility of lower extrusion pressures.

Further research into the mechanisms of, and (optimum) conditions for, solid state deformation will lead to more efficient processes and a yet closer approach to the high theoretical moduli of most semicrystalline thermoplastics.

References

1. K. Nakamura, K. Imada and M. Takayanagi, Intern. J. Polym. Mater. 2, 71 (1972).
2. E. S. Clark and L. S. Scott, Polym. Eng. Sci. 14, 682 (1974).
3. I. Sakurada and K. Kaji, J. Polym. Sci., C, 31, 57 (1970).
4. F. W. Billmeyer, J. Am. Chem. Soc. 75, 6118 (1953).
5. J. K. Beasley, J. Am. Chem. Soc. 75, 6123 (1953).
6. I. Harris, J. Polym. Sci. 8, 353 (1952).
7. C. W. Bunn, Trans. Far. Soc. 35, 482 (1939).
8. R. L. Miller in "Crystalline Olefin Polymers", Part I, R. A. V. Raff and K. W. Doak, Eds., Interscience, New York, 1965, Ch. 12.
9. E. R. Walter and F. P. Reding, J. Polym. Sci. 21, 561 (1956).
10. A. Renfrew and P. Morgan, Eds., "Polythene", Interscience, New York, 1960.
11. H. D. Keith and F. J. Padden, Jr., J. Polym. Sci. 39, 101 (1959).
12. H. D. Keith and F. J. Padden, Jr., J. Polym. Sci. 39, 123 (1959).
13. A. Keller, J. Polym. Sci. 39, 151 (1959).
14. F. P. Price, J. Polym. Sci. 39, 139 (1959).
15. L. Mandelkern in "Growth and Perfection of Crystals", R. H. Doremus, B. W. Roberts and D. Turnbull, Eds., John Wiley, New York, 1958, p. 467.
16. S. Buckser and L. H. Tung, J. Phys. Chem. 63, 763 (1958).
17. L. Mandelkern, M. Nellman, B. W. Brown, D. E. Roberts and F. A. Quinn, J. Res. Nat'l. Bur. Standards 58, 137 (1957).
18. P. H. Lindenmeyer, Polym. Eng. Sci. 14, 456 (1974).

19. J. Schultz, "Polymer Materials Science", Prentice-Hall, Englewood Cliffs, New Jersey, 1974.
20. F. J. Balta-Calleja, D. C. Bassett and A. Keller, *Polymer* 4, 269 (1963).
21. I. C. Sanchez, J. P. Colson and R. K. Eby, *J. Appl. Phys.* 44, 4332 (1973).
22. I. C. Sanchez, A. Peterlin, R. K. Eby and F. L. McCrackin, *J. Appl. Phys.* 45, 4216 (1973).
23. D. P. Pope and A. Keller, *J. Polym. Sci.-Phys.* 14, 821 (1976).
24. M. Yashuniwa, C. Nakafuku and T. Takemura, *Polym. J.* 4, 526 (1973).
25. M. Kyotani and H. Kanetsuna, *J. Polym. Sci.-Phys.* 12, 2331 (1974).
26. Y. Maeda and H. Kanetsuna, *J. Polym. Sci.-Phys.* 12, 255 (1974).
27. B. Wunderlich and T. Arakawa, *J. Polym. Sci.* A2, 3697 (1964).
28. P. Geil, F. R. Anderson, B. Wunderlich and T. Arakawa, *J. Polym. Sci.*, A2, 3707 (1964).
29. D. V. Rees and D. C. Bassett, *J. Polym. Sci.*, A2, 9, 385 (1971).
30. J. M. Lupton and J. W. Regester, *J. Appl. Polym. Sci.* 18, 2407 (1974).
31. G. E. Attenburrow and D. C. Bassett, *J. Mater. Sci.* 12, 192 (1977).
32. D. C. Bassett, *Polymer* 17, 460 (1976).
33. Y. Kinoshita, *Makromol. Chem.* 33, 1 (1959).
34. G. Champetier and R. Aelion, *Bull. Soc. Chim. France*, 683 (1948).
35. R. Hill and E. E. Walker, *J. Polym. Sci.* 3, 609 (1948).
36. D. D. Coffman, N. L. Cox, E. L. Martin, W. E. Moche1 and F. J. Van Natta, *J. Polym. Sci.* 3, 85 (1948).



37. D. D. Coffman, G. J. Berchet, W. R. Peterson and E. W. Spanagel, J. Polym. Sci. 2, 306 (1947).
38. C. W. Bunn and E. V. Garner, Proc. Roy. Soc. (London), A189, 39 (1957).
39. V. V. Korshak and T. M. Frunze, Zhur. Obshchei Khim. 26, 732 (1956).
40. D. S. Trifan and J. F. Terenzi, J. Polym. Sci. 28, 443 (1958).
41. A. Miyake, J. Polym. Sci. 44, 223 (1960).
42. M. I. Kohan, "Nylon Plastics", John Wiley, New York, 1973.
43. D. R. Holmes, C. W. Bunn and D. J. Smith, J. Polym. Sci. 17, 159 (1955).
44. I. Sandeman and A. Keller, J. Polym. Sci. 19, 401 (1956).
45. R. Hosemann, Polymer 3, 349 (1962).
46. E. M. Bradbury, L. Brown, A. Elliott and D. A. D. Parry, Polymer 6, 465 (1965).
47. H. Arimoto, J. Polym. Sci., A-2, 2, 2283 (1964).
48. B. D'Alo, G. Coppola and B. Pallesi, Polymer 15, 130 (1974).
49. M. G. Northolt, B. J. Taylor and J. J. Van Aartsen, J. Polym. Sci., A-2, 10, 191 (1972).
50. K. Inoue and S. Hoshino, J. Polym. Sci., Polym. Phys. Ed. 2, 1077 (1973).
51. T. Ishikawa, A. Sugihara, T. Hamada, S. Nagai, N. Yasuoka and N. Kasai, Kagaku 9, 1744 (1973).
52. R. J. Fredericks, J. Polym. Sci., A-2, 4, 899 (1956).
53. M. Tsuruta, H. Arimoto and M. Ishibashi, Kobunshi Kagaku 15, 619 (1958).
54. Y. Kinoshita, Makromol. Chem. 33, 21 (1959).

55. D. C. Vogelsong and E. M. Pearce, J. Polym. Sci. 45, 546 (1960).
56. H. Arimoto, Kobunshi Kagaku 19, 212 (1962).
57. K. Miyasaka and K. Makishima, Kobunshi Kagaku 23, 870 (1966).
58. R. Brill, J. Prakt. Chem., 161 (1942).
59. P. W. Allen, Research (London) 5, 492 (1952).
60. H. M. Heuvel, R. Huisman and K. C. J. B. Lind, J. Polym. Sci., Polym. Phys. Ed. 14, 921 (1976).
61. R. Huisman and H. M. Heuvel, J. Polym. Sci., Polym. Phys. Ed. 14, 941 (1976).
62. W. P. Slichter, J. Polym. Sci. 36, 259 (1959).
63. W. P. Slichter, J. Polym. Sci. 35, 77 (1959).
64. M. Genas, Angew. Chem. 74, 535 (1962).
65. S. Onogi, T. Asada, Y. Fukui and I. Tachinaka, Bull. Inst. Chem. Res., Kyoto Univ., 52 (2), 368 (1974).
66. R. Aelion, Ann. Chim. (Paris) 3, 5 (1948).
67. R. J. Barriault and L. F. Gronholtz, J. Polym. Sci. 18, 393 (1955).
68. H. W. Starkweather, Jr. and R. E. Brooks, J. Appl. Polym. Sci. 1, 236 (1959).
69. H. W. Starkweather, Jr., G. E. Moore, J. E. Hansen, T. M. Roder and R. W. Brooks, J. Polym. Sci. 21, 189 (1956).
70. H. W. Starkweather, Jr., J. Appl. Polym. Sci. 2, 129 (1959).
71. H. W. Starkweather, Jr., J. Macromol. Sci., Phys., B-3, 727 (1969).
72. J. L. Koenig and M. C. Agboatwalla, J. Macromol. Sci., Phys., B-2, 391 (1968).
73. C. G. Cannon and P. H. Harris, J. Macromol. Sci., Phys., B-3, 357 (1969).

74. F. Khoury, J. Polym. Sci. 33, 389 (1958).
75. E. S. Clark and C. A. Garber, Inter. J. Polym. Mat. 1, 31 (1971).
76. A. Keller and M. J. Machin, J. Macromol. Sci. (Phys.), B-1, 41 (1967).
77. M. J. Hill and A. Keller, J. Macromol. Sci. (Phys.), B-3, 153 (1969).
78. J. Mann and L. Roldan-Gonzales, J. Polym. Sci. 60, 1 (1962).
79. J. H. Magill, J. Polym. Sci., A-2, 4, 243 (1966).
80. C. R. Lindegren, J. Polym. Sci. 50, 181 (1961).
81. D. V. Badami and P. H. Harris, J. Polym. Sci. 41, 540 (1959).
82. C. G. Cannon, F. P. Chappel and J. I. Tidmarsh, J. Text. Inst. 54, T210 (1963).
83. J. V. McLaren, Polymer 4, 175 (1963).
84. U . S. Patent 3,080,345 (March 5, 1963) to E. I. duPont deNemours & Company.
85. A. D. McLaren and J. W. Rowen, J. Polym. Sci. 7, 289 (1951).
86. S. Gogolewski and A. J. Pennings, Polymer 14, 463 (1973).
87. S. Gogolewski and A. J. Pennings, Polymer 16, 673 (1975).
88. T. Zylinski, "Fiber Science", S.P.F.C.C.C.I.S.T.E.I., Warsaw, 1964.
89. A. Peterlin, J. Polym. Sci. C, 15, 427 (1966).
90. A. Peterlin, J. Polym. Sci., A-2, 9, 67 (1971).
91. N. W. Wyckoff, J. Polym. Sci. 62, 83 (1962).
92. W. G. Perkins, J. N. Capiati and R. S. Porter, Polym. Eng. Sci. 16, 200 (1976).
93. W. Urbanczyk, J. Polym. Sci. 59, 215 (1962).
94. D. C. Prevorsek and R. K. Sharma, Polym. Eng. Sci. 14, 778 (1974).



95. D. C. Prevorsek, P. J. Harget, R. K. Sharma and A. C. Reimschuessel, J. Macromol. Sci., Phys., B-8 (1-2), 127 (1973).
96. A. C. Reimschuessel and D. C. Prevorsek, J. Polym. Sci., Polym. Phys. Ed. 14, 485 (1976).
97. A. Peterlin, Polym. Eng. Sci. 9, 172 (1969).
98. A. Peterlin, J. Mater. Sci. 6, 490 (1971).
99. A. Peterlin, Text. Res. J. 42, 20 (1972).
100. A. Peterlin, Ann. Rev. Mater. Sci. 2, 349 (1972).
101. J. Becht, K. L. DeVries and H. H. Kausch, Eur. Polym. J. 7, 105 (1971).
102. J. Becht and H. Fischer, Kolloid-Z-Polym. 240, 766 (1970).
103. H. D. Keith and F. J. Padden, J. Polym. Sci. 41, 525 (1959).
104. D. C. Prevorsek, J. Polym. Sci., C, 32, 343 (1971).
105. A. Peterlin, J. Polym. Sci., A-2, 7, 1151 (1969).
106. G. Meinel and A. Peterlin, J. Polym. Sci., A2, 9, 67 (1971).
107. G. Meinel, A. Peterlin and K. Sakaoku in "Analytical Calorimetry", R. S. Porter and J. F. Johnson, Eds., Plenum Press, New York, 1968.
108. A. Peterlin, J. Macromol. Sci.-Phys. B8, 83 (1973).
109. A. Peterlin in "Copolymers, Polyblends and Composites", N. A. J. Platzer, Ed., Adv. Chem. Ser. No. 142, Am. Chem. Soc., 1975, p. 1.
110. A. Peterlin, Colloid & Polym. Sci. 253, 809 (1975).
111. A. Peterlin, Polym. Eng. Sci. 17, 183 (1977).
112. P. J. Barham, private communication.
113. M. Takayanagi and T. Kajiyama, J. Macromol. Sci.-Phys. B8, 1 (1973).
114. D. A. Zaukelies, J. Appl. Phys. 33, 2797 (1962).
115. R. Hosemann, C. R. C. Crit. Rev. Macromol. Sci. 1, 351 (1972).

116. R. Hosemann, Acta. Crystallogr. 4, 520 (1950).
117. D. H. Reneker, J. Polym. Sci. 59, 39 (1962).
118. W. Pechhold, Kolloid Z. 228, 1 (1968).
119. W. Pechhold and S. Blasenbrey, Kolloid Z. 216, 235 (1967).
120. J. J. Point, M. Dosiere, M. Gilliot and A. Goffin-Gerin, J. Mater. Sci. 6, 479 (1971).
121. D. M. Gezovich and P. H. Geil, J. Mater. Sci. 6, 531 (1971).
122. P. B. Bowden and R. J. Young, J. Mater. Sci. 9, 2034 (1974).
123. R. G. C. Arridge, P. J. Barham and A. Keller, J. Polym. Sci., Polym. Phys. Ed. 15, 389 (1977).
124. I. L. Hay and A. Keller, Kolloid-Z-Polym. 204, 43 (1965).
125. H. D. Keith and F. J. Padden, J. Polym. Sci. 41, 525 (1969).
126. K. Sasaguri, S. Hoshino and R. S. Stein, J. Appl. Phys. 35, 47 (1964).
127. P. Erhardt, K. Sasaguri and R. S. Stein, J. Polym. Sci., C, 5, 179 (1964).
128. R. S. Stein, S. Onogi, K. Sasaguri and D. A. Keedy, J. Appl. Phys. 34, 80 (1963).
129. Y. F. Yu and R. Ullman, J. Polym. Sci. 60, 55 (1962).
130. P. Ingram and A. Peterlin, J. Polym. Sci., B-2, 739 (1964).
131. J. L. Cooney, J. Appl. Polym. Sci. 8, 1889 (1964).
132. R. S. Stein, S.P.E. Trans. 4, 1 (1964).
133. R. S. Stein, Polym. Eng. Sci. 9, 320 (1969).
134. R. S. Stein, J. Polym. Sci., C, 1, 185 (1966).
135. R. S. Stein, Polym. Eng. Sci. 9, 320 (1969).
136. R. S. Stein, Rheology 5, 121 (1972).

137. R. S. Stein, *Accts. Chem. Res.* 5, 121 (1972).
138. R. Yang and R. S. Stein, *J. Polym. Sci., A-2*, 5, 939 (1967).
139. R. J. Samuels, "Structured Polymer Properties", John Wiley, New York, 1974.
140. R. J. Samuels, *J. Polym. Sci.* C13, 37 (1966).
141. R. J. Samuels, *J. Polym. Sci.*, A3, 1741 (1965).
142. R. G. Crystal and D. Hansen, *J. Polym. Sci., A-2*, 6, 981 (1968).
143. M. Matsuo, H. Hattori, S. Nomura and H. Kawai, *J. Polym. Sci., Polym. Phys. Ed.* 14, 223 (1976).
144. S. Nomura, M. Matsuo and H. Kawai, *J. Polym. Sci., Polym. Phys. Ed.* 10, 2489 (1972).
145. T. W. Haas and P. H. MacRae, *S.P.E. J.* 24, 27 (1968).
146. T. W. Haas and R. H. MacRae, *Polym. Eng. Sci.* 9, 423 (1969).
147. H. Olf and A. Peterlin, *J. Coll. Sci.* 47, 628 (1974).
148. W. Glenz and A. Peterlin, *J. Macromol. Sci., B-4*, 473 (1970).
149. E. W. Fischer, H. Goddar and G. F. Schmidt, *Makromol. Chem.* 118, 144 (1968).
150. F. P. Chappel, *Polymer* 1, 409 (1960).
151. R. S. Stein and F. H. Norris, *J. Polym. Sci.* 21, 391 (1956).
152. T. Yemni and R. H. Boyd, *J. Polym. Sci., Polym. Phys. Ed.* 14, 499 (1976).
153. R. J. Samuels, *J. Polym. Sci.*, C20, 253 (1967).
154. H. C. Zachmann, *Z. Naturforsch.* 19a, 1397 (1964).
155. P. F. Dismore and W. O. Statton, *J. Polym. Sci.*, B-2, 1116 (1964).
156. P. F. Dismore and W. O. Statton, *J. Polym. Sci.*, C13, 133 (1966).
157. D. R. Beresford and H. Bevan, *Polymer* 5 (5), 247 (1963).



158. K. Sakaoku, N. Morosoff and A. Peterlin, J. Polym. Sci., Polym. Phys. Ed. 11, 31 (1973).
159. W. T. Mead and R. S. Porter, J. Appl. Phys. 47, 4278 (1976).
160. N. E. Weeks. Ph.D. Dissertation, University of Massachusetts, Amherst, 1974.
161. J. H. Dumbleton and T. Murayama, Kolloid-Z-Polymer 238, 410 (1970).
162. T. Murayama and B. Silverman, J. Polym. Sci., Polym. Phys. Ed. 11, 1873 (1973).
163. K. H. Illers, Colloid & Polym. Sci. 253, 329 (1975).
164. T. Murayama, J. H. Dumbleton and M. L. Williams, J. Makromol. Sci., Phys., B-1, 1 (1967).
165. M. Takayanagi, K. Imada and T. Kajiyama, J. Polym. Sci., C15, 263 (1966).
166. A. Miyagi and B. Wunderlich, Bull. Am. Phys. Soc. (11), 16, 410 (1971).
167. T. Seto, T. Hara and K. Tanaka, Jap. J. Appl. Phys. 7, 31 (1968).
168. W. P. Slichter, J. Polym. Sci. 21, 141 (1956).
169. P. W. Teare and D. R. Holmes, J. Polym. Sci. 24, 496 (1957).
170. A. Turner-Jones, J. Polym. Sci. 62, 853 (1962).
171. H. Kiho, A. Peterlin and P. H. Geil, J. Appl. Phys. 35, 1599 (1964).
172. K. Tanaka, T. Seto and T. Hara, J. Phys. Soc. Japan 17, 873 (1962).
173. R. J. Young and P. B. Bowden, Phil. Mag. 29, 1061 (1974).
174. M. Bevis and E. B. Crellin, Polymer 12, 666 (1971).
175. H. Kiho, A. Peterlin and P. H. Geil, J. Polym. Sci., B3, 157 (1965).
176. H. Kiho, A. Peterlin and P. H. Geil, J. Polym. Sci., B3, 263 (1965).
177. K. Miyasaka and K. Maskishima, J. Polym. Sci., A1, 5, 3017 (1967).

178. D. R. Holmes, C. W. Bunn and D. J. Smith, J. Polym. Sci. 17, 159 (1955).
179. A. Ziabicki, Colloid-Z. 167, 132 (1960).
180. H. Arimoto, M. Ishibashi and M. Hirai, J. Polym. Sci., A-3, 317 (1965).
181. P. I. Vincent, "Fracture", Ch. 5 in "Mechanical Properties of Polymers", N. M. Bikales, Ed., John Wiley, 1971, pp. 105-174.
182. L. E. Nielsen, "Mechanical Properties of Polymers", Reinhold Publishing Corp., 1962, Ch. 5.
183. G. Capaccio and I. M. Ward, Polym. Eng. Sci. 15, 219 (1975).
184. E. I. duPont deNemours & Company, U.S. Pat. 604,667.
185. J. Miklowitz, J. Colloid Sci. 2, 193 (1974).
186. I. Marshall and A. B. Thompson, Proc. Roy. Soc., A, 221, 541 (1954).
187. F. H. Muller, Rub. Chem. Tech. 30, 1027 (1957).
188. K. Jackel, Colloid-Z. 137, 130 (1954).
189. J. S. Lazurkin, J. Polym. Sci. 30, 595 (1958).
190. P. I. Vincent, Polymer 1, 7 (1960).
191. Y. A. Antsupov, U. P. Volodin and E. V. Kuvshinskii, Mekhanika Polimerov 4 (3), 509 (1968).
192. J. M. Andrews and I. M. Ward, J. Mater. Sci. 5, 411 (1970).
193. G. Capaccio and I. M. Ward, Nature Phys. Sci. 243, 143 (1973).
194. G. Capaccio and I. M. Ward, Polymer 15, 233 (1974).
195. G. Capaccio and I. M. Ward, Polymer 16, 239 (1975).
196. P. J. Barham and A. Keller, J. Mater. Sci. 11, 27 (1976).
197. P. J. Barham and A. Keller, J. Polym. Sci., B13, 197 (1975).

198. H. D. Noether and R. W. Singleton, U.S. Pat. 3,161,709 (December 15, 1964).
199. W. C. Sheehan and T. B. Cole, J. Appl. Polym. Sci. 8, 2359 (1964).
200. S. N. Zhurkov, B. Y. Levin and A. V. Savitskii. Doklady Phys., Chem. 186, 296 (1969).
201. J. H. Southern and R. S. Porter, J. Macromol. Sci., Phys., B-4, 541 (1970).
202. J. H. Southern and R. S. Porter, J. Appl. Polym. Sci. 14, 2305 (1970).
203. J. S. Southern, N. E. Weeks and R. S. Porter, Makromol. Chem. 162, 19 (1972).
204. R. S. Porter, J. H. Southern and N. E. Weeks. Polym. Eng. Sci. 15, 213 (1975).
205. K. Imada, T. Yamamoto, K. Shigamatsu and M. Takayanagi, J. Mater. Sci. 6, 537 (1971).
206. P. Predecki and W. O. Statton, J. Polym. Sci., B-10, 87 (1972).
207. Carroll Edgar, "Fundamentals of Manufacturing Processes and Materials", Addison-Wesley, Reading, Massachusetts, 1965.
208. N. J. Capiati, S. Kojima, W. G. Perkins and R. S. Porter, J. Mater. Sci. 12, 334 (1977).
209. N. E. Weeks and R. S. Porter, J. Polym. Sci., Polym. Phys. Ed. 12, 635 (1974).
210. N. J. Capiati and R. S. Porter, J. Polym. Sci., Polym. Phys. Ed. 13, 1177 (1975).
211. D. L. M. Cansfield, G. Capaccio and I. M. Ward, Polym. Eng. Sci. 16, 721 (1976).



212. A. Buckley and H. A. Long, Polym. Eng. Sci. 9, 115 (1969).
213. K. Imada, Y. Kondo, K. Kanekiyo and M. Takayanagi, Rep. Prog. Polym. Phys. Jap. 14, 393 (1971).
214. C. D. Denson, Polym. Eng. Sci. 13, 125 (1973).
215. S. Maruyama, K. Imada and M. Takayanagi, Inter. J. Polym. Mater. 2, 125 (1973).
216. L. E. Nielsen, J. Polym. Sci. 42, 357 (1960).
217. T. Niikuni and R. S. Porter, J. Mater. Sci. 9, 389 (1974).
218. T. F. Ballenger and J. L. White, J. Appl. Polym. Sci. 15, 1949 (1971).
219. A. E. Everage, Jr. and R. L. Ballman, J. Appl. Polym. Sci. 18, 933 (1974).
220. M. T. Shaw, J. Appl. Polym. Sci. 19, 2811 (1975).
221. F. N. Cogswell, Polym. Eng. Sci. 12, 64 (1972).
222. S. Maruyama, K. Imada and M. Takayanagi, Inter. J. Polym. Mater. 2, 105 (1973).
223. J. J. Benbow and P. Lamb, S.P.E. Trans. 7 (January, 1963).
224. K. Imada and M. Takayanagi, Inter. J. Polym. Mater. 2, 89 (1973).
225. R. Hill, "The Mathematical Theory of Plasticity", Oxford Clarendon Press, 1950.
226. J. B. Smith, G. R. Davies, G. Capaccio and I. M. Ward, J. Polym. Sci., Polym. Phys. Ed. 13, 2331 (1975).
227. K. D. Pae, D. R. Meares and J. A. Sauer, J. Polym. Sci., B-6, 733 (1968).
228. S. Kojima and R. S. Porter, J. Appl. Polym. Sci.

229. A. G. Kolbeck and D. R. Uhlmann, J. Polym. Sci., Polym. Phys. Ed. 15, 27 (1977).
230. A. G. Gibson, I. M. Ward, B. N. Cole and B. Parsons, J. Mater. Sci., Letters, 9, 1193 (1974).
231. T. Williams, J. Mater. Sci. 8, 59 (1973).
232. H. N. Yoon, K. D. Pae and J. A. Sauer, Polym. Eng. Sci. 16, 567 (1976).
233. F. J. Fuchs in "Engineering Solids Under Pressure", H. L. D. Pugh, Ed., Inst. Mech. Engs., London, 1971.
234. J. M. Alexander, Mater. Sci. Eng. 10, 70 (1972).
235. L. A. Davis, Polym. Eng. Sci. 14, 641 (1974).
236. K. Nakayama and H. Kanetsuna, Kobunshi Kagaku 30, 713 (1973).
237. K. Nakayama and H. Kanetsuna, Kobunshi Ronbunshu 31, 256 (1974).
238. K. Nakayama and H. Kanetsuna, Kobunshi Ronbunshu 31, 321 (1974).
239. S. K. Bhakja and K. D. Pae, J. Polym. Sci., B-10, 531 (1972).
240. J. R. Collier, T. Y. Taitam, J. Newcombe and N. Dinos, Polym. Eng. Sci. 16, 204 (1976).
241. G. S. Farshyn, V. G. Baranov and S. Ya. Frenkel, Vysok. Soedin. A12, 1574 (1970).
242. V. G. Baranov, T. I. Volkov, G. S. Farshyn and S. Ya. Frenkel, J. Polym. Sci., C30, 305 (1970).
243. V. G. Baranov, N. I. Bychkovsky, A. Sh. Goikhman and M. P. Nosov, J. Polym. Sci., C38, 327 (1972).
244. T. Hashimoto, K. Nagatoshi, A. Todo and H. Kawai, Polymer 17, 1063 (1976).
245. A. Keller and M. J. Machin, J. Macromol. Sci. B1, 41 (1967).

246. T. T. Wang, H. S. Chen and T. K. Kwei, Polym. Letters 8, 505 (1970).
247. T. K. Kwei, T. T. Wang and H. E. Bair, J. Polym. Sci., C, 31, 87 (1970).
248. D. M. Bigg, Polym. Eng. Sci. 16, 725 (1976).
249. S. L. Cannon, G. B. McKenna and W. O. Statton, J. Polym. Sci., Macromol. Rev. 11, 209 (1976).
250. A. W. Christiansen, E. Baer and S. V. Radcliffe, Phil. Mag. 24, 451 (1971).
251. J. A. Sauer, Polym. Eng. Sci. 17, 150 (1977).
252. M. G. Northolt, J. Polym. Sci., C38, 205 (1972).
253. G. A. Gordon, J. Polym. Sci., A2, 9, 1693 (1971).
254. P. Lindenmeyer, J. Appl. Polym. Sci. 21, 821 (1977).

The following conversion factors may be beneficial in comparing data from various researchers:

$$1 \text{ GPa} = 10^9 \frac{\text{GN}}{\text{m}^2}$$

$$1 \text{ GPa} = 10^{10} \frac{\text{dynes}}{\text{cm}^2}$$

$$1 \text{ GPa} = 10^5 \text{ atm; bar; } \frac{\text{kg}}{\text{cm}^2}$$

$$1 \text{ GPa} = 1.45 \times 10^5 \text{ PSI}$$

$$1 \text{ GPa} = \frac{(12,800 \times \text{S.G.}) \frac{\text{gm}}{\text{denier}}}{1.45 \times 10^5}$$



Captions for Figures

1. Melting points of polyamides: — from hexamethylenediamine and dibasic acids; ----- from heptamethylenediamine and dibasic acids; ..... from diamines and azelaic acid; — - — - from  $\omega$ -amino acids. [After Kinoshita (33).]
2. Arrangement of sheets of molecules in  $\alpha$  and  $\beta$  crystals. Lines represent chain molecules; circles oxygen atoms. [After Bunn and Garner (38).]
3. (A) Crystal structure A of the  $\gamma$  form of nylon 12 (a) projection on the ab plane, (b) projection on the plane perpendicular to the a axis. (B) Crystal structure B of the  $\gamma$  form of nylon 12 (a) projection on the ab plane, (b) projection on the plane perpendicular to the a axis. [After Inoue and Hoshino (50).]
4. Effect of spherulite size on the yield point: (O) compression-molded films; (0) injection-molded bars. N is the number of spherulite boundaries per millimeter. [After Starkweather and Brooks (68).]
5. Tensile modulus of oriented nylon in the machine direction. [After Starkweather (71).]
6. Structural model of nylon 6 fibers (fiber axis vertical). [After Prevorsek, et al. (95).]
7. Microfibrillar model of fiber structure: A, interfibrillar; B, intrafibrillar tie molecule. [After Peterlin (98).]

8. Schematic diagrams of crystal slip. (a) Fine slip. A displacement of one lattice vector has occurred on every other lattice plane in the crystal. (b) Coarse slip. The same total shear has been produced by a displacement of two lattice vectors on every fourth plane. The direction  $n$  is the normal to the surface of the crystal which has rotated relative to the chain axis,  $c$ , during deformation. [After Bowden and Young (122).]
9. Graphs of  $f_a$ ,  $f_c$  and  $f_u$  vs. extension ratio for different values of  $C$ . Symbols explained in text. [After Chappel (150).]
10. Change of orientation of nylon 66 with temperature. [After Dismore and Statton (156).]
11. Change of breaking strength with temperature of three-month old samples of nylon 66. [After Dismore and Statton (156).]
12. (a) Model comprising folded chains having well defined lamellar regions. (b) Arrangement of folded sheets which do not give low angle reflections. [After Beresford and Bevan (157).]
13. Temperature dependence of  $E'$  and  $E''$  along and perpendicular to the drawing direction for the cold-drawn samples of linear polyethylene at 110 cycle/sec. [After Takayanagi, et al. (165).]
14. Temperature dependence of  $E'$  and  $E''$  along and perpendicular to the drawing direction for the annealed samples of polyethylene at 110 cycle/sec. [After Takayanagi, et al. (165).]
15. All hydrogen bonds made perfectly by inverting alternate chains. [After Holmes, Bunn and Smith (178).]
16. A schematic stress-strain curve. [After Nielsen (182).]

17. The effect of strain rate on the yield stress and drawing stress. [After Andrews and Ward (192).]
18. Model of continuous crystal matrix with chain-fold defects. [After Clark and Scott (2).]
19. Schematic of solid state ram extrusion apparatus. [After Buckley and Long (212).]
20. Long period of extrudates vs. extrusion temperature. Points represent draw ratios from 4 to 25. [After Maruyama, Imada and Takayanagi (222).]
21. Schematic of solid state hydrostatic extrusion apparatus. [After Buckley and Long (212).]
22. Effect of deformation ratio on the modulus of the extrudate. [After Gibson, Ward, Cole and Parsons (230).]
23. Variation of birefringence with deformation ratio. [After Gibson, Ward, Cole and Parsons (230).]
24. Extrusion pressure vs. die angle. Extrusion ratio: 6.4. Plunger velocity: 5 mm/min. (X): stick-slip. [After Nakayama and Kanetsuna (236).]
25. Extrusion pressure vs. temperature. (O) extrusion ratio: 6.1. (O) extrusion ratio: 11.3. [After Nakayama and Kanetsuna (237).]
26. Extrusion rate vs. pressure at extrusion temperatures shown. Extrusion ratio: 9.0. [After Nakayama and Kanetsuna (237).]
27. Relationships between the critical extrusion pressure,  $P_o$ , and die angle ( $2\alpha$ ).  $R_E'$ : extrusion ratio (from 4.8 - 9).  $T_E$ : extrusion temperature (from  $30^0$  -  $110^0\text{C}$ ). [After Nakayama and Kanetsuna (238).]



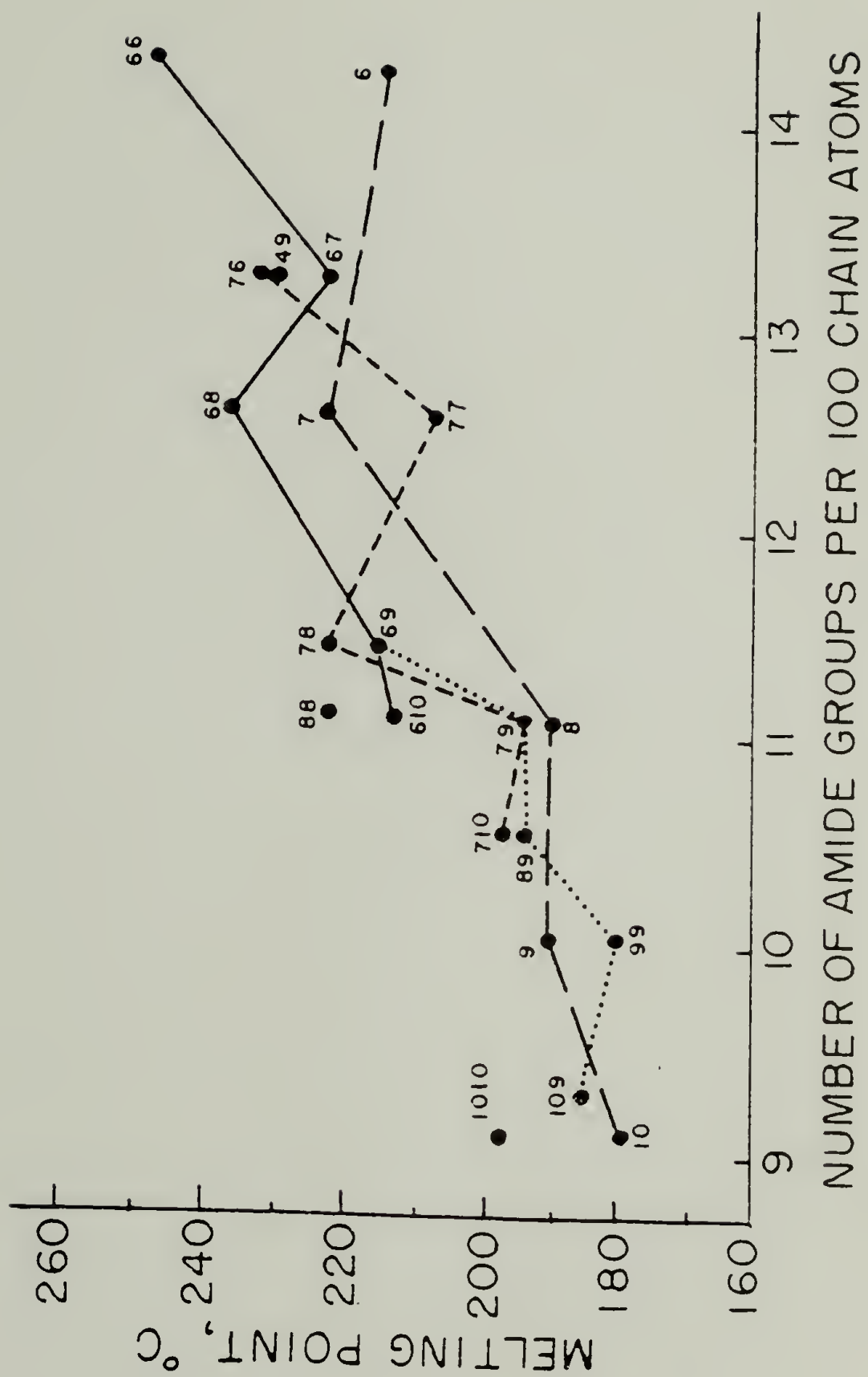


Figure 1

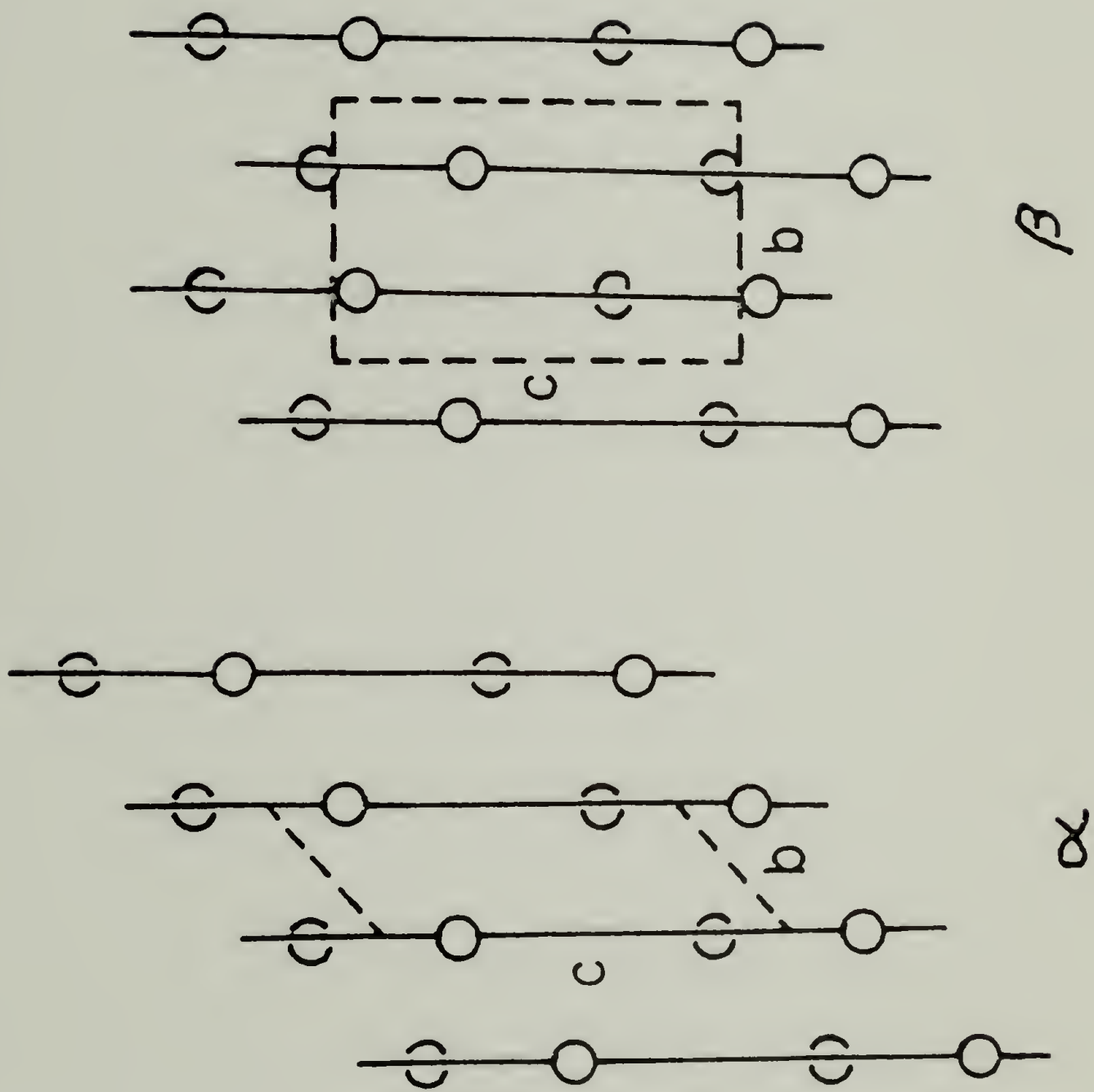


Figure 2

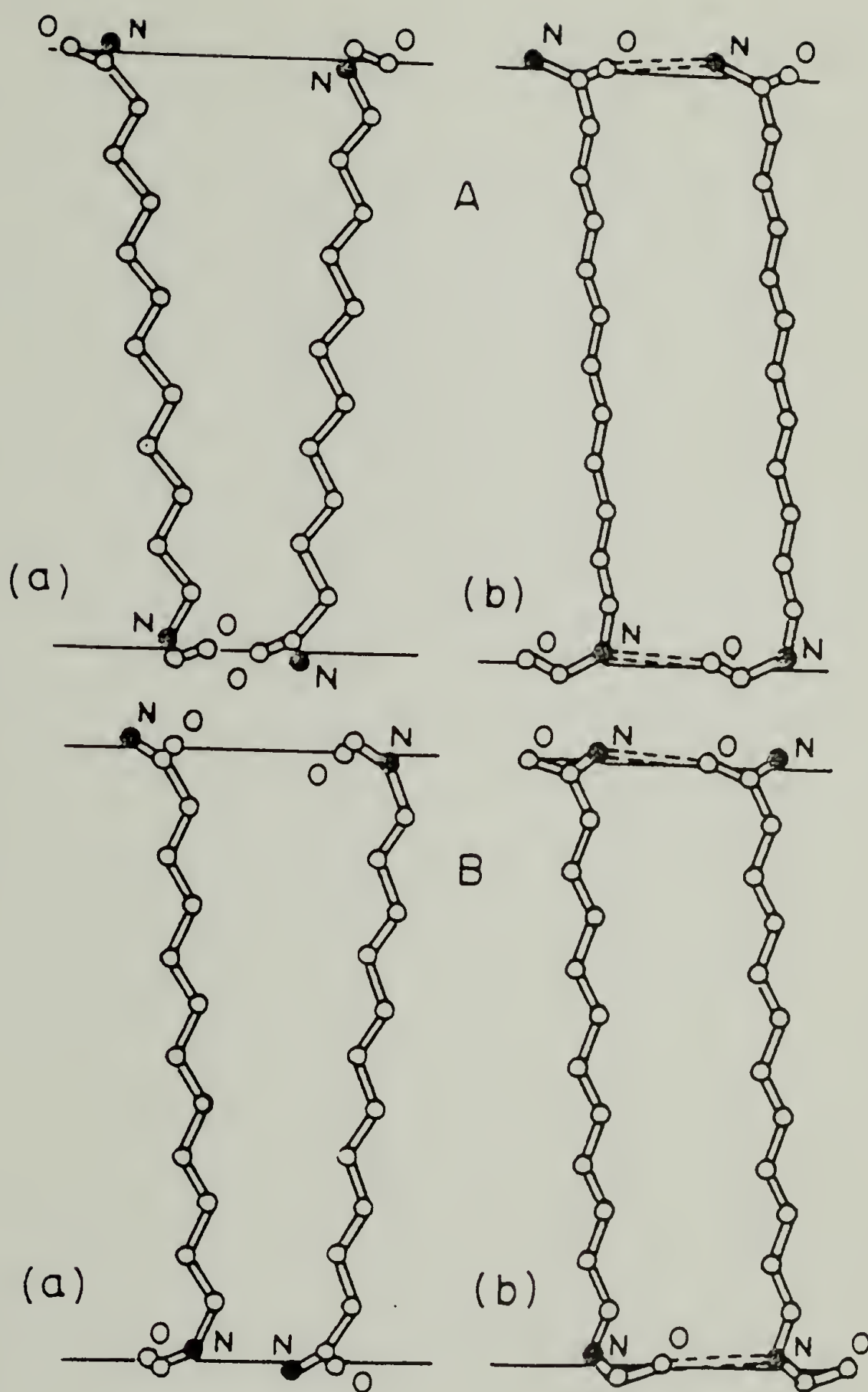


Figure 3



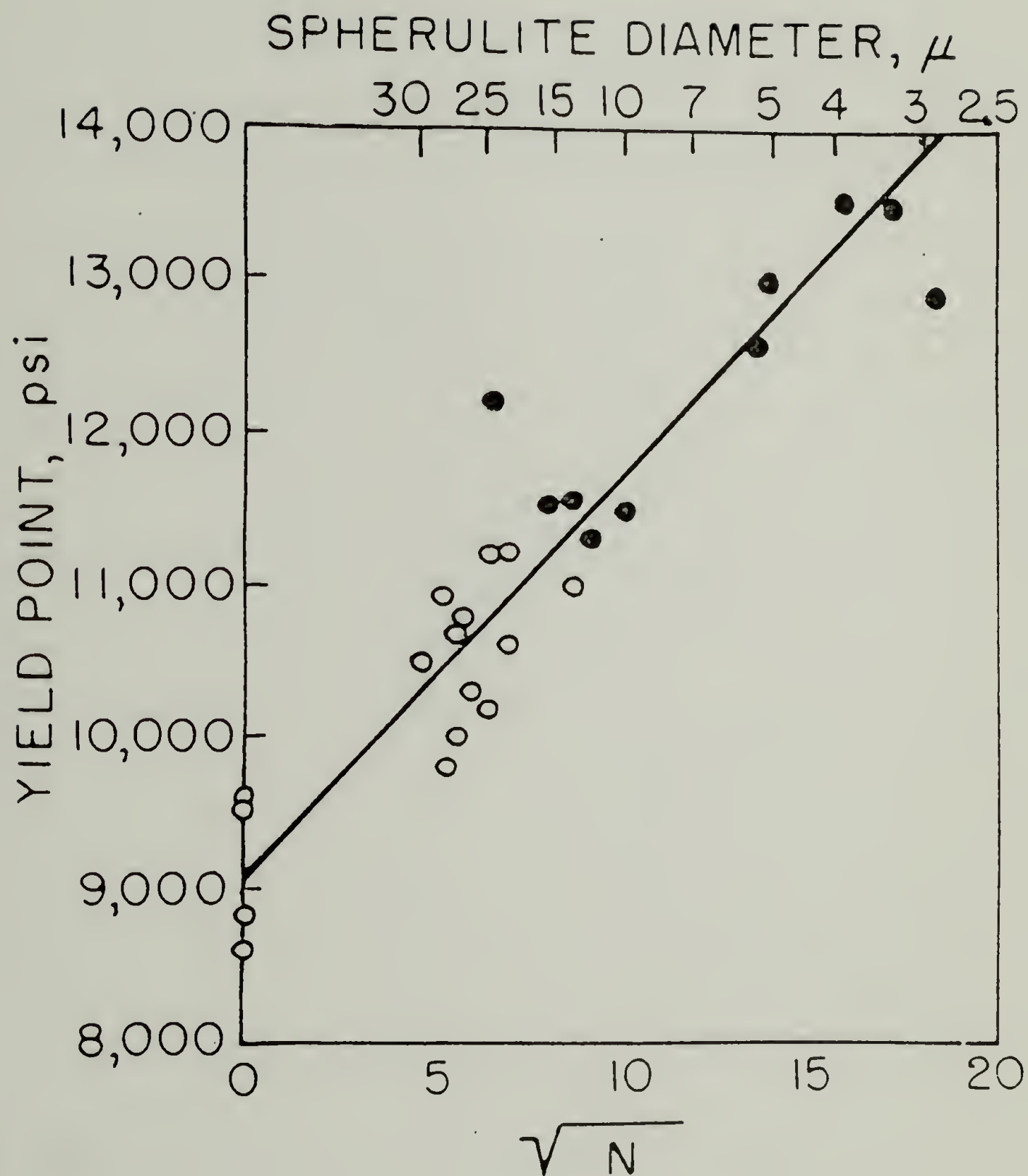


Figure 4

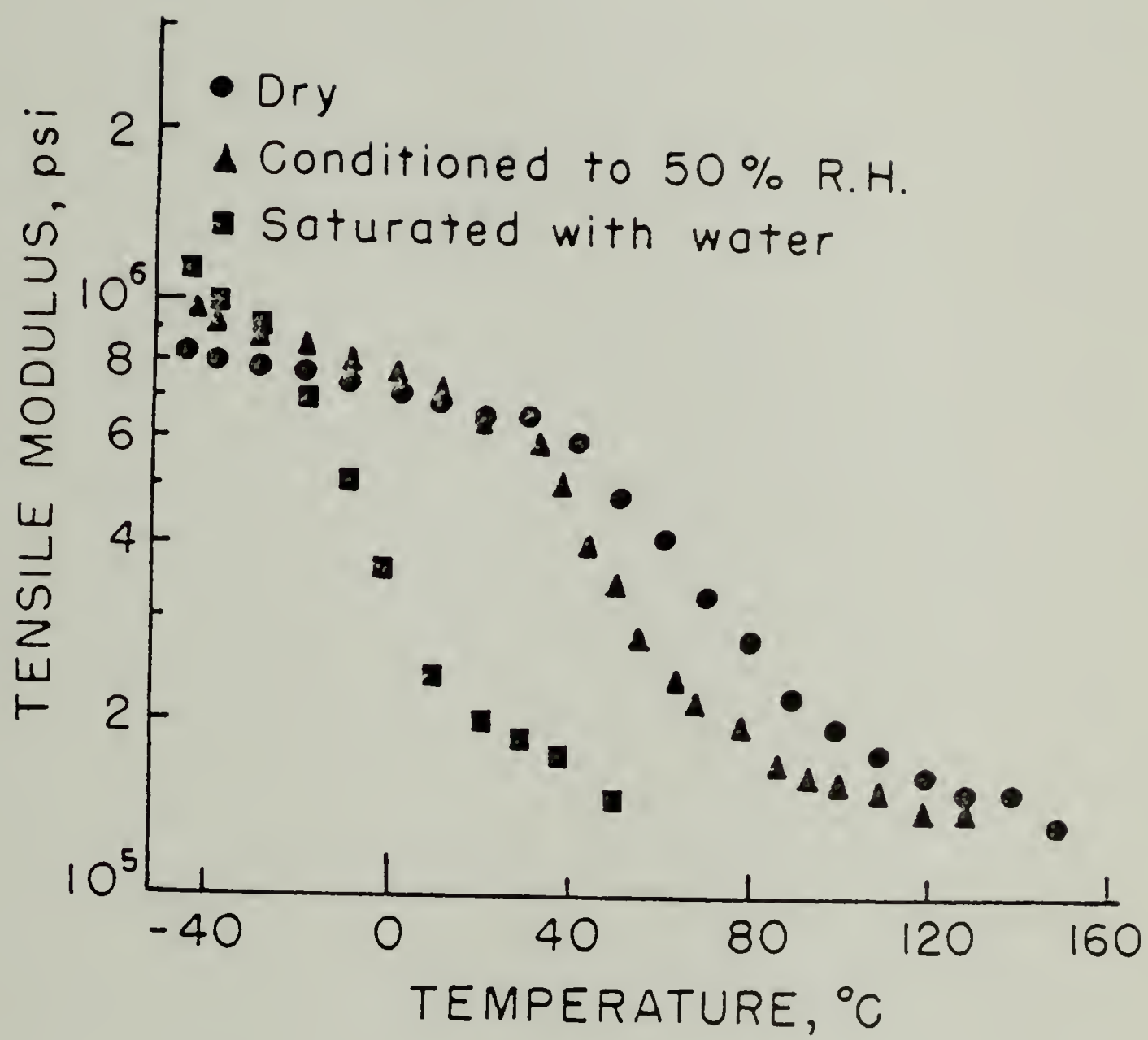


Figure 5

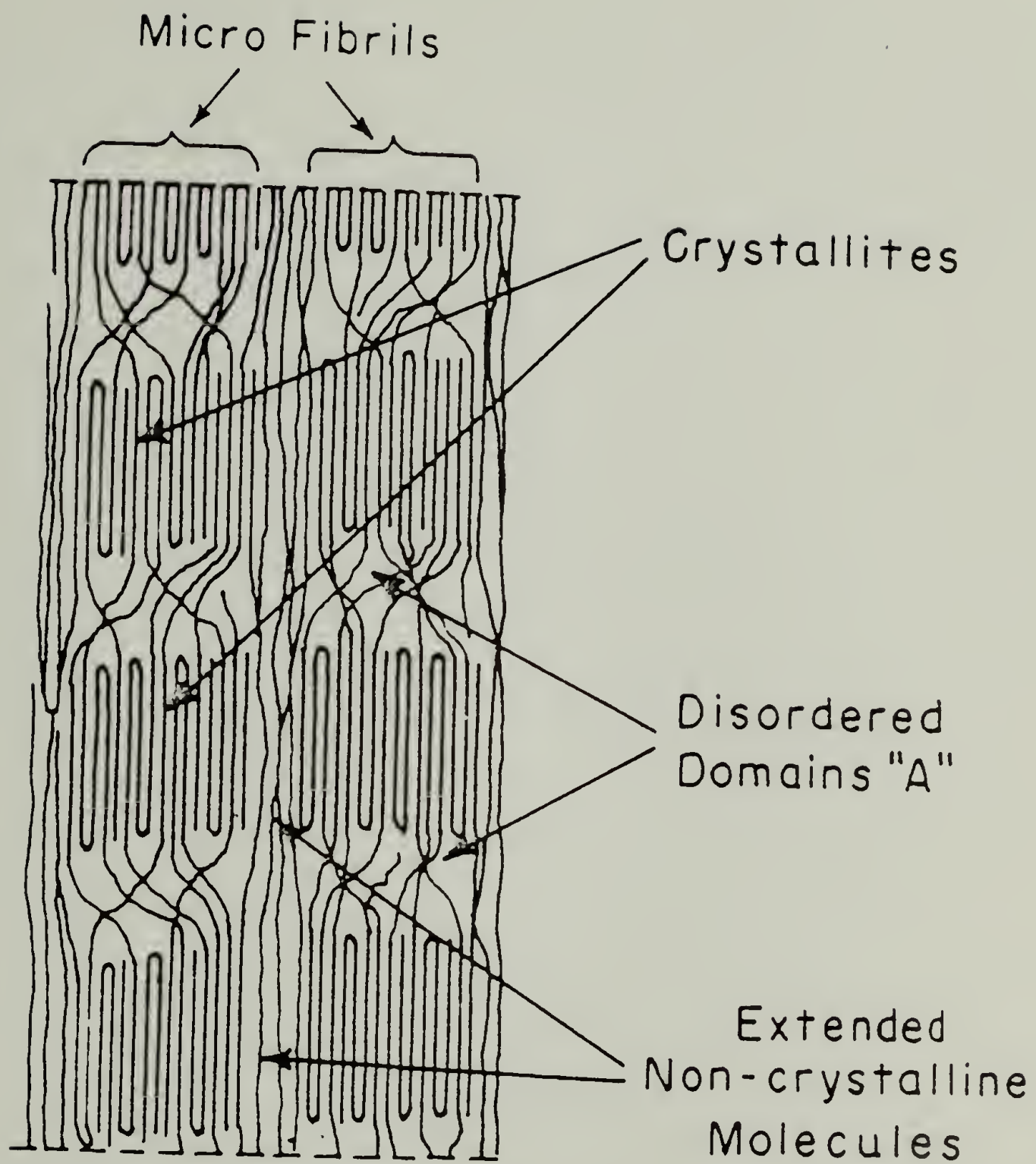


Figure 6



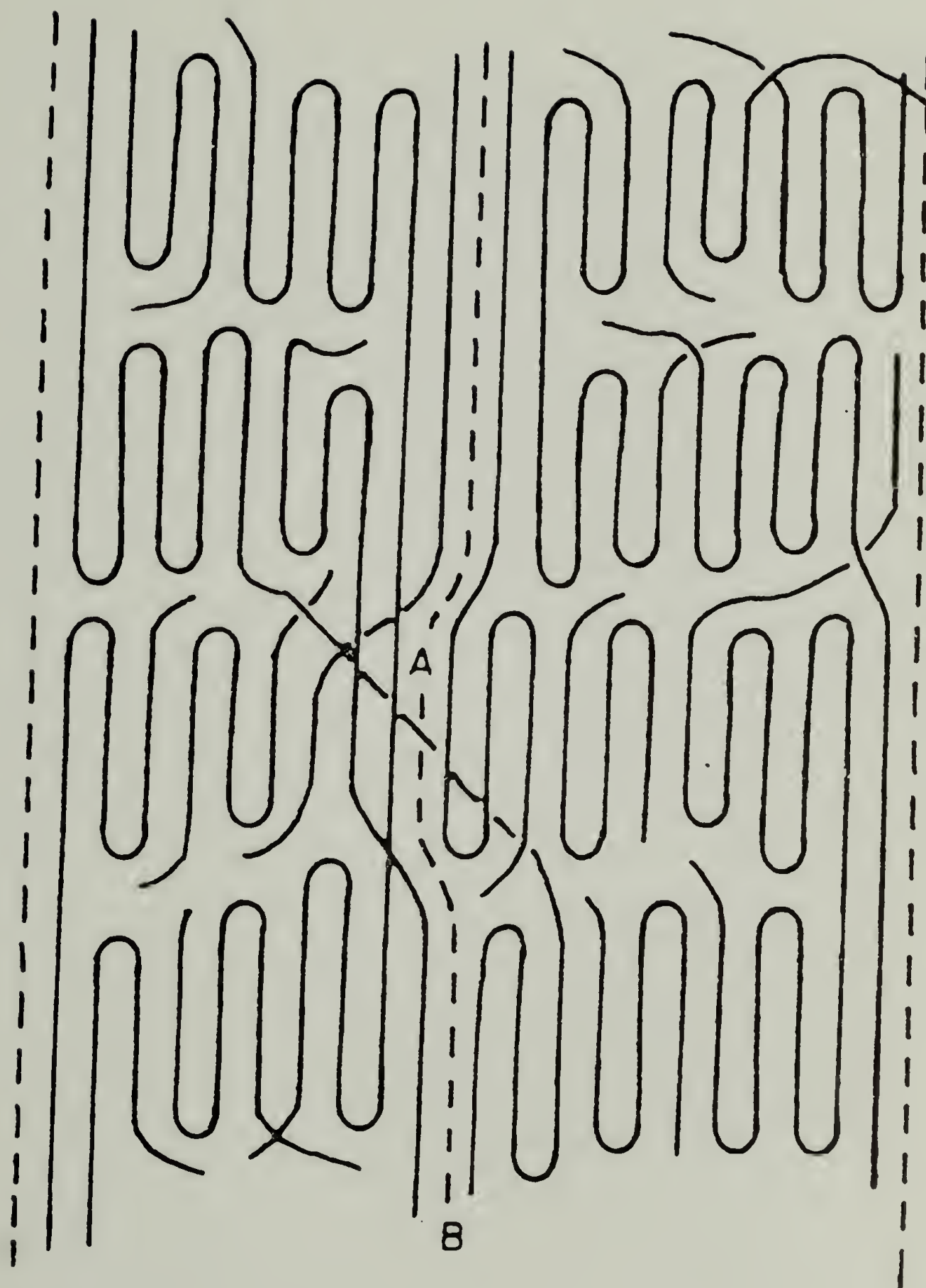


Figure 7

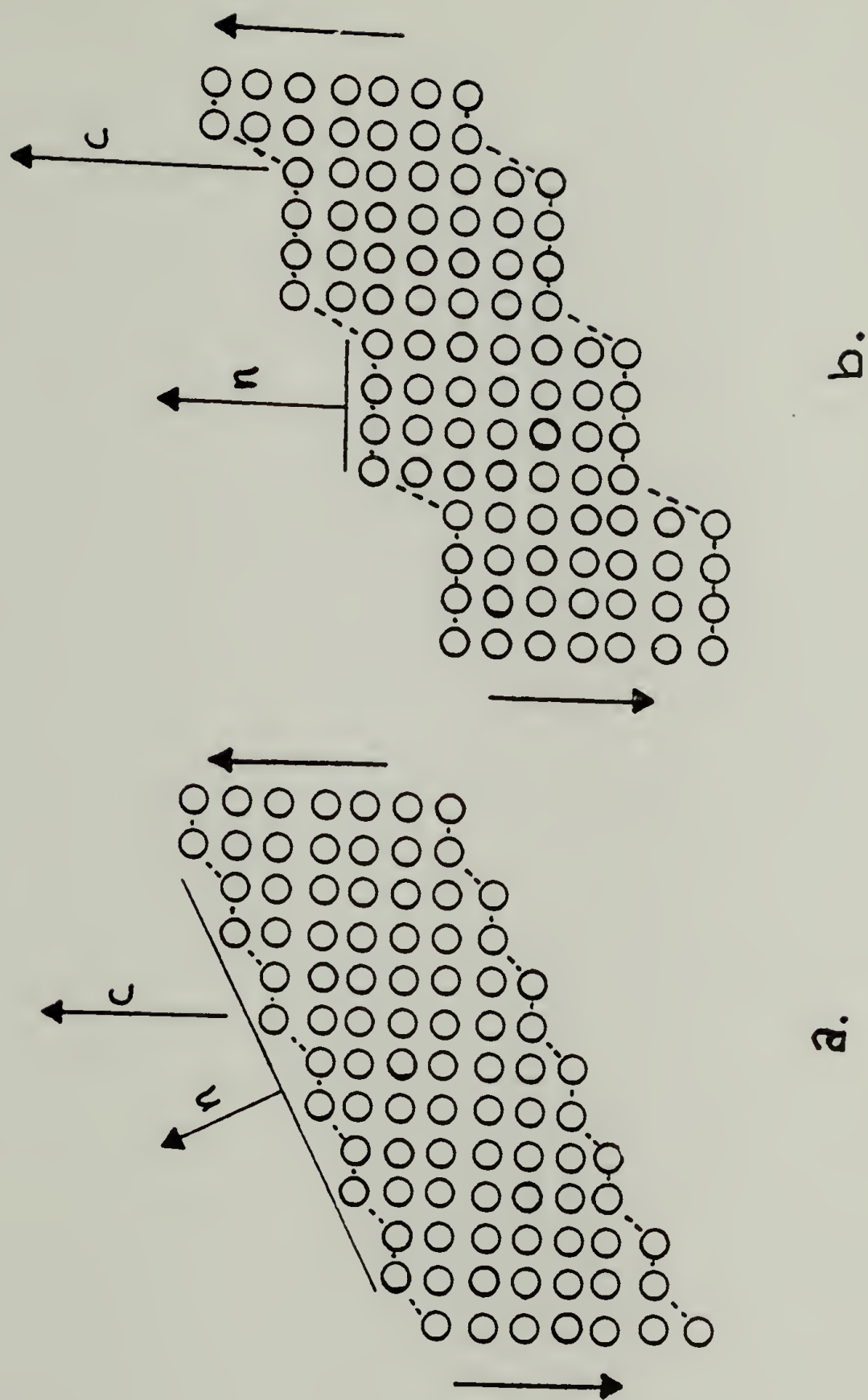


Figure 8

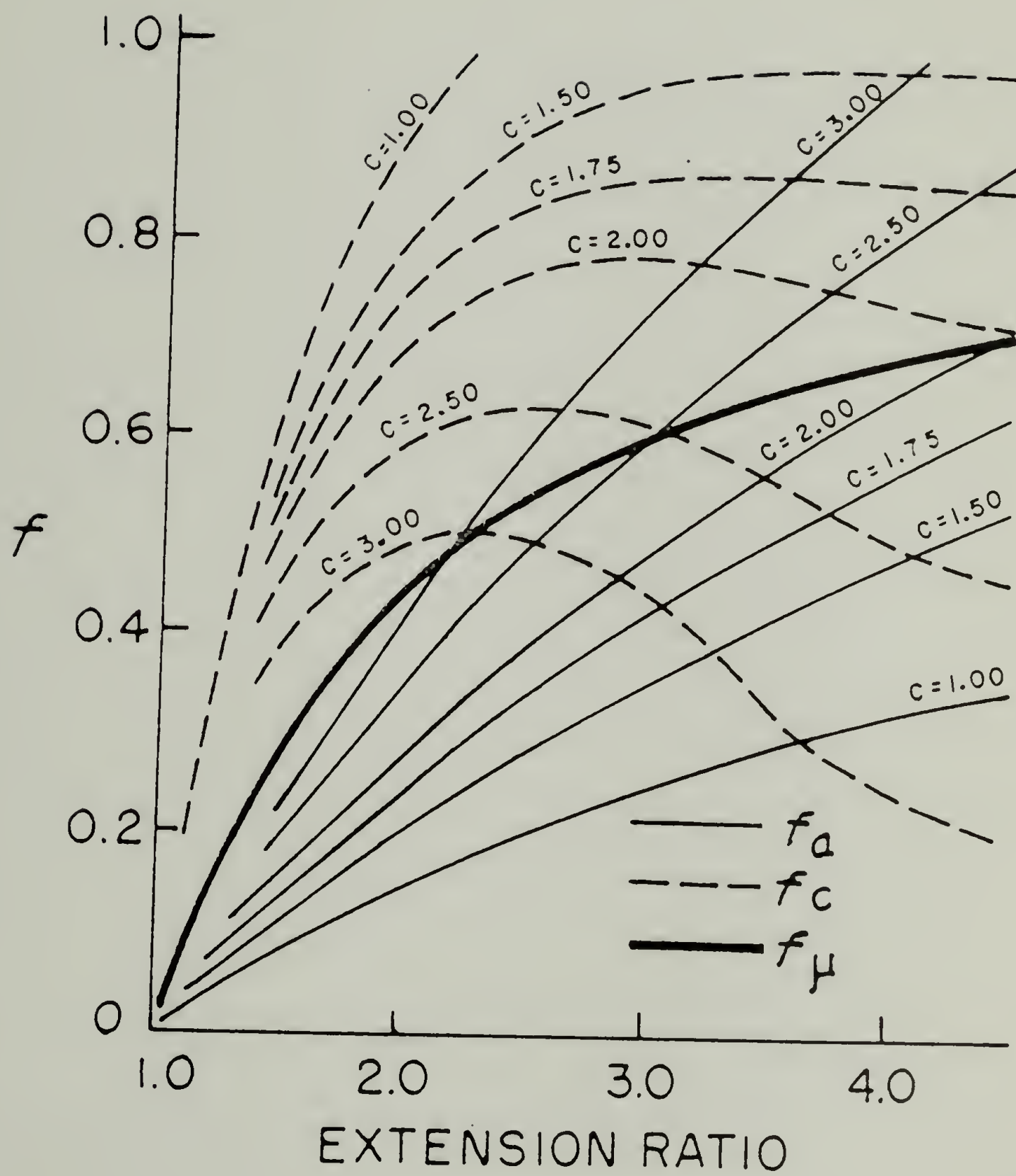


Figure 9

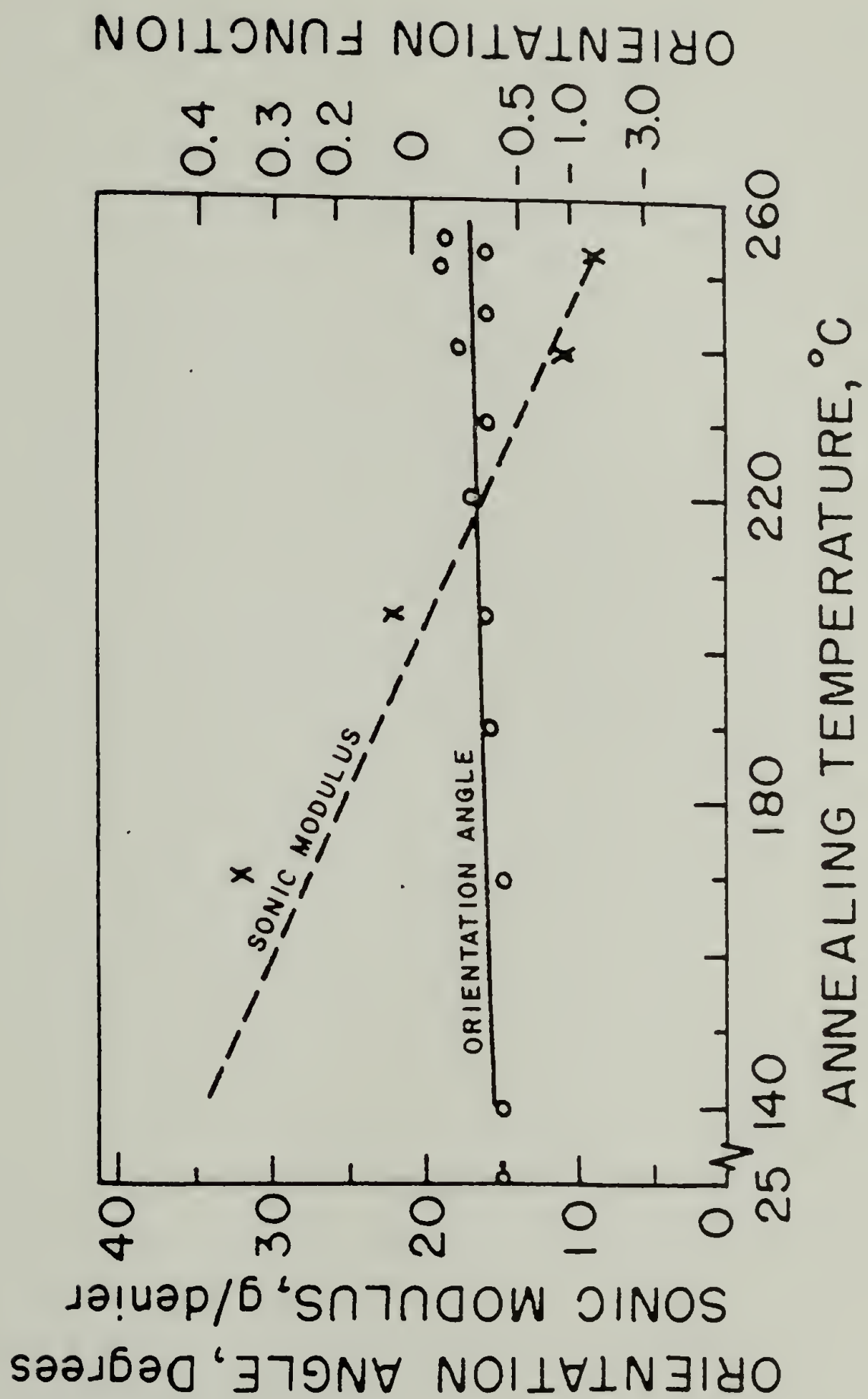


Figure 10



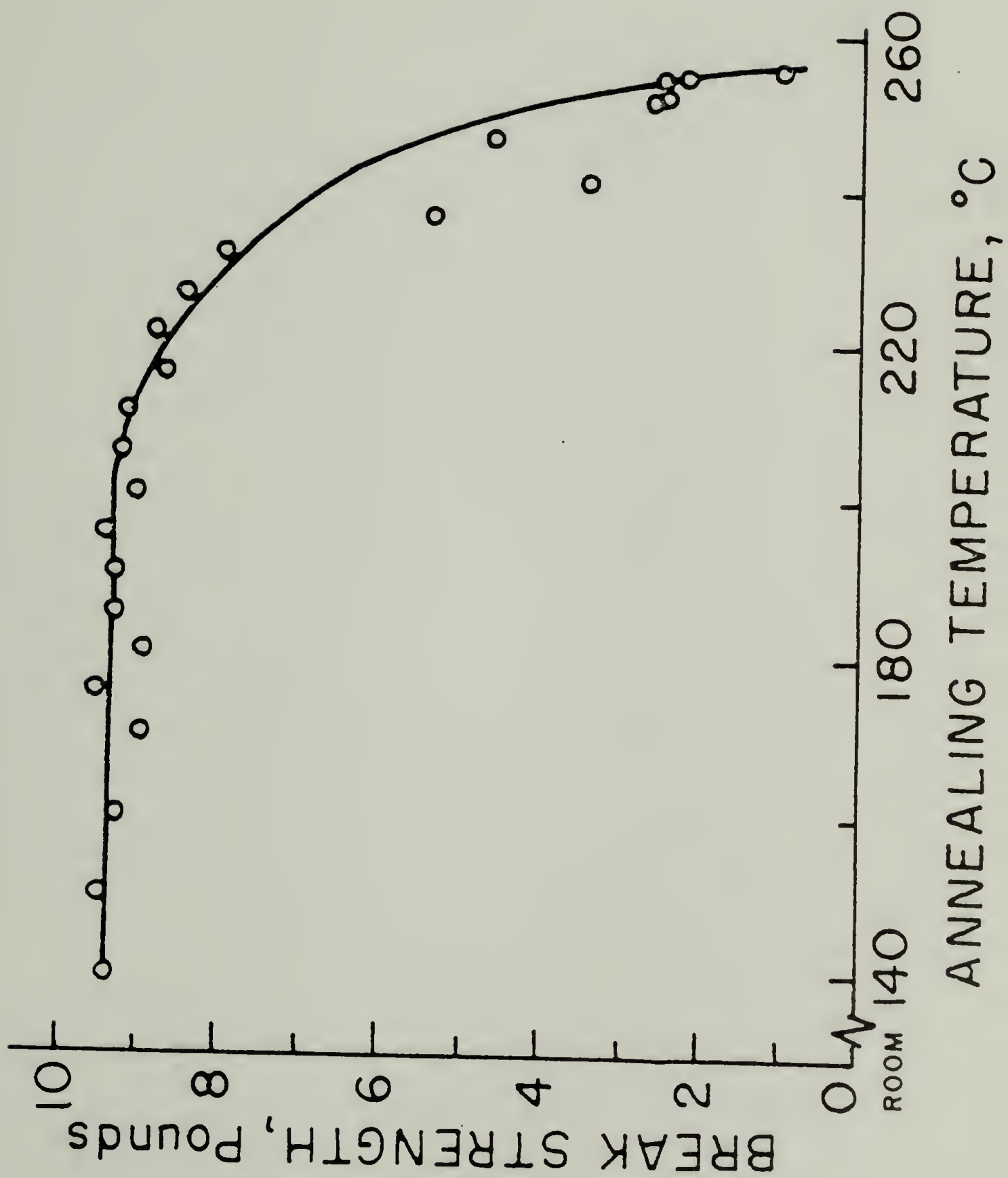


Figure 11

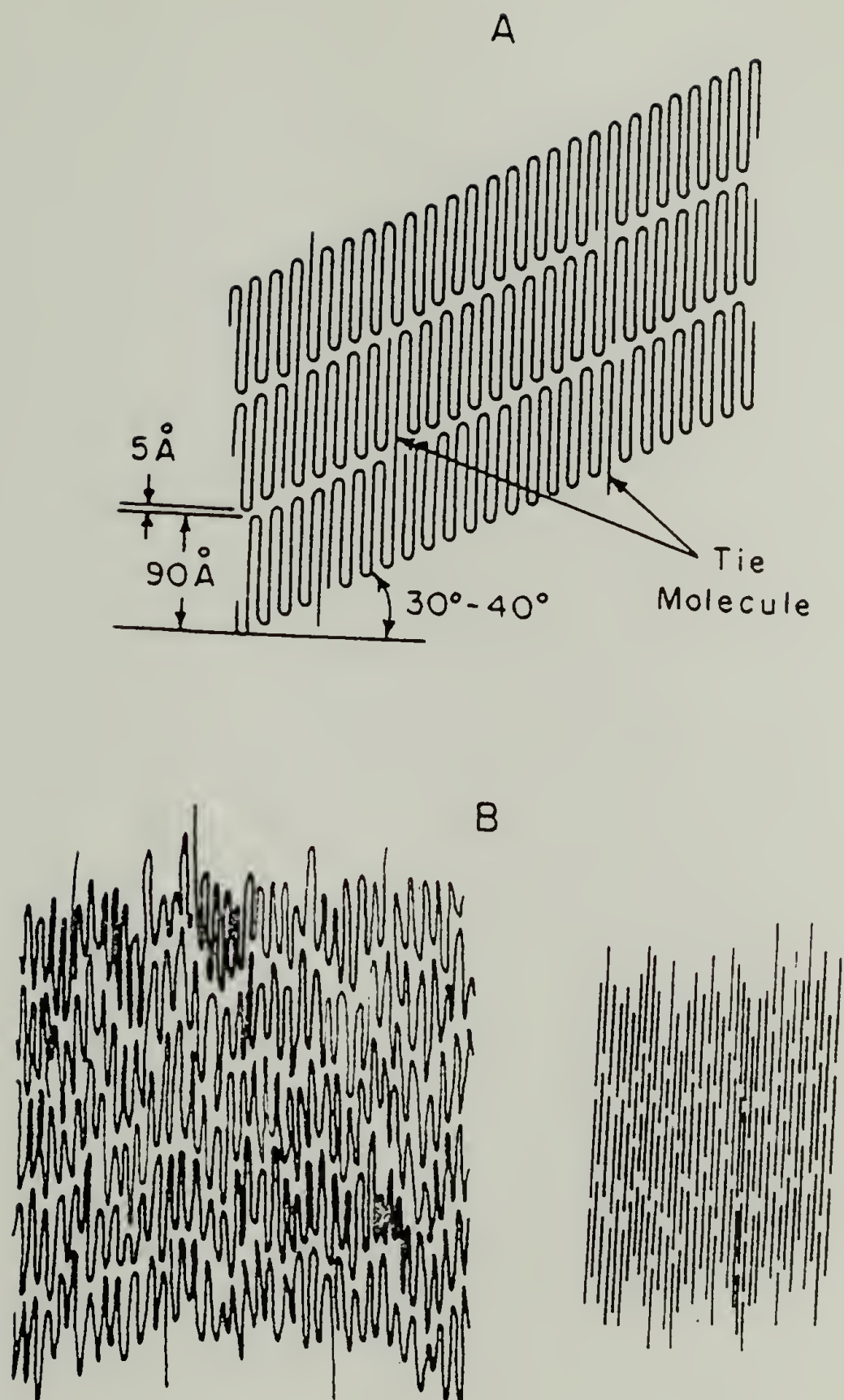


Figure 12

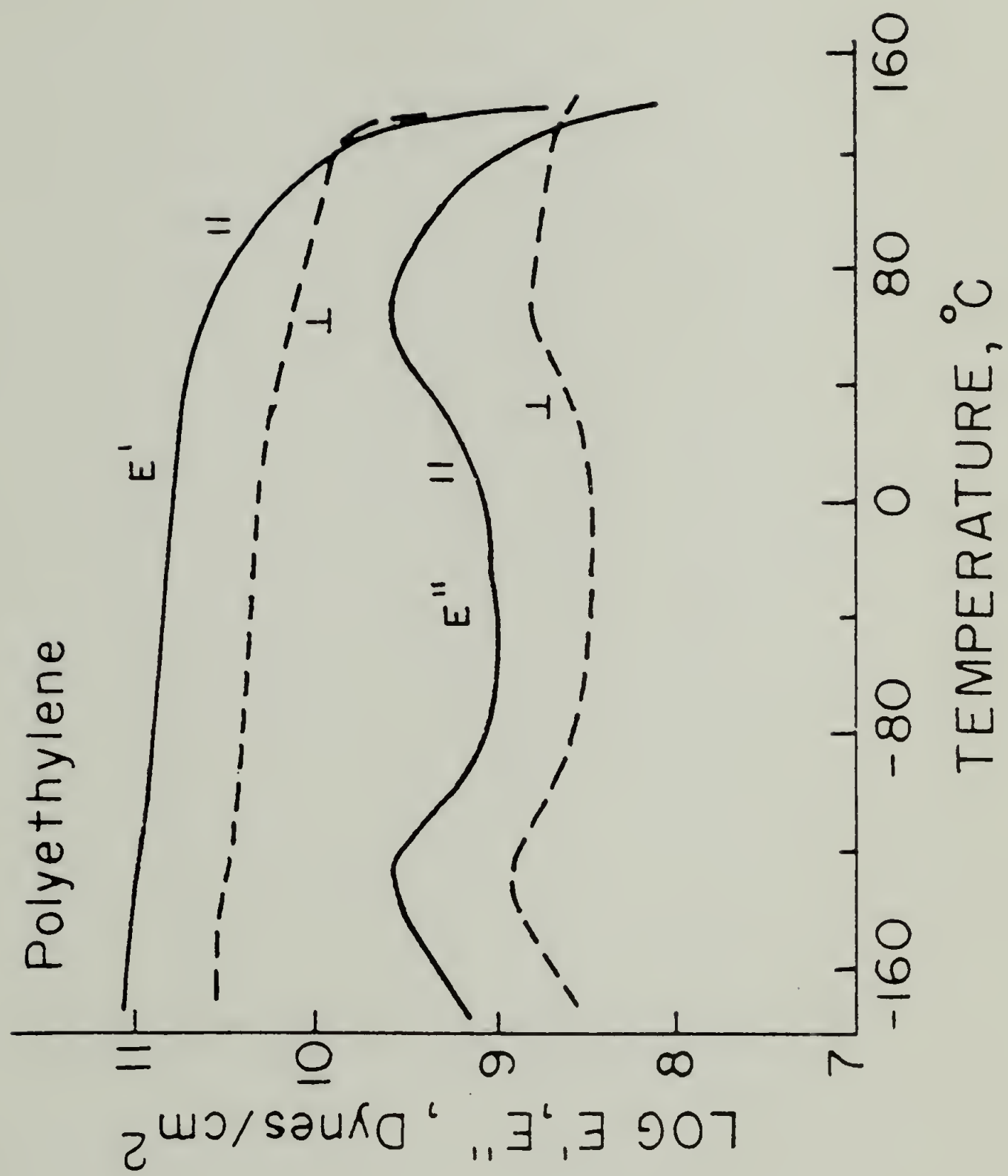


Figure 13

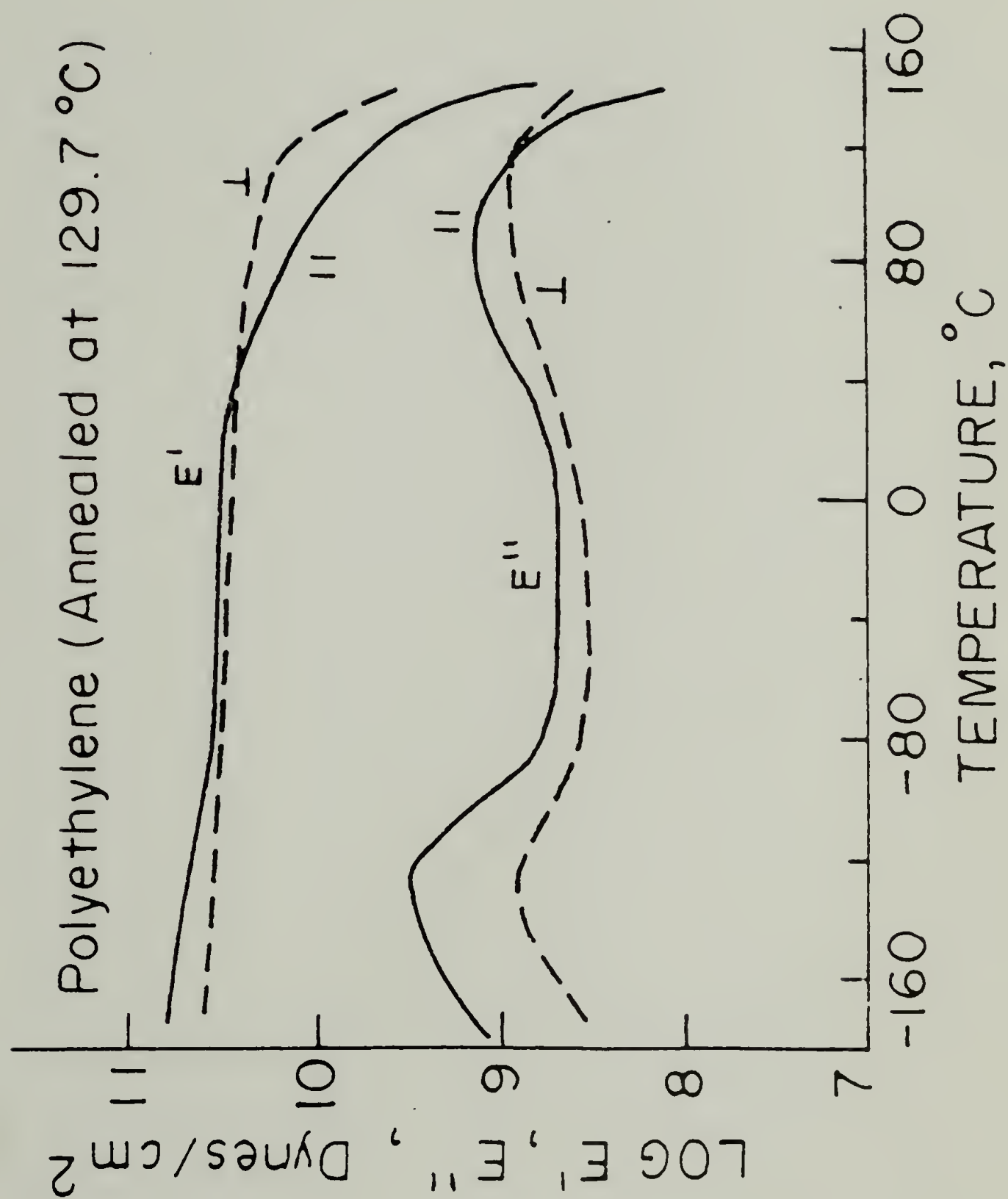


Figure 14



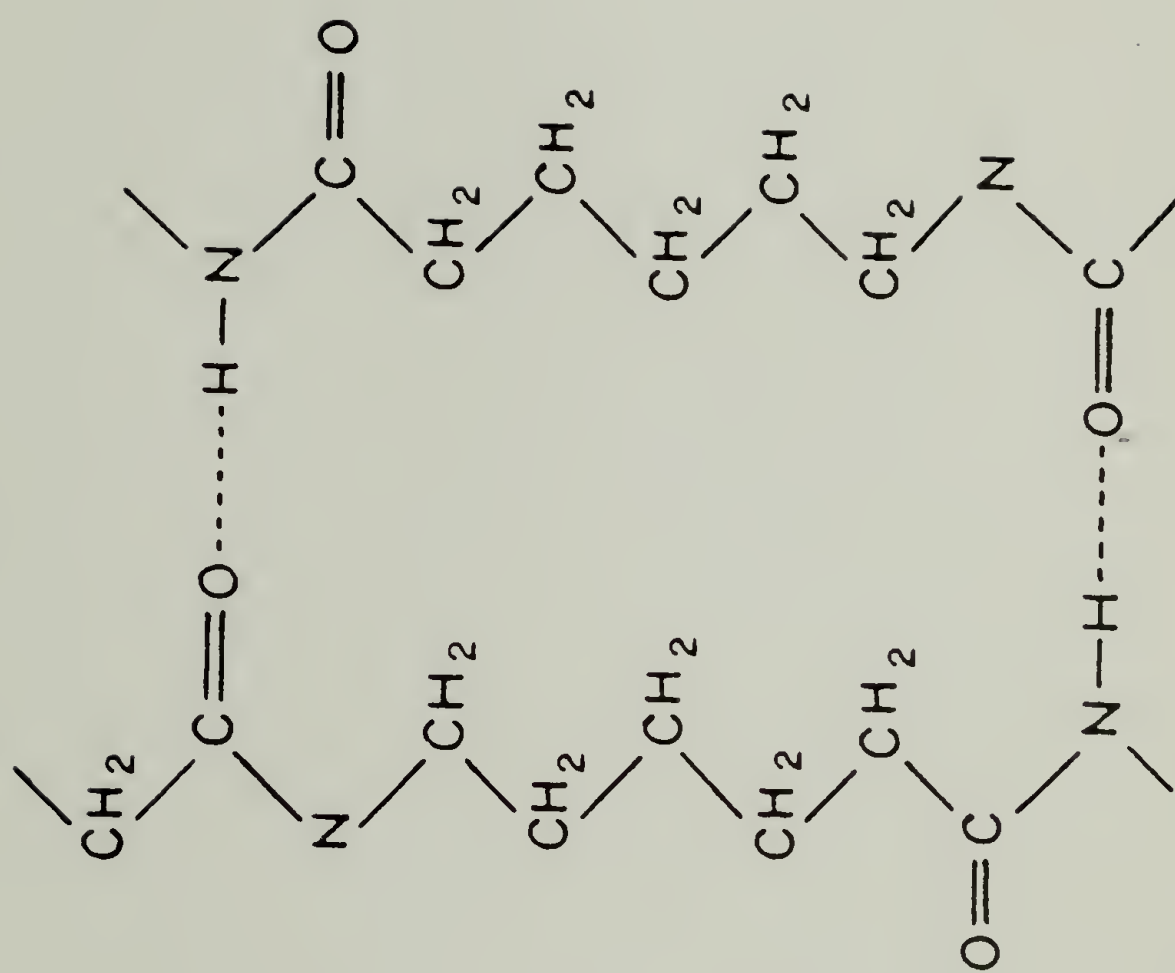


Figure 15

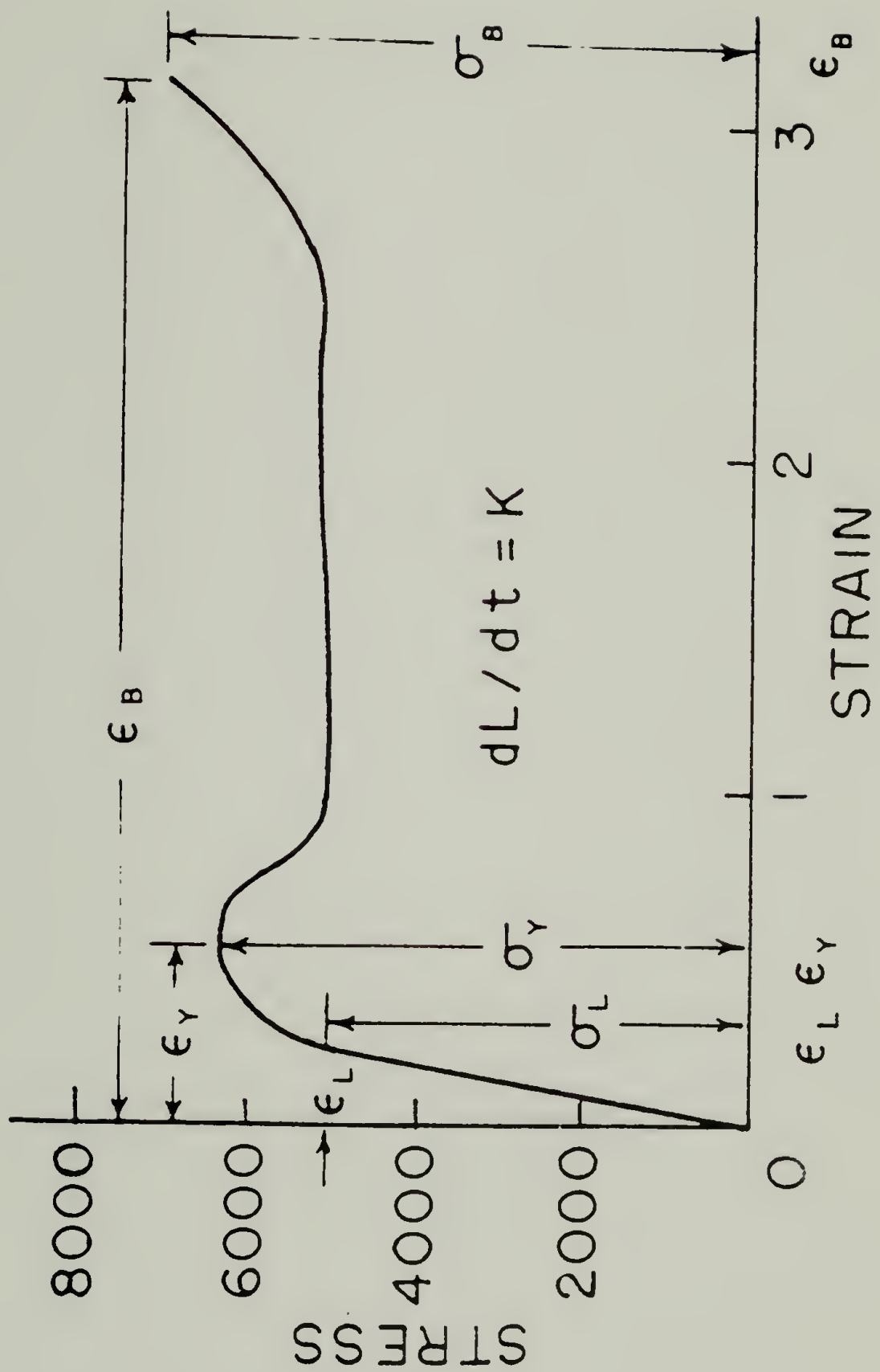


Figure 16

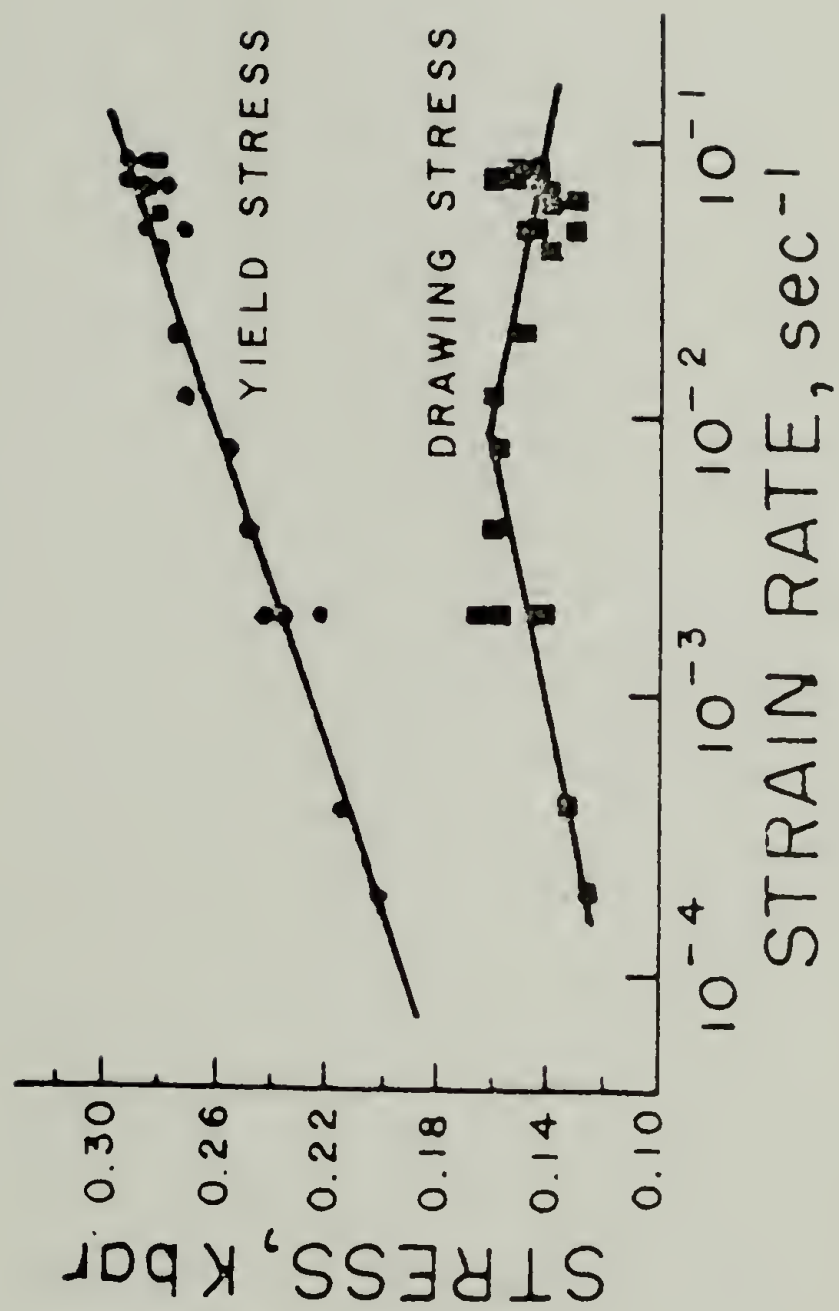


Figure 17

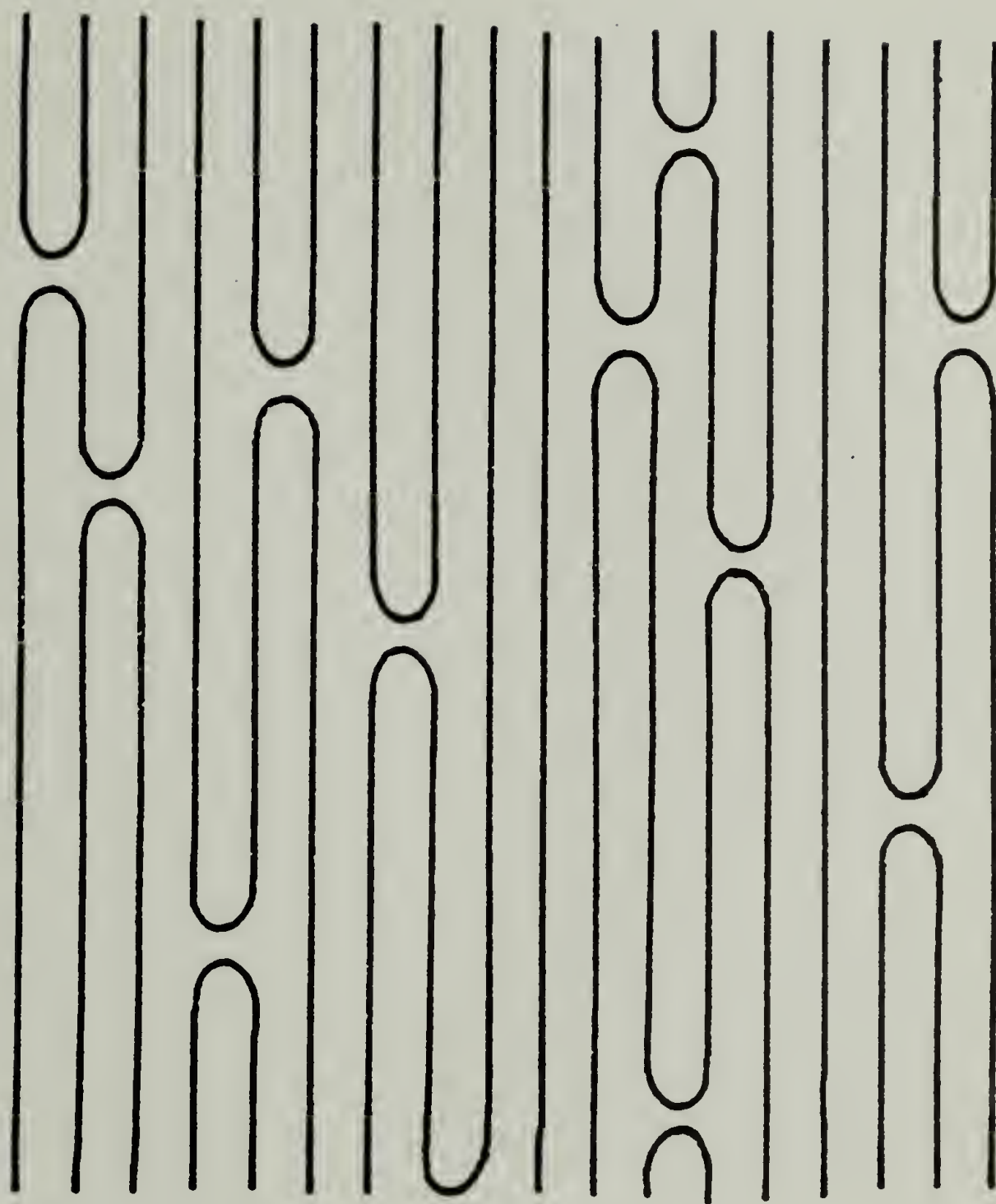


Figure 18



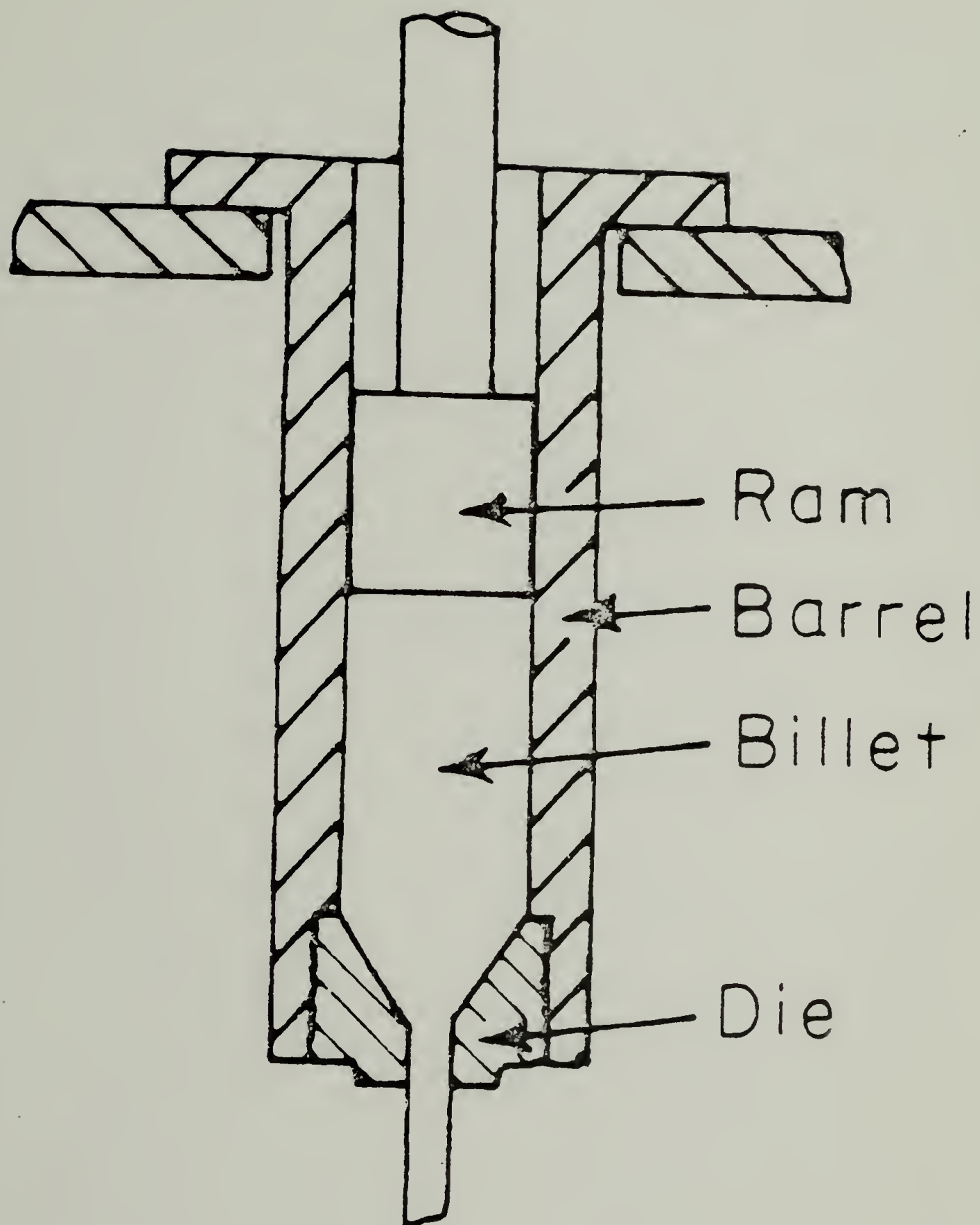


Figure 19

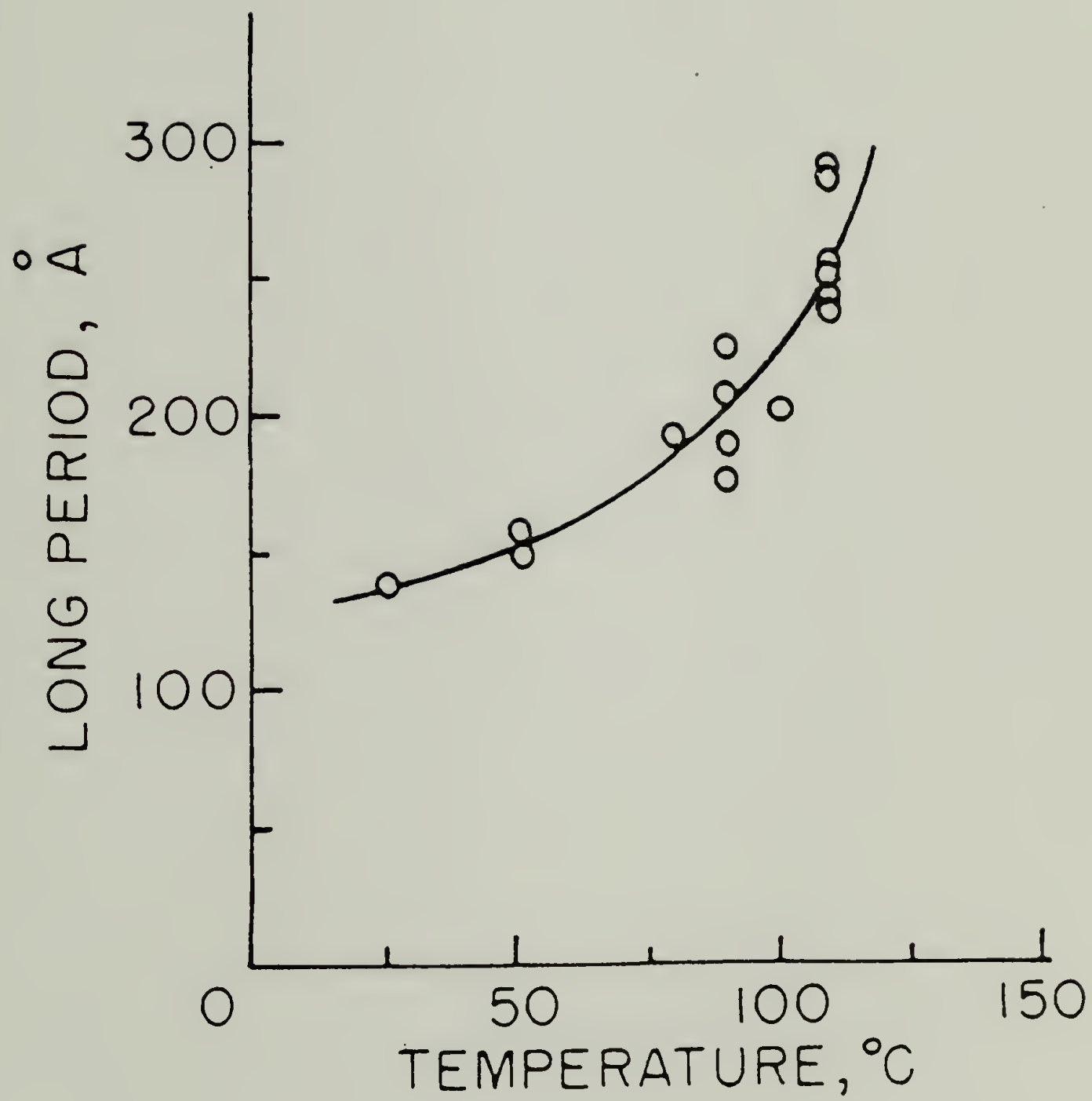


Figure 20

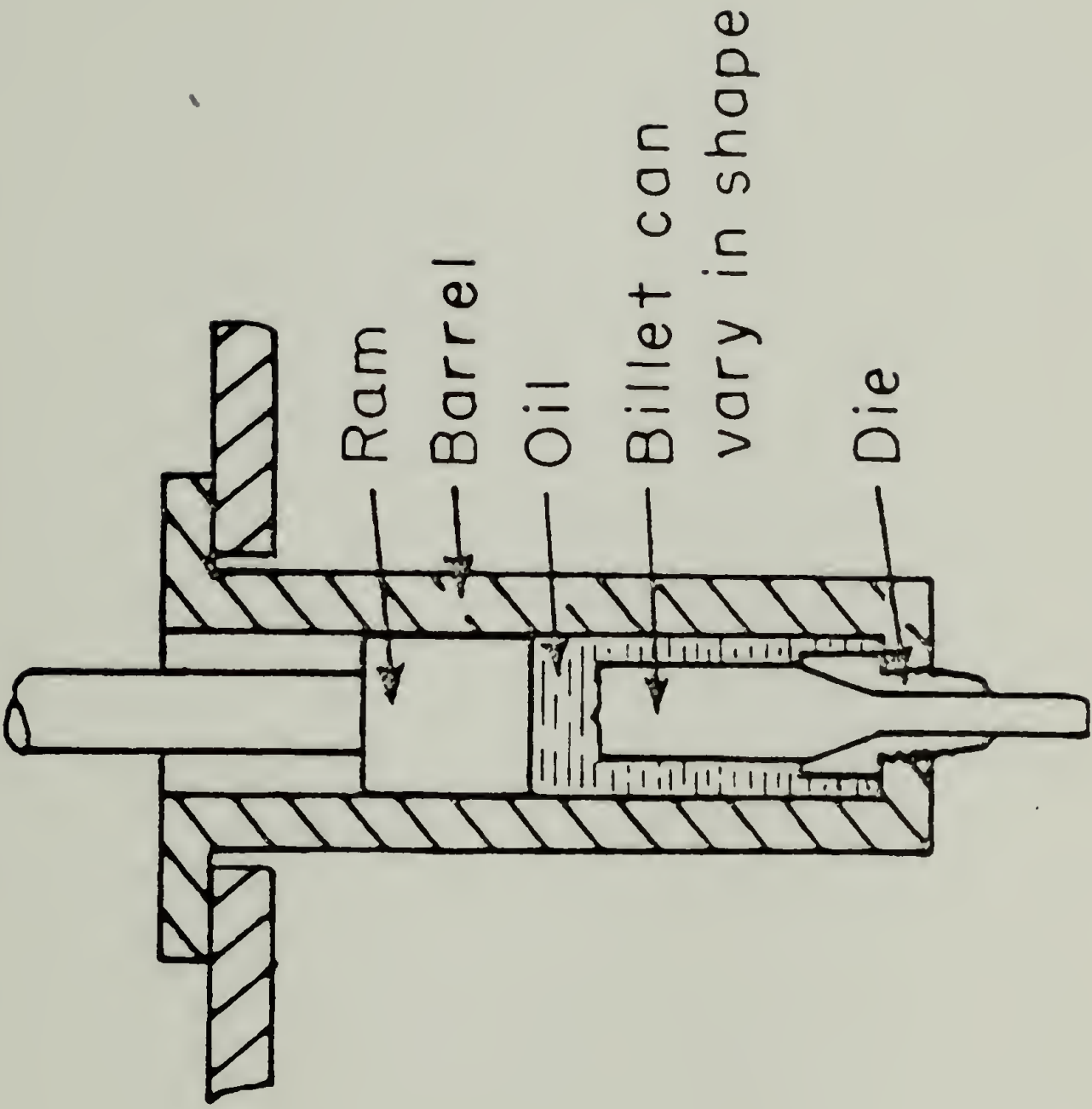


Figure 21

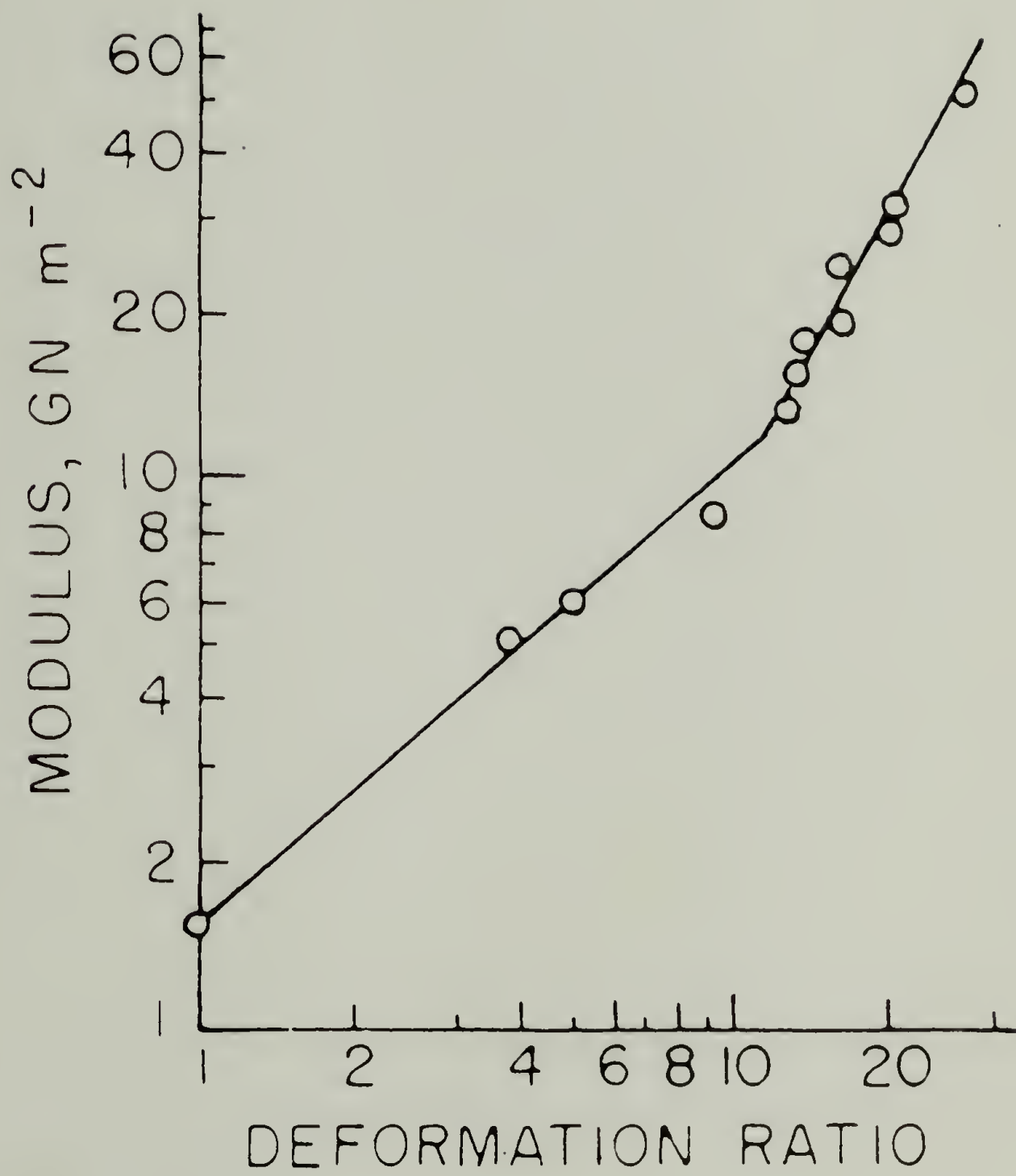


Figure 22



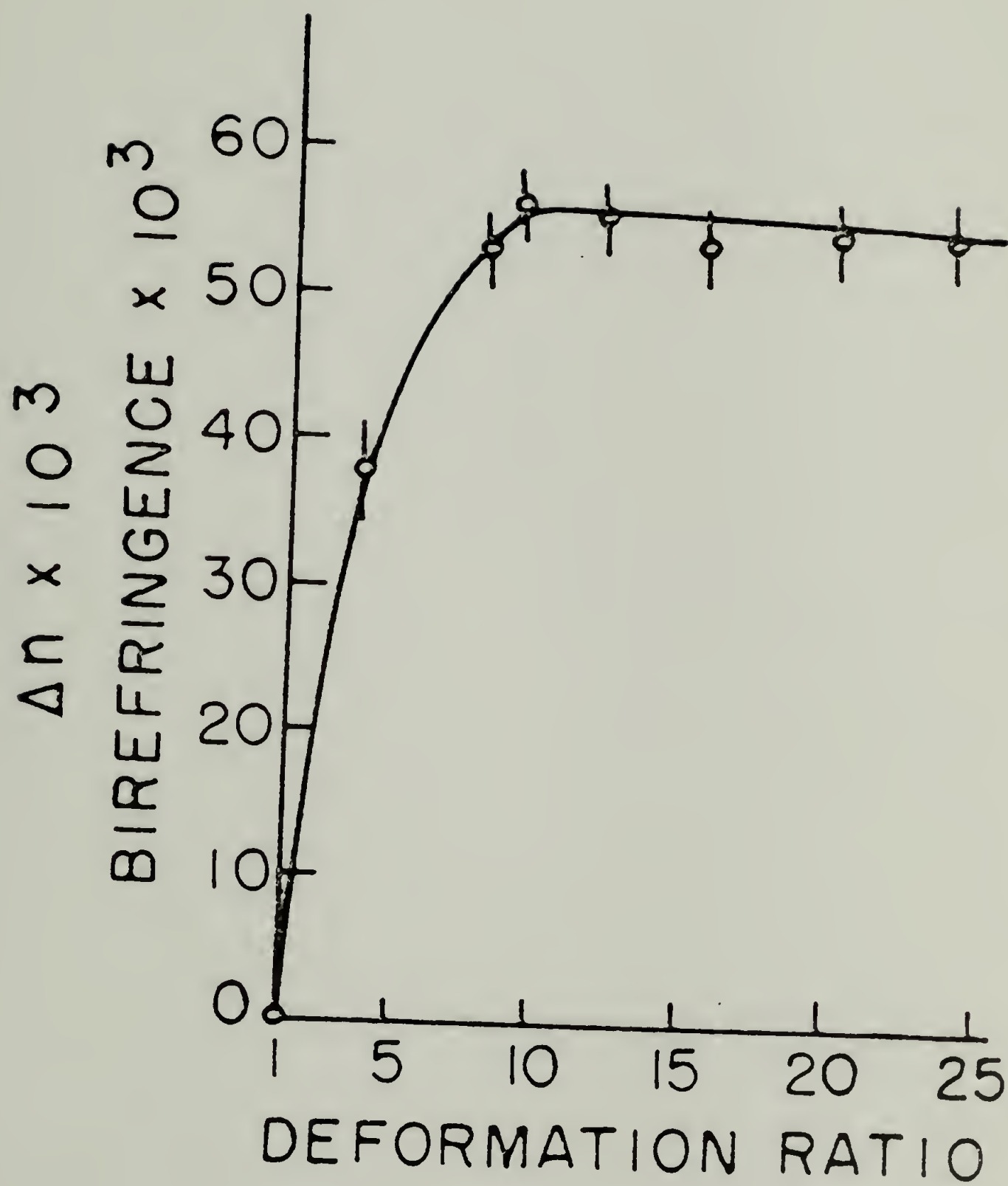


Figure 23

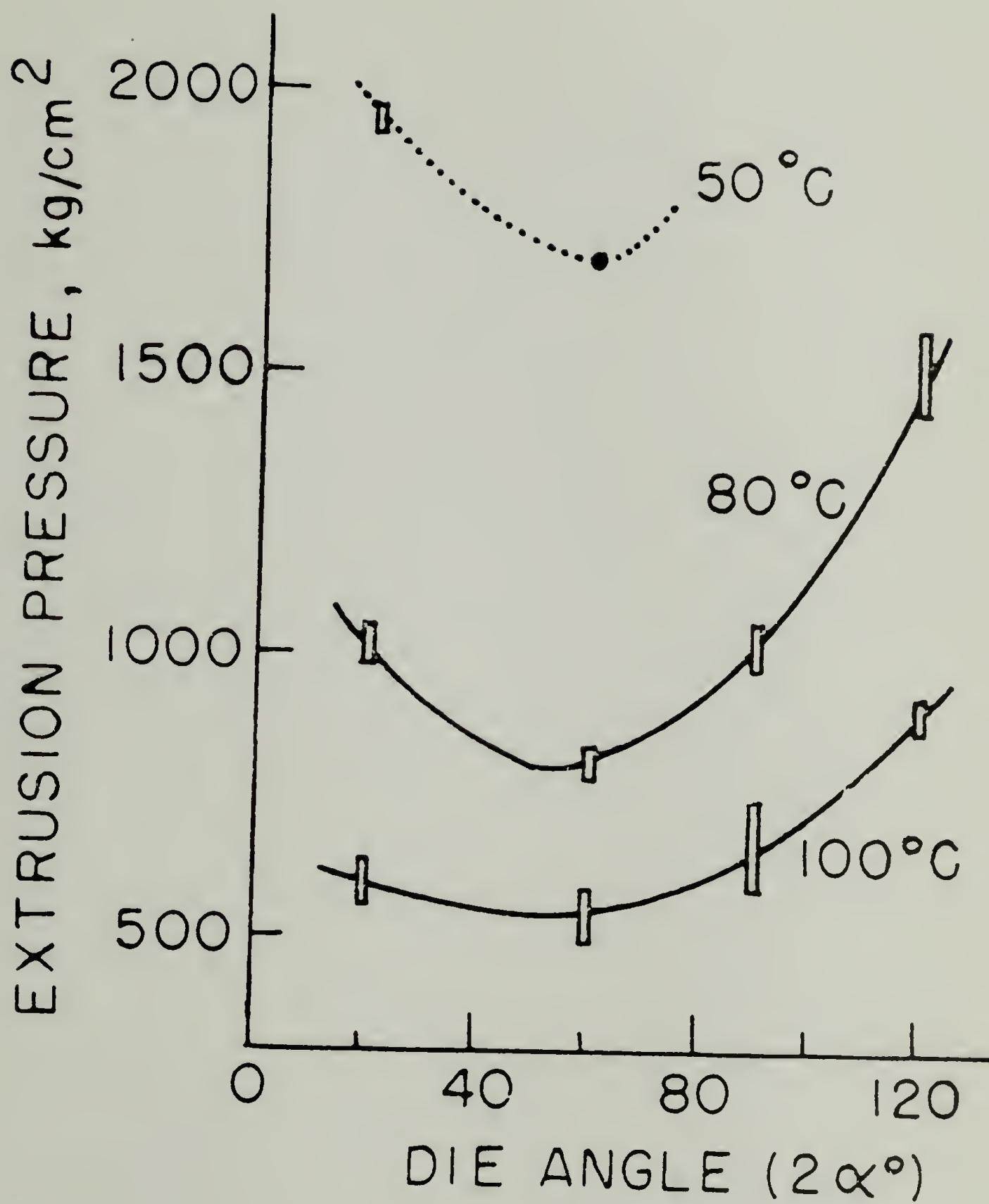


Figure 24

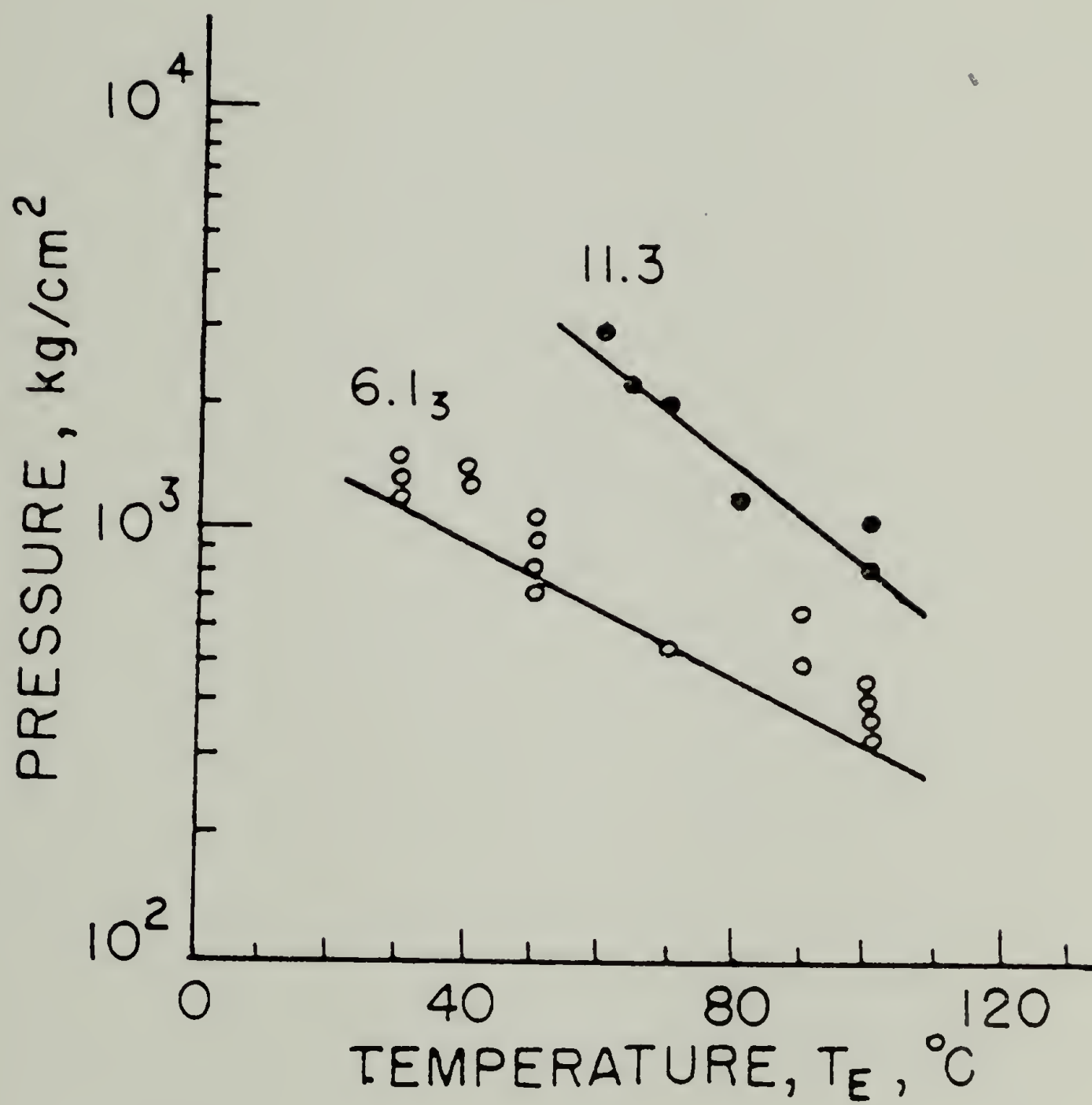


Figure 25

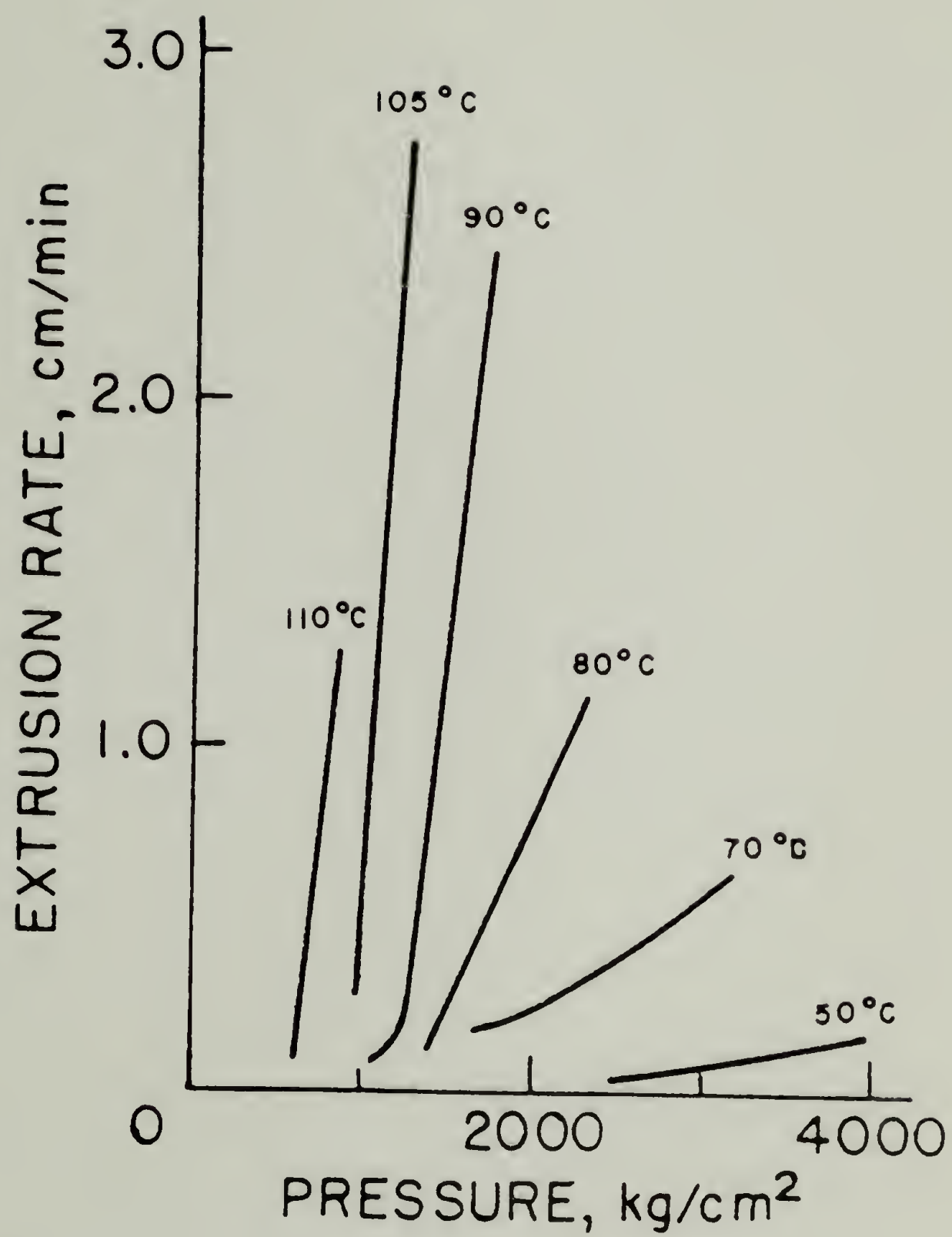


Figure 26



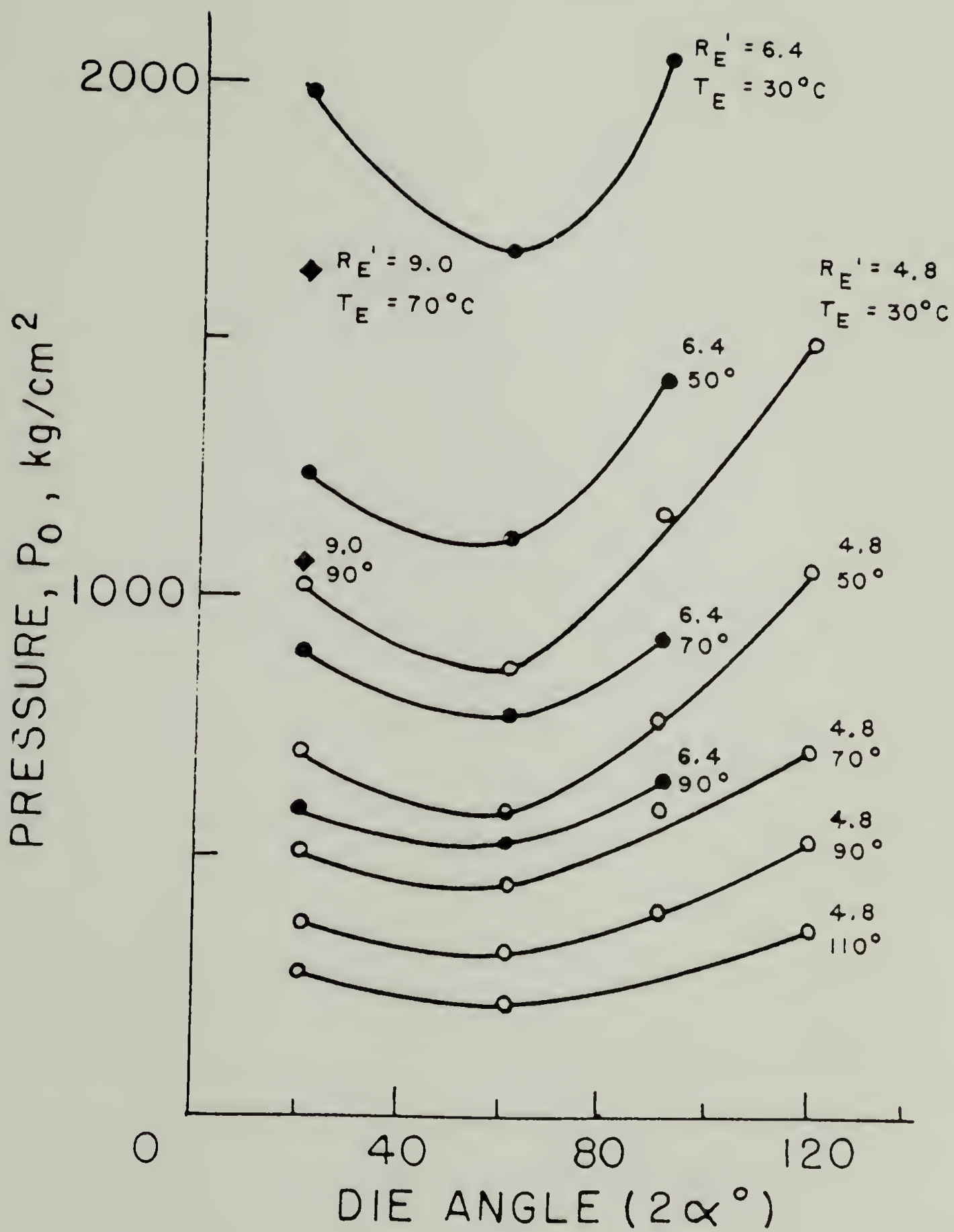


Figure 27

# CHAPTER I I

## ON PREPARATION OF AN ULTRA-ORIENTED POLYETHYLENE MORPHOLOGY

### I. Preparation Procedure

The molecular chains of a crystalline linear polymer, when perfectly extended, can have a longitudinal stiffness similar to that of steel (1,2). However, commercial plastics usually exhibit tensile moduli from 20 to over 100 times lower (3). Even for highly-oriented synthetic fibers the modulus will be relatively low unless a proportion of the chains are highly extended. It is the extended chains which provide the longitudinal continuity that leads to a high tensile modulus (4-7).

The methods available to obtain highly-oriented and extended-chain materials can be divided in two categories: those in which the flow or deformation is purely extensional (7-9) and those bearing an important shear component (10-13). Peterlin (14) and Ziabicki (13) and, more recently, Frank and coworkers (1,9) have emphasized the importance of the elongational deformation to achieve a considerable chain extension. In shear flow, the velocity gradient normal to the flow direction induces a superposed motion of rotation and translation on each material element. This effect restricts the molecular extension achievable.

The concepts described here are substantially different from the alternate ways to promote orientation (drawing, spinning, solution-grown crystals under shear, etc.). This chapter contains a description of the

method we currently use. It differs from the procedure used previously in this laboratory by J. Southern, N. Weeks and by T. Niikuni both in the capillary geometry and in the conditions for crystallization prior to extrusion (15). We currently reach an equilibrium crystallization before deformation is induced. We then perform a solid-state extrusion rather than one in a highly-viscous liquid state. This minimizes the shear (rotational) flow and favors an elongational deformation which provides a higher efficiency for chain orientation and extension.

The prior reports remain entirely valid as far as we know (15). They may, nonetheless, be misleading since we have subsequently developed a much more efficient and, importantly, essentially continuous method for producing high density polyethylene strands of extreme orientation. We therefore offer this standard method which is now being used in several research laboratories including our own.

Strong, ultra-oriented strands and film strips of high density polyethylene now can be extruded, free of defects and of indefinite length, in an Instron Capillary Rheometer. Pressure, temperature and capillary geometry are among the important parameters in preparation of the ultra-oriented morphologies. A typical material used is DuPont Alathon 7050 high density polyethylene,  $M_w = 59,000$ ,  $M_n = 20,000$ . Many other high density polyethylenes have been shown amenable to these procedures including Alathons with a range of molecular weights and comparable samples from the Phillips Company.

The preparation procedure can be separated in three steps: (1) Conditioning of the test specimens, (2) crystallization under pressure and (3) morphological changes produced under solid-state, high-pressure extrusion.

1. Preparation: The polyethylene is placed in the reservoir of an Instron rheometer and compacted in a conventional way at a temperature just below ( $\sim 5^{\circ}\text{C}$ ), the polymer melting point. The plunger is placed into the rheometer barrel and a restrictor is placed at the base of the capillary. The restrictor is a simple, conically-tipped steel needle which can be screwed firmly between the Instron base and the rheometer to plug the capillary. The temperature is then increased at atmospheric pressure up to around  $170^{\circ}\text{C}$  to melt the polyethylene. Next the heaters are shut off and the temperature reduced towards working conditions. When temperature nears the set point, the automatic temperature controller is switched on and temperature is allowed to stabilize.

2. Crystallization under Pressure: Pressure is now increased by moving down the rheometer plunger with the Instron crosshead at a fixed speed (a typical value is 1 cm/min). When the working pressure is reached (for example 2400 atm), the crosshead speed is reduced gradually towards the minimum value (.005 cm/min) to maintain a constant and high pressure, commonly near the upper limit of the Instron. For convenience, the instrument may be put on cyclic loading at a force corresponding to the desired pressure. The crosshead motion is stopped and started automatically in a close interval around the desired pressure. The crystallization is presumed to reach equilibrium when the volume reduction approaches zero which



is detected by pressure constancy with the crosshead still. Figure 1 shows the volume change with time during a typical run at 135°C and 2000 atm. Pressure increased from 1 to 2000 atm. in the first 41 seconds. Since the crosshead speed is constant, the change in volume is a linear function of time in this region. A plot of pressure vs. time, Figure 2, shows the onset of crystallization at about 500 atm. At this point a decrease in slope, corresponding to a lower resistance to volume change, indicates the crystallization initiation. Once the working pressure is reached, the crosshead speed is reduced gradually. Here the volume reduction slows down progressively with time beyond the linear region. As can be seen in Figure 1, the volume change decreases rapidly and in relatively short times, about 100 seconds, reaches an equilibrium value indicating the end of this step.

3. Morphology Preparation under Stress and Pressure during Extrusion: The restrictor is taken off and extrusion initiated. A 600 gram weight is clamped onto the end of the emerging fiber. This weight keeps the fiber straight during the extrusion process. This weight is sufficiently small compared to the extrusion pressure that it does not increase the extrusion rate. Alternatively, no weight is used, but the polymer is extruded through a glass tube to insure straightness. The crosshead motion is periodically reset to maintain a constant, high and predetermined pressure near the Instron maximum. The subsequent morphological transformation during extrusion is achieved by the combined effect of pressure and tensile deformation in the capillary entrance region.

The flow rate is highest at the beginning in successful extrusions. Still at constant and high pressure, the flow slows down until a constant and slow rate of extrusion is reached. This is commonly about one cm min<sup>-1</sup>. The first portions (~ 20 cm) of the extruded strands have lower perfection, i.e. lower melting points, heats of fusion, moduli and tensile strengths, than the subsequent portions. This is consistent with the idea of more perfect morphologies produced during steady extrusion at higher draw ratios.

The method described above differs in two essential ways from the former published procedure (15).

1. The Use of a Restrictor with the Consequent Result of a Two-Stage Process for Morphology Preparation: Niikuni and earlier workers on this project crystallized polyethylene directly from the melt, inducing the first nuclei by shear stress plus some pressure. Pressure increased abruptly in this former process only when the flow was arrested by extensive crystallization in shear.

With the present method, pressure is imposed before any crystallization takes place and the first stage of crystallization is carried out at the working pressure but without shear. This produces an equilibrium, spherulitic morphology at an undercooling corresponding to the elevation of melting point due to pressure of about 20°C per 1000 atm (16). The polymer is subsequently extruded and the second stage of morphology preparation, i.e. the crystal-crystal transformation, is induced.

2. The Capillary Geometry: Niikuni used only capillaries of 90° entrance angle. The best results were subsequently obtained here using a

capillary of  $20^\circ$  included angle. Also the former capillary lengths were relatively large (the shortest was 2.5 cm). Instead, lengths smaller than 2 cm now appear to be desirable for producing long strands of good perfection for ultra-oriented polyethylene. Capillary length itself, however, may not be a sensitive variable in these studies.

## II. Comments on Capillary Geometry

The lengths of extrudable strands, free of defects, that can be obtained are very sensitive to the cleanliness and smoothness of the inner surface of the capillary and entrance region. Lubrication with Teflon spray (bonding grade) proved to be useful. The Teflon adheres to the capillary wall forming a very thin layer with an extremely low friction coefficient. The application of the Teflon is done by spraying against the entrance zone while pulling a vacuum on the back (capillary) end. The Teflon coating is also buffed in.

Long strands, over 14 inches (35 cm), of clear, strong polyethylene are obtained using a brass capillary of draw ratio 52 with  $20^\circ$  entrance angle, polished and Teflon lubricated. With capillaries of lower draw ratio, continuous extrusion is achieved.

Both entrance angle and draw ratio influence the maximum strand length achievable before fracture starts to appear. Experiments developed with different entrance angles for capillaries of the same length and diameter show a consistent increase in strand length with a reduction of angle. However, the maximum extrusion ratio attainable decreases regularly with a reduction in entrance angle. The smallest angle tried was  $6^\circ$ .



Extrudate length is not analogous to extrudate extrusion ratio where dies of different entrance angles are involved (see below).

Another important aspect of capillary geometry is real vs. nominal draw ratio. The nominal draw ratio is the ratio of cross-sectional areas of the rheometer barrel to the die exit. However, as material is initially extruded from the capillary die conical entrance region, the draw ratio of the resulting extrudate continually increases up to the maximum. This actual draw ratio equals the nominal draw ratio only when all the material originally in the die entrance region is extruded. At this point, steady-state, or continuous, extrusion at the limiting length ratio is attained. Figure 3 shows the real draw ratio as a function of extrudate length for a series of capillaries having the nominal, i.e. maximum, extrusion draw ratios shown.

### III. Billet Length and Extrusion Pressure

The length of the polymer billet in the rheometer barrel prior to extrusion markedly influences the extrusion rate as shown in Figures 4 and 5. A billet of Alathon 7050 high density polyethylene was extruded until the extrudate fractured. The restrictor was then replaced in the die exit and the billet was remelted above  $160^{\circ}\text{C}$  and recrystallized under pressure. A second extrusion run was carried out, again until fracture. This procedure was repeated six times and the extrudate length vs. extrusion time curves for each run were plotted in Figure 4. The initial slope of these curves was plotted against billet length in Figure 5. Billet length at the beginning of each run was determined from the crosshead position indicator dial on the Instron. It is apparent from Figure 5 that initial



extrusion rate has a strong inverse dependence on billet length. This is most likely due to a large pressure drop through the billet arising from friction between the billet and the die. Consistent with this effect, it has been observed that for a given billet length, initial extrusion rates are higher in the case of lubricated dies. Steady state extrusion rates appear to be independent of billet length.

#### IV. Pressure Effects

Another interesting point is the effect of pressure on the extrusion characteristics and physical properties of the ultra-oriented strands. Figure 6 shows two plots of extrudate length vs. extrusion time. The polyethylene in the upper plot was crystallized and extruded under 4000 atm. pressure. Its maximum length before fracturing was 58 cm., corresponding to a draw ratio of 47! The lower plot is data from the same polyethylene crystallized and extruded at 2400 atm. Its maximum length at fracture was 38.5 cm., or a draw ratio of 36. Although the steady state (long times) extrusion rates are approximately the same, the initial rate for the high pressure run is notably higher as might be expected.

Physical/mechanical properties of solid state extruded Alathon 7050 as a function of crystallization/extrusion pressure are shown in Table 1. Crystalline melting temperature is invariant with preparation pressure history, whereas percent crystallinity and Young's modulus rise slightly with increasing pressure. This probably results from the closer packing of crystals with higher pressure. Tensile strength at break rises

significantly with samples prepared under increasingly high pressure before levelling off. This may be due to increased entanglements brought about by closer chain packing during high pressure crystallization.

#### V. Possibilities of This Method

An interesting alternative to these procedures involves crystallization at higher temperatures. With the previous method used by Niikuni and Weeks, it is not possible to reach enough shear stress to allow massive crystallization above  $137^{\circ}\text{C}$ . Thus strands produced up to now have been extruded at temperatures no higher than  $136^{\circ}\text{C}$  and 5000 atm. pressure. By the following method, there is no temperature limitation. The equilibrium melting point at 2000 atm. pressure for linear polyethylene is near  $168^{\circ}\text{C}$  (16). Therefore, assuming a  $135^{\circ}\text{C}$  operation temperature, the supercooling is  $33^{\circ}\text{C}$ . This relatively high supercooling leads to a rapid crystallization in the reservoir, but the crystal thickness will be quite small. With a supercooling of  $15^{\circ}\text{C}$ , primary crystallization is completed in about 30 minutes (18). Furthermore, the increase in lamellar thickness with reduction of supercooling is remarkable (for example, 65% increase on passing from  $33^{\circ}\text{C}$  to  $15^{\circ}\text{C}$  supercooling). Apparently we can obtain considerably thicker crystals by operating at  $150^{\circ}\text{C}$  ( $18^{\circ}$  supercooling) during the first stage of crystallization and the crystallization time will not be unreasonably large (not much longer than 30 min.). Once crystallized at  $150^{\circ}\text{C}$  and 2000 atm., either the temperature can be reduced at  $135^{\circ}\text{C}$  and the extrusion started or the material can be extruded at  $150^{\circ}\text{C}$  using a

cooling system at the exit to avoid the strand melting. This interesting experiment has not yet been done. Indeed, we await a major area of research which will involve decoupling the pressure effects on morphology preparation and on extrusion rate. Our basic method now allows us to prepare crystals under a variety of conditions prior to extrusion.

### References

1. F. C. Frank, Proc. Roy. Soc. London, A, 319, 127 (1970).
2. I. Sakurada and K. Kaji, J. Polym. Sci., C, 31, 57 (1970).
3. J. Brandrup and E. H. Immergut, "Polymer Handbook," Interscience, New York, 1966.
4. R. S. Porter, ACS Meeting, Washington, D.C., 1971, "Symposium on Unsolved Problems in Polymer Science."
5. A. Peterlin, J. Mater. Sci. 6, 490 (1971).
6. A. Peterlin, Tex. Res. J. 42, 20 (1972).
7. N. J. Capiati and R. S. Porter, J. Polym. Sci., Polym. Phys. Ed. 13, 1177 (1975).
8. T. T. Wang, H. S. Cheng and T. K. Kwei, J. Polym. Sci., B, 8, 505 (1970).
9. F. C. Frank, A. Keller and M. R. Mackley, Polymer 12, 467 (1971).
10. K. Imada, T. Yamamoto, K. Shigematsu and M. Takayanagi, J. Mater. Sci. 6, 537 (1971).
11. A. J. Pennings, J. Polym. Sci. 16, 1799 (1967).
12. A. J. Pennings and A. M. Kiel, Koll. Z. Polym. 205, 160 (1965).
13. A. Ziabicki, J. Appl. Polym. Sci. 2, 24 (1959).
14. A. Peterlin, J. Polym. Sci., B, 4, 287 (1966).
15. T. Niikuni and R. S. Porter, J. Mater. Sci. 9, 389 (1974).
16. B. Wunderlich and T. Arakawa, J. Polym. Sci., A2, 3697 (1964).
17. P. Predecki and W. O. Statton, J. Polym. Sci., B, 10, 87 (1972).
18. P. D. Calvert and D. R. Uhlmann, J. Polym. Sci., A-2, 10, 1811 (1972).



CRYSTALLIZATION - EXTRUSION PRESSURE (GPa)	0.24	0.29	0.33	0.36	0.39
AMBIENT CRYSTALLINE MELTING POINT (°C)	139.0	139.3	139.0	139.2	139.2
PERCENT CRYSTALLINITY ±1%	86	87	90	90	89
YOUNG'S MODULUS, GPa ±10%	49	45	64	55	54
TENSILE STRENGTH, GPa 10%	0.37	0.48	0.54	0.53	0.53

TABLE 1

Physical Properties of Alathon 7050 HDPE ( $\bar{M}_w$ : 59,000;  $\bar{M}_n$ : 19,900)  
Crystallized and Solid State Extruded at 134°C and at pressures shown.

Captions for Figures

1. Volume decrease for polyethylene on increasing pressure to 2000 atm. with time at  $135^{\circ}\text{C}$ . Initial slope due to instrument response.
2. Change of pressure with time in the Instron Rheometer showing crystallization of high density polyethylene at  $135^{\circ}\text{C}$ .
3. Real draw ratio as a function of strand length for selected dies.
4. Extrudate length vs. extrusion time for a series of billet lengths; billet lengths decreasing from 1 to 6.
5. Initial extrusion rate of high density polyethylene versus length of original billet.
6. Extrudate length versus extrusion time for high density polyethylene samples crystallized and extruded at two different pressures.

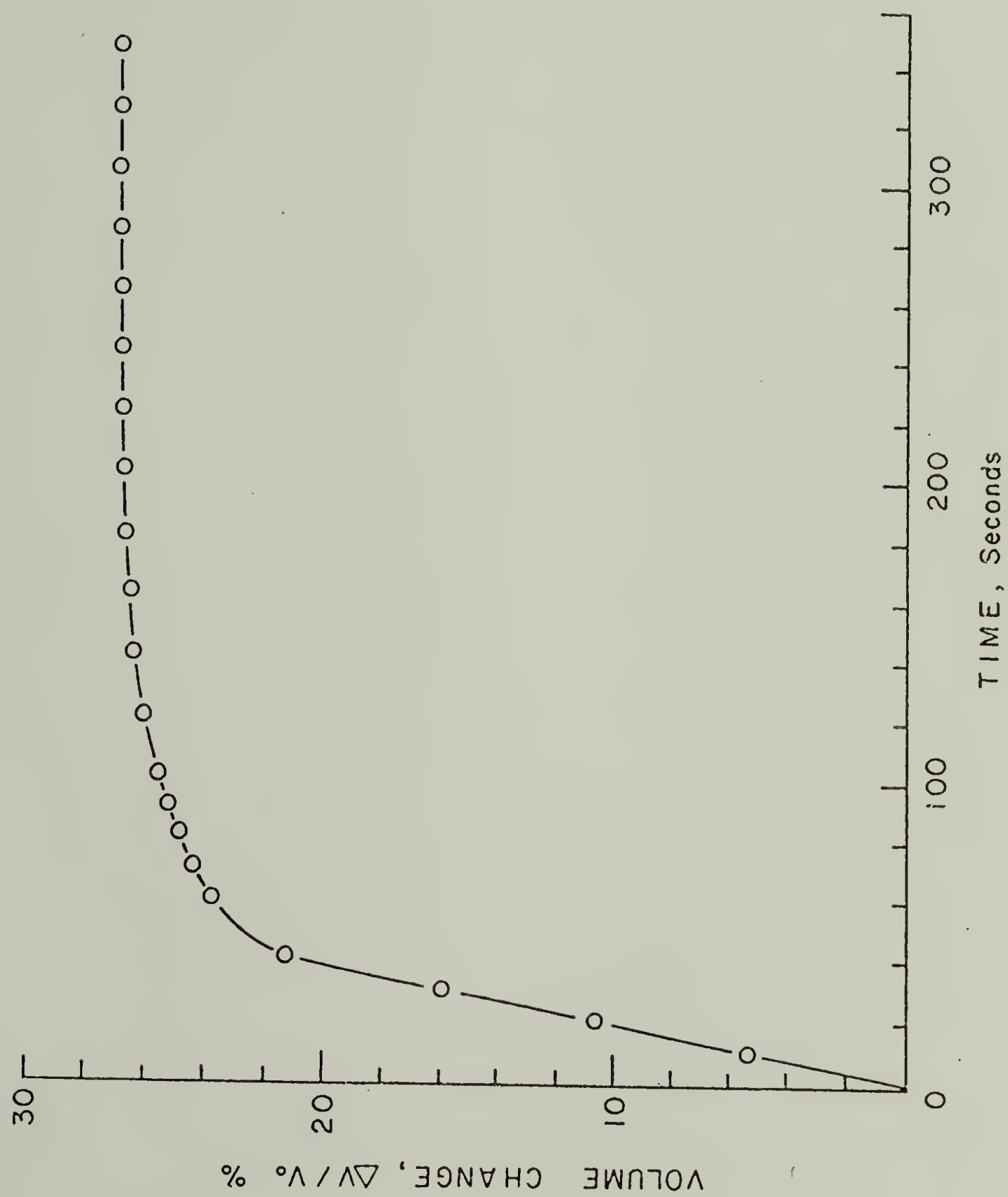


Figure 1

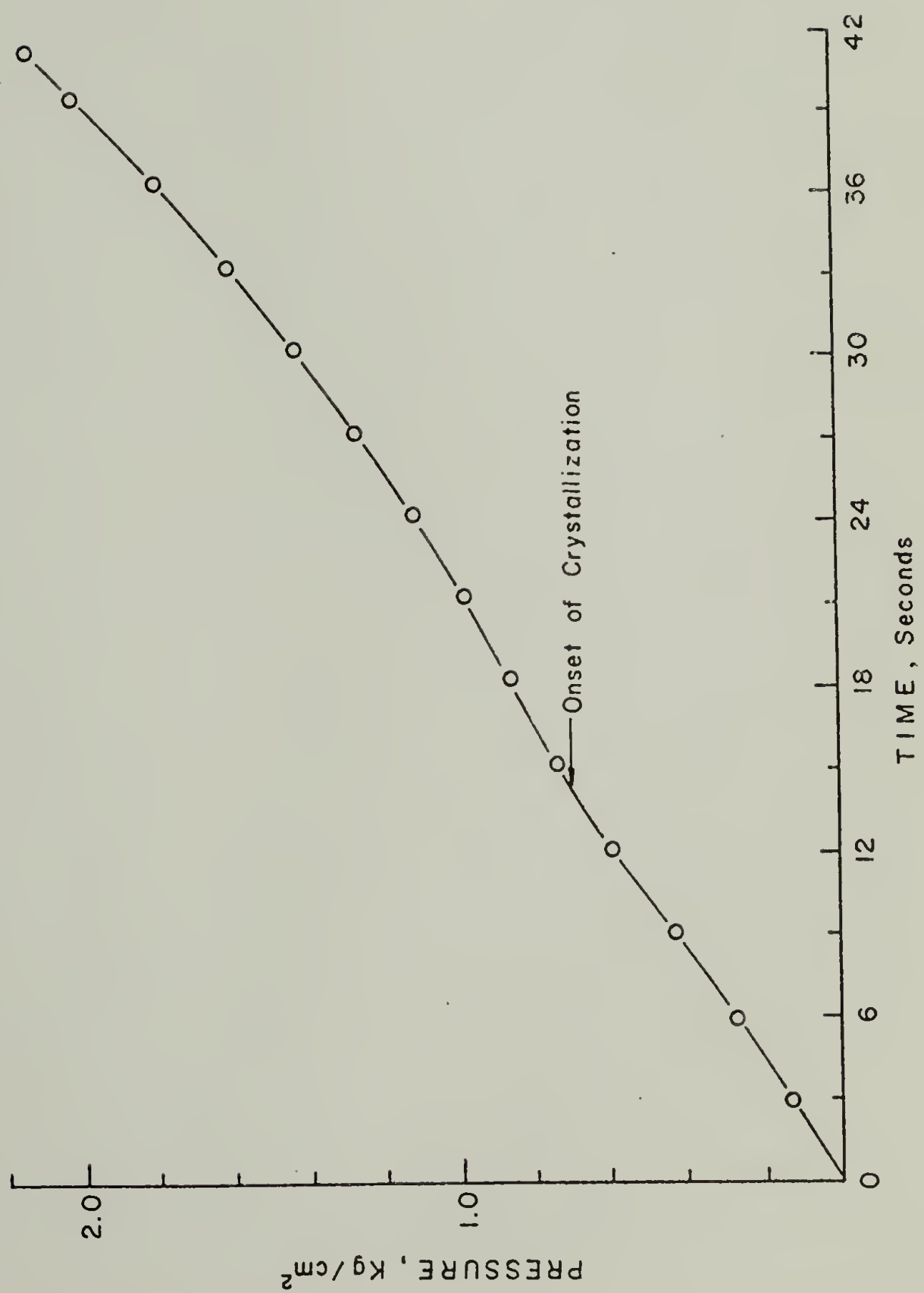


Figure 2



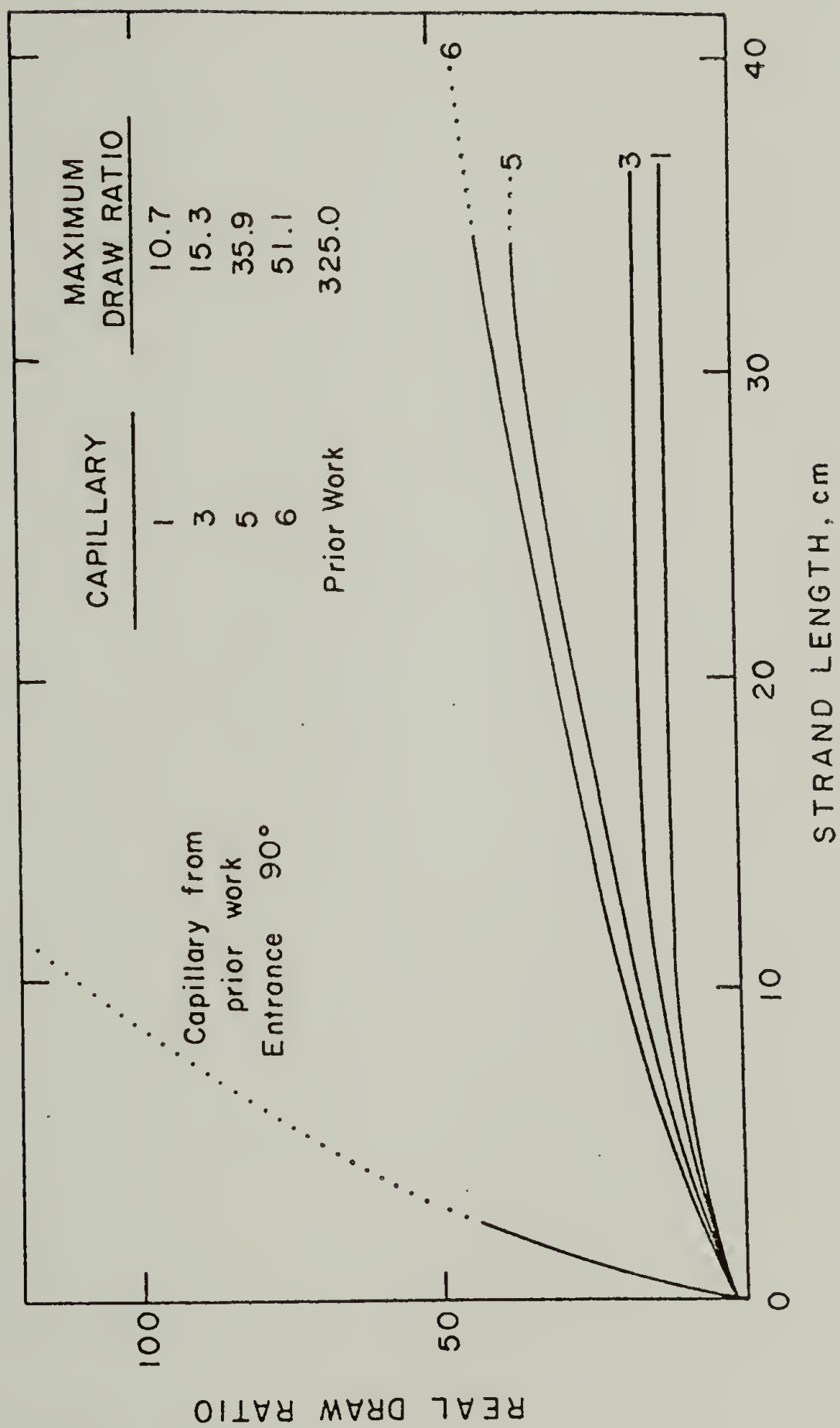


Figure 3

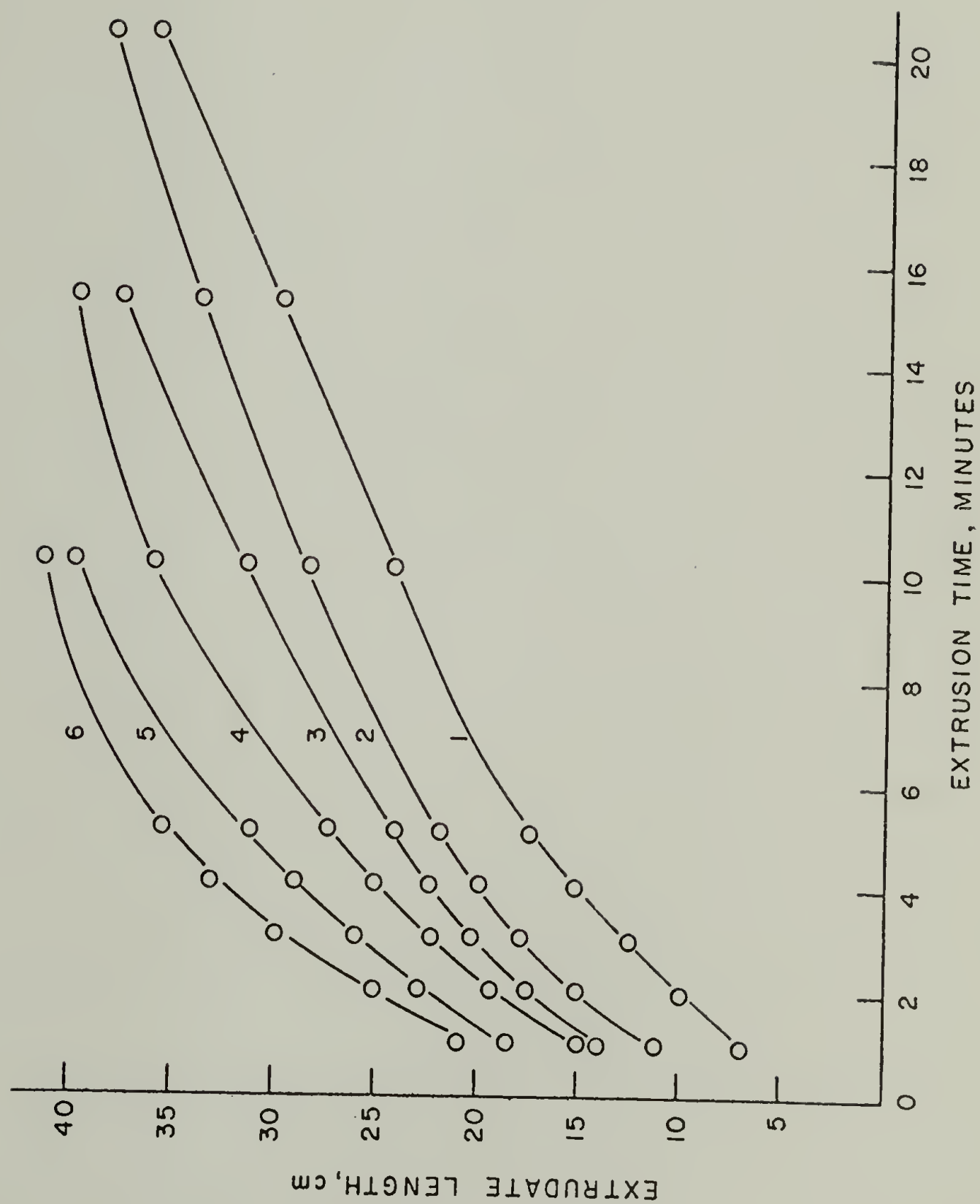


Figure 4

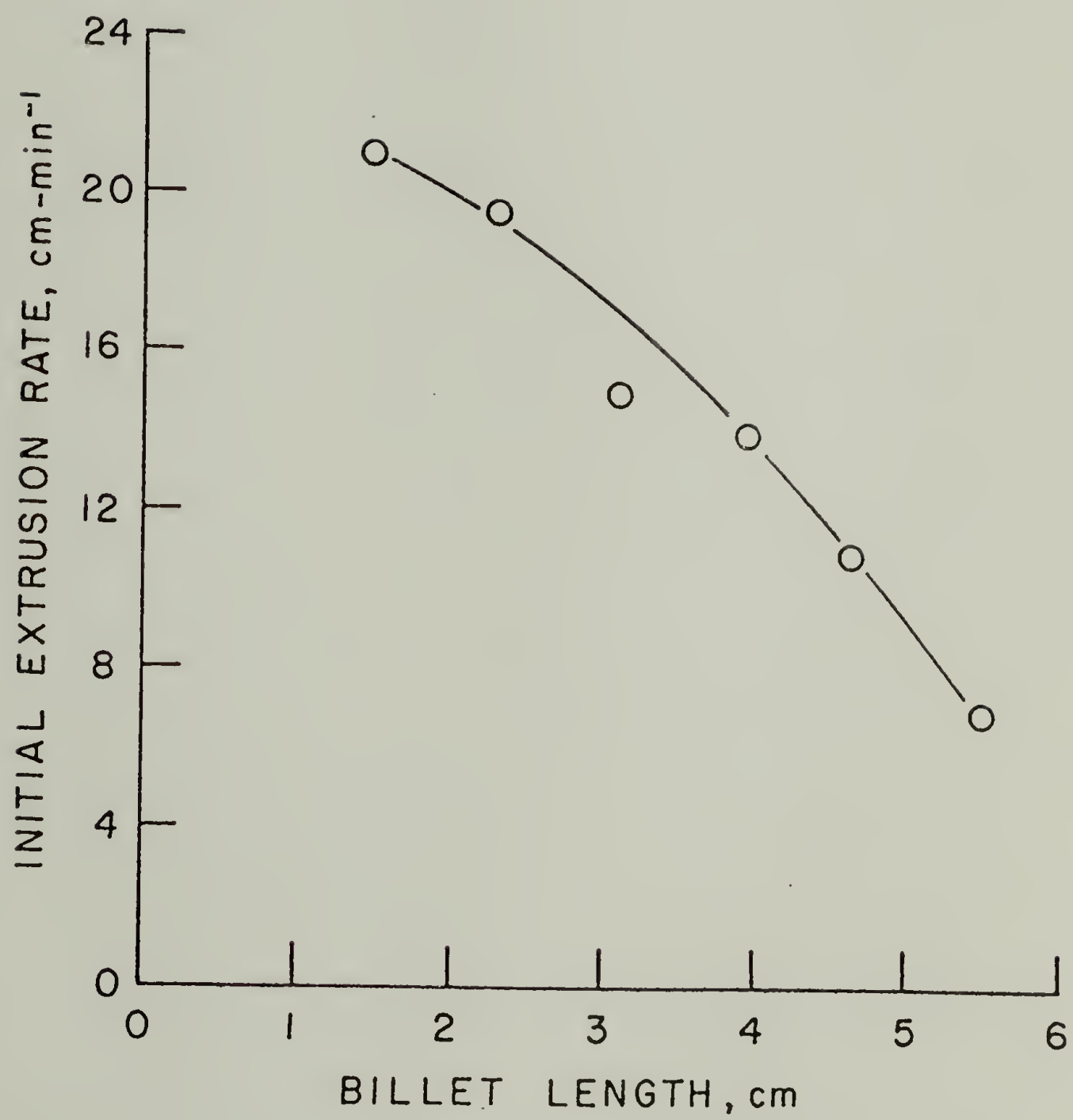


Figure 5

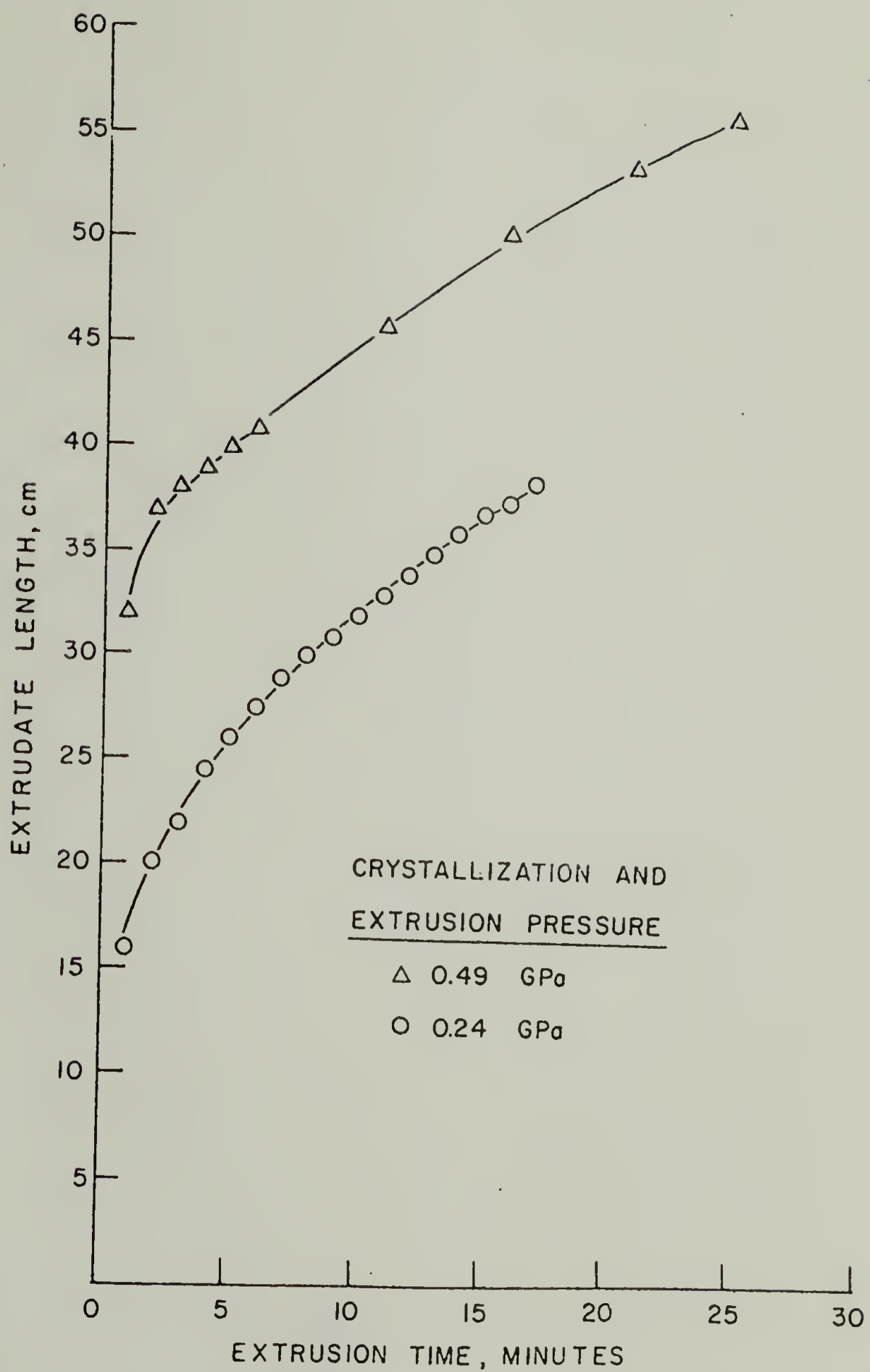


Figure 6



C H A P T E R   I I I  
EXTRUSION PROPERTIES OF HIGH DENSITY POLYETHYLENE  
AS A FUNCTION OF CAPILLARY DIE ENTRANCE ANGLE

I. Introduction

Ultra-oriented high density polyethylene (HDPE) films and fibers have been produced in this laboratory by solid state extrusion using an Instron capillary rheometer (1). A typical die is of brass with a  $20^{\circ}$  included entrance angle ( $2\alpha$ ) and a nominal extrusion draw ratio of 52. However, actual extrusion ratios on samples are generally less. This is because the total volume of polymer initially in the tapered die entrance region is not extruded before the extrudate fractures. This means that the maximum potential extrusion draw can be difficult to achieve. This study is an attempt to clarify the importance and efficiency of the capillary die entrance angle with respect to extrusion characteristics and physical properties of the extrudates for HDPE.

In even a qualitative analysis of the deformation undergone by the polymer in solid state extrusion, one must consider both the shear and extensional forces and flows occurring within the die entrance region. Such discussions in the literature are limited to melt flow so that such results are considered here only as analogous to solid state flow. Under the high extrusion pressures commonly encountered in the process ( $\leq 0.49$  GPa), consideration must also be given the effect of pressure on the

transitions and yield properties of the polymer being extruded.

According to Cogswell (2), "simple shear deformation takes place when the flow streamlines are parallel, but correspond to different material velocities." This corresponds to entrance regions having angles, which in the geometrical limit, as  $2\alpha$  approaches zero, are straight tubes. Cogswell continues, "Extensional flow occurs when the streamlines through a cross-section correspond to constant material velocities, but are not parallel." This is the case involving larger entrance angles, which in a limit would be  $180^\circ$ , or a square entrance region. In his review on the processing of ultra-high modulus polymers, Bigg (3) states that a high elongation velocity gradient is needed to develop the necessary molecular structure for superior extrudate physical properties. He speculates that small entrance angles most probably cannot produce such a gradient. On the other hand, Bigg goes on to say that a uniform elongational velocity gradient is difficult to realize at large die angles, because of localized high elongation of the material at the entrance to the capillary portion of the die.

Although a well-developed elongational velocity gradient is seen as important for enhancement of extrudate physical properties, excessively high extensional stresses are believed to cause gross extrudate fracture. Shaw (4) postulates that lubrication of the die entry region minimizes or eliminates shear stresses, thus generating high extensional stresses which result in melt fracture. A balance of shear and extensional deformation was also seen as important by Predecki and Statton (5) who noted that die lubrication reduced the efficiency of the molecular orientation process

by reducing shear stresses. Everage and Ballman (6) calculated a critical recoverable extensional strain, and state that once this strain is attained, the material cannot elastically deform fast enough to reach a steady-state extensional stress level, and fracture may result. They conclude that melt fracture can be a consequence of tensile failure of the material in extensional deformation. Metzger, et al. (7), show that the magnitude of the shear stresses developed during melt extrusion of HDPE are proportional to the molecular weight. From Cogswell's calculations relating extensional and shear stresses to entrance angle, one would expect smaller extensional stresses at larger entrance angles. This means a higher extrusion ratio before fracture should be possible for higher molecular weight materials extruded through larger entrance angles. This would appear to be the case for the Nakayama and Kanetsuna study (8) on hydrostatic extrusion of HDPE where the optimum entrance angle (lowest extrusion pressure required) was found to be  $60^{\circ}$ , at a HDPE molecular weight twice as high as the Alathon 7050 used in this study. Imada and Takayanagi (9), processing HDPE via solid state extrusion, found the optimum included entrance angle to be  $20-40^{\circ}$ , using a HDPE having approximately the same molecular weight as the Alathon 7050 used here.

Pugh (10) believes that two important factors influence the choice of optimum die entrance angle. One is the "redundant work," caused by shearing of the material as it enters the deformation (entrance) zone and flows toward the die orifice. This factor increases with increasing die angle. The other factor is the frictional work at the billet-die



interface. This decreases with increasing die angle. Pugh concludes that there would quite naturally be a minimum in the relation between extrusion pressure and die angle. He further observed that this minimum shifts toward smaller angles as the coefficient of friction between the billet material and the die decreases.

The effect of high pressure on the mechanical properties of polymers must be considered in an analysis of solid state extrusion since the material being extruded is under high pressure in both the die and rheometer barrel. It is generally concluded that both the modulus and yield stress rise substantially with increasing hydrostatic pressure. Ainbinder, et al. (11), attribute the modulus increase at 2,000 atm to a decrease in specific volume, analogous to cooling the polymer  $> 100^{\circ}\text{C}$ . They further state that the nature of the deformation of crystalline polymers in the presence of (all around) compression seems to depend largely on the percent crystallinity. For highly crystalline polymers (such as HDPE), the deformational process cannot be very dependent on conformational movements; the decisive factor will therefore be the extent of deformation. Because the material undergoes less total deformation in large entrance angle dies (smaller entry volume), one might conclude that shear stress buildup will be less and maximum extrusion ratios higher.

Pae, et al. (12), believe, from the behavior of polyethylene single crystals, that bulk polymer under hydrostatic pressure will principally deform via shear modes. If this is indeed the case, die angles which reduce such stresses will allow larger deformations without fracture;



these are the larger angles. As stated by Mears, et al. (13), under high pressure a higher applied pressure is required to initiate the molecular mobility associated with plastic yielding. This is because as the material is compressed, the free volume is reduced and the secondary forces between neighboring segments are therefore increased. This agrees with the general contention that yield stress increases with high pressure and strain to fracture decreases during tensile tests in a high pressure environment. Therefore, the higher pressures necessary for solid-state extrusion are also responsible for the ultimate failing of the extrudate at high extrusion ratios. From the data of Mears, et al. (13), and Ward, et al. (14), the tensile yield stress increases more rapidly with increasing pressure than does the shear yield stress. Therefore, larger entrance angles, where shear stresses (not strains) are larger, should allow attainment of greater extrusion ratios.

## II. Experimental

The high density polyethylenes used exclusively in this study were DuPont Alathon 7050 ( $\overline{M}_w$ : 59,000;  $\overline{M}_n$ : 19,900) and Alathon 7030 ( $\overline{M}_w$ : 92,000;  $\overline{M}_n$ : 26,000) (15). Fibers were extruded through brass capillary dies having entrance angles of 10, 14, 20, 30, 60, 90, 120 and 180<sup>0</sup> (see Figure 1). A 6<sup>0</sup> entrance angle die was also tested, but anomalous results and subsequent inspection of the die revealed faulty die machining, so these results were not included.

Capillary length for all entrance angles was 1.0 cm and diameter was 0.132 cm. Extrusions were done at 2,400 atm pressure and 134°C. Teflon film-bonding grade lubricant was sprayed on the highly polished dies prior to extrusion. The solid state extrusion technique was as previously described (1) except that no weight was attached to the emerging extrudates, which were instead extruded through a glass tube to insure straightness. The extrusion rate at each entrance angle was measured with a cathetometer under steady state conditions. Characterization techniques applied to the extrudate included differential scanning calorimetry; birefringence, thermomechanical analysis, and mechanical testing.

Differential scanning calorimetry (DSC) was performed with a Perkin-Elmer DSC-1B at a heating rate of 10°C-min<sup>-1</sup> to yield heats of fusion (converted to percent crystallinity) and crystalline melting points.

Birefringence measurements were carried out on a Zeiss polarizing microscope equipped with an Ehringhaus rotary compensator consisting of double calcite plates. The compensator can measure up to 133 orders of retardation in white light. The magnitude of the birefringence was calculated from

$$\Delta = \frac{\delta\lambda}{t}$$

where  $\Delta$  = total birefringence of the fiber,  $\delta$  = retardance,  $\lambda$  = wavelength of white light ( $5674\text{\AA}$ ), and  $t$  = fiber thickness (diameter).

A Perkin-Elmer TMS-1 thermomechanical analyzer attachment to the DSC-1B was used for measurement of the linear expansion coefficient,  $\alpha$ , as well as thermal transitions. Sample preparation for this test was as previously described (16). A small load of 3 grams was used with the expansion probe, and the scanning rate was  $10^{\circ}\text{C-min}^{-1}$ . Test sample length was approximately 1 centimeter. Scans were made from  $-110$  up to  $120^{\circ}\text{C}$ .

For studies of mechanical properties on extruded fibers, an Instron tensile testing machine, model TTCM, was used, equipped with a strain-gauge extensometer. Load-elongation curves were obtained at room temperature using a fixed elongation rate of  $0.02\text{ cm-min}^{-1}$  for accurate modulus measurements, and  $0.50\text{ cm-min}^{-1}$  for determination of tensile strength and strain-at-break. The fibers had to be gripped by special clamps described elsewhere (17) to prevent slippage in the jaws. The Young's modulus was determined as the tangent to the stress-strain curve at 0.1% strain.

### III. Results

#### A. Extrusion Rate.

The rate of extrusion for HDPE (Alathon 7050) plotted against die entrance angle is shown in Figure 2. The steady state rate decreases rapidly from  $1.16\text{ cm-min}^{-1}$  at the  $10^{\circ}$  entrance angle to  $0.2\text{ cm-min}^{-1}$  at an entrance angle of  $120^{\circ}$ . At still larger angles, the rate remains fairly

constant at  $\sim 0.2 \text{ cm-min}^{-1}$ . For Alathon 7030 ( $\overline{M}_w$ : 92,000), the extrusion rates, although generally slower, behave similarly. They decrease from  $0.43 \text{ cm-min}^{-1}$  at the  $10^\circ$  entrance angle to  $0.72 \text{ cm-min}^{-1}$  at  $120^\circ$ , thereafter remaining nearly constant. These steady-state extrusion rates appear well before the entrance cone volume is expended (see Chapter II).

### B. Deformation Intensity.

The concept of deformation intensity was developed in a paper by Capiati, et al. (1), and plotted as a function of extrusion draw ratio. Deformation intensity (DI) is defined as the rate change of draw which reaches a maximum at the entrance cone exit

$$\left. \frac{d(ER)}{dH} \right|_{\max} = 2R_a^2 \tan\alpha / R_b^3$$

where  $\left. \frac{d(ER)}{dH} \right|_{\max}$  = maximum deformation intensity,  $R_a$  = rheometer barrel (reservoir) radius,  $R_b$  = extrudate radius, and  $\alpha$  = entrance cone semi-angle.  $H$  = axial distance along die.

Figure 3 is a plot of deformation intensity vs. entrance angle. It is seen that DI rapidly increases with increasing entrance angle. According to Capiati, et al. (1), the relationship between DI and extensional shear rate is given by



$$\frac{dV}{dH} = V_a \frac{d(ER)}{dH}$$

where  $V$  and  $V_a$  are material velocities at two points within the conical die entrance region. Since extensional shear rate is shown above to be proportional to  $DI$ , and present data show  $DI$  to increase with larger entrance angles, one can conclude that extensional shear rates increase with increasing entrance angles. This indicates a more efficient molecular extension at larger angles and higher ultimate extrusion ratios would be expected at the larger angles.

#### C. Extrusion Length at Fracture.

The curves showing extrusion length at fracture vs. entrance angle shown in Figure 4 are similar to those of extrusion rate vs. entrance angle. A rapid decrease in maximum extrudate length from  $10^\circ$  to  $60^\circ$  is followed by a more gradual decrease at larger angles. The two molecular weight curves cross at a projected entrance angle of  $85^\circ$ . The  $14^\circ$  data for the lower molecular weight Alathon 7050 is anomalously low and may be due to a less well polished die.

#### D. Maximum Extrusion Ratio.

The maximum extrusion ratio ( $ER$ ) obtainable is plotted as extrusion ratio at fracture vs. die entrance angle in Figure 5. These data mark

the points where extrudate fracture began. The maximum ER possible with the dies used in this study was 52, found by dividing the cross-sectional area of the capillary exit into the cross-sectional area of the Instron rheometer barrel. This ER was realized with Alathon 7050 in the  $120^\circ$  entrance angle die. Lowering the entrance angle from  $120^\circ$  to  $20^\circ$  at this same molecular weight ( $\overline{M}_w$ : 59,000) produced a linear decrease in the maximum obtainable ER. For strands extruded through dies having entrance angles less than  $20^\circ$ , fracture occurs at significantly lower ER's, as shown in Figure 5. For the higher molecular weight Alathon 7030, the maximum ER obtainable also occurred with the  $120^\circ$  die. However, the maximum was only 49. Maximum ER's for this polymer decreased linearly from 49 at the  $120^\circ$  angle to 43.5 at the  $10^\circ$  entrance angle. The maximum ER for the lower molecular weight strands is inexplicably low for fibers extruded through the  $14^\circ$  entrance angle die. Another noteworthy feature of this plot is the crossing of the two curves at a projected angle of  $\sim 85^\circ$ .

#### E. Birefringence.

Birefringence, a measure of total (amorphous and crystalline) orientation, is plotted as a function of extrusion ratio in Figures 6 and 7 for all entrance angles. Figure 6, a plot of birefringence vs. ER curves for Alathon 7050, shows that all extrudates exhibit low orientation at low ER's ( $\sim 10$ ) with the  $120^\circ$  strands quite low. At an ER of 20, orientation has increased to a fairly high value for the  $20^\circ$ ,  $30^\circ$ , and  $60^\circ$  fibers, to

a somewhat lower value for 14 and  $90^{\circ}$  fibers, and to an even lower value for the fibers extruded through the  $120^{\circ}$  entrance angle die. Moving up to an ER of 24, where mechanical properties were measured, one sees that the 20, 30, 60, and  $90^{\circ}$  strands exhibit high orientation, whereas the 14 and the  $120^{\circ}$  strands remain lower. The curves appear to approach a limiting birefringence of 0.062. The curve for the  $10^{\circ}$  fiber is not shown since these strands were not sufficiently transparent to allow birefringence measurements.

Figure 7 is a plot of birefringence vs. ER for the higher molecular weight Alathon 7030. At low extrusion ratios the values are lower than those of the Alathon 7050 resin. At an ER of 20, the  $20^{\circ}$  extrudates appear to be the most highly oriented, while the 60 and  $90^{\circ}$  extrudates remain quite low, and the  $120^{\circ}$  strands appear to be still less oriented. At an ER of 24, the 20 and  $30^{\circ}$  fibers show the highest orientation, while the 90 and  $120^{\circ}$  fibers remain least oriented. However, both Figures 6 and 7 show that at above an extrusion ratio of  $\sim 35$ , strands extruded through a  $90^{\circ}$  entrance angle die are the most highly oriented whereas those extruded through a  $120^{\circ}$  entrance region are least oriented. Except for the  $90^{\circ}$  extrudates, birefringence values for the 7030 fibers tend toward a limit at 0.061. Nakayama and Kanetsuna (8) found that x-ray (crystal) orientation was invariant with die entrance angle up to  $90^{\circ}$ . Extrudates from the  $120^{\circ}$  die showed lower crystal orientation. Anomalies in the present results may then be due to amorphous phase orientation.

The literature value calculated for maximum birefringence of a perfectly oriented HDPE crystal is 0.059 (18). In this laboratory, Mead, Desper and Porter (19) have observed a maximum birefringence of ultra-oriented HDPE of 0.062.

#### F. Calorimetry.

Differential scanning calorimetry (DSC) results for crystalline melting point and percent crystallinity of the two molecular weight HDPE's are shown in Tables 1 and 2. Measurements were made at an extrusion ratio of 10. The fibers extruded through the  $120^{\circ}$  die have the lowest melting point and percent crystallinity. Strands extruded through dies at the other angles show no significant variation in melting point or percent crystallinity.

#### G. Thermomechanical Analysis.

Thermomechanical analysis (TMA) yielded values of linear expansion coefficients ( $\alpha$ ) over various temperature ranges. These coefficients, in  $^{\circ}\text{C}^{-1}$ , are obtained from the slopes of plots of normalized sample length change vs. scanning temperature. Values of  $\alpha_1$ , the coefficient measured from  $-110$  to  $-80^{\circ}$  for Alathon 7050 and measured from  $-110$  to  $-73.5^{\circ}$  for Alathon 7030, are plotted against die entrance angle in Figures 8 and 9, respectively. Measurements were taken at an ER of 20. The 7050 data had rather large scatter, but appeared to show a maximum between the  $30$  and  $90^{\circ}$  entrance angle. The higher molecular weight (7030) data in Figure 9 show an increase to a maximum at the  $20$ - $30^{\circ}$  angles, then a gradual



decline at larger angles.

#### H. Mechanical Testing.

Mechanical properties were measured at an ER of 24. Stress-strain curves run at low ( $< 1\%$ ) strain yielded values of Young's modulus vs. die entrance angle as shown in Figures 10 and 11. Values for 7050 fibers in Figure 10 show a maximum at a die angle of  $20$  to  $30^\circ$ , then a slow drop to a constant value at larger entrance angles. The higher molecular weight 7030 data shown in Figure 11 is similar except that the maximum occurs at die angles of  $14 - 20^\circ$  and the absolute values are slightly higher.

Tensile strength at break is plotted against die entrance angle in Figures 12 and 13. The strength of 7050 fibers increases with increasing entrance angle up to  $20 - 30^\circ$ , then decreases and levels off at larger entrance angles. The higher molecular weight fibers (Figure 13) show an increase to a maximum at  $14 - 20^\circ$ , then the strength drops somewhat and levels off at the larger entrance angles. Values for the higher molecular weight extrudates are generally higher than their lower molecular weight counterparts.

Strain at break is plotted against entrance angle in Figures 14 and 15. The 7050 plot is analogous to the tensile strength data in that values rise to a maximum at an entrance angle of  $20 - 30^\circ$  then drop and level off at higher angles. The higher molecular weight 7030 fibers show a rise in breaking strain to a maximum at  $14 - 20^\circ$ , followed by a

drop. Ultimate properties of strands extruded through larger entrance angles are difficult to obtain due to their short lengths and subsequent slippage in the testing machine grips. For this reason, some larger angle data is missing in these plots.

Figure 16 shows schematically two types of load-cycling curves obtained during the (low strain) mechanical tests. Curve (a) is typical for the fibers extruded through the die with the  $10^0$  entrance region, whereas curve (b) is typical for fibers extruded through all other angles for both molecular weights. The area within a given (open) loop is a measure of the energy dissipated,  $E_d$ , for that particular cycle. A plot of  $E_d$  vs. die entrance angle is shown in Figure 17. The data for both molecular weights fall on the same curve. There is a drop from the  $10^0$  entrance angle to the  $14^0$  angle, followed by a plateau, then slow rise at higher angles.

Figure 18 relates the energy dissipated to Young's modulus for both 7050 and 7030 strands at an ER of 24. Again the data for both molecular weights fall on the same curve. It is seen that there is an inverse relationship between the energy dissipated in a stress-strain cycle and Young's modulus, more pronounced at lower moduli values. The unusually high  $E_d$  values for the 7030 extrudate at low Young's moduli correspond to extrudates formed by the  $10^0$  entrance angle die.

#### IV. Discussion and Conclusions

##### A. Extrusion Rate.

The results of the extrusion rate data, plotted in Figure 2, indicate that the deformation process is facilitated by a streamlined (more gradually tapered) entrance region, at least up to angles of  $120^{\circ}$ . As the entrance angles tend toward  $0^{\circ}$ , the extrusion rates tend toward very high values. This would be expected as the deformation becomes increasingly parallel to the primary compressive force applied by the Instron plunger. However, although these smaller angles result in faster extrusion rates and longer extrudates, the actual maximum extrusion ratio attainable increases with increasing entrance angle. This indicates that a large extensional component is necessary for optimum crystalline state deformation efficiency. This occurs with larger entrance angles.

##### B. Extrusion Length and Extrusion Ratio at Fracture.

The curves of maximum extrusion length vs. entrance angle cross at a projected angle of  $85^{\circ}$ . At smaller angles, the higher molecular weight Alathon 7050 produces longer extrudates, while at larger (than  $85^{\circ}$ ) angles, both molecular weights produce approximately equal lengths at a given angle. There is an unexplained low value in the Alathon 7050 curve at an entrance angle of  $14^{\circ}$ . The extrusion ratio at fracture vs. entrance angle curves for the two molecular weights cross at the projected  $85^{\circ}$  entrance angle. Below this angle the higher molecular weight HDPE allows attainment of greater extrusion ratios, whereas above the crossover point,

the lower molecular weight HDPE results in fibers having greater maximum ER's. Both maximum extrusion length and extrusion ratio results indicate that the cold extrusion process is more efficient at smaller entrance angles for higher molecular weight HDPE and more efficient at larger entrance angles for lower molecular weight HDPE. Possibly the two curves in Figures 4 and 5 cross because the higher molecular weight HDPE cannot utilize effectively the high elongational deformation taking place at the larger entrance angles while the lower molecular weight HDPE is not deformed efficiently at the smaller angles.

### C. Birefringence.

Birefringence measurements indicate that greater total orientation is achieved for the lower molecular weight fibers at any given extrusion ratio and entrance angles greater than  $20^{\circ}$ . The  $20^{\circ}$  entrance angle curves for both HDPE's cross at extrusion ratios of 15 and  $35^{\circ}$  whereas the  $14^{\circ}$  curve for the higher molecular weight strands shows greater birefringence (total orientation). Again, the deformation process for the lower molecular weight HDPE appears more efficient at large entrance angles while for the higher molecular weight HDPE, smaller entrance angles seem to be more advantageous. At the  $120^{\circ}$  entrance angle, both molecular weights give poorly oriented extrudates. This could result from annealing of the extrudate in the die as it emerges at the slow rates characteristic of high angles.



#### D. Calorimetry.

Measurement of crystalline melting point and percent crystallinity indicates that no great change in crystal size and/or perfection results from altering the die entrance angle except at an angle of  $120^{\circ}$ , where the crystal quality is apparently lower at an ER of 10. This is likely due to the lower total orientation of fibers extruded through this die, as shown by birefringence. The melting points and crystallinity for the Alathon 7050 fibers are slightly higher in the  $20-60^{\circ}$  entrance angle range whereas those in the  $14-30^{\circ}$  entrance angle range are higher for the higher molecular weight Alathon 7030 strands. These differences, however, border on the range of experimental error.

#### E. Coefficient of Expansion.

The magnitude of the negative linear expansion coefficient in the orientation direction is a qualitative measure of the extent of chain extension in ultra-oriented systems (15). The results in this study suggest that maximum chain extension occurs in fibers extruded through the middle angle ( $30 - 90^{\circ}$ ) dies for Alathon 7050 and through the smaller angle ( $20 - 30^{\circ}$ ) dies for the higher molecular weight Alathon 7030. There was a large amount of scatter in the 7050 measurements. Both the  $10^{\circ}$  and  $120^{\circ}$  entrance angle fibers exhibited notable positive expansion coefficients in orientation direction shortly before the melting range. This indicates that the extended chain crystals in these extrudates are somewhat unstable.

Possibly there is a relaxation (annealing) of the ultra-oriented morphology during extrusion. Such annealing would increase with slower extrusion rates (larger angles) and result in lower fiber orientation. This would explain why the high molecular weight HDPE reaches a maximum at smaller angles than the lower molecular weight HDPE. For a given molecular weight, the extrusion rate is faster the smaller the angle. This phenomenon is competing with the present contention that larger angles result in more efficient deformation.

#### F. Mechanical Testing.

Curves of Young's modulus, tensile stress at break, and tensile strain at break, each vs. entrance angle, all show a similar trend. There is a maximum at an entrance angle of  $20 - 30^{\circ}$  for the lower molecular weight strands followed by a decrease and levelling off. For the higher molecular weight strands, the curve is similar except the maximum occurs at an angle of  $14 - 20^{\circ}$ .

These data imply that the overall efficiency of the solid state deformation process depends on the molecular weight of the polymer as well as the capillary die entrance angle. Higher molecular weight polyethylene should be extruded through a smaller entrance angle die than lower molecular weight material if maximum deformation efficiency and physical properties are to be realized.

The type of fracture commonly observed during mechanical testing is shown in Figure 19. A fibrillar fracture surface is observed and the

load-elongation curves show that fibrils comprising the strands fracture stepwise as opposed to all breaking at once. The fibrillar morphology is shown at high magnification in Figure 20. These are scanning electron micrographs of ultra-oriented HDPE fractured along the orientation direction.

#### G. Elastic Hysteresis.

The elastic hysteresis, or energy dissipated through viscous heating during the stress-strain cycle, is a measure of the elasticity of the test specimen. Smaller values imply a more highly elastic material, while larger values indicate a more viscous material with consequently poorer tensile properties. The hysteresis curves in Figure 16 indicate that the fibers extruded through the  $10^0$  entrance angle (curve a) are less elastic than the strands extruded through other dies. The plot of energy dissipated vs. die entrance angle (Figure 17) shows that the 14, 20, and  $30^0$  entrance angles produce the most elastic extrudates followed by the 60, 90, and finally  $10^0$  angles. The relationship between dissipated energy and Young's modulus is shown in Figure 18 where one sees an inverse relationship between the two parameters. Higher modulus materials, which by definition exhibit greater elasticity at small strains, dissipate less energy during strain cycling. Less elastic materials of lower tensile modulus lose large amounts of energy during cyclic deformation, as shown in the plot. The Young's moduli reported herein were measured as the tangent to the 5th cycle hysteresis curve. Further cycling produces no change in moduli values, which increase to a steady-state value at 5 cycles.

### V. Summary

Optimum entrance angles for capillary dies used in solid state extrusion for HDPE vary with molecular weight. Other considerations such as extrusion temperature and type of polymer may well be equally important, as they may dictate the limiting shear and extensional stresses that the material can withstand before failing. A balance of shear and extensional forces is seen as important for the efficient deformation and chain unfolding necessary for high extrusion ratios and thus superior physical properties. The optimum condition is one where extensional strains are large and extensional stresses are minimized. However, shear forces must also be present for maximum deformation efficiency. The actual entrance angle where these conditions exist will vary with the material being extruded and with the extrusion conditions.

In conclusion, ultimate extrusion ratios increase and extrusion rates decrease with larger entrance angles. Deformation efficiency is seen to increase at larger angles but is probably counteracted somewhat by annealing effects caused by the slower extrusion rates at large entrance angles.



References

1. N. J. Capiati, S. Kojima, W. G. Perkins and R. S. Porter, J. Mater. Sci. 12, 334 (1977).
2. F. N. Cogswell, Polymer Eng. Sci. 12, 64 (1972).
3. D. M. Bigg, Polymer Eng. Sci. 16, 725 (1976).
4. M. T. Shaw, J. Appl. Polym. Sci. 19, 2811 (1975).
5. P. Predecki and W. O. Statton, J. Polym. Sci.-B, 10, 87 (1972).
6. A. E. Everage and R. L. Ballman, J. Polym. Sci.-B, 18, 933 (1974).
7. A. P. Metzger, C. W. Hamilton and E. H. Merz, S.P.E. Trans., p. 21, January, 1963.
8. K. Nakayama and H. Kanetsuna, Kobunshi Kagaku 30, 713 (1973).
9. K. Imada and M. Takayanagi, Intern. J. Polym. Mater. 2, 89 (1973).
10. H. L. D. Pugh, Ed., "Mechanical Properties of Materials Under Pressure," Elsevier, Amsterdam, 1970.
11. S. B. Ainbinder, M. G. Laka and I. Yu. Majors, Mekhanika Polimerov 1, 65 (1965).
12. K. D. Pae, D. R. Mears and J. A. Sauer, J. Polym. Sci.-B, 6, 773 (1968).
13. D. R. Mears, K. D. Pae and J. A. Sauer, J. Appl. Phys. 40, 4229 (1969).
14. S. Rabinowitz, I. M. Ward and S. S. C. Parry, J. Mater. Sci. 5, 29 (1970).
15. W. G. Perkins, N. J. Capiati and R. S. Porter, Polym. Eng. Sci. 16, 200 (1976).

16. R. S. Porter, N. E. Weeks, N. J. Capiati and R. J. Krzewki, J. Therm. Anal. 8, 547 (1975).
17. N. J. Capiati and R. S. Porter, J. Polym. Sci., Phys. Ed. 13, 1177 (1975).
18. C. W. Bunn and R. Daubeny, Trans. Faraday Soc. 50, 1173 (1954).
19. W. T. Mead, C. R. Desper and R. S. Porter, to be published.

TABLE I

ENTRANCE ANGLE	CRYSTALLINE MELTING POINT, °C	PERCENT CRYSTALLINITY
10°	136.3	77.5
14°	135.8	78.5
20°	136.0	79.5
30°	136.0	79.5
60°	136.3	81.5
90°	136.0	78.0
120°	135.0	74.5

Crystalline melting points and percent crystallinities for solid state extruded Alathon 7050 extruded through dies having entrance angles shown. Measurements made at ER = 10.

TABLE 2

ENTRANCE ANGLE	CRYSTALLINE MELTING POINT, °C	PERCENT CRYSTALLINITY
10°	137.5	71.0
14°	138.3	72.0
20°	137.0	72.0
30°	138.0	71.0
60°	137.5	71.3
90°	137.7	71.0
120°	136.8	68.3

Crystalline melting points and percent crystallinities for solid state extruded Alathon 7030 extruded through dies having entrance angles shown. Measurements made at ER = 10.



Captions for Figures

1. Schematic cross-sectional views of typical extrusion capillary dies showing tapered (conical) entrance region and relative volumes.
2. Extrusion rate vs. die entrance angle for two HDPE polymers;  $\overline{M}_w$ 's as shown.
3. Maximum deformation intensity vs. die entrance angle. See text for explanation.
4. Maximum extrusion length prior to fracture vs. die entrance angle for two HDPE polymers;  $\overline{M}_w$ 's as shown.
5. Extrusion ratio (ER) at fracture vs. die entrance angle for two HDPE polymers;  $\overline{M}_w$ 's as shown.
6. Birefringence vs. extrusion ratio for Alathon 7050 HDPE extruded through dies of various entrance angles.
7. Birefringence vs. extrusion ratio for Alathon 7030 HDPE extruded through dies of various entrance angles.
8. Negative linear expansion coefficient vs. die entrance angle for Alathon 7050 HDPE. Measurements made at ER = 20.
9. Negative linear expansion coefficient vs. die entrance angle for Alathon 7030 HDPE. Measurements made at ER = 20.
10. Young's modulus vs. die entrance angle for Alathon 7050 HDPE. Measurements made at ER = 24.
11. Young's modulus vs. die entrance angle for Alathon 7030 HDPE. Measurements made at ER = 24.

12. Tensile strength at break vs. die entrance angle for Alathon 7050 HDPE. Measurements made at  $ER = 24$ .
13. Tensile strength at break vs. die entrance angle for Alathon 7030 HDPE. Measurements made at  $ER = 24$ .
14. Strain at break vs. die entrance angle for Alathon 7050 HDPE. Measurements made at  $ER = 24$ .
15. Strain at break vs. die entrance angle for Alathon 7030 HDPE. Measurements made at  $ER = 24$ .
16. Strain-cycling curves for (a) HDPE extruded through a  $10^0$  entrance angle die and (b) HDPE extruded through dies of all other angles.
17. Energy dissipated vs. die entrance angle for two HDPE polymers;  $\overline{M}_w$ 's as shown. For explanation see text.
18. Energy dissipated vs. Young's modulus for two HDPE polymers;  $\overline{M}_w$ 's as shown. For explanation see text.
19. Typical fracture surface of solid state extruded HDPE, broken in a stress-strain tensile test.
20. SEM photographs of solid state extruded HDPE, peeled under liquid nitrogen. Orientation direction horizontal. Upper: magnification 1,000X. Lower: magnification 11,000X.
21. Schematic stress-strain curve of typical solid state extruded HDPE fiber.

Cross-Sections for Brass Capillaries 0.052" D x 0.39" L  
Identical Dimensions Except for Entrance Angle,  $2\alpha$

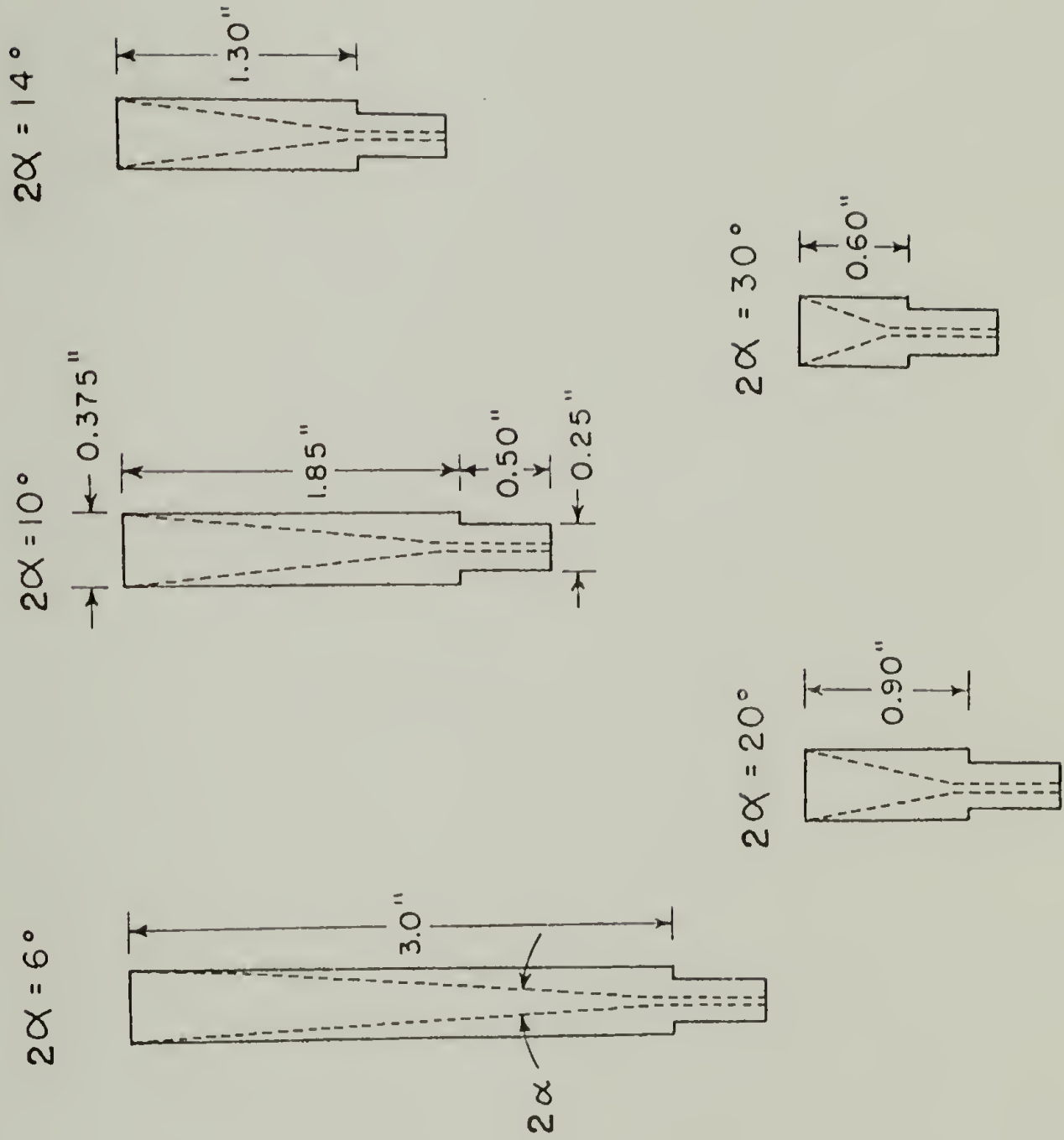


Figure 1

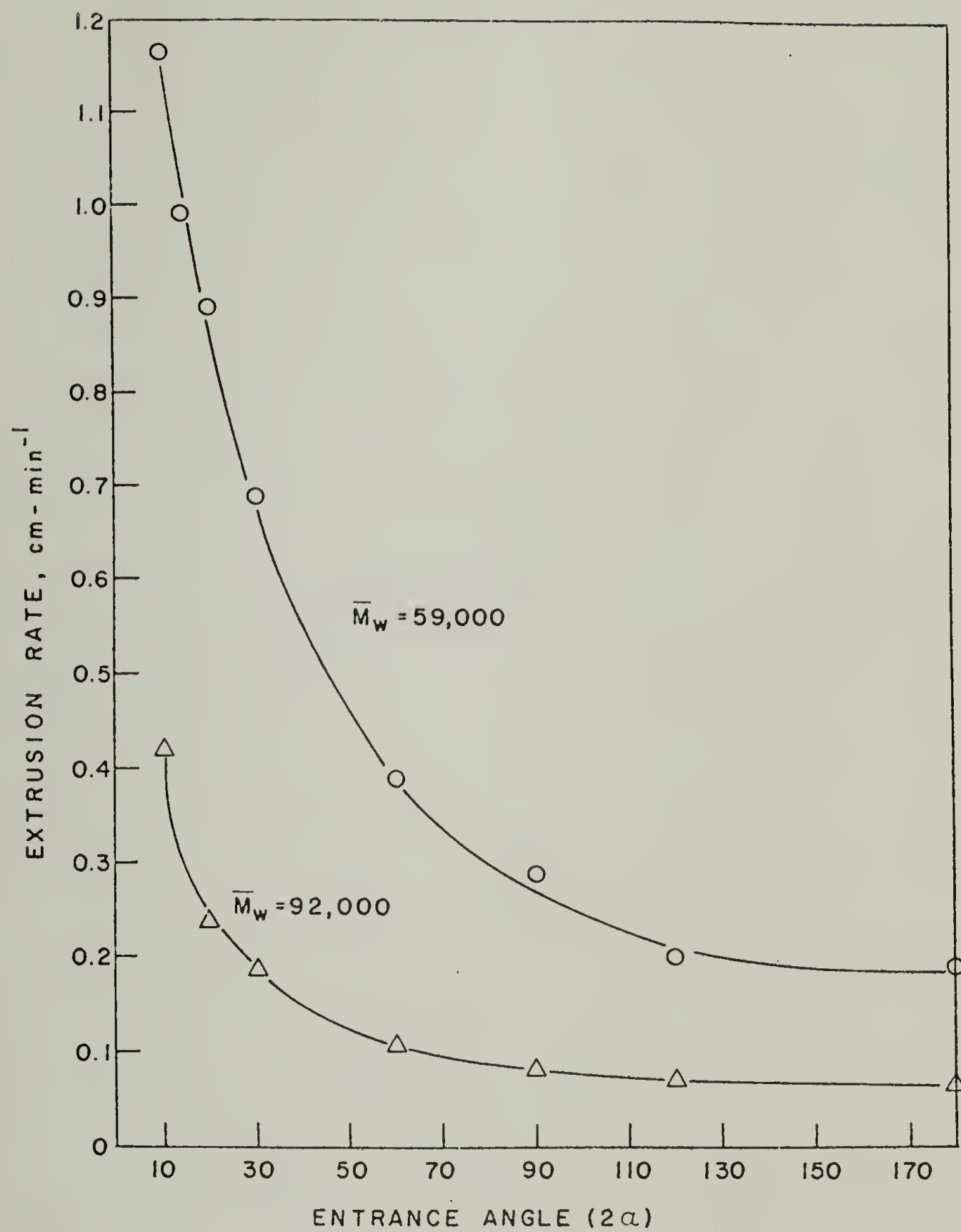


Figure 2



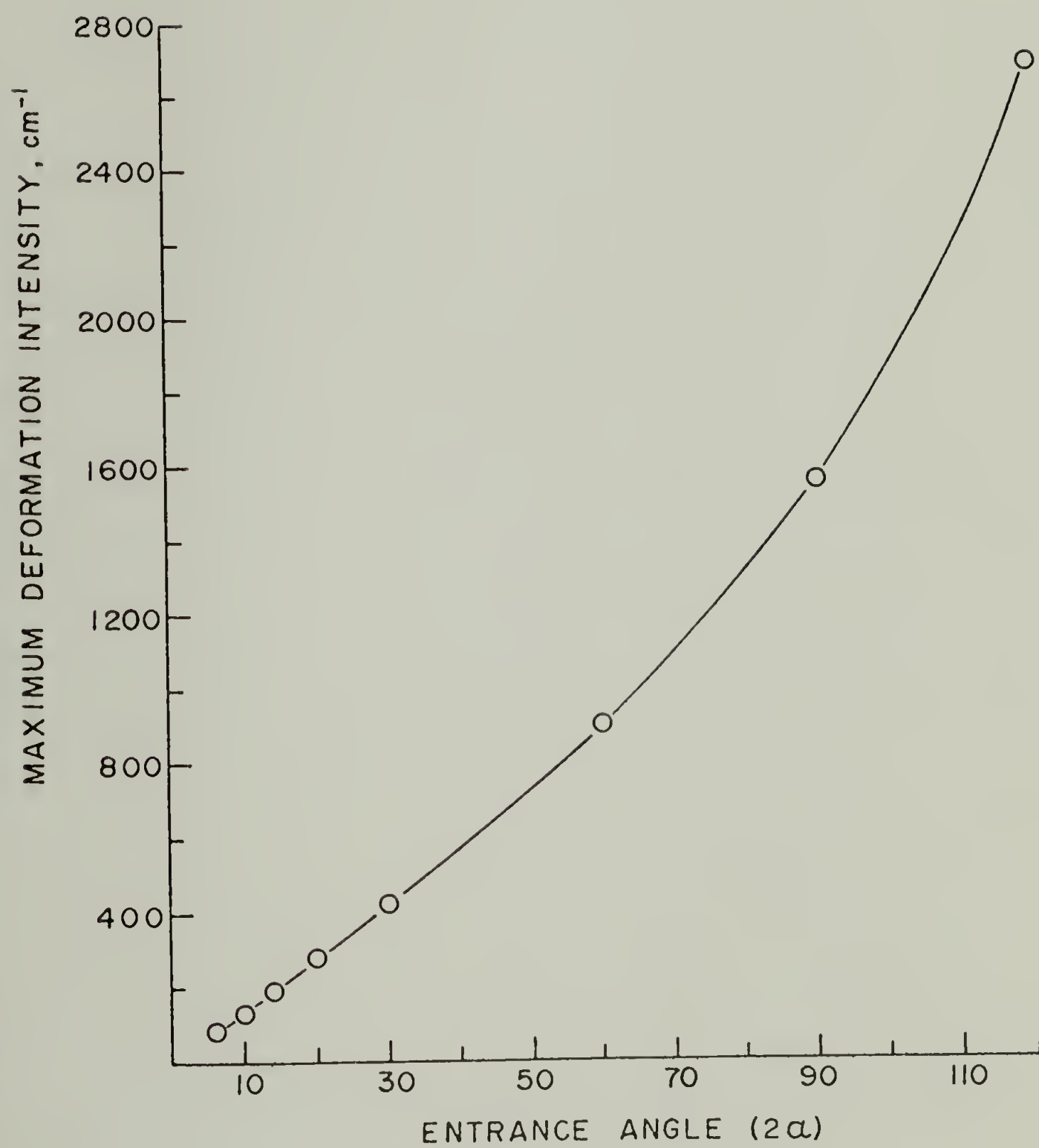


Figure 3

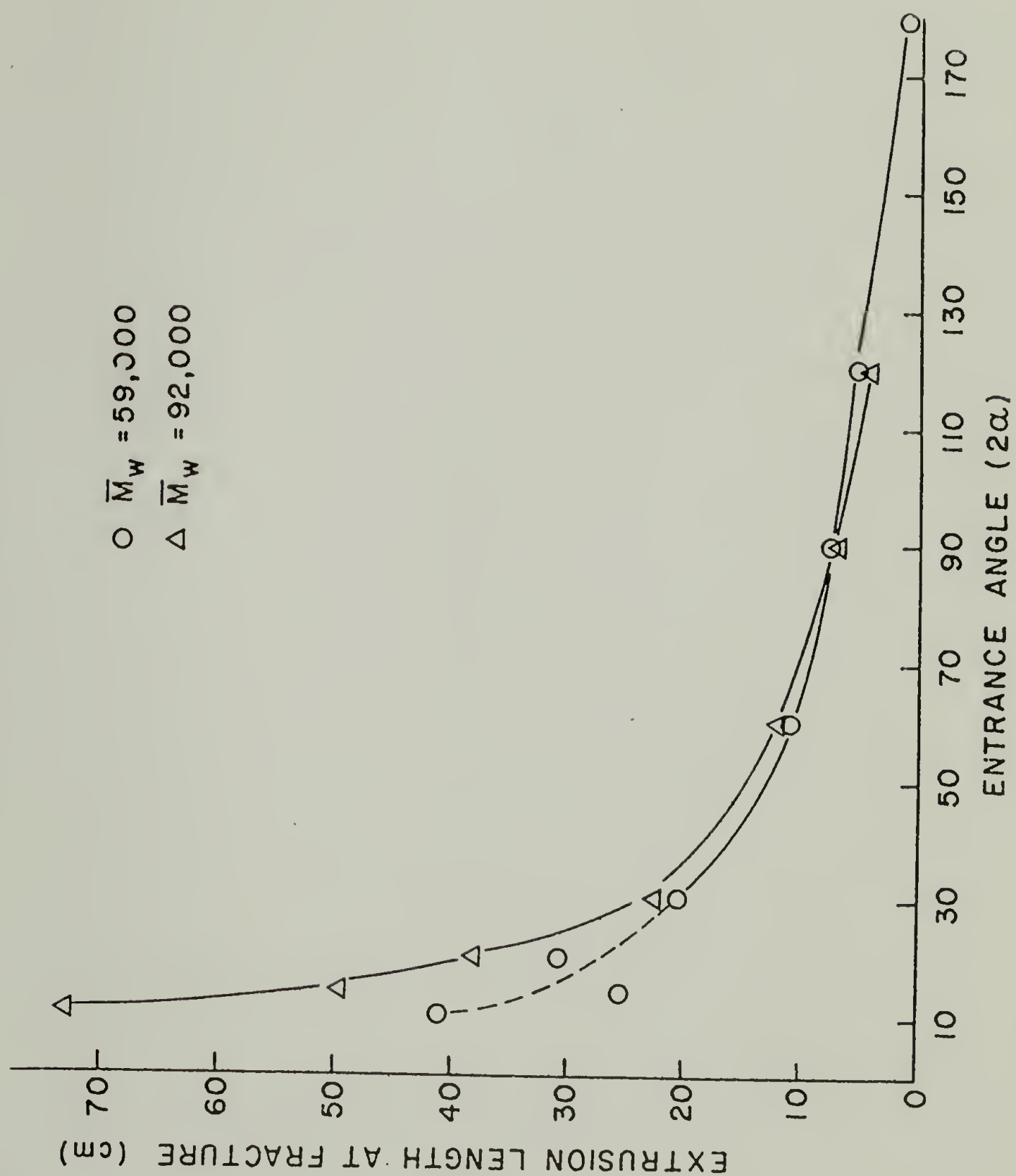


Figure 4

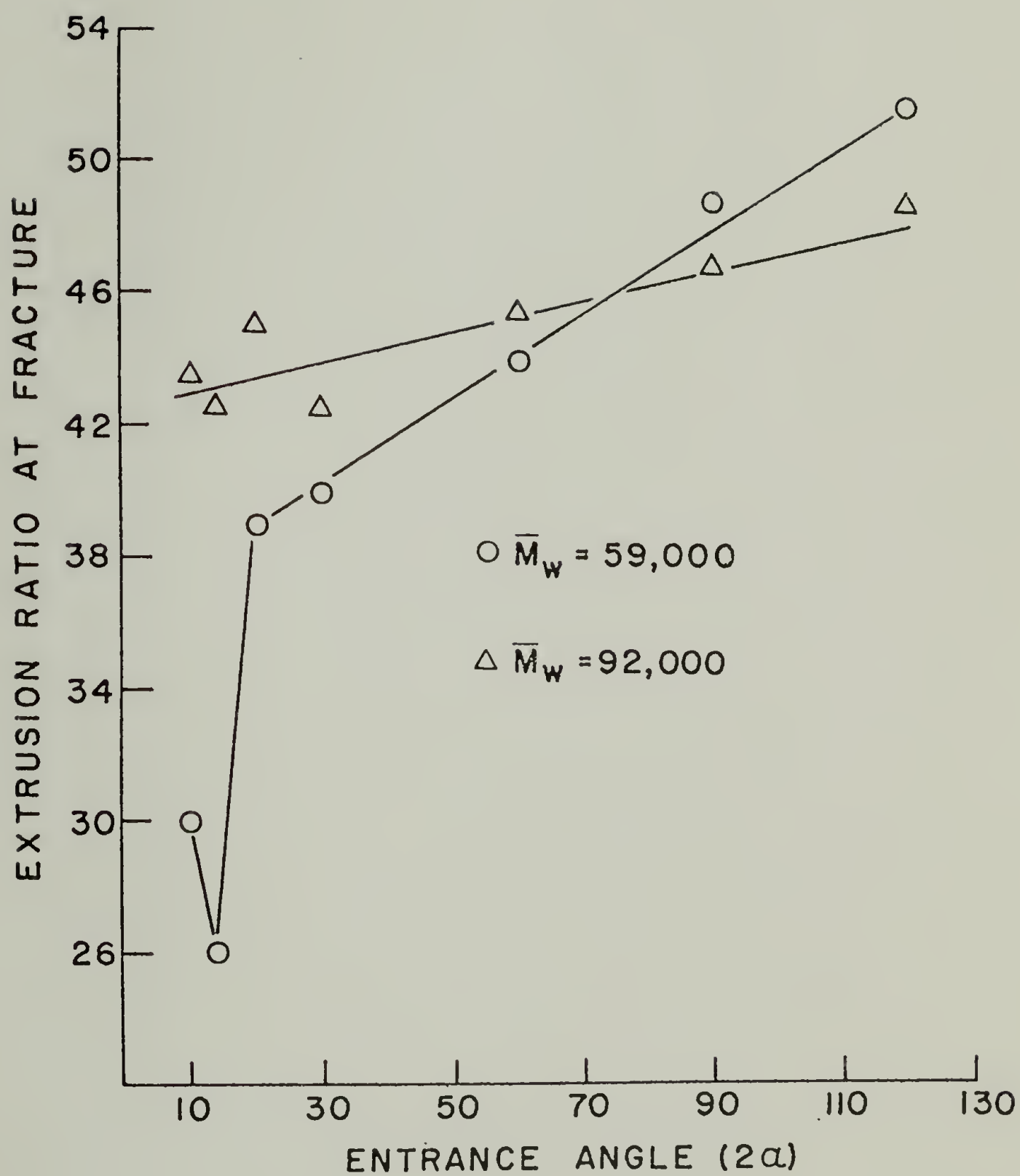


Figure 5

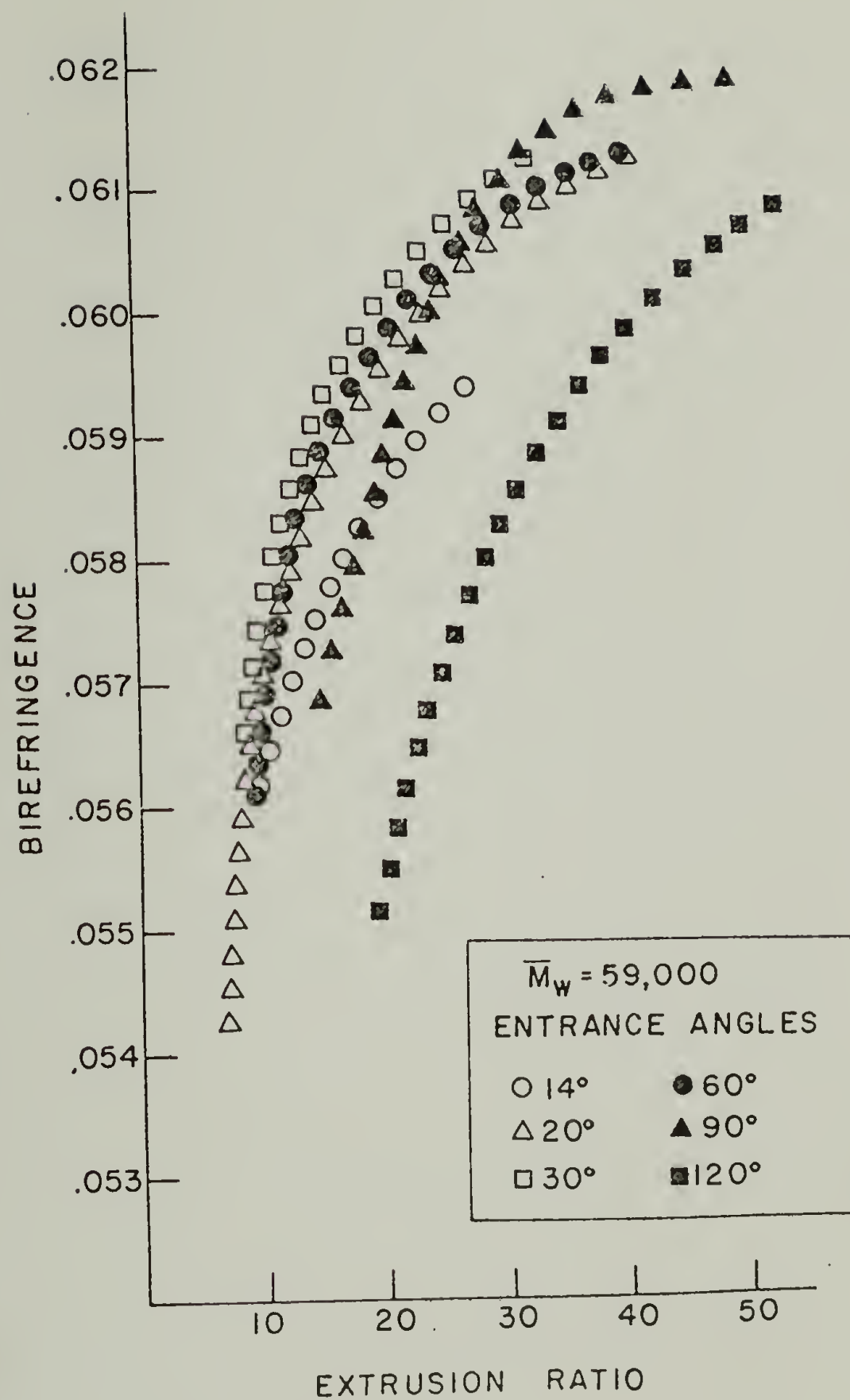


Figure 6



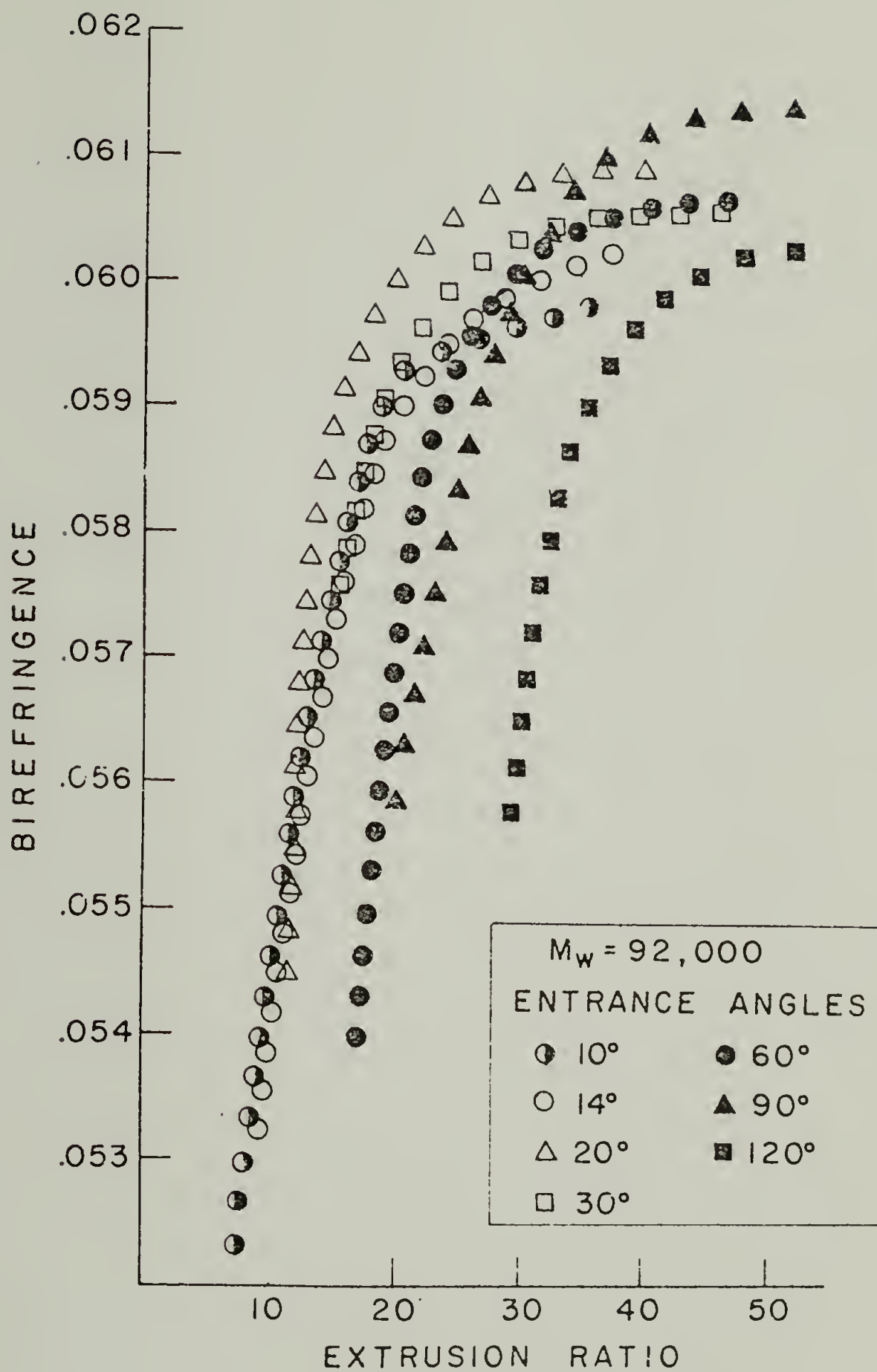


Figure 7

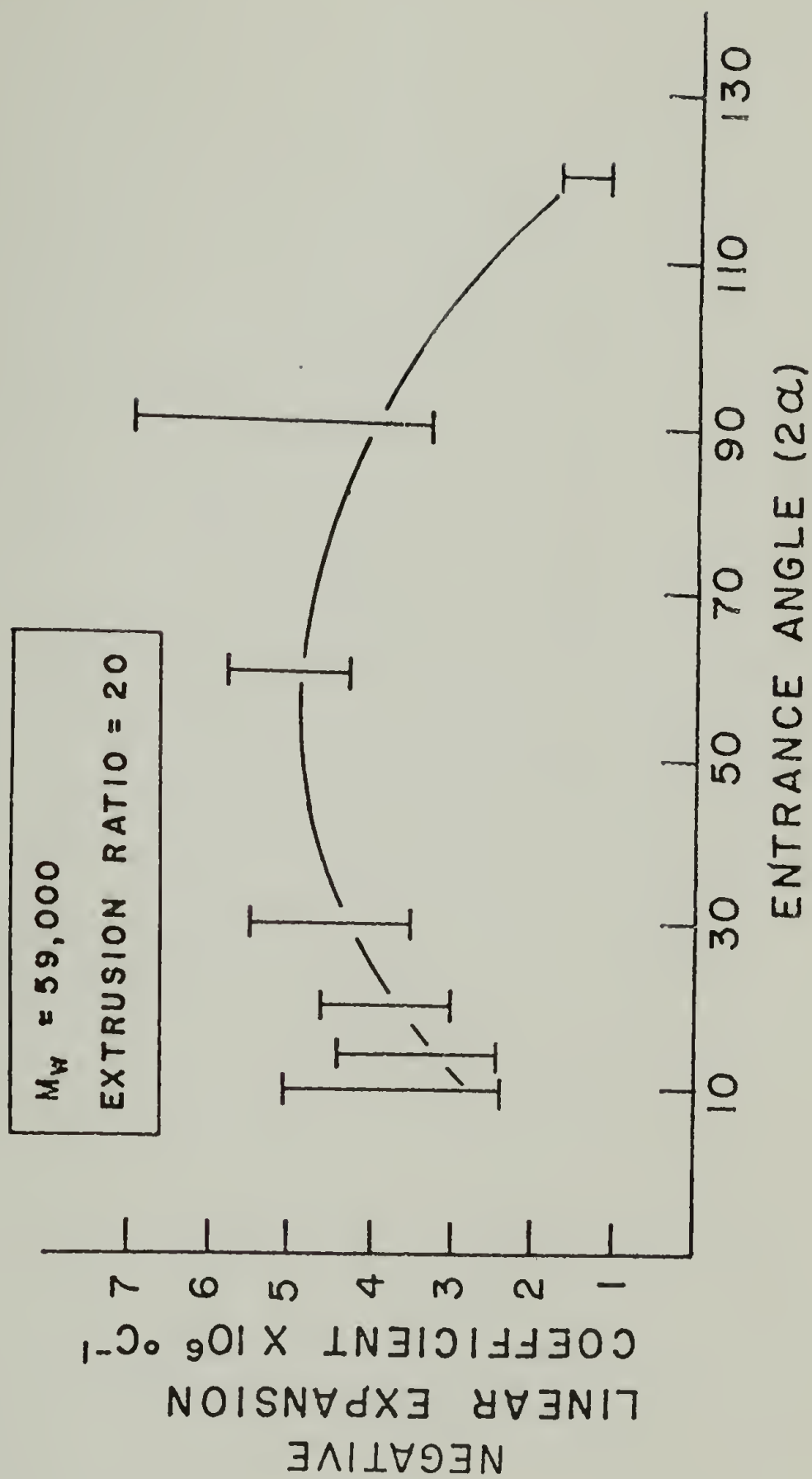


Figure 8

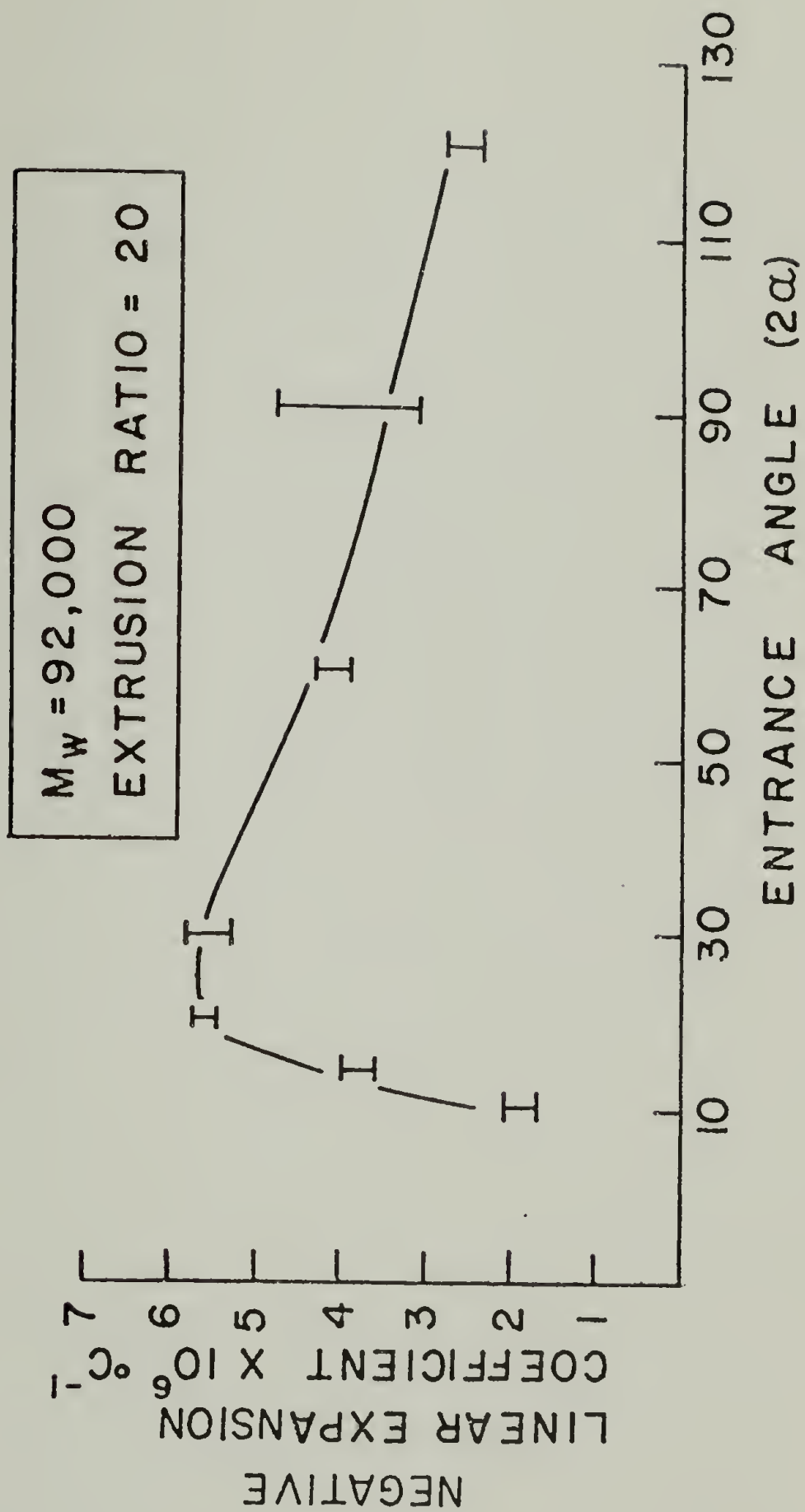


Figure 9

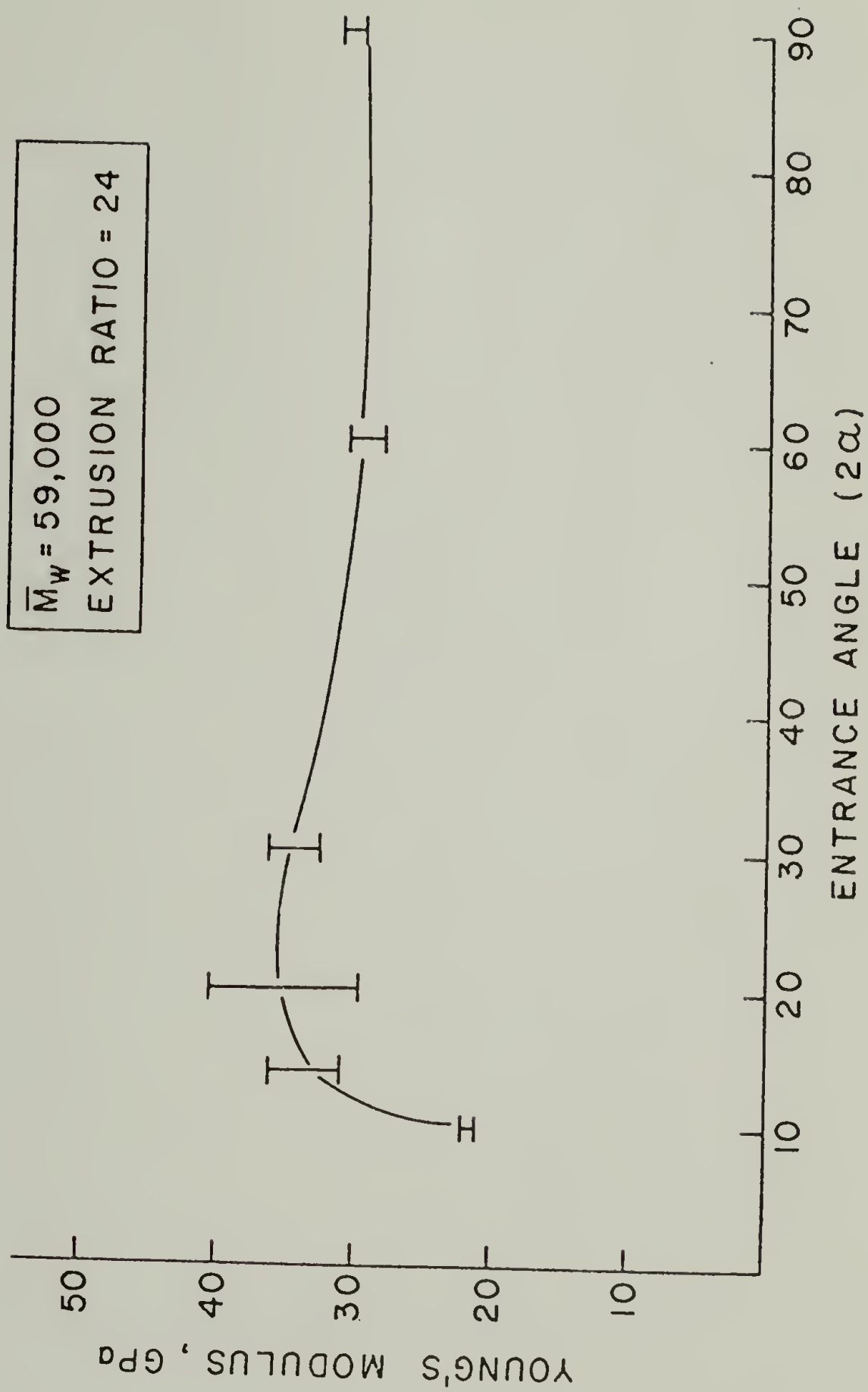


Figure 10



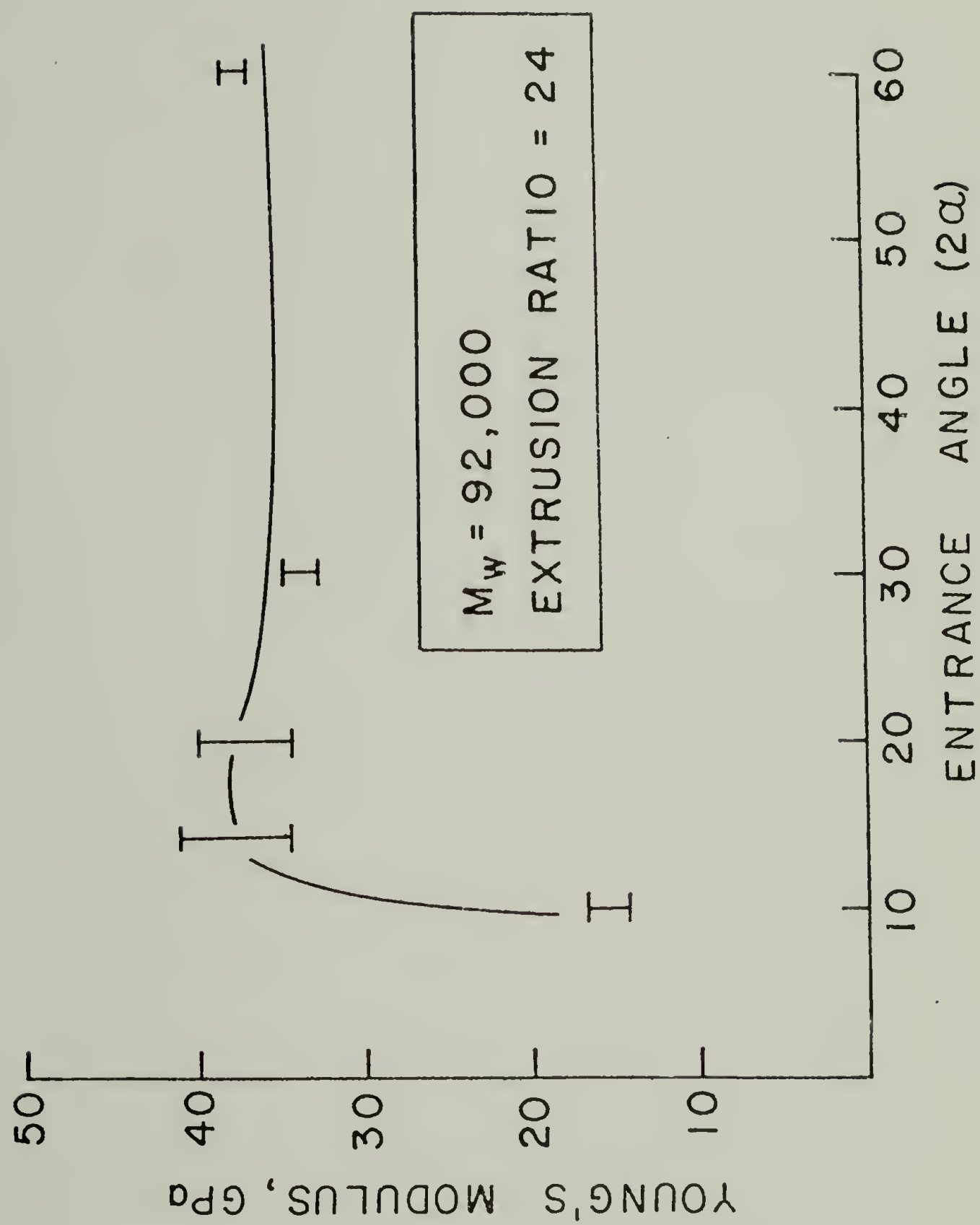


Figure 11

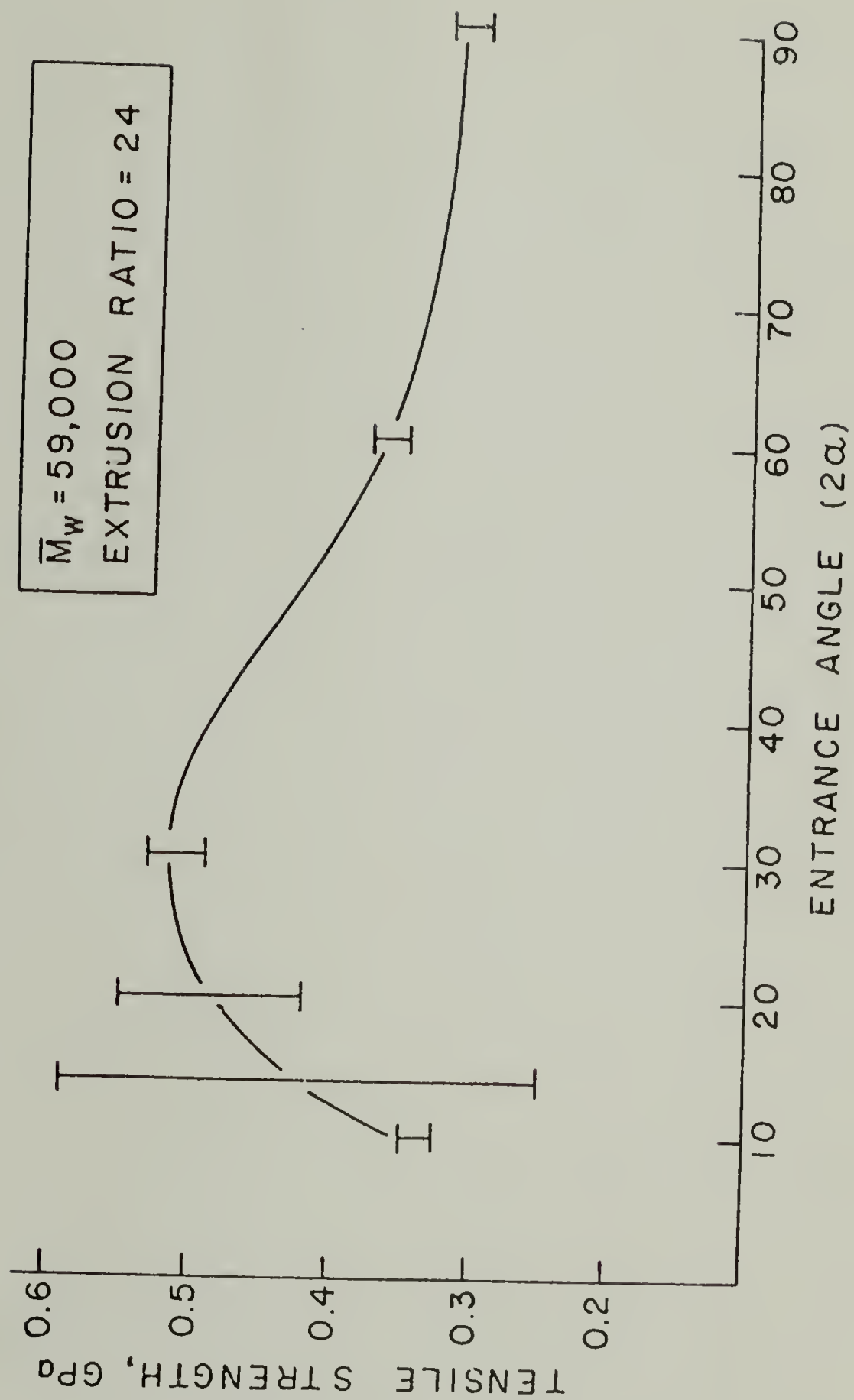


Figure 12

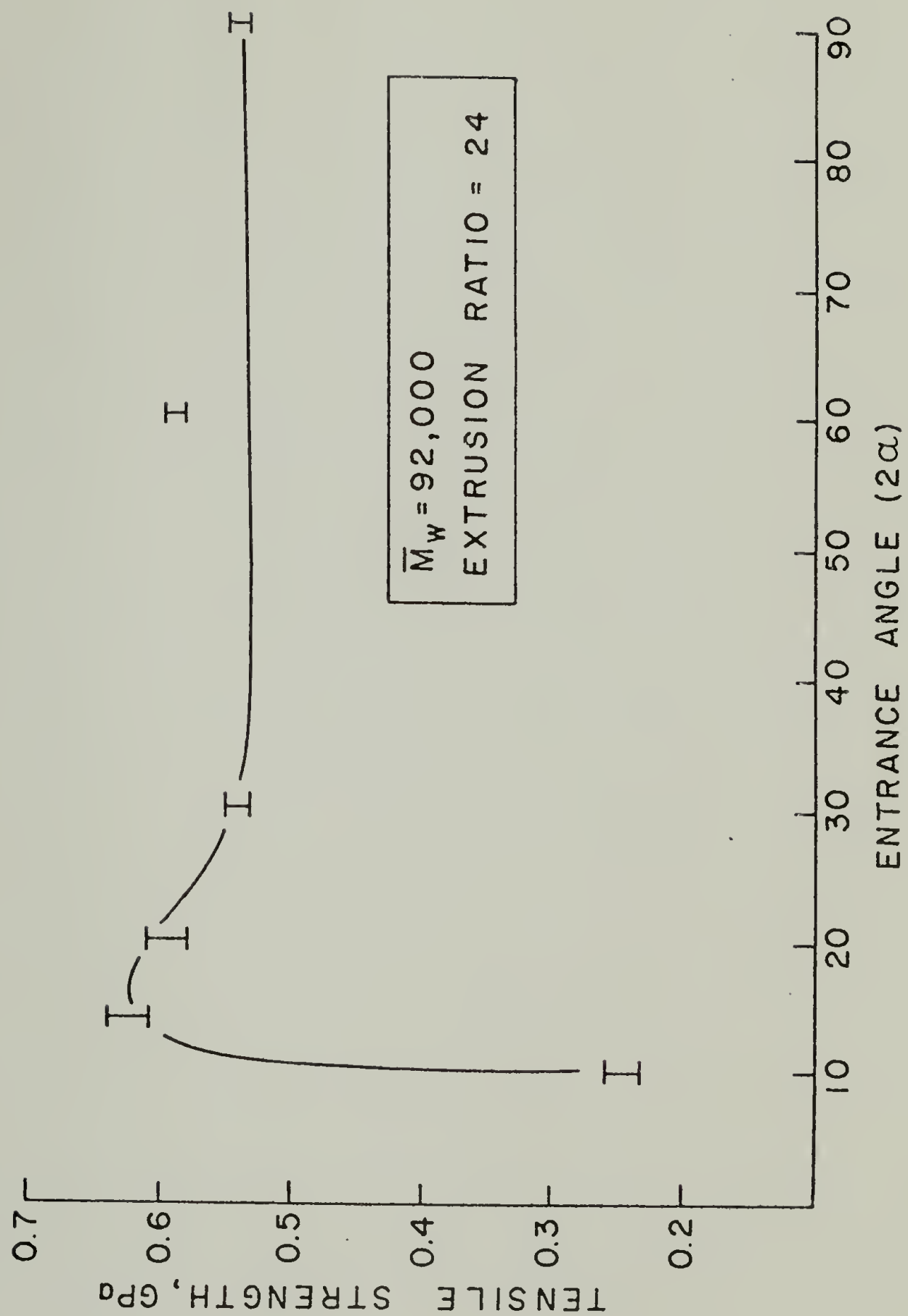


Figure 13

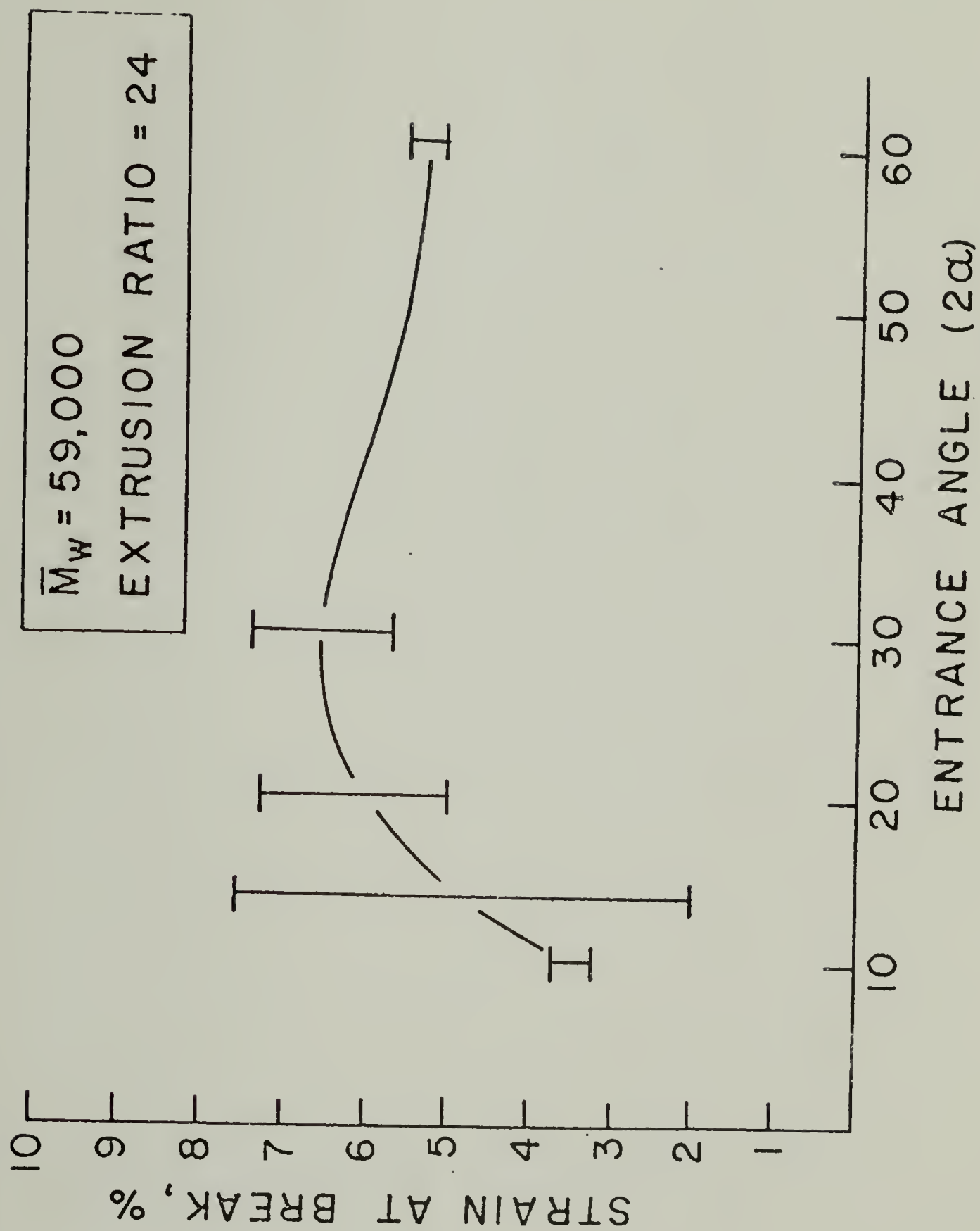


Figure 14



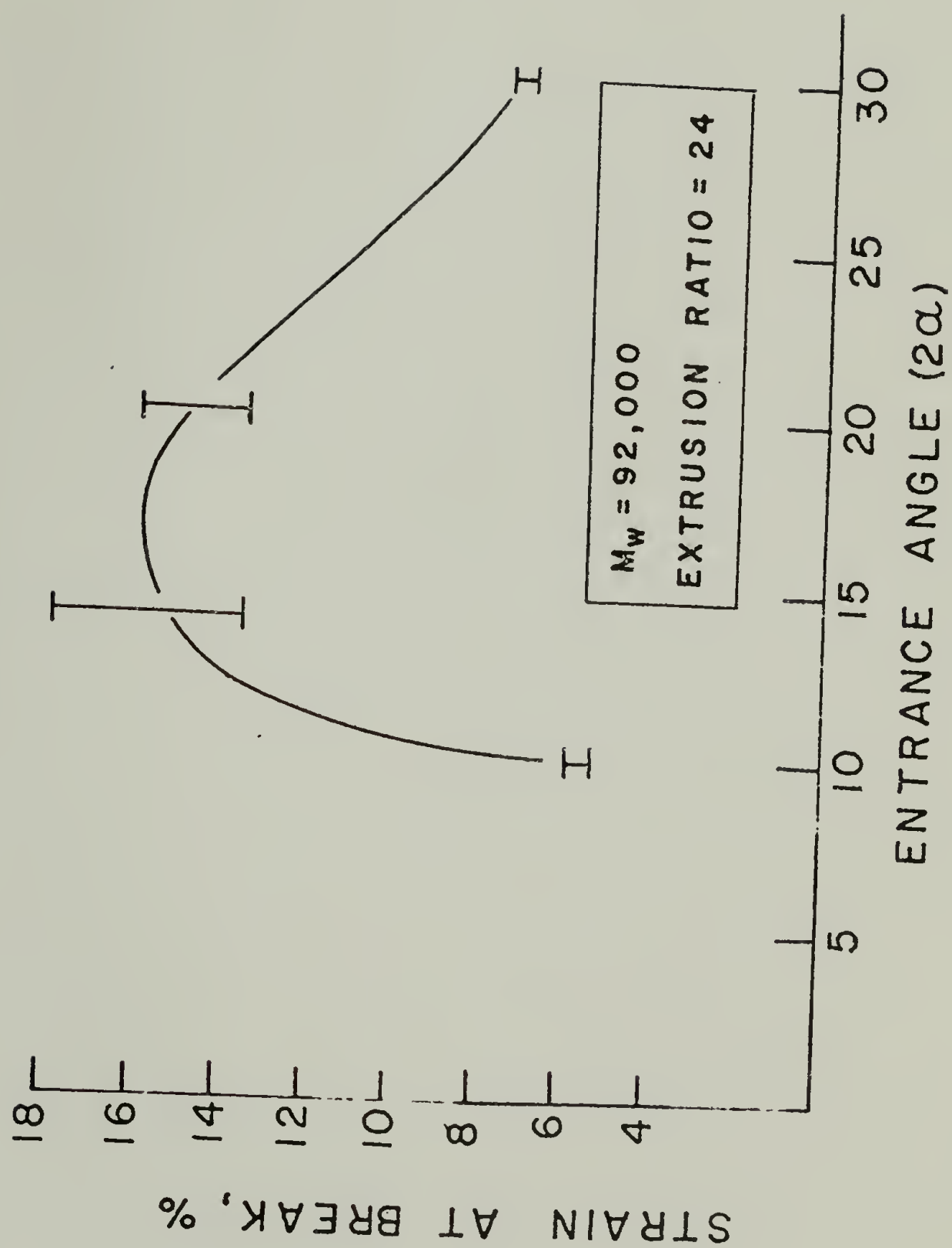


Figure 15

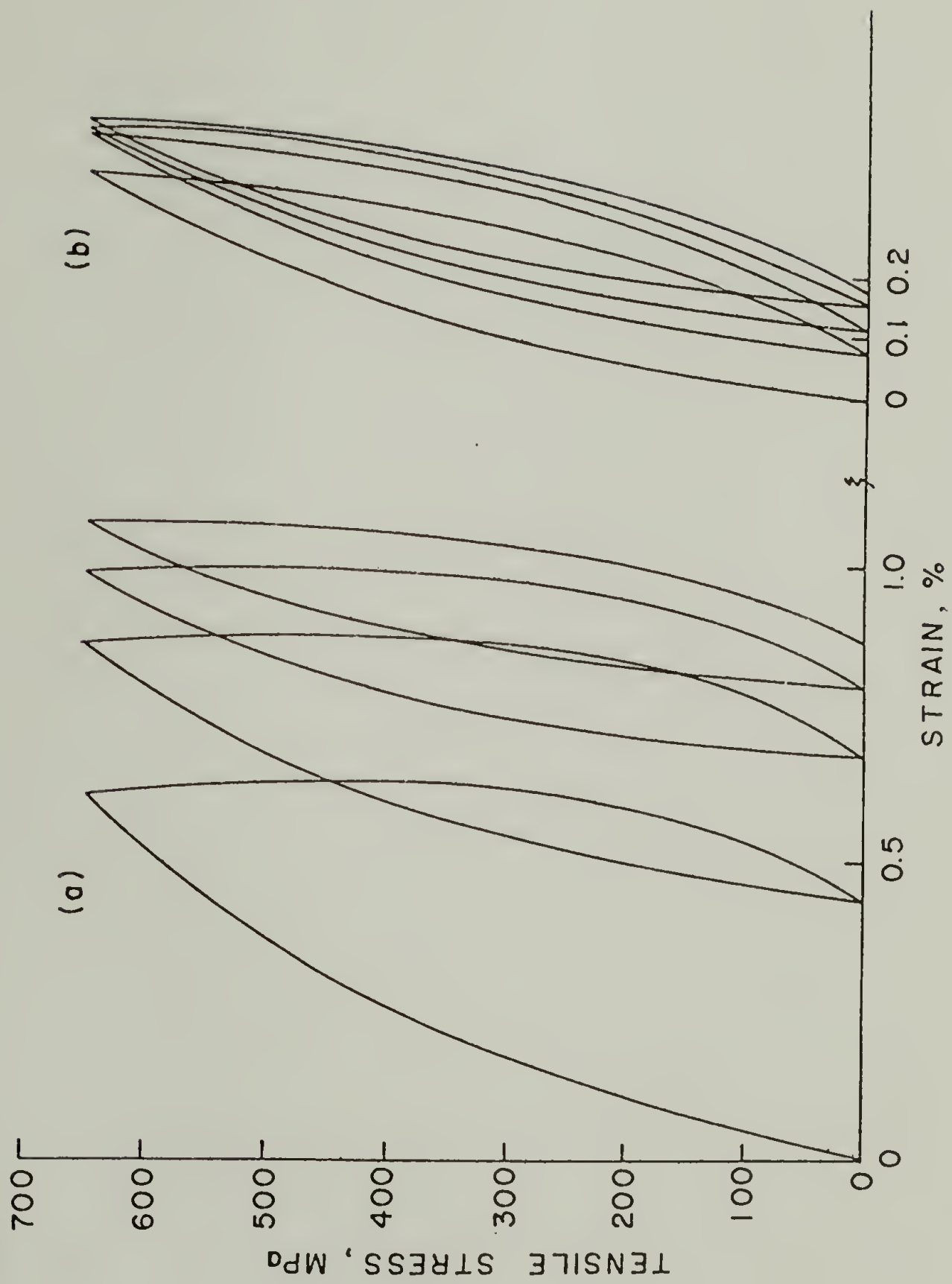


Figure 16

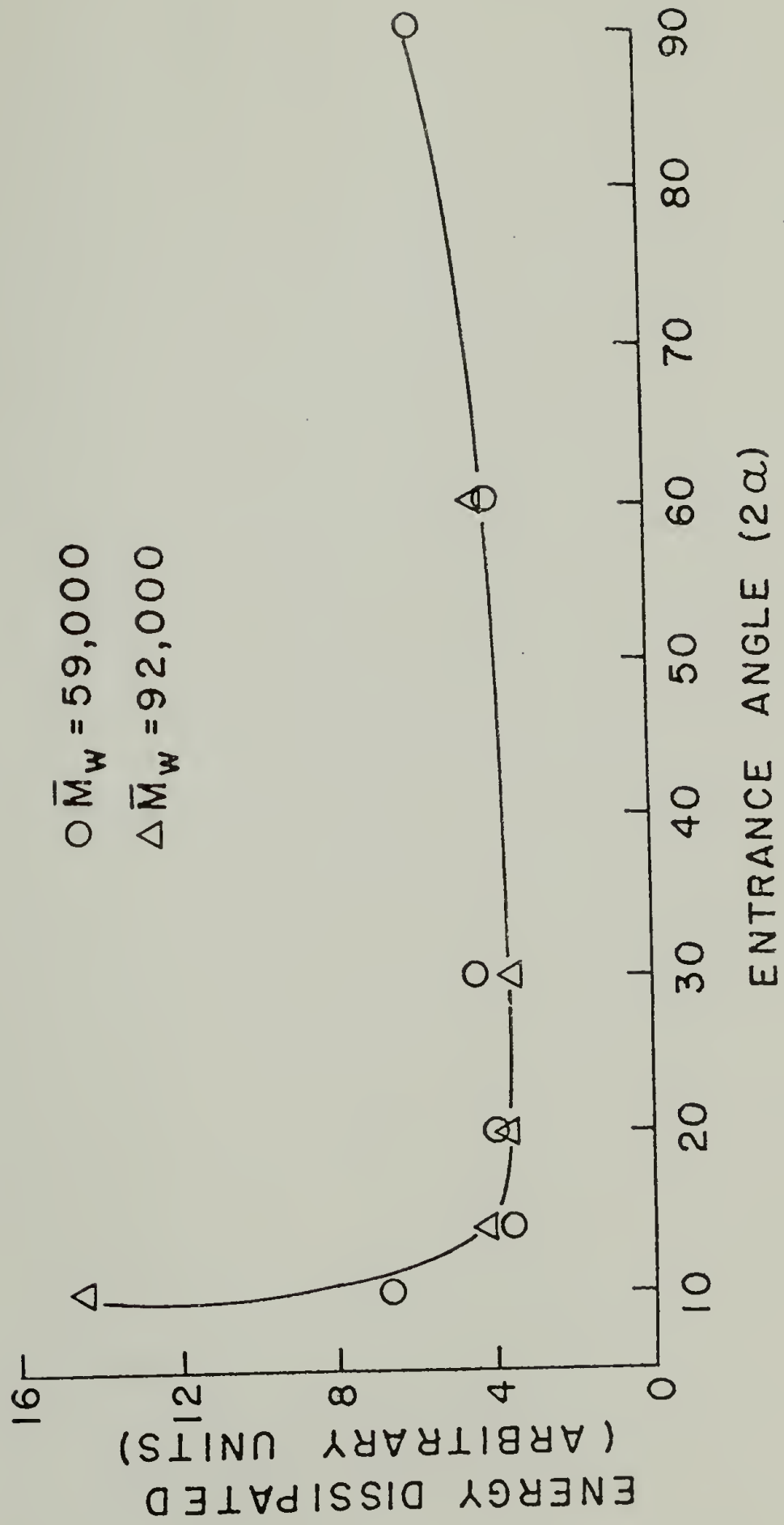


Figure 17

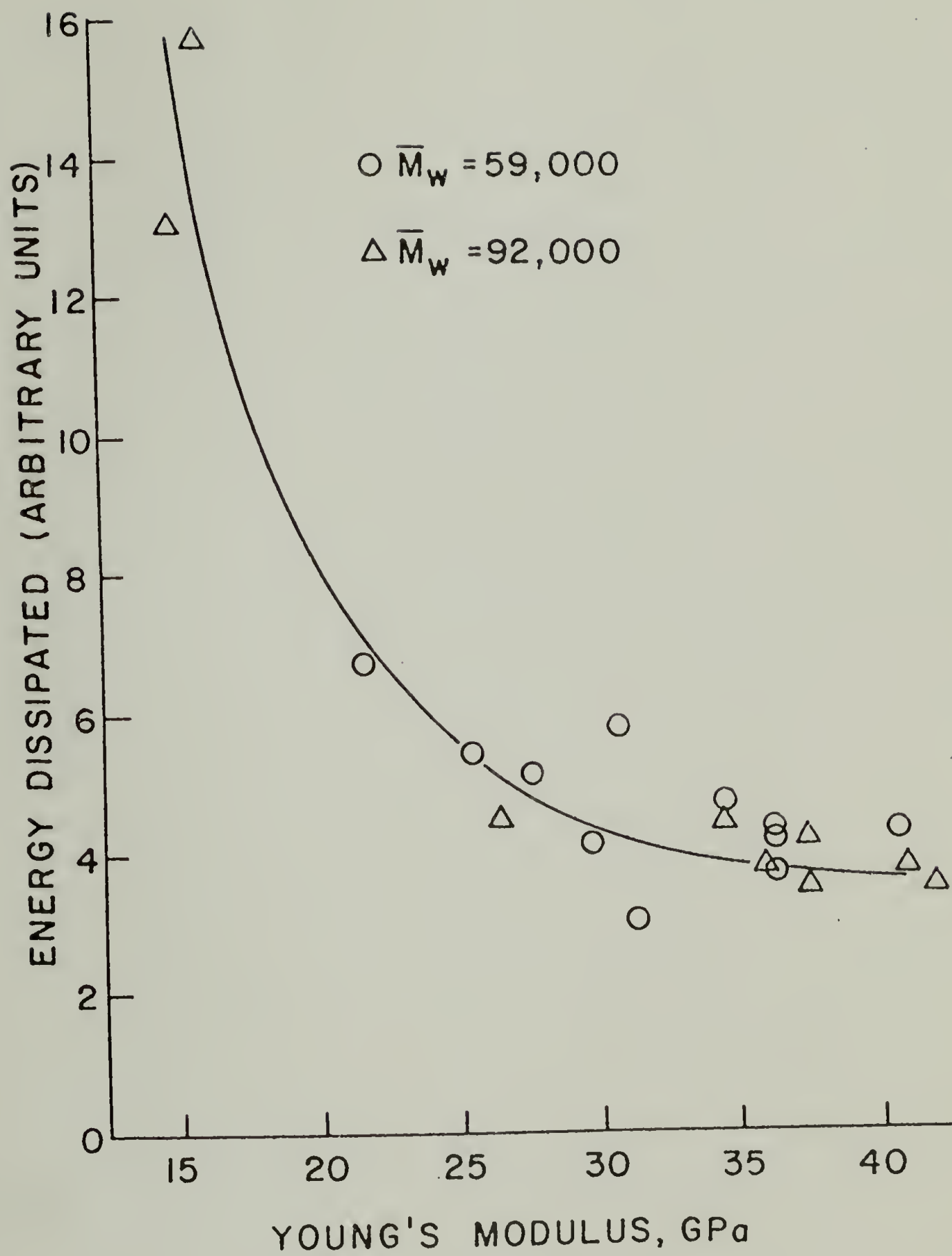


Figure 18





Figure 19



a.

 $\overline{\quad}$   
1  $\mu$ 

b.

 $\overline{\quad}$   
1  $\mu$ 

Figure 20

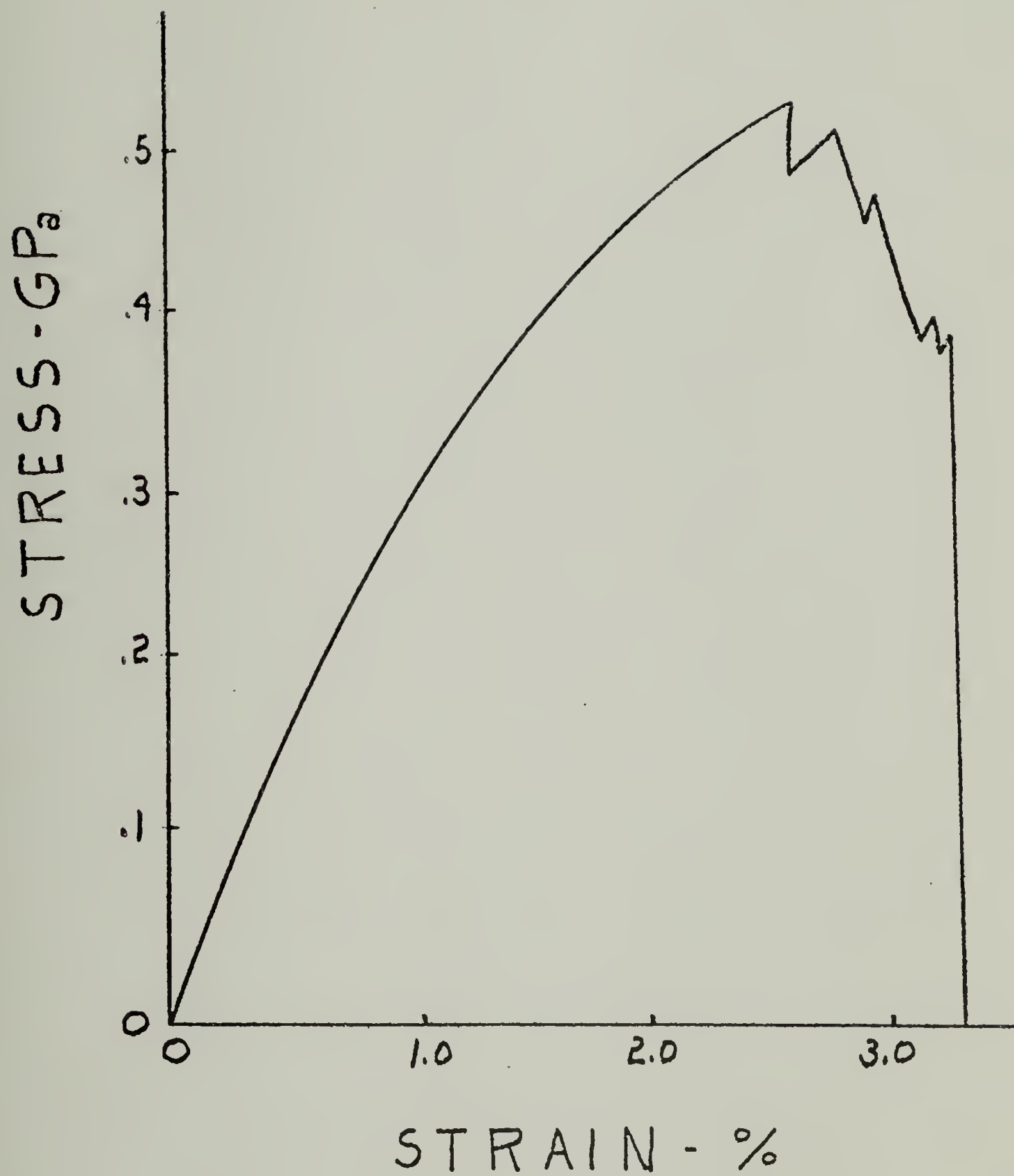


Figure 21

## C H A P T E R   I V

### THE EFFECT OF MOLECULAR WEIGHT ON THE PHYSICAL AND MECHANICAL PROPERTIES OF ULTRA-DRAWN HIGH DENSITY POLYETHYLENE

#### I. Introduction

During the past several years considerable effort has been spent studying the mechanism and properties of cold-drawn semicrystalline polymers and, in particular, polyethylene (1-5). This has led to a plausible model for the morphological changes on cold drawing (6,7). Models entail the transformation of spherulites into microfibrils consisting of folded chains, amorphous regions and tie molecules. The tie molecules may be appreciably extended and at least partially crystalline and as such have been called "continuous crystals" (8). The amount of chain extension depends on the magnitude and conditions of drawing. The cold extrusion process used here, which has similarities to conventional cold drawing, involves first crystallization and then extrusion of the polymer under high pressure and at a temperature below its melting point. Such a process has been developed in this laboratory (9-12) and is believed to produce a significant fraction (~ 15 percent) of extended-chain crystals (13-15). Other workers (16-21) have produced related morphologies by variations of the cold-drawing process. Ward and coworkers (17-19) have obtained interesting results by investigating different molecular weights of high density polyethylene (HDPE) drawn somewhat less than the samples used in the present study. Here we present new data concerning the effect



of molecular weight on the physical and mechanical properties of ultra-drawn HDPE which help explain the predicted morphology of such materials and the corresponding remarkable properties.

## II. Experimental

The fibers evaluated in this study were prepared by a cold extrusion process using an Instron capillary rheometer (9-12). This method involves high pressure crystallization of the polymer near its ambient melting point and subsequent extrusion in the semicrystalline state (24). The process is known to produce highly oriented, optically clear films and fibers of high density polyethylene (9-12). The extrusion temperature and pressure were  $134^{\circ}\text{C}$  and 2.4 kbar. A brass capillary having a  $20^{\circ}$  included entrance angle, 1.5 cm length, 0.132 cm diameter and a nominal draw ratio of 52, was employed throughout the study. The actual average draw ratios will be less due to portions of the strand coming from the lower region of the capillary entrance cone. The draw ratio was calculated as the ratio of cross-sectional areas of the rheometer barrel to the straight portion of the capillary. For convenience, fibers were produced in lengths of about 35 cm with extrusion times varying from ~ 20 min. for Alathon 7050 to about 3 hrs. for Alathon 7026. The four polymers used in this investigation were from DuPont's Alathon 7000 series HDPE resins, with average molecular weights and distributions as shown in Table 1. The molecular weight averages used in this study were those determined by GPC at Chalmers University, Sweden.

Melting curves were determined by differential scanning calorimetry (DSC) using a Perkin-Elmer model DSC-1B. Single, sharp peaks were obtained

consistent with the results of Southern and Porter (9) and of Harland, Khadr and Peters (22), also for highly drawn polyethylene. Heating rates were varied from 0.625 to  $20^{\circ}\text{C min.}^{-1}$  and peak melting points were extrapolated to zero rate. The pellets of virgin HDPE were all subjected to the same thermal treatment and crystallization conditions. They were initially heated to  $182^{\circ}\text{C}$  and then cooled to  $75^{\circ}\text{C}$  at  $20^{\circ}\text{C min.}^{-1}$ , then, after each run, were cooled from 147 to  $75^{\circ}\text{C}$  at  $20^{\circ}\text{C min.}^{-1}$ . The degree of crystallinity for both the virgin and extruded HDPE was obtained from the areas under the melting curves following calibration of the DSC with indium. The coefficients of expansion measurements were made on a TMS-1 thermomechanical analyzer attachment for the Perkin-Elmer DSC-1B. Sample preparation and experimental details for these tests were as reported by Porter, et al. (23).

For studies of the fiber mechanical properties, an Instron tensile testing machine, model TTCM, equipped with a strain-gauge extensometer, was used. Load-elongation curves were obtained at room temperature using a fixed elongation rate of  $0.05 \text{ cm. min.}^{-1}$  for modulus measurements and  $0.50 \text{ cm. min.}^{-1}$  for determination of tensile strength and strain to break. The fibers had to be gripped by special clamps described elsewhere (24) to prevent slippage in the jaws. The Young's modulus was determined as the tangent to the stress-strain curve at a strain level of 0.1 percent. Values of moduli, tensile strength and breaking strain presented here represent averages of from 8 to 14 samples at each molecular weight tested. The values for modulus have a standard deviation of  $\pm 0.58$ . The range of tensile strength values can be seen in Figure 3, while those of ultimate strain are presented in Figure 4.

### III. Results and Discussion

#### A. Melting Point and Degree of Crystallinity.

The melting point of the virgin pellets of different molecular weight HDPE extrapolated to zero scanning rate was found to be  $131.4^{\circ}\text{C}$  as shown in Figure 1. Each point represents the four molecular weights investigated. The apparent melting point rose with increasing scanning rate to  $133.6^{\circ}\text{C}$  at  $20^{\circ}\text{C min.}^{-1}$ . Since the pellets are assumed to consist of folded-chain crystals which do not appreciably superheat (25,26), the increase in melting point is attributable to a lag in response between sample and instrument. Thus, such curves were used, see Figure 1, to calibrate the melting of fibers which were of similar size and geometry in order to evaluate possible superheating effects due to extended-chain crystals. That such superheating is present can be seen qualitatively from the greater slope of the fiber curves which is consistent with the presence of extended-chain crystals (13). Any differences between individual fiber curves are likely masked by the spread of data. The peak melting point of the fibers increased with molecular weight from  $136.2^{\circ}\text{C}$  for HDPE (7050) to  $139.4^{\circ}\text{C}$  for the highest molecular weight HDPE (7026), all values extrapolated to zero scanning rate. If the extended-chain crystal content is equal for all four samples, something else must be responsible for raising the melting point of the higher molecular weight samples. Figure 2, a plot of degree of crystallinity ( $X_c$ ) vs. molecular weight, indicates that for the original pellets,  $X_c$  (as measured from heat of fusion) decreases linearly with increasing molecular weight. This is believed to result from the difficulty of long polymer chains to efficiently pack into a



crystal lattice. At high molecular weights, different parts of the same chain probably crystallize into separate folded-chain lamellae which are joined by stressed portions of the molecule. These stressed portions are known as tie chains, which can become extended during cold-drawing to form extended-chain crystals. With the extruded fibers, however,  $X_c$  (as shown in Figure 2) remains nearly constant. Therefore, one may conclude that the type, and not the amount, of folded-chain crystals varies with molecular weight. Lower molecular weight fibers have higher orientation (27) but less perfect folded-chain crystals due to a greater concentration of end group defects (28). Therefore,  $X_c$  can be constant while the melting point increases with molecular weight. The latter can occur because the drastic alteration of intramolecular structure associated with melting is facilitated in a crystal system containing more defects (chain ends). In other words, such "defective" crystals constitute a less thermodynamically-stable system (29) with a subsequently lower melting point. This idea of chain ends not being able to pack into a regular crystalline lattice was set forth in an early work by Flory (30).

#### B. Coefficient of Expansion.

Measurement of the coefficient of thermal expansion in the direction of the fiber (C axis) yielded the results shown in Table 2. Two values were obtained for each molecular weight:  $\alpha_1$  is the coefficient for the temperature range  $-130$  to  $-54^\circ\text{C}$  and  $\alpha_2$  is the coefficient measured from  $-48$  to  $60^\circ\text{C}$ . Expansion coefficients were determined by drawing a tangent to the thermogram over each temperature range, followed by the determination of the slope and division by sample length. At a temperature of  $-51^\circ\text{C} \pm 3^\circ$  a



distinct change in slope was noted on the plots of  $\Delta L$  vs.  $T$ , the change in sample length vs. temperature, indicating a transition of some type as previously noted (23). The value of  $\alpha_1$  averaged  $-7.06 \times 10^{-6} \text{ }^\circ\text{C}^{-1}$  and  $\alpha_2$  averaged  $-10.4 \times 10^{-6} \text{ }^\circ\text{C}^{-1}$ . Previous unpublished work done in this laboratory resulted in an  $\alpha_1$  of  $-7.3 \times 10^{-6} \text{ }^\circ\text{C}^{-1}$  and an  $\alpha_2$  of  $-10.6 \times 10^{-6} \text{ }^\circ\text{C}^{-1}$  for the temperature ranges  $-140$  to  $-45^\circ\text{C}$  and  $-45$  to  $70^\circ\text{C}$ , respectively. Three or four samples of each molecular weight were tested and the resulting  $\alpha$  values averaged to give the  $\alpha$  values in Table 2. It is believed that extended-chain crystals are responsible for the negative expansion coefficient (23). Since these values remain nearly constant with increasing molecular weight, increasing molecular weight apparently has no significant effect on the content of extended-chain crystals in highly-drawn fibers of high density polyethylene.

### C. Modulus, Tensile Strength, and Strain to Break.

It was found, see Table 3, that the Young's modulus of the strands was essentially independent of molecular weight over the range investigated. If the modulus of ultra-drawn fibers increases with increasing extended-chain crystal content and is solely dependent on such content, the latter is again indicated not to vary with molecular weight. The ultimate tensile strength increased linearly with molecular weight (Figure 3). These results support the theory that an increase in molecular weight leads to an increase in the number of intercrystalline tie chains which run both longitudinally in each microfibril as well as laterally between the microfibrils, giving cohesion to the system. Because these tie molecules are not fully extended, they do not contribute to the modulus values at low strains ( $< 1$  percent).

However, on greater elongation, as in the tensile strength test, they become extended and help prevent the microfibrils from slipping with respect to each other, thus increasing the fiber tensile strength. The fact that one can increase the tensile strength of such fibers without sacrificing modulus is a benefit of the cold-extrusion process, as mentioned by Frank (31). The ultimate elongation, plotted as strain to break in Figure 4, shows a decided increase with increasing molecular weight. This again is likely due to the greater number of non-extended intercrystalline tie chains linking the microfibrils and resisting the separation of the latter which leads to fracture. The fibers made from lower molecular weight HDPE would contain fewer and shorter intercrystalline tie chains, resulting in less extension before the breaking stress is reached.

#### IV. Conclusions

The data presented here have led to several conclusions regarding ultra-drawn polyethylene fibers. (1) Higher molecular weight polyethylenes give higher strength fibers while having no apparent effect on the Young's modulus. (2) The amount of extended-chain crystals appears to be independent of molecular weight over the range studied. (3) Melting points of the drawn fibers increase with molecular weight while the degree of crystallinity remains constant, indicating a variation in the type of folded-chain crystal in the fibers. (4) Strain to break increases with increasing molecular weight, indicating increasing intercrystalline tie-chain content with molecular weight.

References

1. R. E. Robertson, J. Polym. Sci., Polym. Phys. Ed. 10, 2437 (1972).
2. R. S. Stein, Accounts Chem. Res. 5, 121 (1972).
3. A. Peterlin, J. Polym. Sci., C, 15, 427 (1966).
4. A. Peterlin, J. Polym. Sci., A-2, 7, 1151 (1969).
5. G. Meinel and A. Peterlin, J. Polym. Sci., A-2, 9, 67 (1971).
6. A. Peterlin, J. Mater. Sci. 6, 490 (1971).
7. A. Peterlin, Text. Res. J. 42, 20 (1972).
8. E. S. Clark and L. S. Scott, Polym. Eng. Sci. 14, 682 (1974).
9. J. H. Southern and R. S. Porter, J. Macromol. Sci., Phys., B-4, 541 (1970).
10. J. H. Southern and R. S. Porter, J. Appl. Polym. Sci. 14, 2305 (1970).
11. J. H. Southern, N. E. Weeks and R. S. Porter, Makromol. Chem. 162, 19 (1972).
12. R. S. Porter, J. H. Southern and N. E. Weeks, Polym. Eng. Sci. 15, 213 (1975).
13. N. E. Weeks, Ph.D. Dissertation, University of Massachusetts, Amherst, 1974.
14. B. Crist, Jr., Personal Communication.
15. S. Krimm, J. H. C. Ching and V. L. Folt, Macromolecules 7, 537 (1974).
16. K. Imada, T. Yamamoto, K. Shigematsu and M. Takayanagi, J. Mater. Sci. 6, 537 (1971).
17. J. M. Andrews and I. M. Ward, J. Mater. Sci. 5, 411 (1970).
18. G. Capaccio and I. M. Ward, Polymer 15, 233 (1974).
19. G. Capaccio and I. M. Ward, Polym. Eng. Sci. 15, 219 (1975).

20. L. A. Davis, Polym. Eng. Sci. 14, 641 (1974).
21. S. Muruyama, K. Imada and M. Takayanagi, Intern. J. Polym. Mat. 1, 211 (1972).
22. W. G. Harland, M. M. Khadr and R. H. Peters, Polymer 15, 81 (1974).
23. R. S. Porter, N. W. Weeks, N. J. Capiati and R. J. Krzewski, J. Thermal Anal. 8, 547 (1975).
24. N. J. Capiati and R. S. Porter, J. Polym. Sci., Polym. Phys. Ed., 13, 1177 (1975).
25. F. Liberti and B. Wunderlich, J. Polym. Sci., A-2, 6, 833 (1968).
26. J. L. Koenig and A. J. Carrano, Polymer 9, 359 (1968).
27. J. Steidl and Z. Pelzbauer, J. Polym. Sci., C, 38, 345 (1972).
28. P. Predecki and W. O. Statton, J. Appl. Phys. 37, 11 (1966).
29. L. Mandelkern, J. Polym. Sci., C, 15, 129 (1966).
30. P. J. Flory, J. Chem. Phys. 17, 223 (1949).
31. F. C. Frank, Proc. Roy. Soc. Lond. A319, 127 (1970).
32. P. S. Francis, R. C. Cooke, Jr. and J. H. Elliott, J. Polym. Sci. 31, 453 (1958).



TABLE 1  
Molecular Weights for High Density Polyethylenes Studied\*

<u>Data Source</u>	<u>DuPont HDPE</u>	<u><math>M_n \times 10^{-3}</math></u>	<u><math>M_w \times 10^{-3}</math></u>	<u><math>M_w/M_n</math></u>
Polymer Group, Chalmers	7050	19.9	59	2.96
University, Sweden (GPC)	7040	21.1	71	3.36
	7030	26.0	92	3.54
	7026	33.4	147	4.40
DuPont	7050	22.0	60	2.73
	7040	25.2	84	3.34
	7030	28.0	115	4.10
	7026	33.0	175	5.30
From $M_v$ and Reference 32	7050		56	
Relating $M_v$ to $M_w$	7040		78	
	7030		112	
	7026		135	

\* Number-and weight-average molecular weights and molecular weight distributions for Alathon high density polyethylene, as obtained from three sources, by gel permeation chromatography and dilute solution viscometry.

TABLE 2

Linear Expansion Coefficient ( $\alpha$ ) for Ultra-Drawn Strands  
of High Density Polyethylene Measured Along Fiber Axis  
for Four Molecular Weights\*

$\underline{M_w \times 10^{-3}}$	$\underline{-\alpha_1 \times 10^{6**}}$	$\underline{-\alpha_2 \times 10^{6***}}$
59	8.01	11.2
71	6.94	10.2
92	6.72	10.6
147	6.58	9.51

\* Numbers are average values.

\*\*  $\alpha_1$  from  $-130$  to  $\sim -54^\circ\text{C}$ .

\*\*\*  $\alpha_2$  from  $\sim -48$  to  $+60^\circ\text{C}$ .

TABLE 3

Young's Modulus of Ultra-Drawn Strands of High  
Density Polyethylene Obtained at Molecular Weights Shown\*

$\underline{M_w \times 10^{-3}}$	$\underline{E \times 10^{-11}}$ $\underline{\text{dynes/cm}^2}^{**}$	$\underline{E \times 10^{-6},}$ $\underline{\text{psi}}$
59	7.01	10.2
71	6.06	8.78
92	6.44	9.33
147	6.59	9.55

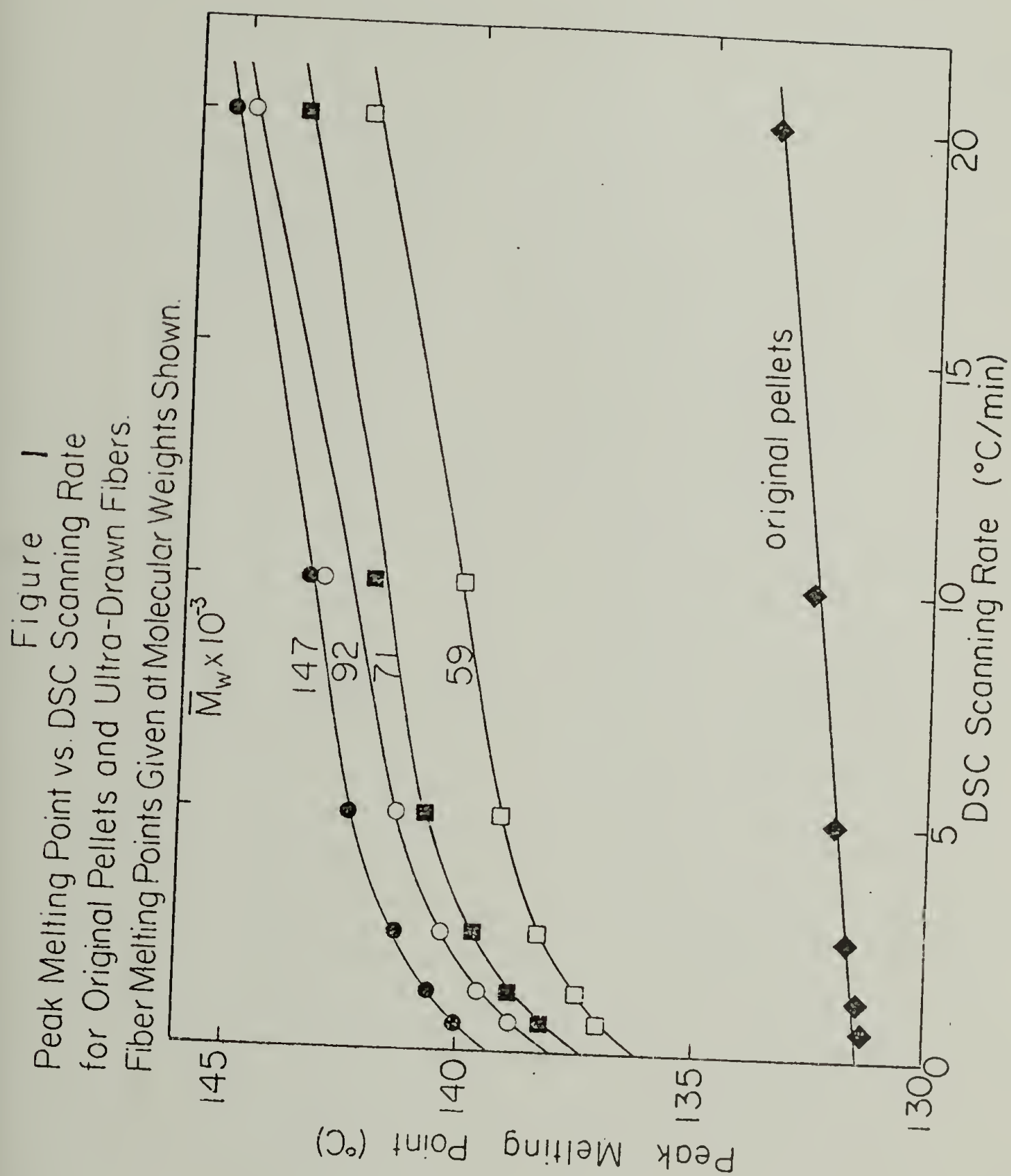
\* Numbers are average values.

\*\*Times 0.1 for S.I. units of  $\text{N/m}^2$ .

Captions for Figures

1. Peak melting point vs. DSC scanning rate for original pellets and ultra-drawn fibers. Fiber melting points given at molecular weights shown.
2. Degree of crystallinity vs. molecular weight for pellets and ultra-drawn fibers. Pellets were crystallized by cooling from 147°C at 20°C/minute.
3. Ultimate tensile strength vs. molecular weight for ultra-drawn high density polyethylene fibers.
4. Strain to break vs. molecular weight for ultra-drawn high density polyethylene fibers.





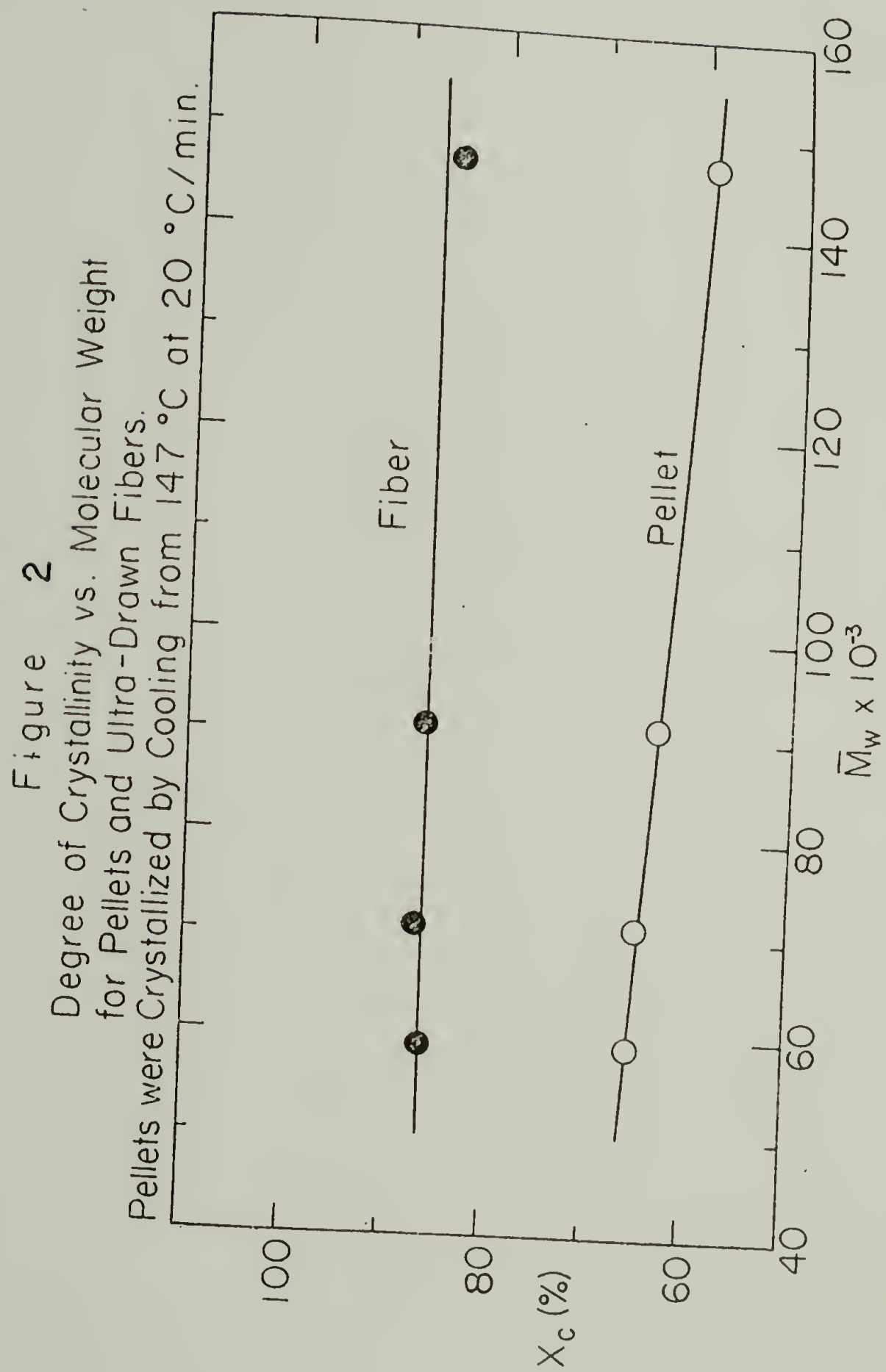


Figure 3  
Ultimate Tensile Strength vs. Molecular Weight  
for Ultra-Drawn High Density Polyethylene Fibers.

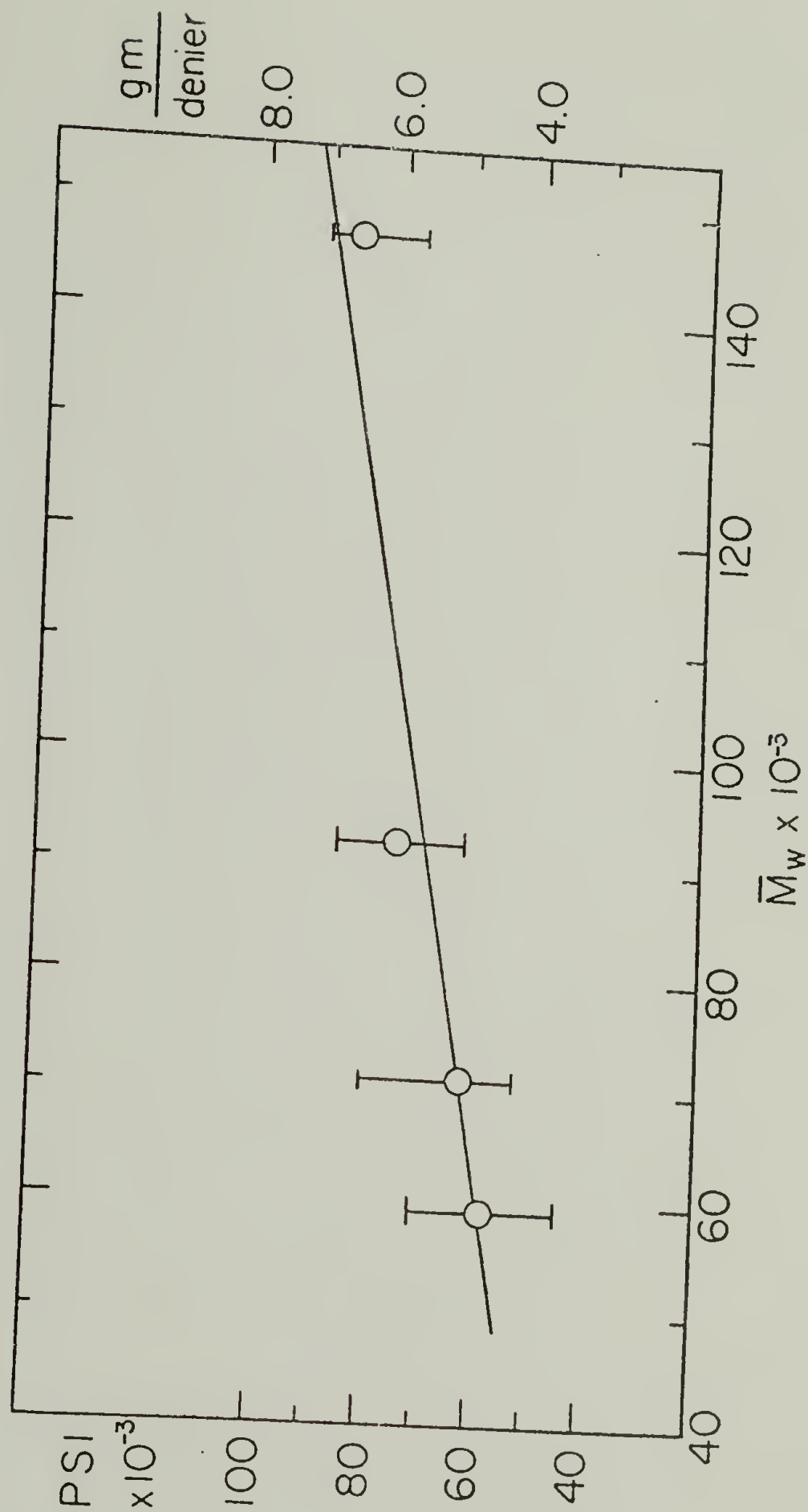
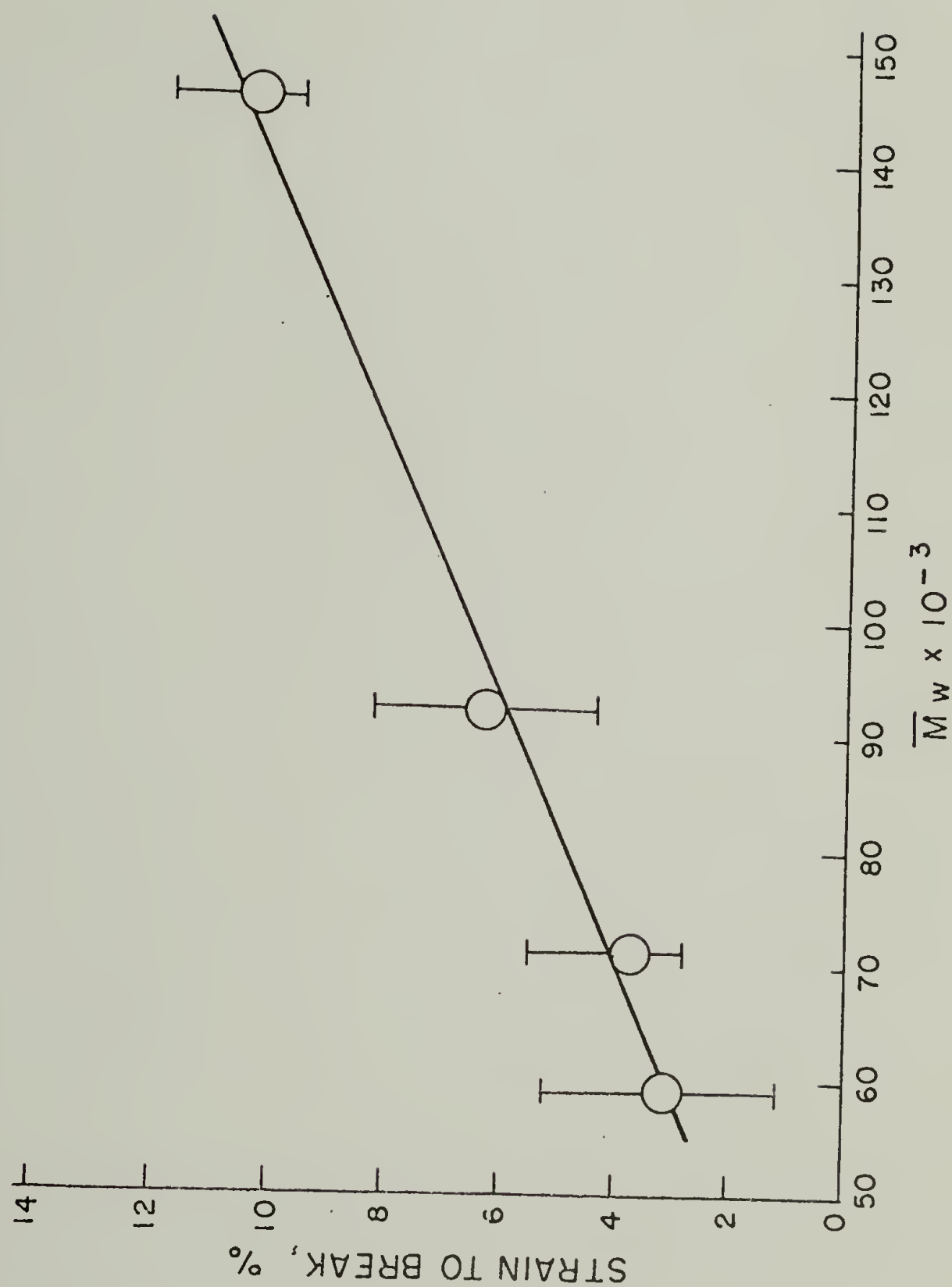


FIGURE 4  
STRAIN TO BREAK VS. MOLECULAR WEIGHT FOR  
ULTRA-DRAWN HIGH DENSITY POLYETHYLENE FIBERS





C H A P T E R   V  
THE EFFECT OF  $\gamma$  RADIATION AND ANNEALING  
ON ULTRA-ORIENTED POLYETHYLENE

I. Introduction

The radiochemical transformations occurring in polymers as a result of irradiation have been reviewed (1-3). The two major effects of ionizing radiation on polymers are crosslinking and main-chain rupture. Either process can predominate, depending on the polymer and conditions. Polyethylene preferentially crosslinks with the ratio between the number of main-chain cleavages and the number of crosslinks not exceeding 0.1 for irradiation in the absence of oxygen (4). The mechanism of radiation crosslinking is generally believed to proceed by hydrogen atom abstraction followed by crosslinking between adjacent polymer chains. For crosslinking to occur, the chains must be mobile, as at higher temperatures, or in an inert solvent.

Patel and Keller (5,6) have proposed that radiation-induced crosslinking of bulk polymer occurs exclusively in the fold surface (amorphous) regions of polyethylene, i.e. no crosslinking occurs within the crystal lattice. This does not exclude radical formation within crystals. However, those that may be created are unable to migrate sufficiently to form a crosslink. Jenkins and Keller (7) attribute decreases in melting point and crystallinity of an irradiated polyethylene to the difficulty of chains to regularly refold on recrystallization as can their unirradiated counterparts. Selikhova, et al. (8), conclude that radiation doses > 80 MRad

are necessary to suppress polyethylene recrystallization. Considerable hindrance to recrystallization was first noted at 80 MRad.

Ionizing radiation also disrupts polymer crystals to some extent, thus lowering the first melting point. Kusy and Turner (9,10) have, in fact, used the depression of the initial melting point to estimate the number of crystalline units destroyed by the irradiation. Jenkins and Keller have observed that crosslinking efficiency is inversely related to the degree of crystallinity: the lower the crystallinity the more developed is the resultant network (7). They also note that details of the lamellar morphology may be influential. Peterlin's model (11,12) for highly oriented semicrystalline polymers incorporates many intra- and interlamellar tie molecules. These can form effective crosslinks which contribute to mechanical strength in contrast to intramolecular loop crosslinking, which does not contribute to mechanical properties.

In the present investigation ultra-oriented filaments of high density polyethylene (HDPE) have been prepared by solid state extrusion using an Instron capillary rheometer (13). These filaments possess remarkable mechanical properties (14-17) due to extreme crystal (c-axis) chain orientation and extension, and the resultant microfibrillar morphology (18). Because of the unusual and interesting nature of these filaments, further investigations into their mechanical and physical properties continue in this and other laboratories.

The effect of ionizing ( $\gamma$ ) radiation on the highly oriented fibers is of interest primarily from the standpoint of annealing effects on the partially chain-extended morphology. Research has been conducted into use of the filaments in self-reinforcement, i.e. composites formed from two

morphologies of the same polymer. Ultra-oriented fibers melt 5-10°C higher than the (spherulitic) precursor from which they are formed. The filaments can, therefore, be embedded without melting in a matrix of high or low density polyethylene at a temperature between the melting points for the fiber and matrix, and then cooled, to form a new class of self-reinforced thermoplastic composites. Above 120°C, however, the ultra-oriented fibers anneal (19) which reduces their superior tensile properties and is thus a limitation in their use as a reinforcement. If the filaments are irradiated while in the oriented state, it is conceivable that their special morphology might become partially fixed through intermolecular crosslinks, enabling the preparation of the composite without the aforementioned deleterious crystal reorganization. This is thus the basis for the present investigation.

## II. Experimental

Ultra-oriented HDPE fibers were prepared from DuPont Alathon 7050 ( $\bar{M}_w = 59,000$ ) at an extrusion (draw) ratio of 26. The fibers were extruded at 2400 atm and 134°C through a 20° entrance angle brass capillary die. Separate extrudates were then irradiated under vacuum by gamma ( $\gamma$ ) rays from a cobalt-60 source at doses of 10, 15, 20, 40 and 60 megarads (MRad). The dose rate was 0.42 MRad/hr. Samples were degassed at  $10^{-5}$  mm H<sub>g</sub> for 24 hours then stored in the dark for 10 days at 30°C. This was to insure decay of any trapped radicals which can cause oxidative degradation. For comparison, one set of extrudates irradiated at each dose was immersed (annealed) in a silicone oil bath for 1/2 hour at 128°C. Such annealing of these morphologies is well above the minimum time needed for any structural



reorganization since Mead and Porter (19) found that 10 minutes is sufficient at  $129^{\circ}$  and 30 minutes is sufficient at  $126^{\circ}$ . A second set of extrudates was given no post-irradiation treatment. Characterization of the resultant morphologies included differential scanning calorimetry, birefringence, thermomechanical analysis, and mechanical testing.

Differential scanning calorimetry (DSC) was performed with a Perkin-Elmer DSC-1B at a heating rate of  $10^{\circ}\text{C}\cdot\text{min}^{-1}$  to yield heats of fusion [converted to percent crystallinity ( $X_c$ )] and crystalline melting points ( $T_m$ ). The melted fibers were also recrystallized at  $107^{\circ}$  after first heating and then remelted, for a second set of melting values.

Birefringence measurements were carried out on a Zeiss polarizing microscope equipped with an Ehringhaus rotary compensator consisting of double calcite plates. The compensator can measure up to 133 orders of retardation in white light.

A Perkin-Elmer TMS-1 thermomechanical analyzer attachment to the DSC-1B was used for measurement of the linear expansion coefficient,  $\alpha$ , as well as thermal transitions. Sample preparation for this test was as previously described (20). A load of 3 grams was used with the expansion probe and the scanning rate was  $10^{\circ}\text{C}\cdot\text{min}^{-1}$ . Test sample length was approximately one centimeter. Scans were made from  $-120^{\circ}\text{C}$  up to  $120^{\circ}\text{C}$ .

For studies of fiber mechanical properties, an Instron tensile testing machine, model TTCM, equipped with a strain-gage extensometer, was used. Load elongation curves were obtained at room temperature using a fixed elongation rate of  $0.02\text{-cm min}^{-1}$  for modulus measurements and  $0.50\text{-cm}\cdot\text{min}^{-1}$  for determination of tensile strength and strain at break. The fibers had to be gripped by special clamps described elsewhere (16) to



prevent slippage in the jaws. The Young's modulus was determined as the tangent to the stress-strain curve at 0.1% strain.

### III. Results and Discussion

#### A. Unannealed Samples.

##### 1. Calorimetry.

Figure 1 shows that the crystalline melting point of the ultra-oriented fibers decreases linearly with increasing radiation from about  $137^{\circ}\text{C}$  at 0 dose to  $134^{\circ}\text{C}$  at 60 MRad. Upon recrystallization and remelting of this series the same trend is observed only more pronounced; i.e. the melting point drops from  $129^{\circ}\text{C}$  to  $123^{\circ}\text{C}$ . The depression of the first melting point is about  $0.05^{\circ}\text{C}$  per megarad. This is close to the value of  $0.03 - 0.04^{\circ}\text{C}$  per megarad found by Kusy and Turner (9) and leads to a G value of 10 for the loss of crystalline units. This can be compared with a G value of 4.9 for chemically changed units (9). This would imply that two crystalline units are lost for each chemical change as found also by Kusy and Turner for poly(ethylene oxide) (10). This approach is fully discussed in References 9 and 10.

Percent crystallinity, calculated from heat of fusion data, is shown in Figure 2. An initial drop from 0 to 10 MRad of 5% is followed by a gradual decrease at even higher doses. The curve for second melting depicts the same trend; however, the depression is greater and tends to level off at the highest doses. These results are consistent with melting point data in that the crystal lattices are only slightly disrupted upon initial irradiation yet are unable to reform effectively once melted and recooled. The leveling off of the percent crystallinity at higher doses while the melting

point continues to drop would indicate that fewer large crystals are formed upon recrystallization favoring formation of smaller, less perfect crystals.

## 2. Birefringence.

The measurements of morphology birefringence in Table 1 indicate that total orientation is unchanged by  $\gamma$  radiation at the doses employed in this study.

## 3. Thermomechanical Analysis (TMA).

Previous measurements of linear expansion coefficients, ( $\alpha$ ), on similar (unirradiated) fibers having a somewhat higher extrusion ratio produced values of  $\alpha_1$  (from  $-130$  to  $-54^\circ\text{C}$ ) of  $-7.06 \times 10^{-6} \text{ }^\circ\text{C}^{-1}$  and  $\alpha_2$  (from  $-48$  to  $60^\circ\text{C}$ ) equal to  $-10.4 \times 10^{-6} \text{ }^\circ\text{C}^{-1}$  (15). The small negative values for  $\alpha$  in the chain direction result from the inability of extended (all trans) chains to increase their length when thermally excited. The only motion possible in the chain-extended crystals is vibration and rotation about carbon-carbon bonds, a situation that will cause the chains to shorten, i.e. contract, when heated. Along the direction perpendicular to the orientation axis,  $\alpha$  is positive and larger, on the order of  $10^{-4} \text{ }^\circ\text{C}^{-1}$ . The unannealed strands examined in this study also exhibited negative thermal expansion coefficients which were essentially invariant with radiation dose, see Table 2. This again is consistent with irradiation effects only in the amorphous regions since disruption of the chain-extended crystals would show a marked effect on  $\alpha$ . As in the previous study (17), two values of  $\alpha$  were observed. The average value of  $\alpha_1$  (measured from  $-120$  to  $-75^\circ\text{C}$ ) was  $-7.0 \pm 0.05 \times 10^{-6} \text{ }^\circ\text{C}^{-1}$ , while  $\alpha_2$  (measured above  $-75^\circ$ ; see Table 2) averaged  $-9.88 \pm 1.0 \times 10^{-6} \text{ }^\circ\text{C}^{-1}$ . The determination of  $\alpha$  was made from the slope(s) of plots of the normalized change in sample length ( $\Delta L/L_0$ ) vs. temperature

(T). The temperature range over which  $\alpha_2$  could be measured varied with radiation dose. A break occurs in the curves of  $\Delta L/L_0$  vs. T at  $-75^\circ\text{C}$ ;  $\alpha_1$  is the coefficient below, and  $\alpha_2$ , above, this point. For samples irradiated at 40 MRad, there are two breaks in the curves; thus there are three  $\alpha$  values, as shown in Table 2.  $\alpha_3$  is the coefficient above the second break. Since these measurements reflect the extended chain content of the ultra-oriented fibers, the data indicate that  $\gamma$  radiation up to 60 MRad does not disrupt this conformation.

#### 4. Mechanical Testing.

Stress-strain curves yielded values of Young's modulus, stress-at-break (tensile strength), and strain-at-break vs. radiation dose (Figures 3, 4 and 5). Fracture in all cases was fibrillar in nature, i.e. long, needle-like fracture surfaces were produced, indicating a shear deformation as the predominant fracture mode. Modulus increased 20% from 0 to 40 MRad, then levelled off at higher dosages. Both tensile strength and elongation-at-break increased significantly to a projected maximum at between 10 and 20 MRad, then dropped off to nearly constant values at higher doses, approaching those of the unirradiated samples. Lyons and Vaughn (21), working with low and high density polyethylene and an ionomer, also noticed an increase in tensile strength on irradiation to a maximum at 15 to 30 MRad. Tynny and Velikovskii (22) observed a similar effect with high density polyethylene. The invariance of the linear expansion coefficient with dose would predict the same behavior for Young's modulus since both properties depend upon extended chain content, which appears not to vary with dose. The slight increase in modulus with radiation dose is likely due to a stiffening of the morphology by crosslinks between



extended molecular chains and/or between the oriented folded chain component of the morphology.

Increases in tensile strength and elongation-at-break at moderate radiation doses can be due to an effective increase in molecular weight by the addition of radiation-induced crosslinks. This results in more trapped entanglements. The subsequent decrease in these properties at higher radiation doses may be attributable to a more brittle morphology at high crosslink density.

## B. Annealed Samples.

### 1. Calorimetry.

Curves of crystalline melting point and degree of crystallinity vs. radiation dose for annealed samples are shown in Figures 6 and 7. These plots are essentially identical to those in Figures 1 and 2 for unannealed samples. Absolute values of first-melting crystallinity are about 7% higher for the annealed samples while the absolute melting points are the same for both annealed and unannealed samples. This indicates that annealing at 128°C allows the formation of more crystallites, but that these new crystallites are small and imperfect, apparently due to restricted mobility of the irradiated (i.e. crosslinked) chains which hinders crystal formation.

### 2. Birefringence.

Birefringence measurements on annealed fibers are shown in Table 3. It is seen that annealing lowers total orientation for the unirradiated samples but has no disorienting effect on fibers irradiated at all doses. This again is apparently because the disruption of amorphous orientation by annealing is suppressed by radiation crosslinking.



### 3. Thermomechanical Analysis.

Linear expansion coefficients of annealed samples are shown in Table 4. The values of  $\alpha_1$  and  $\alpha_2$  (expansion coefficients at temperatures below and above the aforementioned break at  $-75^\circ\text{C}$  in plots of  $\Delta L/L$  vs. temperature) remain approximately constant from 10 to 60 MRad radiation dose, where  $\alpha_1$  averages  $-5.87 \pm 0.6 \times 10^{-6} \text{ }^\circ\text{C}^{-1}$  and  $\alpha_2$  averages  $-9.54 \pm 0.75 \times 10^{-6} \text{ }^\circ\text{C}^{-1}$ . There appears to be a slight maximum at 15 MRad. The values of both  $\alpha_1$  and  $\alpha_2$  are lower for the unirradiated annealed fiber.

### 4. Mechanical Testing.

Plots of Young's modulus, tensile strength at break, and elongation at break vs. radiation dose for annealed samples are shown in Figures 8, 9 and 10. The modulus vs. dose plot (Figure 8) parallels the coefficient of expansion data as values increase from 0 to 15 MRad, then drop slightly and level off. Tensile strength (Figure 9) and elongation at break (Figure 10) curves have similar shape (as was the case for unannealed samples). Both rise sharply with increasing irradiation from 0 to 40 MRad, then essentially flatten out. The initial increase in these properties is significant; a 100% increase in tensile strength and a 75% increase in strain at break.

All the data pertaining to annealed fibers can be used to explain what is occurring when irradiation is accompanied by annealing in highly oriented morphologies. Curves of modulus and linear expansion coefficient, both properties related to extended chain content, are similar in shape. Each increases from 0 to 15 MRad, then drops slightly and remains constant. This indicates that annealing disrupts the chain-extended morphology in the case of unirradiated fibers, while having no apparent effect on the extended chain morphology for irradiated fibers. The maximum at 15 MRad is unexplained

at present but is apparently due to two opposing effects of irradiation. Tensile strength and breaking strain increase with radiation dose as the effective molecular weight is increased by intermolecular crosslinking. However, at higher doses the values do not drop as they do for the unannealed fibers, but rather continue to rise, then level off. Both these properties depend on (initially) unstressed interlamellar tie chains which become stretched upon sample extension, resisting fracture and allowing further extension. For unannealed samples, these tie molecules are crosslinked by radiation while unstressed, and so are unable to stretch appreciably upon deformation. This is consistent with the brittle behavior (at high crosslink density) commonly observed in network structures. Annealing of crosslinked tie molecules apparently increases the mobility of the interlamellar phase sufficiently to allow the recombination of dangling ends and split chains, thus providing a greater number of unstressed tie molecules which tend to strengthen the structure. At the highest doses the tensile strength and breaking strain level off, probably because mobility reaches saturation as crosslink density increases. At this point there is a balance between the (desirable) effective molecular weight increase and the creation of tie molecules on the one hand and the (undesirable) induced brittleness on the other.

#### IV. Conclusions

It has been found that the irradiation of ultra-oriented morphologies of HDPE can prevent large-scale morphological disruption and subsequent reduction in the mechanical properties of such extrudates. The tensile strength for annealed, irradiated fibers is doubled while tensile modulus

remains constant. Other annealing temperatures may produce yet stronger samples. Sohma and coworkers (23) working with high density polyethylene noticed an increase in free radical decay at the temperature region of  $-73^{\circ}\text{C}$ . This corresponds closely with the  $(-75^{\circ}\text{C})$  temperature at the break in our  $\Delta L/L$  vs.  $T$  plots of linear expansion coefficients. They propose that, based on investigations of Hideshima, et al. (24), the  $-73^{\circ}\text{C}$  temperature corresponds to the glass transition temperature of high density polyethylene. This question remains moot.

Jenkins and Keller (7) note that differences in initial morphology as manifested by property differences after irradiation are most evident in the range 10 to 30 MRad. In the present work, maximums in tensile strength and elongation at break for unannealed samples and maximums in modulus and linear expansion coefficient for annealed samples occur in this same irradiation range.

### References

1. F. A. Makhlis, "Radiation Physics and Chemistry of Polymers," Halsted Press, New York, 1975.
2. A. Charlesby in "Polythene," A. Renfrew and P. Morgan, Eds., Liffé and Sons, London, 1960, Ch. 12.
3. R. F. Gould, Ed., "Irradiation of Polymers," Adv. Chem. Ser., No. 66, Am. Chem. Soc., Washington, D.C., 1967.
4. P. Alexander and D. J. Toms, J. Polym. Sci. 22, 343 (1956).
5. G. N. Patel and A. Keller, J. Polym. Sci., Polym. Phys. Ed. 13, 303 (1975).
6. G. N. Patel and A. Keller, J. Polym. Sci., Polym. Phys. Ed. 13, 323 (1975).
7. H. Jenkins and A. Keller, J. Macromol. Sci. B11, 301 (1975).
8. V. I. Selikhova, N. F. Bakeyev, Yu. A. Zubov, N. M. Kovov, F. F. Sikhov, V. S. Shchirets and G. P. Belov, Vysokomol. Soy A17, 1814 (1975).
9. R. P. Kusy and D. T. Turner, Macromolecules 4, 337 (1971).
10. R. P. Kusy and D. T. Turner, Macromolecules 10, 493 (1977).
11. A. Peterlin, J. Mater. Sci. 6, 490 (1971).
12. A. Peterlin, Polym. Eng. Sci. 17, 183 (1977).
13. N. J. Capiati, S. Kojima, W. G. Perkins and R. S. Porter, J. Mater. Sci. 12, 334 (1977).
14. N. E. Weeks and R. S. Porter, J. Polym. Sci., Polym. Phys. Ed. 12, 635 (1974).
15. R. S. Porter, J. H. Southern and N. E. Weeks, Polym. Eng. Sci. 15, 213 (1975).



16. N. J. Capiati and R. S. Porter, J. Polym. Sci., Polym. Phys. Ed. 13, 1177 (1975).
17. W. G. Perkins, J. N. Capiati and R. S. Porter, Polym. Eng. Sci. 16, 200 (1976).
18. C. R. Desper, J. H. Southern, R. D. Ulrich and R. S. Porter, J. Appl. Phys. 41, 4284 (1970).
19. W. T. Mead and R. S. Porter, J. Appl. Phys. 47, 4278 (1976).
20. R. S. Porter, N. E. Weeks, N. J. Capiati and R. J. Krzewki, J. Thermal Anal. 8, 547 (1975).
21. B. J. Lyons and C. Vaughn, Chapter 10 in "Irradiation of Polymers," Adv. Chem. Ser., No. 66, Am. Chem. Soc., Washington, D.C., 1967.
22. A. N. Tynnyi and A. A. Velikovskii, Fiz., Khim. Mekh. Mater. 3, 602 (1967).
23. S. Nara, S. Shimada, H. Kashiwabara and J. Sohma, J. Polym. Sci., A-2, 6, 1435 (1968).
24. M. Kakizaki, Y. Morita, K. Tsuge and T. Hideshima, Repts. Prog. Polym. Phys. Japan 10, 397 (1967).

TABLE I  
 BIREFRINGENCE OF UNANNEALED,  
 IRRADIATED, ULTRA-ORIENTED  
 HIGH DENSITY POLYETHYLENE FIBERS

SAMPLE	RADIATION DOSE (MRad)					
	0	10	15	20	40	60
A	.061	.060	.060	.061	.061	—
B	.060	.062	—	.061	.061	.061

TABLE 2

COEFFICIENT OF EXPANSION vs.  
 RADIATION DOSE FOR UNANNEALED  
 IRRADIATED, ULTRA-ORIENTED  
 HIGH DENSITY POLYETHYLENE FIBERS

COEFFICIENT OF EXPANSION ( $\times 10^{-6} \text{ }^{\circ}\text{C}^{-1}$ )	RADIATION DOSE (MRad)				
	0	10	20	40	60
$-\alpha_1$	6.64	6.59	7.22	7.42	7.08
$-\alpha_2$	9.51	10.29	9.34	9.24	11.03
$-\alpha_3$	—	—	—	12.31	—

TABLE 3

BIREFRINGENCE OF ANNEALED,  
IRRADIATED, ULTRA-ORIENTED  
HIGH DENSITY POLYETHYLENE FIBERS

SAMPLE	RADIATION DOSE (MRad)					
	0	10	15	20	40	60
A	.058	.061	.061	.062	.061	.061
B	.058	.060	.060	.061	.061	.061



TABLE 4

COEFFICIENT OF EXPANSION vs.  
RADIATION DOSE FOR ANNEALED  
IRRADIATED, ULTRA-ORIENTED  
HIGH DENSITY POLYETHYLENE FIBERS

COEFFICIENT OF EXPANSION ( $\times 10^{-6} \text{ }^{\circ}\text{C}^{-1}$ )	RADIATION DOSE (MRad)					
	0	10	15	20	40	60
$-\alpha_1$	4.66	5.06	6.24	5.97	5.78	5.59
$-\alpha_2$	7.95	9.65	10.12	9.27	9.54	8.82

Captions for Figures

1. Crystalline melting point vs. radiation dose for unannealed, irradiated, ultra-oriented high density polyethylene fibers. Upper curve depicts first melting; lower, curve, second melting (see text).
2. Degree of crystallinity vs. radiation dose for unannealed, irradiated, ultra-oriented high density polyethylene fibers. Upper curve depicts first melting; lower curve, second melting (see text).
3. Young's modulus vs. radiation dose for unannealed, irradiated, ultra-oriented high density polyethylene fibers.
4. Tensile strength vs. radiation dose for unannealed, irradiated, ultra-oriented high density polyethylene fibers.
5. Elongation at break vs. radiation dose for unannealed, irradiated, ultra-oriented high density polyethylene fibers.
6. Crystalline melting point vs. radiation dose for annealed, irradiated, ultra-oriented high density polyethylene fibers. Upper curve depicts first melting; lower curve, second melting (see text).
7. Degree of crystallinity vs. radiation dose for annealed, irradiated, ultra-oriented high density polyethylene fibers. Upper curve depicts first melting; lower curve, second melting (see text).
8. Young's modulus vs. radiation dose for annealed, irradiated, ultra-oriented high density polyethylene fibers.
9. Tensile strength vs. radiation dose for annealed, irradiated, ultra-oriented high density polyethylene fibers.
10. Elongation at break vs. radiation dose for annealed, irradiated, ultra-oriented high density polyethylene fibers.

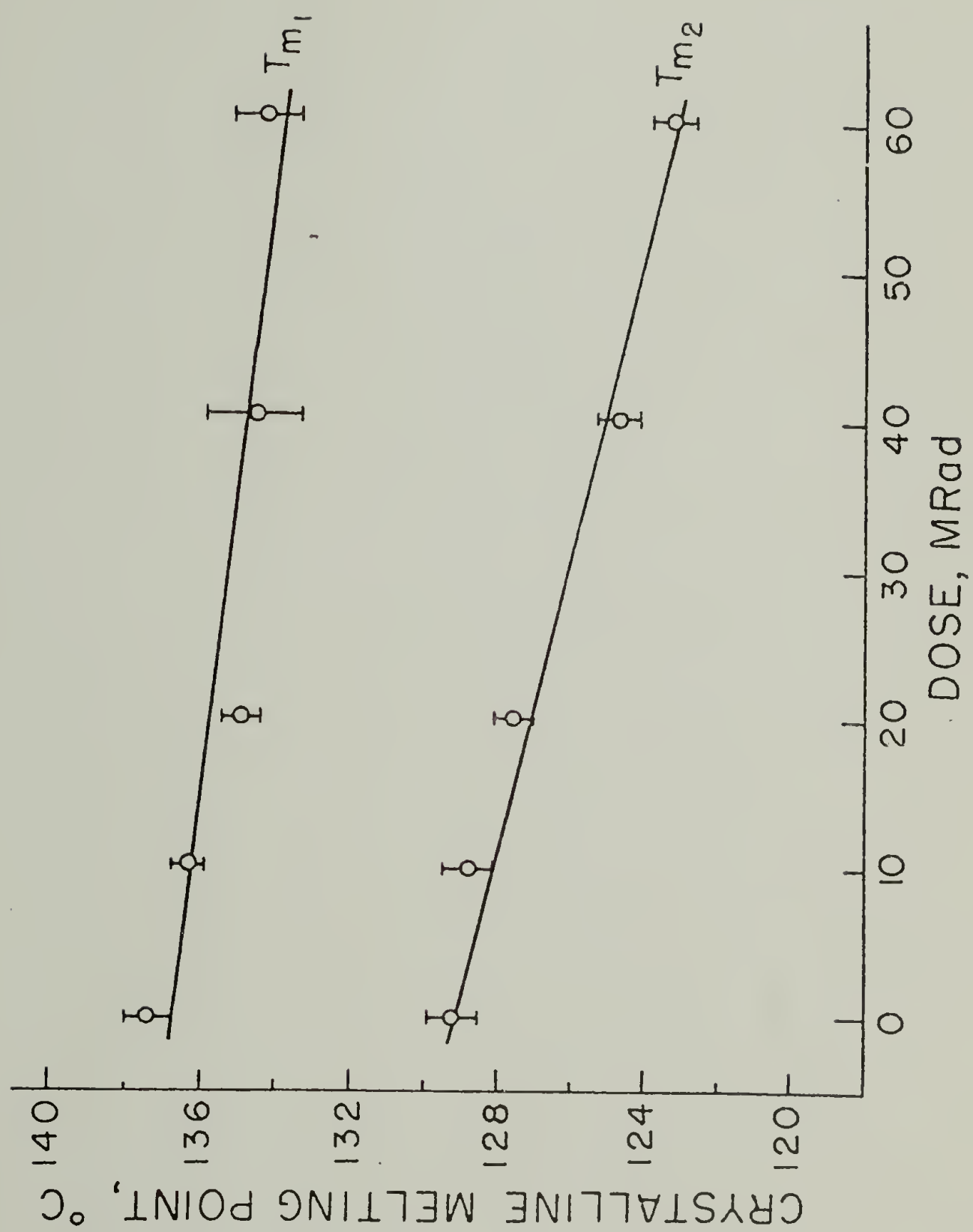


Figure 1

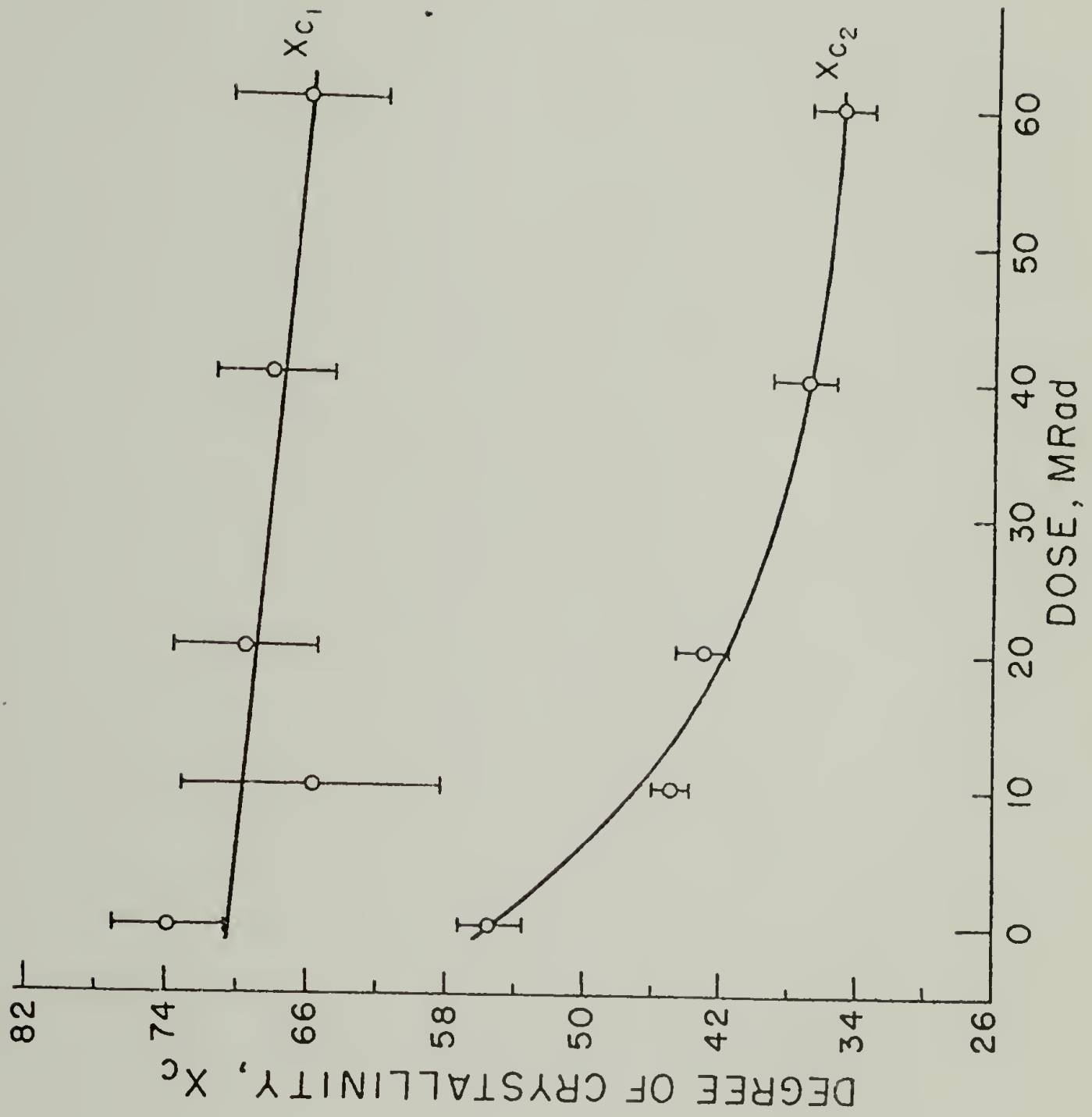


Figure 2



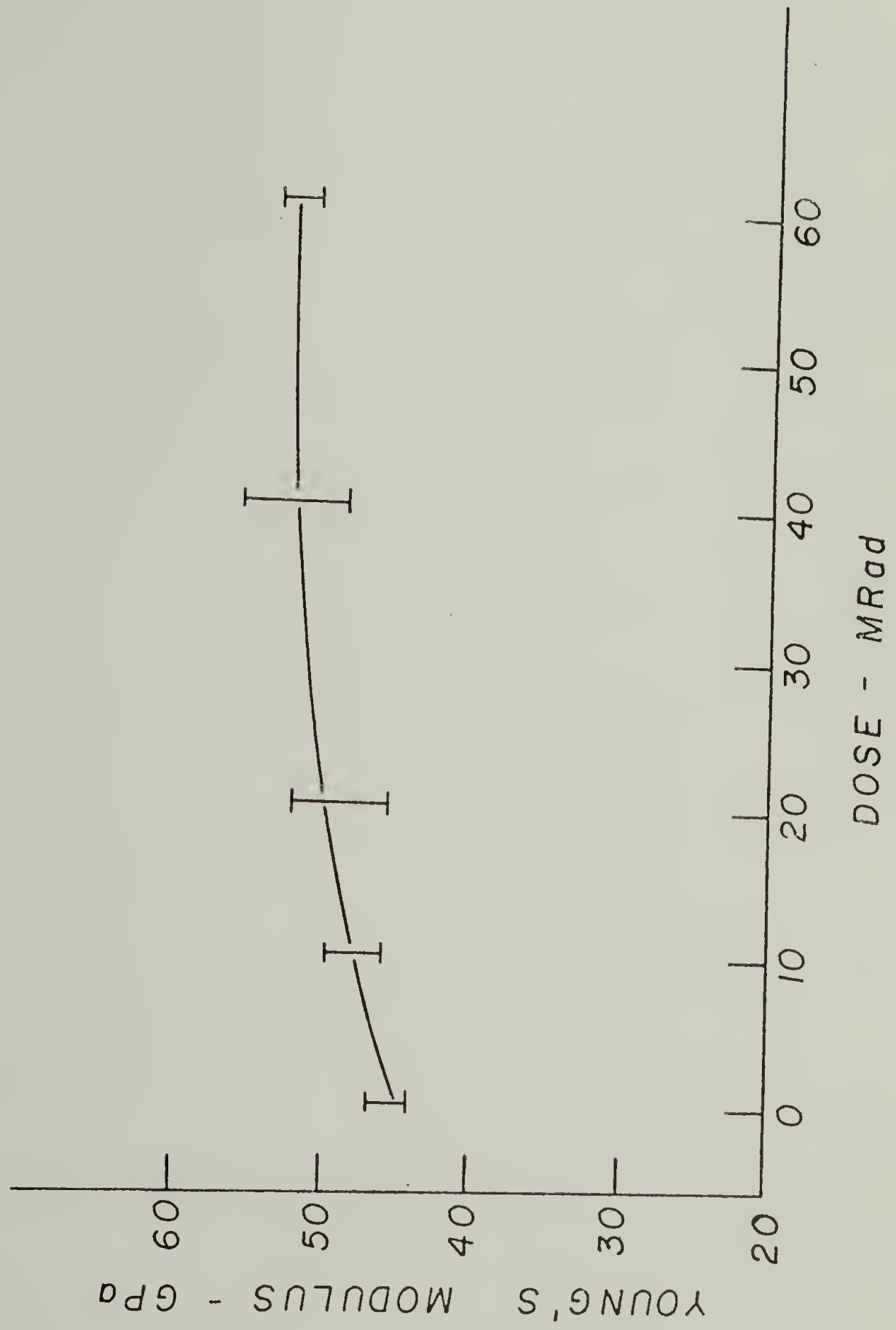


Figure 3

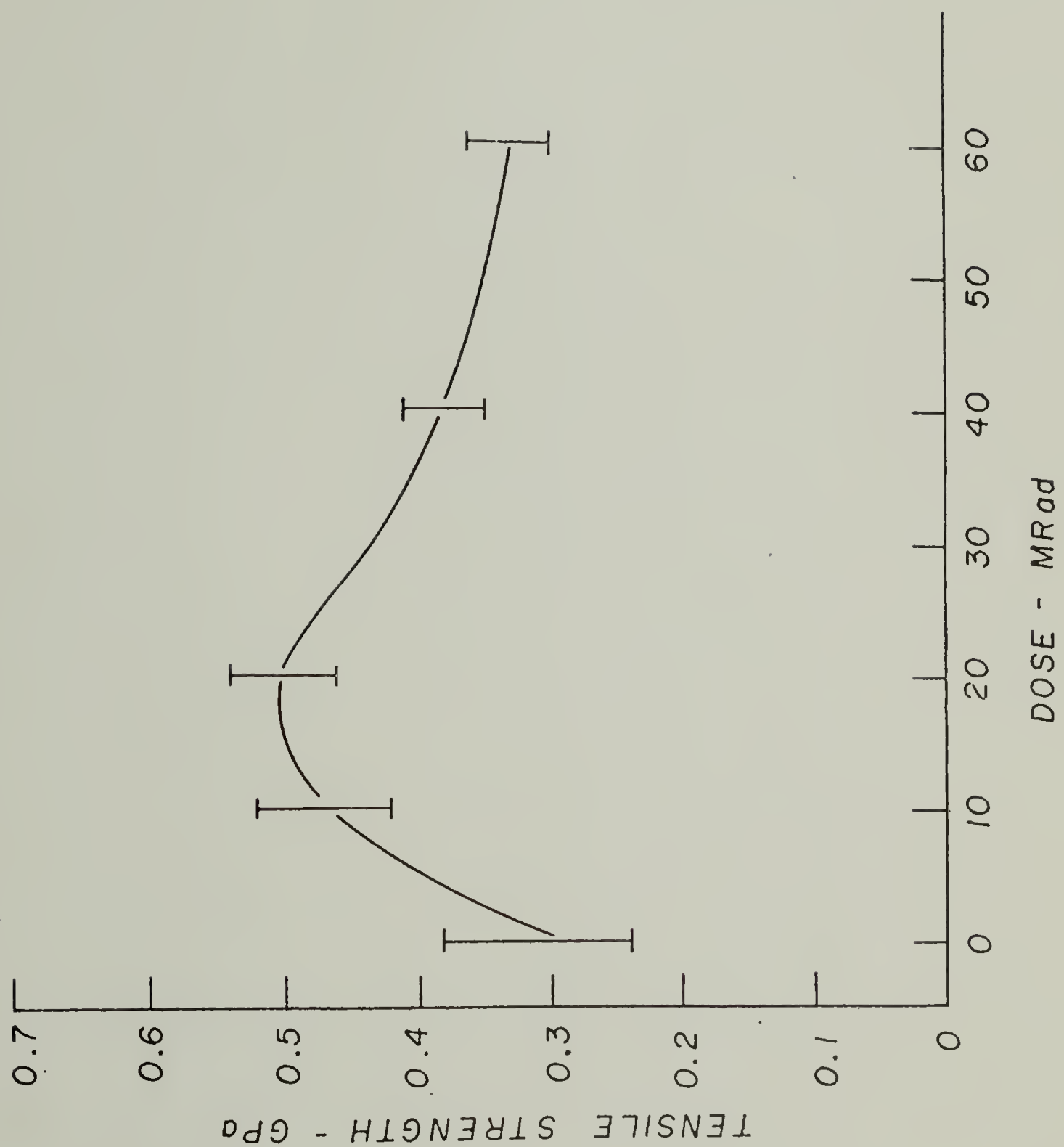


Figure 4

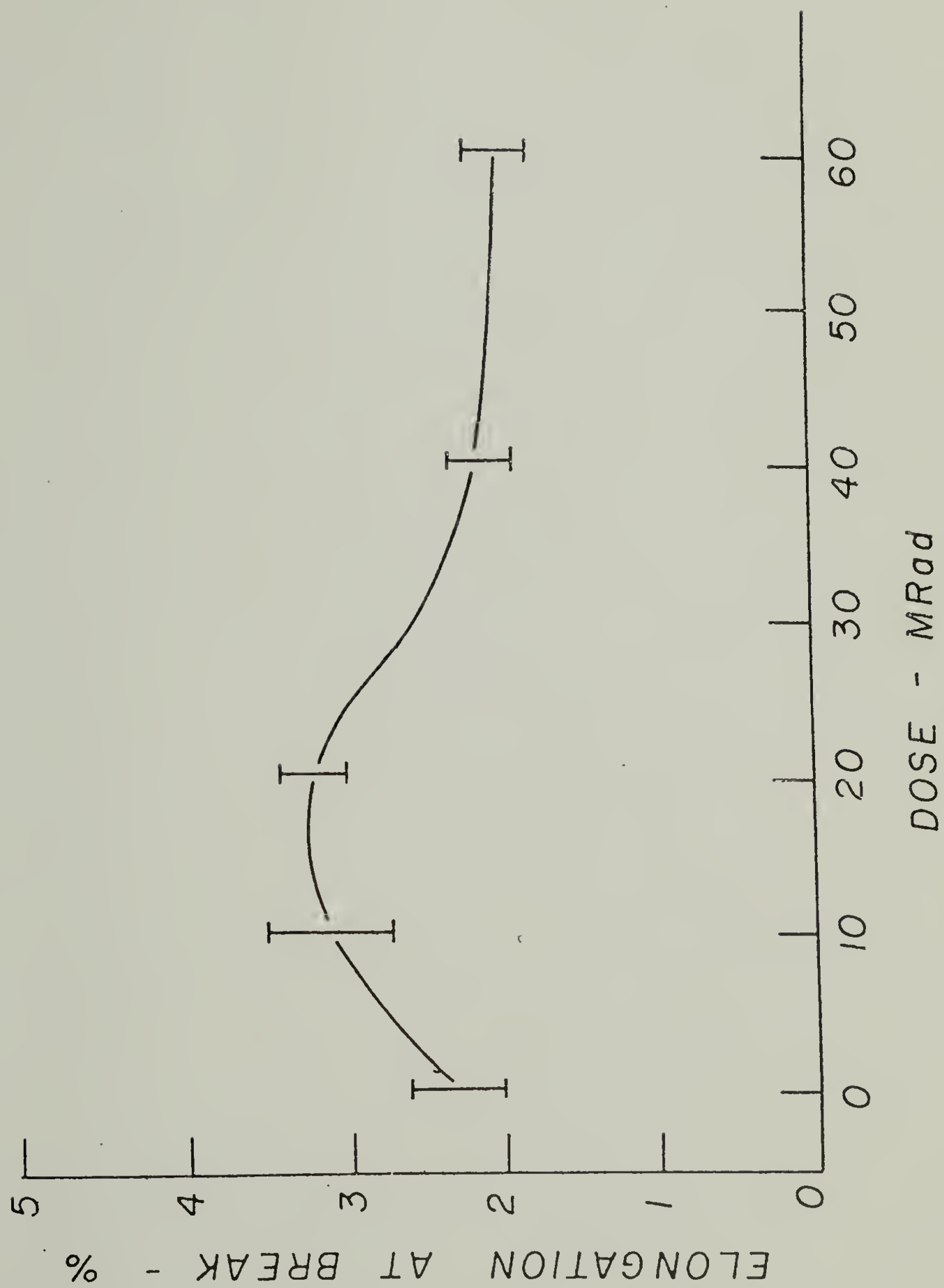


Figure 5

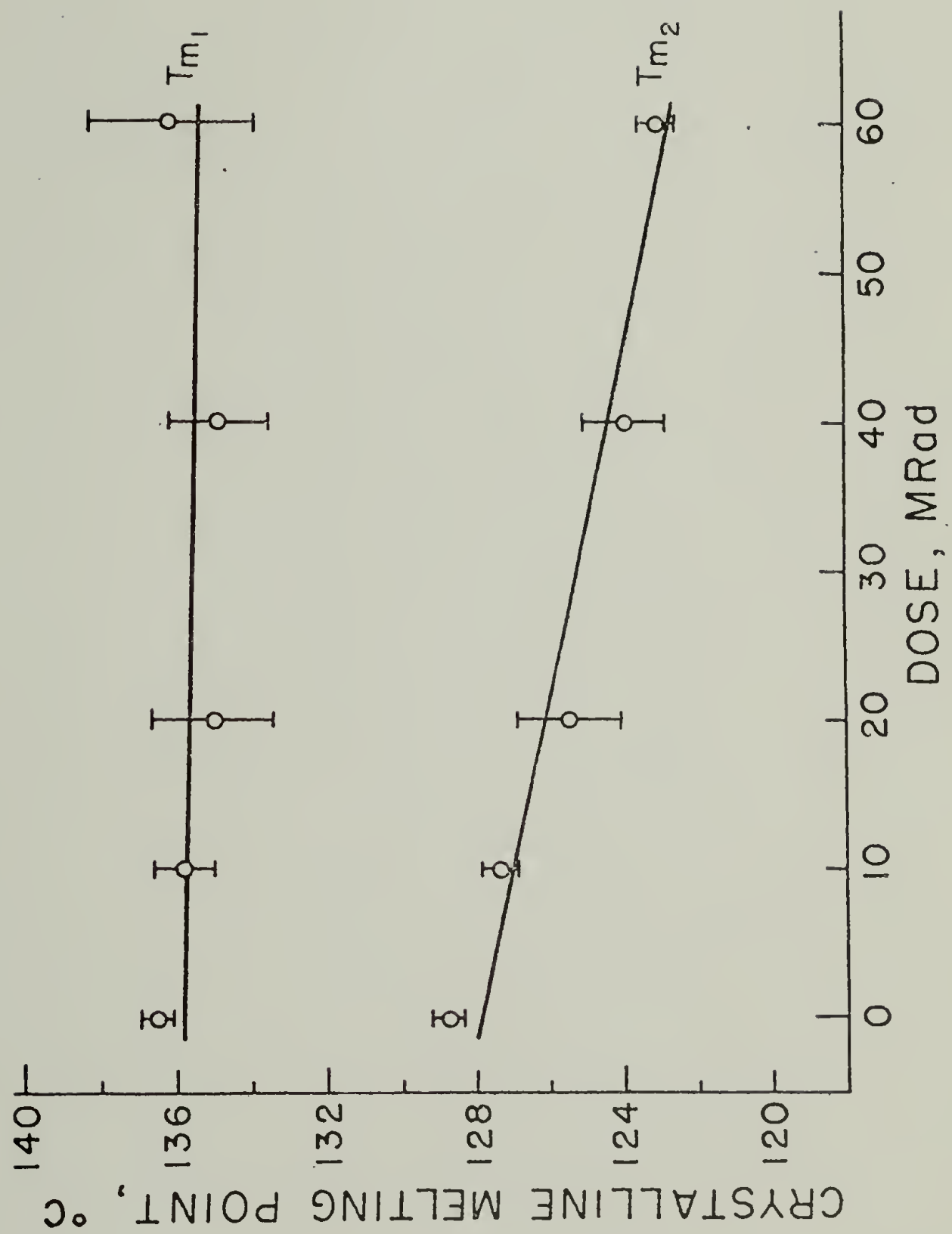


Figure 6



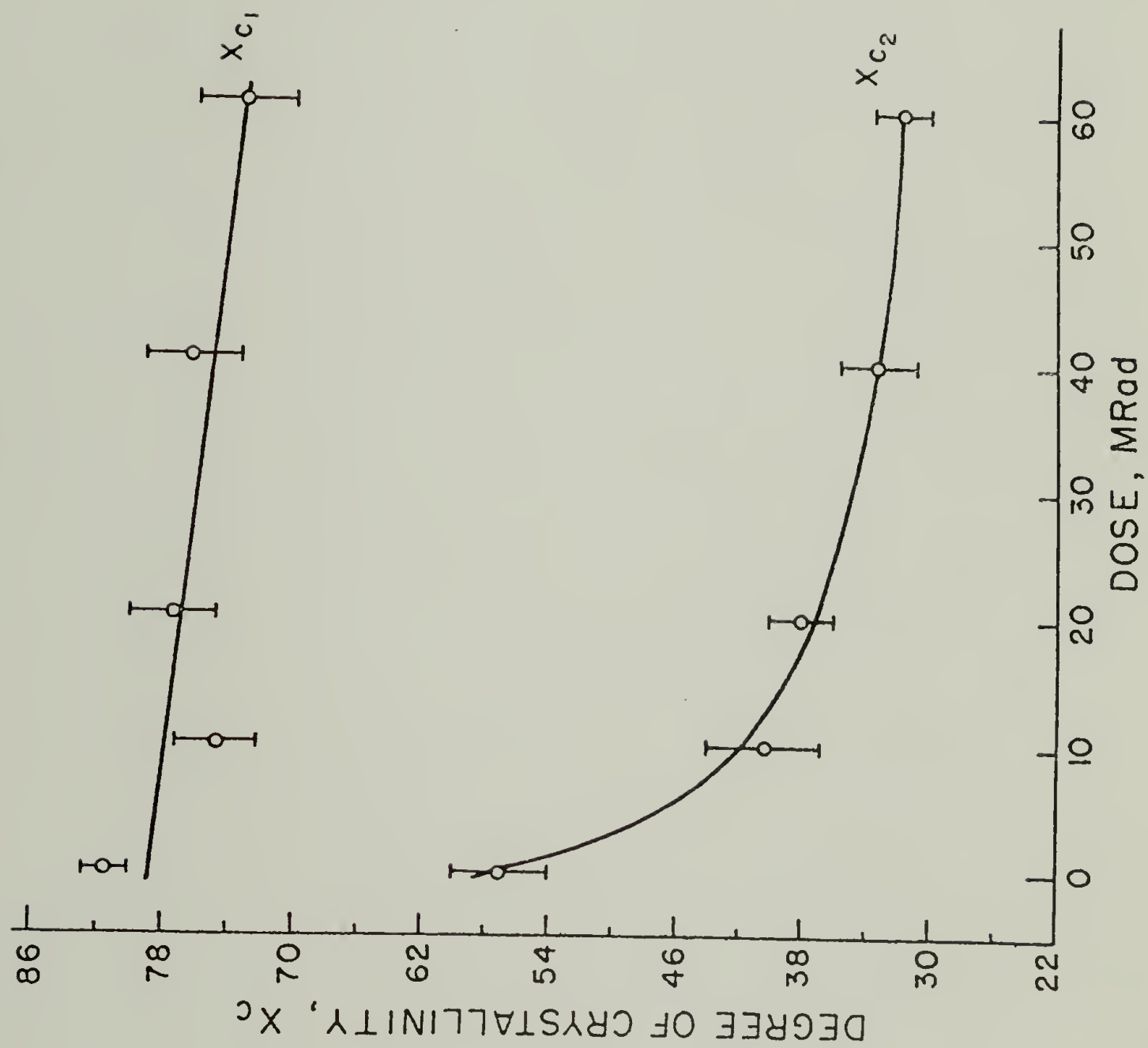


Figure 7

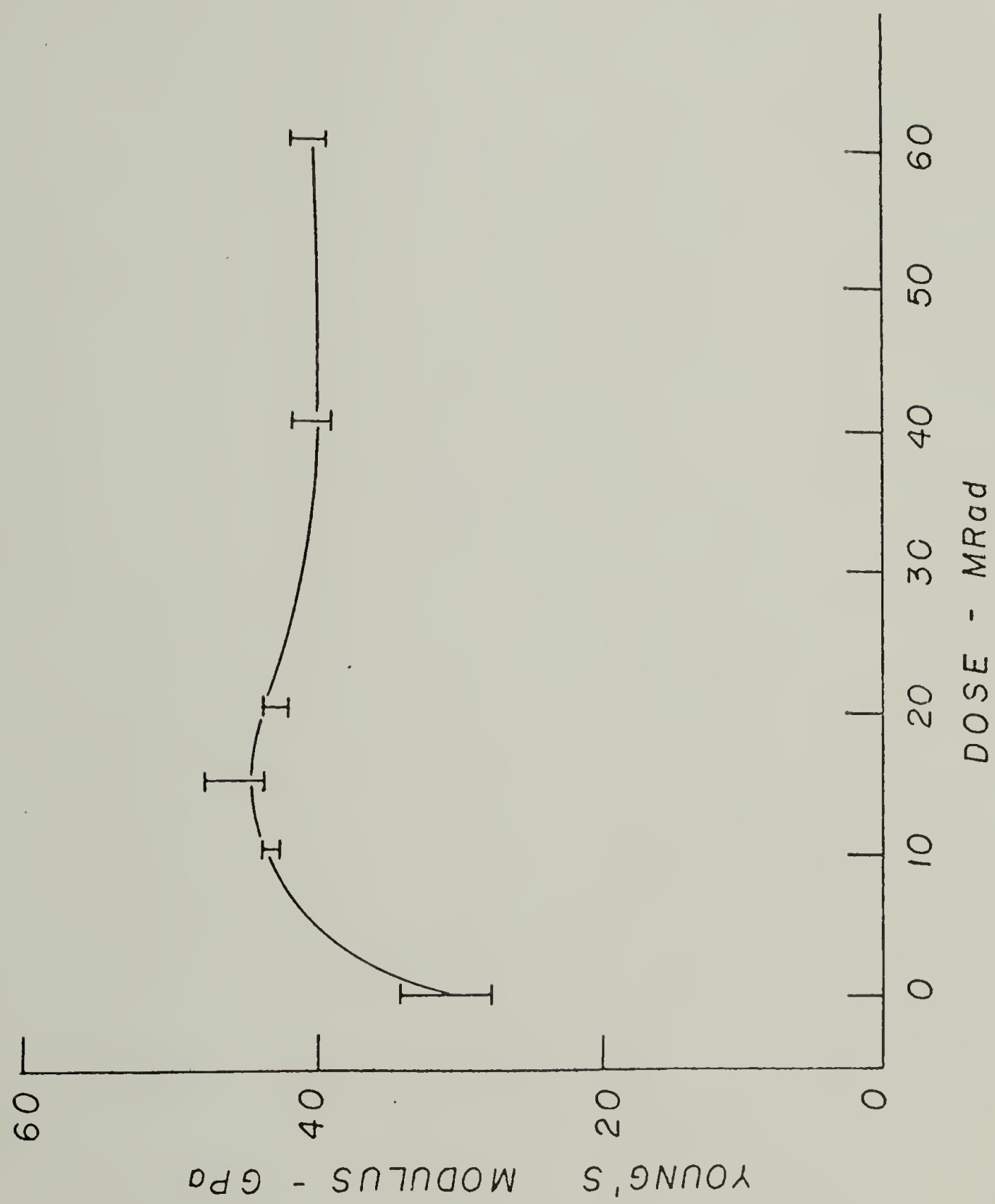


Figure 8

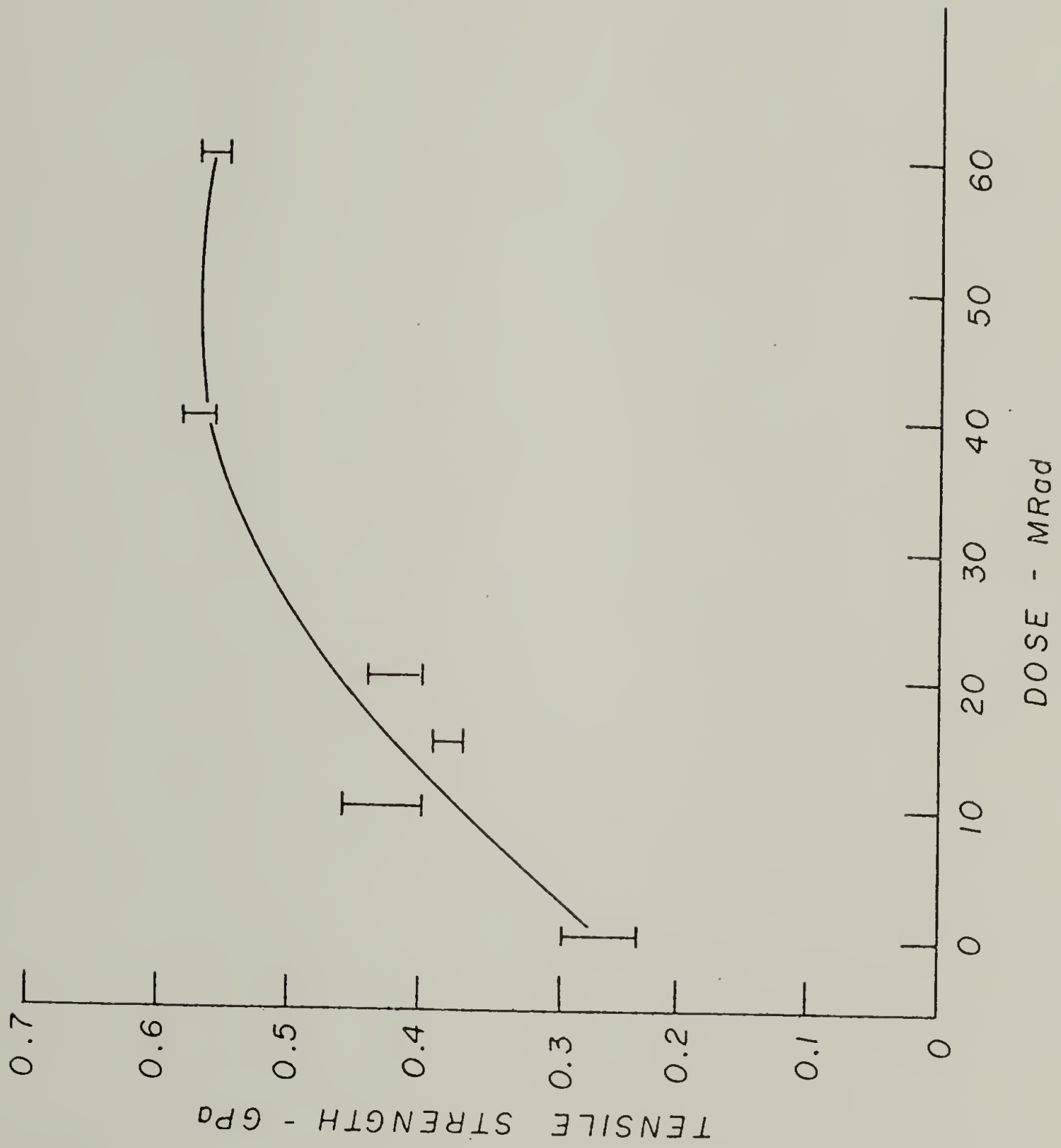


Figure 9

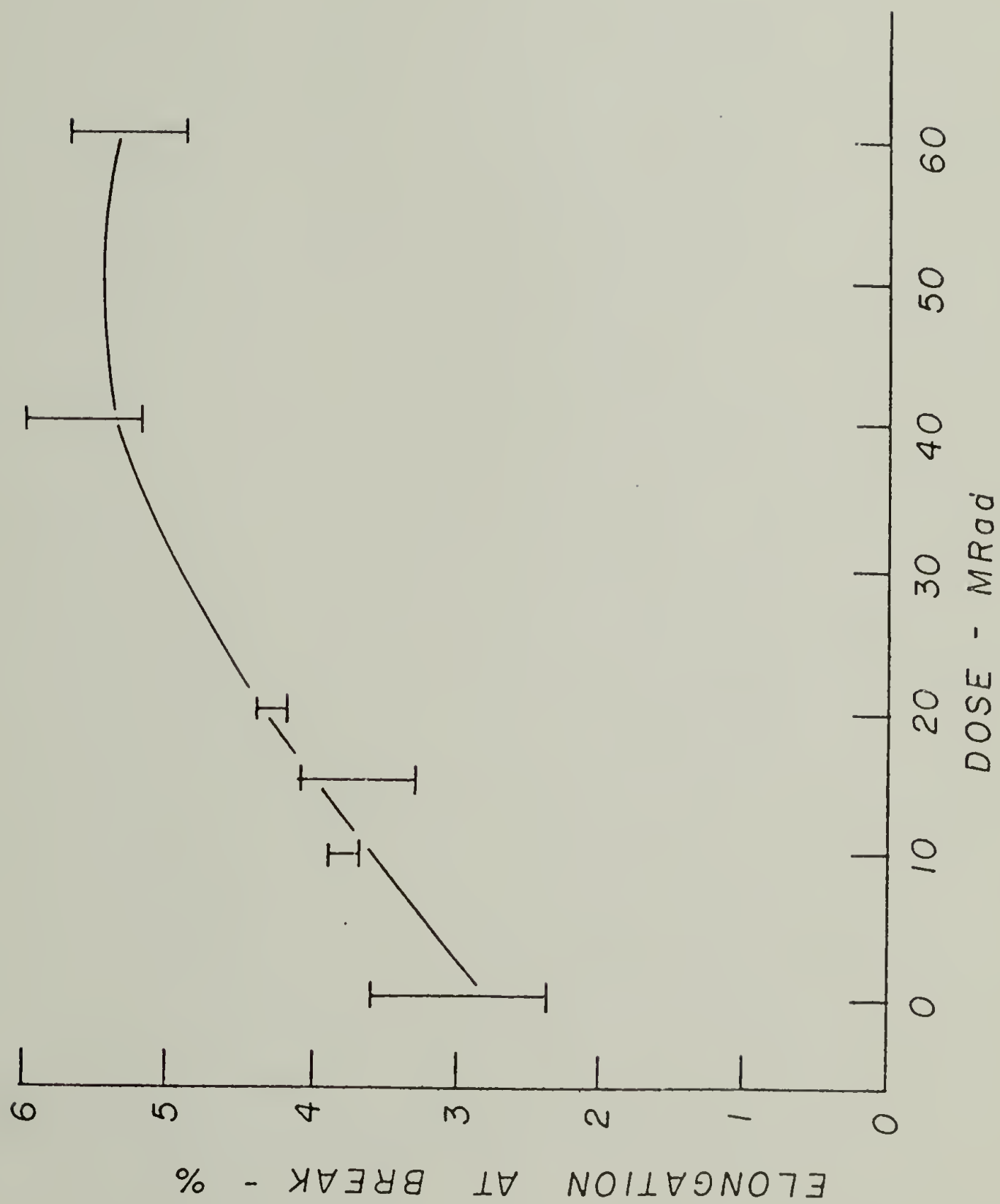


Figure 10



C H A P T E R   V I  
SOLID STATE EXTRUSION OF NYLONS 11 AND 12;  
PROCESSING, MORPHOLOGY AND PROPERTIES

I. Introduction

Solid state extrusion of high density polyethylene has provided films and fibers of exceptionally high modulus and tensile strength (1,2). It was thought that studies with the hydrogen-bonded nylons would expand the state-of-the-art of crystalline-state extrusion into polymers having more interesting starting morphologies, i.e. strong intermolecular secondary bonding. Such bonding results in higher crystalline melting points than attained in polymers which are intermolecularly bonded only by weaker van der Waals interactions. These higher melting points may result in useful products. Nylon 66 was the polymer of choice but proved extremely difficult to extrude in the solid state. The higher nylons, therefore, were chosen because of their longer olefinic segments, and the study of solid state extruded nylons was begun.

This chapter details the investigation of the process-structure-property relationships of nylon 11 [poly(11-amino-undecanoic acid)] and nylon 12 [poly(laurylactam)] extruded in the crystalline state. Discussion of experimental results is divided into two parts. Part I is on nylon 11 and part II is on nylon 12.

## II. Experimental

Solid state extruded nylon morphologies were prepared in an Instron capillary rheometer by the technique detailed previously (3). Variations on the process included crystallization and extrusion at several temperatures and pressures, as well as extrusion at constant rates (fixed crosshead speed) up to a predetermined maximum pressure. When the maximum pressure was attained, the load was cycled between narrow limits to maintain the pressure constant. By this method, strain hardening was minimized, as extrusion pressure was allowed to rise slowly up to the desired maximum.

Differential scanning calorimetry (DSC) was performed on the starting nylons and extrudates with a Perkin-Elmer DSC-1B at a heating rate of  $10^{\circ}\text{C}\cdot\text{min}^{-1}$  to yield heats of fusion (converted to percent crystallinity,  $X_c$ ) and crystalline melting points,  $T_m$ . Entropy of fusion was calculated from the above parameters through their thermodynamic relationship.

A Perkin-Elmer TMS-1 thermomechanical analyzer attachment to the DSC-1B was used for measurement of the linear expansion coefficient,  $\alpha$ . Sample preparation for this test was as previously described (4). A load of 3 grams was used with the expansion probe, and the scanning rate was  $10^{\circ}\text{C}\cdot\text{min}^{-1}$ . Test sample length was approximately 1 cm. Scans were made from  $-140^{\circ}\text{C}$  up to  $190^{\circ}\text{C}$ .

For studies of fiber mechanical properties, an Instron tensile testing machine, model TTCM, equipped with a strain-gauge extensometer, was used. Load-elongation curves were obtained at room temperature using a fixed elongation rate of  $0.02 \text{ cm-min}^{-1}$  for modulus measurements and  $0.50 \text{ cm-min}^{-1}$  for determination of tensile strength and strain at break. Samples were gripped in special clamps described elsewhere (1) to prevent slippage in the jaws. Nevertheless, slippage occurred during testing of nylon 11 ultimate properties, rendering impossible determination of tensile strength and strain at break. Strain rates for determination of Young's modulus and tensile strength (nylon 12) were  $3.33 \times 10^{-4} \text{ sec}^{-1}$  and  $1.67 \times 10^{-3} \text{ sec}^{-1}$ , respectively. The Young's modulus was determined as the tangent to the stress-strain curve at 0.2% strain.

Dilute solution viscosity measurements were conducted in a silicone oil bath using a #100 Ubbelohde viscometer. The solvent was m-cresol and test temperature was  $50^{\circ}\text{C}$ . Efflux time for the solvent was  $\sim 300 \text{ sec}$ .

### III. Part I - Nylon 11

#### A. Introduction.

Nylon 11 is the polyamide of 11-amino-undecanoic acid, which polymerizes on heating



The nylon 11 used in this study was supplied by the Rilsan Corporation, Glen Rock, New Jersey, having a reported  $\overline{M}_w = 34,000$  and  $\overline{M}_n = 13,000$ . The crystalline melting point of the as-recorded material was  $189^{\circ}\text{C}$  and the heat of fusion,  $11.26 \text{ cal-gm}^{-1}$ . This corresponds to ~ 21% crystallinity, as the heat of fusion for 100% crystalline nylon 11 has been calculated to be  $53 \text{ cal-gm}^{-1}$  (5,6).

The principal crystal structure of nylon 11 has been investigated by several authors (7-11) and found to exist in a planar zigzag conformation. The unit cell contains one monomer unit and is triclinic, having dimensions  $a = 4.9\text{\AA}$ ,  $b = 5.4\text{\AA}$ ,  $c$  (chain axis)  $= 14.9\text{\AA}$ ;  $\alpha = 49^{\circ}$ ,  $\beta = 77^{\circ}$ ,  $\gamma = 63^{\circ}$  (8). Polymorphism exists in nylon 11 as it does in virtually all the polyamides. Genas (6) found that, above  $70^{\circ}\text{C}$ , the  $a, b$  (basal) plane of the triclinic cell assumes pseudo-hexagonal packing. Onogi, et. al (11) observed that quenched film of nylon 11 contains  $\gamma$  (pseudo-hexagonal) crystals, while film solution-cast from *m*-cresol contains  $\alpha$  (triclinic) crystals. When films containing  $\gamma$  crystals were annealed above  $90^{\circ}\text{C}$ , they transformed into the  $\alpha$  modification. This  $\gamma \rightarrow \alpha$  transformation can also occur by stretching (12). Figure 1b is a wide angle x-ray photograph of a nylon 11 extrudate solid state extruded at an extrusion ratio of 7. Although the photographic reproduction is not good, the diffraction pattern is that commonly observed for the  $\alpha$  (triclinic) modification. It has been suggested (13,14) that the "parallel" structure of nylon 11, wherein the polar amide groups are tilted with respect to the chain axes, represents a stronger hydrogen bond association than does the "antiparallel" modification. This is consistent with the triclinic unit cell generally observed



at room temperature (8,9,11). The parallel modification arises when neighboring chains lie all in the same direction. In the antiparallel form, the chains alternate in direction. There is a difference between the two forms because the sequence of chain atoms encountered in going along the chain in one direction for  $\omega$ -amino acid polyamides is the reverse of that found in traveling in the opposite direction (15). For the odd  $\omega$ -amino acid nylons such as nylon 11, both the parallel and anti-parallel forms allow complete hydrogen bonding (8,16). Such is not the case for the even  $\omega$ -amino acid nylons (e.g. nylon 12), discussed in Part II.

The effects of pressure on the crystallization and structure of nylon 11 have recently been studied (17,18). Gogolewski and Pennings (17) found that pressures exceeding 3 Kbar (0.294 GPa) and temperatures higher than 230°C are sufficient for growth of chain-extended crystals, either by pressure-induced crystallization from the melt or by annealing of the folded chain crystals. They note that the  $\alpha$  (triclinic) crystalline modification, commonly found for folded chain crystals of nylon 11, was preserved in the high pressure crystallization and annealing experiments. They concluded that during the initial stages of crystallization under pressure, folded chain crystals are formed, with a crystalline order and long spacing larger than that of the starting nylon 11. These authors noted a 16°C/Kbar melting point increase with pressure.

Newman, et al. (18), performed a detailed x-ray structure analysis on nylon 11 at various temperatures and pressures. They concluded that

the chain conformation of Slichter (8) was distorted (shortened) along the c-axis at ambient temperature/pressure. No phase transformations from the  $\alpha$  crystal structure were observed at room temperature up to pressures of 19.5 Kbar (1.9 GPa). However, a crystal transition at atmospheric pressure was observed at 95°C, the triclinic ( $\alpha$  phase) changing to a pseudohexagonal structure. It was found that the increase in transition temperature with pressure was  $\sim 15^\circ\text{C}/\text{Kbar}$ .

DTA measurements by Gordon (19) show that the commonly observed glass transition at 43°C disappears if a sample is annealed at 75°C for 24 hours. A transition appears instead at 92°C. However, after 3 days at room temperature, samples show transitions at both 40 and 92°C. He concludes that the type of hydrogen bonded network formed from the melt depends on the temperature of formation and the break-up of such networks is responsible for observed glass transitions. He postulates that the network formed at the (ambient) annealing temperature is relatively stable, but the continuing motion of the olefinic linkages leads to generation of another network.

Further work on transitions in nylon 11 was reported by Northolt, et al. (20). Results from DSC, tensile testing and wide angle x-ray measurements on oriented samples aged at various temperatures revealed that the glass transition in nylon 11 shifted to higher temperatures as samples were aged at progressively higher temperatures. This was seen as resulting from amorphous phase hydrogen bond weakening at the higher (aging) temperatures and their subsequent orientation and reformation.

These authors reported no effect of moisture on the observed transitions.

The presence of several relaxations in nylon 11 has been observed by Onogi, et al. (11), from dynamic mechanical spectra. He shows the primary, or glass transition, relaxation at  $\sim 70^{\circ}\text{C}$  and a smaller relaxation at  $-50^{\circ}\text{C}$ . Another relaxation is seen at about  $+160^{\circ}\text{C}$ . This latter dispersion may be analogous to the  $\alpha$  transition observed in polyethylene at from  $80 - 100^{\circ}\text{C}$ . It is generally believed to be due to movements within the crystalline phase such as kink and twist crystal defect motions and chain rotation (21).

#### B. Experimental Results.

The effect of extrusion temperature on extrusion rate is shown in Figures 2 and 3. Figure 2 is a plot of extrudate length vs. extrusion time at two temperatures. Extrusion pressure is 0.24 GPa (2400 atm). As would be expected, the higher extrusion temperature results in an initially higher extrusion rate. However, both extrusion rates reduce with time and essentially stop. Figure 3 shows the effect of extrusion temperature on extrusion rate at a (maximum) extrusion pressure of 0.49 GPa (5000 atm). The results differ somewhat from those at lower extrusion pressure. Although the initial extrusion rate is also slightly higher at higher extrusion temperature, at long times the two (extrudate length vs. extrusion time) curves diverge whereas at the lower pressure (Figure 2), the two curves converge. Also at the high pressure, the curves at both extrusion temperatures are not tending to zero at long



times, although their slopes are decreasing. The effect of extrusion pressure at a single extrusion temperature is clearly shown in Figure 4. At all measured times, both extrudate length and extrusion rate are greater at the higher extrusion pressure.

Table 1 shows the results of dilute solution viscosity measurements done on both virgin nylon 11 pellets and on extruded fibers at several temperatures. No apparent drop in relative viscosities with time at any extrusion temperature indicates that the polymer chains did not undergo degradation during extrusion.

The effect of moisture content on the extrusion rate of nylon 11 is shown in Figure 5. The vacuum dried sample (circles) was dried in a vacuum oven at  $100^{\circ}\text{C}$  for 24 hours then stored in a desiccator over  $\text{P}_2\text{O}_5$  under vacuum. The triangles represent data for nylon 11 which had no conditioning prior to processing. All points fall on the same curve indicating negligible effect of water at ambient conditions on the extrusion rate. A third sample was conditioned by immersion in steam at atmospheric pressure for 71 hours. Upon removal of the restrictor at the beginning of extrusion, the pressure immediately dropped toward zero and a foamed melt rapidly extruded.

The effect of pulling on the emerging extrudate is shown in Figure 6. Nylon 11 was extruded at 0.49 GPa (max) and  $194^{\circ}$  and a 5 kg weight was attached to the extrudate. The initial extrusion rate was somewhat faster than the best runs done under the same conditions but without attached weights. However, at long times no significant increase in extrusion rate was observed.



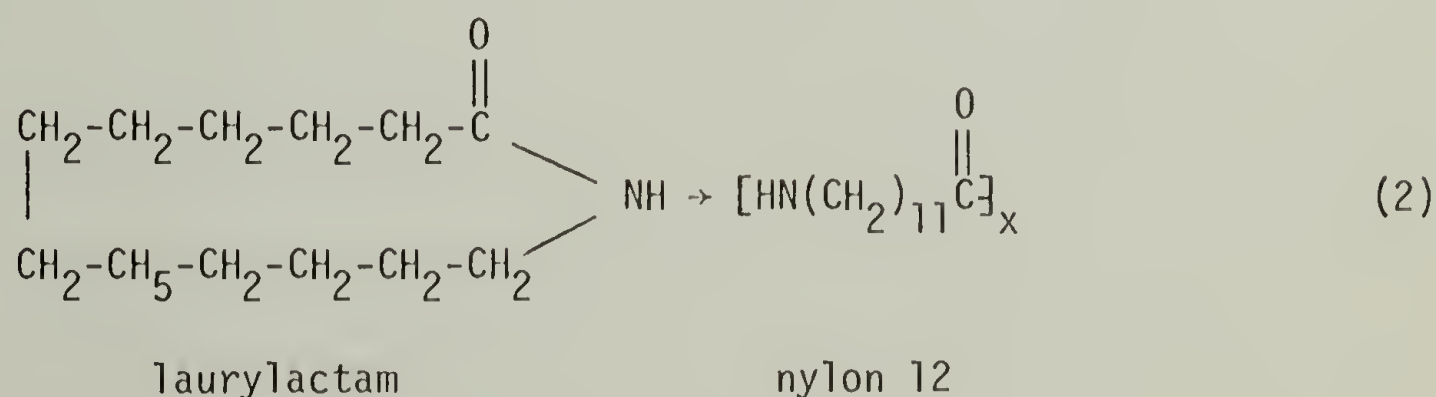
Figures 7 through 10 illustrate some physical properties of solid state extruded nylon 11 and their relationship to extrusion (draw) ratio (ER). Figure 7 is a plot of crystalline melting point ( $T_m$ ) vs. extrusion ratio.  $T_m$  rises with ER to about  $205^{\circ}\text{C}$  at an extrusion ratio of 12. This represents a  $16^{\circ}\text{C}$  increase over the undrawn virgin material ( $\text{ER} = 1$ ). Percent crystallinity ( $X_c$ ) as measured by DSC vs. ER is shown in Figure 8. Crystalline content also increases significantly with ER from  $\sim 21\%$  to  $\sim 44\%$  at an ER of 10. At  $\text{ER} = 12$ , the low values may be due to experimental error. Figure 9 shows the entropy of fusion ( $\Delta S_f$ ) plotted against ER. This parameter rises steeply to  $\text{ER} = 3$  and then approaches a limit.

Figure 10 is a plot of Young's modulus vs. ER. The maximum value attained was  $\sim 5.5$  GPa obtained at an extrusion ratio of 7. Beyond this point the modulus remains constant with ER.

#### IV. Part II - Nylon 12

##### A. Introduction.

Nylon 12 is polymerized from laurylactam, analogously to the use of caprolactam to make nylon 6:



The nylon 12 used in this study was supplied by Dr. Akio Kishimoto of the Toyo Seikan Company, Limited, Yokohama, Japan, having a reported  $\overline{M}_w \approx 28,600$  and  $\overline{M}_n = 14,300$ . The crystalline melting point of the as-received material was  $179^{\circ}\text{C}$  and heat of fusion,  $10.0 \text{ cal/gm}$  corresponding to 18.5% crystallinity since the heat of fusion for 100% crystalline nylon 12 has been calculated to be  $54 \text{ cal/gm}$  (6).

The crystal structure of nylon 12 has been found (22-24) to be a  $\gamma$  modification exclusively wherein the chains are twisted about the methylene groups. Its conformation is planar zigzag. Inoue and Hoshino (23) prepared a sample by drawing a monofilament 3.6X in boiling water then annealing it at  $160^{\circ}\text{C}$  for 10 hours. They found a monoclinic unit cell resembling the  $\gamma$ -form of the other even nylons. From x-ray data they calculated the monoclinic unit cell dimensions as  $a = 9.38\text{\AA}$ ,  $b = 32.2\text{\AA}$  (fiber axis),  $c = 4.87\text{\AA}$  and  $\beta = 121.5^{\circ}$ . There are four repeat monomer units per unit cell. Northolt, et al. (22), found that nylon 12 may exist in two different forms, depending on conditions. Melt-pressed sheet that was quenched in ice water, drawn 4.5X at room temperature, and annealed at  $170^{\circ}\text{C}$  at constant length for several hours under nitrogen, revealed a hexagonal unit cell. Melt-pressed sheet that was quenched in ice water, drawn 7X at just under  $180^{\circ}\text{C}$ , and cooled under stress to room temperature, exhibited what appeared to be a mixture of mono- and triclinic unit cell structures. No transition to the  $\alpha$ -form, wherein chains are antiparallel, is observed for nylon 12 upon stretching or treatment with aqueous phenol. It was therefore decided that the  $\gamma$ -form

of nylon 12 is more stable than for nylon 6, nylon 8 or nylon 10. This led to the conclusion that the longer the molecular chain in the even nylons, the more the crystal shows a tendency to form the  $\gamma$ -phase (23, 25). Nylon 12 is always found in the "parallel" modification (16) wherein neighboring chains are all in the same direction. Because this would result in 50% free NH groups, a twisting of the molecule is necessary for the observed complete hydrogen bond formation. This twisting causes a shortening of the unit cell along the chain (b) axis and results in the  $\gamma$ -form of the crystal. The wide angle x-ray diffraction pattern shown in Figure 1a is a typical pattern for the  $\gamma$ -phase of the even nylons. The strong intensity of the meridional diffraction spots in this picture result from the carbonyl oxygen atoms all lying in planes perpendicular to the fiber axis (25).

Crystallization and annealing under high pressure (4.9 Kbar - 0.48 GPa) was carried out by Stamhuis and Pennings. They noted that a partial transformation of the pseudo-hexagonal or monoclinic  $\gamma$ -crystal structure to an  $\alpha$  modification occurred in samples crystallized at 240°C and 4.9 Kbar for 16 hours. In the pressure range up to 3 Kbar (0.29 GPa) the increase in melting temperature was  $\sim 20^{\circ}\text{C}/\text{Kbar}$ , whereas at a pressure of 8 Kbar (0.78 GPa), the relationship was found to be  $12^{\circ}\text{C}/\text{Kbar}$ . The authors observed no chain-extended crystals, although a broadening of the distribution of crystal dimensions was noted at the higher pressures.

Onogi, et al. (11), found no evidence of an  $\alpha$ -type relaxation for nylon 12 (as is found in polyethylene) by dynamic mechanical testing, as

they did for nylon 11 at 160°C.

### B. Experimental Results.

The effect of extrusion temperature on extrusion rate is shown in Figure 11. The initial rate is higher at the higher temperature but after 15 minutes the rates are both slower and equivalent. At longer extrusion times, the lower temperature extrusion rate begins to level off, while the higher temperature extrusion rate continues to increase, albeit more slowly than at short times.

Figures 12 and 13 show the effect of crystallization/extrusion pressure on crystalline melting point ( $T_m$ ) and percent crystallinity ( $X_c$ ) of extruded nylon 12 fibers. Crystallization and extrusion pressures were equal, and as shown. In Figure 12,  $T_m$  decreases linearly from 0.12 to 0.24 GPa extrusion pressure, then remains constant. Percent crystallinity, shown in Figure 13, rises steadily to 0.24 GPa extrusion pressure before levelling off.

The influence of crystallization/extrusion temperature on the crystalline melting point and crystallinity for nylon 12 fibers is shown in Figures 14 and 15. Here the crystallization and extrusion temperatures were equal, and as shown. The melting point increases about 3°C as crystallization/extrusion temperature is increased from 176 to 196°C. The crystallinity rises from ~ 19% to ~ 30% at an increase in crystallization/extrusion temperature of 8°C, then levels off at higher preparation and processing temperatures.



Figure 16 shows the increase in  $T_m$  from  $179^{\circ}\text{C}$  for undrawn material ( $\text{ER} = 1$ ) to  $183^{\circ}\text{C}$  for fibers extruded to an ER of  $\sim 5$ .

The change in crystallinity with ER is plotted in Figure 17. Crystallinity increased from 19% for undrawn ( $\text{ER} = 1$ ) material to 33% for extrudates drawn about 6X. Both Figures 16 and 17 indicate significant increases in crystalline region perfection with increasing extrusion ratio.

Figure 18 shows how the entropy of fusion ( $\Delta S_f$ ) increases with increasing ER. An initial sharp increase as the material is extruded is followed by a more gradual increase at higher ER's.

Thermomechanical analysis was performed on nylon 12 fiber at an extrusion ratio of 5 (Figure 19). This is a semi-logarithmic plot of the normalized change in length of the fiber, i.e. orientation direction, vs. scanning temperature. The upper curve is for a melt extruded (dis-oriented) fiber whereas the bottom curve depicts the behavior of a solid state extruded fiber ( $\text{ER} = 5$ ) of the same nylon 12. The melt extruded fiber has a large positive expansion coefficient (slope of the curve) up to the melting point of  $179^{\circ}\text{C}$ . The solid state extruded fiber has a smaller positive expansion coefficient up to  $-70^{\circ}\text{C}$ , then contracts rapidly on further heating. Results of temperature cycling in the TMA experiment are shown in Figure 20 and are discussed in the next section.

Figure 21 shows the change in Young's modulus with ER. For an increase in extrusion ratio from 3 to 5.5, the tensile modulus gradually

increases from 2.6 to 3.3 GPa. Mechanical data are compared in Table 2 for molded, commercially melt-spun and cold-drawn, and solid state extruded (ER = 5.5) samples.

### V. Discussion and Conclusions

Several factors come into play during the solid state extrusion of nylon. As with other polymers, strain hardening (defined below) plays an important role, as does molecular weight and conditions for preparation of initial morphology prior to extrusion. Nylon extrusion is also affected by the hydrogen bonding of amide groups between neighboring chains. These bonds have a dissociation energy of  $\sim 8$  Kcal/mole and serve to tie the nylon molecules together. They exist in the non-crystalline as well as crystalline regions of nylons (27).

The influence of intermolecular hydrogen bonding on the flow of polymer melts has been investigated (28) with copolymers of ethylene and acrylic and methacrylic acid. An interesting result of this investigation was that, while the influence of average molecular weight on flow activation energy is minimal, an increase in the amount of hydrogen bonding substantially enhances both flow activation energy and viscosity. By acting as quasi-crosslinks these hydrogen bonds can substantially increase the effective size of a flow unit, leading to increased flow activation energy and viscosity. In this sense, the lower nylons, such as -66 and -6, should be extremely difficult to extrude in the solid state because

of their abundant intermolecular hydrogen bonding. Such bonding would inhibit sliding displacement along consecutive hydrogen bonded planes, the common deformation mode of nylons postulated from x-ray diffraction patterns (29).

The effect of pressure on hydrogen bonding has not been widely investigated but there is evidence (30) that increasing pressure causes a decrease in the distance between the planes containing the hydrogen bonds as well as between the planes held together by van der Waals bonds. This tightening of the structure would likely retard the flow through the die during solid state extrusion.

Flow activation energies ( $E_a$ ) were calculated for nylon 11 in this study at two extrusion pressures using the equation

$$\frac{d(\ln \eta)}{d(1/T)} = \frac{E_a}{R}$$

where  $T$  = extrusion temperature ( $^{\circ}\text{K}$ );  $R$  = gas law constant;  $\eta$  = apparent viscosity, calculated from

$$\eta = \frac{\sigma}{\frac{dL}{dt} \cdot \frac{1}{L}}$$

where  $\sigma$  = shear (applied stress);  $\frac{dL}{dt}$  = shear rate; L = length of extrudate where calculations were made.

The (apparent) activation energy doubled (73 to 124 Kcal/mole) with a doubling of extrusion pressure (0.24 to 0.49 GPa). These values were calculated assuming that solid state extrusion is a limiting case of melt extrusion. Apparent viscosities during extrusion were calculated as  $\sim 10^{14}$  poise at 0.24 GPa extrusion pressure and  $\sim 10^{15}$  poise at 0.49 GPa, both measured at 190°C. High density polyethylene (HDPE) extruded in the solid state commonly exhibits an apparent viscosity of  $10^{12} - 10^{13}$  poise in the steady-state region of extrusion rate curves. Mead and Porter (31) found the flow activation energy of a high density polyethylene to be between 20 and 60 Kcal/mole when the polymer was solid state extruded at temperatures in the vicinity of the ambient melting point. Measurements were made at 0.24 GPa where the nylon 11 value was 73 Kcal/mole.

Nylon 11 exhibits a transition at 160°C whereas nylon 12 shows no such high temperature transition as detected by dynamic mechanical testing (11). This ( $\alpha$ ) transition may well be responsible for the achievement of higher extrusion ratios and faster extrusion rates with nylon 11. Such relaxations are widely reported for other semicrystalline polymers, including polyethylene. They are generally believed to result from the onset of motions within the crystalline phase. Hashimoto, et al. (32), believe that the  $\alpha$  transition in polyethylene results from orientation dispersion of crystallites accompanied by shearing of mosaic crystallites



within the lamellae, and from molecular motion within the crystals. Other investigators have postulated kink (33,34) or twist (35) crystal defect motions, and chain rotation (36-38) as responsible for the observed  $\alpha$  relaxation in polyethylene. These processes may actually occur in nylon 12 but be undetectable by dynamic mechanical testing due to its small magnitude (37). In any case, such a relaxation involving motion in the crystalline phase at temperatures below, or at, solid state extrusion temperatures should aid the extrusion process by imparting mobility into the flow units, which are partially crystalline.

#### A. Strain Hardening.

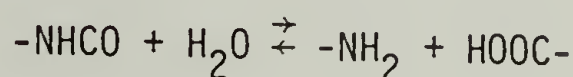
Strain hardening is a phenomenon which is commonly observed in semi-crystalline polymers below their  $T_m$ , and usually somewhat below  $T_g$  for amorphous polymers. During strain hardening the molecules become oriented parallel to the deformation direction. For semicrystalline polymers such as the nylons, the original crystal lamellae are broken up during deformation and aligned in the orientation direction to form microfibrils (39,40). Figures 22 and 23 are scanning electron microscope (SEM) photographs of solid state extruded nylon 12 extrudates fractured along the draw direction. Microfibrils can plainly be seen at each magnification. A result of this fibrillar (non-spherulitic) morphology wherein crystals are fairly uniform in size and perfection is shown in Figure 24. This depicts two extruded nylon 12 fibers photographed over print. The top fiber was melt extruded and is spherulitic and opaque,

whereas the bottom fiber was extruded in the crystalline state and is transparent. Further deformation of this microfibrillar morphology occurs via a stretching of the inter- and intralamellar tie molecules linking the folded lamellae. This deformation of the tie molecules causes the observed strain hardening, or resistance to flow, of solid state extruded polymers at high extrusion ratios.

Extrusion rates for all polymers investigated in this laboratory via the solid state extrusion process decrease at long extrusion times. Strain hardening is believed responsible for this phenomenon. With the high nominal extrusion ratio dies commonly used in this laboratory, extrusion ratio (ER) of the extrudate increases with extrudate length, as explained in Chapter II. In the case of high density polyethylene, maximum attainable ER is limited by a fracture mechanism at extrusion ratios  $\geq 40$ . The nylons investigated in this study also exhibited limiting extrusion ratios. Nylon 12 exhibited a maximum ER of  $\sim 7$ , while nylon 11 attained an ER of  $\sim 12$ . In most cases, however, maximum extrusion ratios were limited not by fracture of the extrudate, as is the case with polyethylene, but rather by the virtual cessation of extrusion. In other words, at long times ( $> 8$  hours), extrusion rates for the nylons declined to  $< 1$  mm/hr. Strain hardening of these polymers apparently reaches the point where even 0.49 GPa is insufficient pressure to force them through the die. The higher yield point of nylons vis-a-vis high density polyethylene is seen as being responsible for the absence of fracture in the majority of nylon extrusions carried out to long extrusion times.

### B. Degradation.

Degradation of nylons generally occurs by a hydrolysis reaction wherein the amide groups combine with water to form an amine and an acid (41).



The reverse reaction (right to left) depicts how amides are formed from amines and acids. The equilibrium constant according to the mass action law is defined as the product of the concentration of the groups produced by the reaction divided by the concentration of the original species

$$K_c = \frac{[\text{NH}_2] [\text{COOH}]}{[\text{NHCO}] [\text{H}_2\text{O}]}$$

If the ratio of concentrations on the right-hand side of Equation (5) is different from  $K_c$ , then that reaction will occur which causes the ratio to approach  $K_c$ ; hydrolysis if the ratio is less than  $K_c$ ; and condensation if the ratio is greater than  $K_c$ . Thus, it is whether the amount of water in the nylon is more or less than the equilibrium value that determines

whether condensation to a higher molecular weight or hydrolysis to a lower molecular weight (degradation) takes place (41). The hydrolysis reaction is endothermic, which means that  $K_c$  increases as temperature increases. Therefore, degradation will be minimized if nylons are processed at the lowest convenient temperatures and in as dry a condition as possible.

At higher molecular weights, the ratio of  $[\text{NHCO}]$  groups to  $[\text{NH}_2]$  and  $[\text{COOH}]$  (chain end) groups increases, so from Equation (5) it is apparent that thermal degradation (hydrolysis) is more likely to occur. Also from Equation (5), the equilibrium amount of water increases for the higher nylons as  $[\text{NHCO}]$  decreases at a given molecular weight.

Degradation via hydrolysis is not a factor in commercial processing of nylons except in unusual instances of excessively high temperatures or excessively long hold up in the processing machine. When decomposition does occur, it involves either breaking of each bond in and adjacent to the amide group (42) or fission of the C-N bond alpha to the amide carbonyl (43,44).

### C. Plasticizers.

Plasticizers for nylons are normally high molecular weight polar compounds of low volatility that are capable of withstanding processing temperatures and interrupt hydrogen bonding between chains by association with the amide groups. These include (41) monomeric carbonamides and sulfonamides, phenolic compounds, cyclic ketones, mixtures of phenols



and esters, sulfonated esters or amides, N-alkylolarylsulfonamides, selected aliphatic diols, and phosphite esters of alcohols such as 9-phenylnonanol-1. Water may be regarded as a non-processable plasticizer and plasticizers lower the glass transition temperature of nylon in the same manner as water. Because plasticizers lower Young's modulus and tensile strength, they would have to be extracted from the extrudate following solid state extrusion. However, the temporary disruption of hydrogen bonds may well be the solution to the problem of low maximum extrusion ratios in nylon crystalline state extrusion.

Solvents used judiciously may act as plasticizers. Disruption of hydrogen bonds in the noncrystalline regions is necessary for a solvent to attack nylons and is a major factor in the plasticizing effect of absorbed solvents. Solvents most likely to swell or dissolve nylons are those containing hydrogen atoms attached to electrophilic groups which increase the positive character of the hydrogen and enable it to compete effectively with the amide hydrogen for association with the electronegative oxygen atom of the amide carbonyl group (41). Water, alcohols, and partially halogenated hydrocarbons such as chloroform are examples of compounds absorbed by nylons. Solvent efficiency increases with increasing temperature and/or decreasing crystallinity, whereas efficiency decreases as the hydrogen bonding capability of the solvent decreases.

Some solutions of salts such as calcium bromide, zinc chloride, or potassium thiocyanate, or alcohol-salt combinations such as methanol-

lithium chloride will serve as solvents for nylons, particularly at high temperatures. Dunn and Sansom (45) suggest that zinc, copper, cobalt and manganese chlorides destroy intermolecular hydrogen bonding by forming metal complexes with the amide carbonyl. Water or alcohol is used to transport the metal ion to the amide group. The effect of lithium and potassium on bulk properties of nylon 6 has been investigated by Acierno, et al. (46). They generally found that the melt viscosity increased with the addition of the salts whereas the activation energy for flow was unaltered. Labile crosslinking from polymer-salt interaction is believed to occur. Equilibrium melting temperature and crystallization rate were significantly depressed by the salts, while shear modulus was unaffected at temperatures below the glass transition temperature. Acierno, et al. (47), in another study, melt-extruded nylon 6-lithium chloride and subsequently drew and annealed the extruded filament. They observed a five-fold increase in Young's modulus following this treatment. These results support their contention that it should be possible to effectively orient a nylon-salt system of low crystallinity, then subsequently recover the crystallinity by annealing or by extracting the salt.

The effect of crystallization pressure on nylons 11 and 12 has been investigated by Pennings, et al. (17,26), as detailed earlier. The pressure range used in the present study for nylon 12 is below the pressure necessary for growth of extended chain crystals. However, that doesn't mean that no chain-extended crystals are present since they may be formed by deformation in the die entrance region rather than by pressure

crystallization (3). The results presented here for nylon 12 indicate that, for the pressure range investigated, increasing crystallization/extrusion pressure causes the formation of a greater amount of crystals, but that these crystals are smaller in size and/or perfection.

Although percent crystallinity and crystalline melting points appear to be levelling off at higher pressures, they may increase further with pressure as the region of extended-chain crystals is reached (26).

The effect of increasing crystallization/extrusion temperature on nylon 12 is to raise the melting point and crystallinity of extrudates. One would expect such increases since the undercooling is less at higher crystallization temperatures at a given pressure. The levelling off of percent crystallinity at higher crystallization/extrusion temperatures may be due to partial melting of smaller crystals at the die exit while the larger, more perfect crystals are unaffected.

Both melting point and heat of fusion (here converted to percent crystallinity) are related to the entropy of fusion by

$$\Delta G_f = \Delta H_f - T_m \Delta S_f$$

where  $\Delta G_f$  = Gibbs free energy of fusion;  $\Delta H_f$  = enthalpy (heat) of fusion;  $T_m$  = melting temperature in degrees Kelvin;  $\Delta S_f$  = entropy of fusion.

At the melting point, the crystalline and molten states are in equilibrium, so  $\Delta G_f = 0$ . Hence

$$\Delta H_f = T_m \Delta S_f$$

or

$$\Delta S_f = \frac{\Delta H_f}{T_m}$$

Tonelli (48) divides the entropy of fusion into two components, a constant volume contribution and a volume expansion contribution. He attributes the former to conformational changes in the polymer chains (increased conformational freedom) which accompany their melting, and is an intramolecular process. The volume expansion contribution to the fusion process is seen as resulting from the increase in energy and entropy attendant upon the increase in the average polymer chain separation. This is an intermolecular process. Tonelli further states that nylons melt at relatively high temperatures due to (relatively) small entropies of fusion. The reason cited (48) for the smaller entropies is



polymorphism or conformational disorder in nylon crystals which lowers the conformational entropy of the system at the fusion temperature.

In the present study, the crystalline melting point increases more rapidly than the percent crystallinity. This apparently results from the small increase in entropy of fusion plotted against extrusion ratio in Figures 9 (nylon 11) and 18 (nylon 12) along with the relationship given in Equation (7). Such entropy behavior is expected from Tonelli's conclusions since both nylon 11 and 12 are known to exhibit polymorphism at elevated temperatures and/or under conditions of solid state deformation (8,9,18,19,22).

Thermomechanical analysis (TMA) can be used as a qualitative measure of extended chain content when measurements are taken along the fiber direction (see Chapters IV or V). Solid state extruded nylon 12 samples all showed an initial positive expansion coefficient that was somewhat smaller than the corresponding melt extruded sample (Figure 19). As the scanning temperature was increased, solid state extruded fibers contracted, and the linear expansion coefficient became negative, in all cases, at temperatures  $< 0^{\circ}\text{C}$ . The initial small positive coefficient of expansion is probably due to a small component of extended chain crystals counteracting the large positive coefficient arising from unoriented amorphous and folded-chain regions (49). This small chain-extended component is apparently fairly stable and remains as the temperature is raised, even though hydrogen bonded sheets are given sufficient mobility to slip with respect to each other, causing a macroscopic shortening of

the fiber. At higher extrusion ratios than tested here by TMA ( $ER = 5$ ), one would expect more highly developed crystallinity (from the present crystallinity plots) and consequently a greater number of stable extended chain structures.

A solid state extruded sample of nylon 12 was heated from  $-130^{\circ}\text{C}$  to  $150^{\circ}\text{C}$  in the thermomechanical analyzer and then cooled again to  $-130^{\circ}\text{C}$  followed by another heating cycle. The behavior on initial heating was as just described. However, upon recooling, the sample at first expanded (in the axial direction), then reached a constant length which did not vary (with cooling and reheating) from  $-25^{\circ}\text{C}$  on the cooling cycle to  $\sim 0^{\circ}\text{C}$  on the heating cycle (see Figure 20). Beyond this point, the sample shortened with increase in temperature up to the melting point as observed earlier in this section for solid state extruded nylon 12 fibers. The plateau in Figure 20 apparently results from annealing of the morphology during the first heating cycle wherein hydrogen bonds are given sufficient mobility to break and reform. A chain-extended component remains but the fiber never regains its initial length. However, the new structure is more stable and retains its dimensional stability up to  $\sim 0^{\circ}\text{C}$ . At this temperature, the data indicate that some instability persists or that the radial expansion is much greater than the axial expansion, since collapse of the macroscopic structure begins at this relatively low temperature. In other words, in the temperature range  $0 \rightarrow 150^{\circ}\text{C}$  (during heating), the fiber behaves the same before and after thermal treatment. Within this range, a quasi-stable state exists. This

state likely consists of unoriented amorphous and crystalline regions stabilized by hydrogen bonds, along with an extended chain component which survives thermal annealing (at least up to 150°C).

Young's modulus of nylon 11 increases more rapidly with draw than nylon 12. However, beyond an ER of 7, the nylon 11 modulus remains constant. Because the tensile modulus of high density polyethylene begins to sharply increase only at extrusion ratios greater than 10, the nylons' potentially high mechanical properties may be realized only when higher ER's are attained. At any rate, nylon 11 fibers cold extruded in this study at an ER of 7 show an 80% increase in tensile modulus over commercial monofilaments. Nylon 12 fibers at an ER of 5.5 display a modulus equal to commercial monofilament.

In conclusion, the nylons appear to offer the promise of highly improved physical and mechanical properties if higher extrusion ratios can be realized. By the incorporation of certain additives prior to crystallization and extrusion, this may be possible. Another route may be the split billet technique recently developed in this laboratory (50). In the present study, mechanical tensile modulus was equal to or greater than that reported in the literature for these polymers. The melting point and crystallinity were significantly increased over virgin material. Further work on nylon systems is warranted.

References

1. N. J. Capiati and R. S. Porter, J. Polym. Sci., Polym. Phys. Ed. 13, 1177 (1975).
2. W. G. Perkins, N. J. Capiati and R. S. Porter, Polym. Eng. Sci. 16, 200 (1976).
3. N. J. Capiati, S. Kojima, W. G. Perkins and R. S. Porter, J. Mater. Sci. 12, 334 (1977).
4. R. S. Porter, N. E. Weeks, N. J. Capiati and R. J. Krzewski, J. Therm. Anal. 8, 547 (1975).
5. M. Inoue, J. Polym. Sci., A-1, 3427 (1963).
6. R. Greco and L. Nicolais, Polymer 17, 1049 (1976).
7. Y. Kimoshita, Makromol. Chem. 33, 1 (1959).
8. W. P. Slichter, J. Polym. Sci. 36, 259 (1959).
9. M. Genas, Angew. Chem. 74, 535 (1962).
10. R. Aelion, Ann. Chim. (Paris) 3, 5 (1948).
11. S. Onogi, K. Asada, Y. Fukui and I. Tachinaka, Bull. Inst. Chem. Res. Kyoto Univ. 52, 368 (1974).
12. T. Sasaki, J. Polym. Sci., B-3, 557 (1965).
13. W. O. Baker and C. S. Fuller, J. Am. Chem. Soc. 64, 2399 (1942).
14. W. O. Baker and N. R. Pope, Paper presented at the 122nd meeting of the American Chemical Society, Atlantic City, New Jersey, September, 1952.
15. R. Hill and E. E. Walker, J. Polym. Sci. 3, 609 (1948).



16. F. W. Lord, Polymer 15, 42 (1974).
17. S. Gogolewski and A. J. Pennings, Polymer 18, 660 (1977).
18. B. A. Newman, T. P. Sham and K. D. Pae, J. Appl. Phys. 48, 4092 (1977).
19. G. A. Gordon, J. Polym. Sci., A-2, 9, 1693 (1971).
20. M. G. Northolt, B. J. Tabor and J. J. van Aartsen, Progr. Colloid and Polym. Sci. 57, 225 (1975).
21. R. Boyd, A.C.S. Organic Coatings and Plastics Preprint 35 (2), 216 (1975).
22. M. G. Northolt, B. J. Tabor and J. J. van Aartsen, J. Polym. Sci., A-2, 10, 191 (1972).
23. K. Inoue and S. Hoshino, J. Polym. Sci., Polym. Phys. Ed. 2, 1077 (1973).
24. T. Ishikawa, A. Sugihara, T. Hamada, S. Nagai, N. Yasuoka and N. Kawai, Kagaku 9, 1744 (1973).
25. D. C. Vogelsong, J. Polym. Sci., A-1, 1055 (1963).
26. J. E. Stamhuis and A. J. Pennings, Polymer 18, 667 (1977).
27. C. G. Cannon, Spectrochim. Acta 16, 302 (1960).
28. L. L. Blyer and T. W. Haas, J. Appl. Polym. Sci. 13, 2721 (1969).
29. J. J. Point, M. Dosiere, M. Gillot and A. Goffin-Gerin, J. Mater. Sci. 6, 479 (1971).
30. S. Gogolewski and A. J. Pennings, Polymer 18, 650 (1977).
31. W. T. Mead and R. S. Porter, submitted to J. Polym. Sci., Polym. Phys. Ed.

32. T. Hashimoto, N. Yasuda, S. Suehiro, S. Nomura and H. Kawai, A.C.S. Polymer Preprints 17 (2), 118 (1976).
33. W. Pechold, S. Blasenbrey and S. Woerner, Kolloid Z. 189, 14 (1963).
34. P. E. McMahon, R. L. McCullough and A. A. Schlegel, J. Appl. Phys. 38, 4123 (1967).
35. D. H. Reneker, J. Polym. Sci. 59, 539 (1962).
36. J. D. Hoffman, G. Williams and E. Passaglia, J. Polym. Sci., C-14, 173 (1976).
37. C. A. F. Tuijnman, Polymer 4, 259 (1963).
38. R. L. McCullough, J. Macromol. Sci.-Phys. 9, 97 (1974).
39. A. Peterlin, J. Mater. Sci. 6, 490 (1971).
40. R. E. Robertson, J. Polym. Sci., Polym. Phys. Ed. 10, 2437 (1972).
41. M. I. Kohan, ed., "Nylon Plastics," John Wiley, New York, 1973.
42. I. Goodman, J. Polym. Sci. 17, 587 (1955).
43. S. Straus and L. A. Wall, J. Res. Nat. Bur. Std. 60, 39 (1958); *ibid*, 63A, 269 (1959).
44. B. Kamerbeek, G. H. Kroes and W. Grolle in "Thermal Degradation of Polymers," S. C. I. Monograph No. 13, London, 1961, p. 357.
45. P. Dunn and G. F. Sansom, J. Appl. Polym. Sci. 13, 1641 (1969).
46. D. Acierno, E. Bianchi, A. Ciferri, B. DeCindio, C. Migliaresi and L. Nicolais in Polym. Symp. Ed. 54, 259 (1976), H. Markovitz and E. F. Casassa, eds., Interscience, New York.

47. D. Acierno, F. P. LaMantia, G. Polizzotti, G. C. Alfonso and A. Ciferri, J. Polym. Sci., Polym. Letters Ed. 15, 323 (1977).
48. A. E. Tonelli in "Analytical Calorimetry," R. S. Porter and J. F. Johnson, eds., Vol. 3, Plenum Press, New York, 1974.
49. D. W. Van Krevelen and P. J. Hoftyzer, "Properties of Polymers," Elsevier, Amsterdam, 1976, Chapter 4.
50. P. D. Griswold, A. E. Zachariades and R. S. Porter, to be published.

TABLE 1

Relative Viscosities of Nylon 11 Fibers Extruded  
at Temperatures Shown and Dissolved  
in m-Cresol at 50°C.

Extrusion Temperature <u>°C</u>	<u>Relative Viscosity</u>
Virgin Pellets	1.14
186	1.16
190	1.21
194	1.13
198	1.23



TABLE 2

Comparison of Mechanical Properties of Molded,  
 Commercially Melt Extruded/Cold-Drawn, and  
 Solid State (Cold) Extruded Nylon 12.  
 The Latter at An Extrusion Ratio of  
 5.5 and  $\bar{M}_w = 34,000$ ,  $\bar{M}_n = 13,000$ .

<u>Property</u>	<u>Molded</u>	<u>Cold- Drawn</u>	<u>Cold- Extruded</u>
Tensile Modulus (GPa)	1.24	2.9	3.3
Tensile Strength (GPa)	.06	.31	.26
Elongation at Break (%)	300	40	38

Captions for Figures

1. Wide angle x-ray photographs of (a) nylon 12 and (b) nylon 11 solid state extruded fibers. Fiber axis vertical.
2. Extrudate length vs. extrusion time for nylon 11 fibers crystallized and extruded at 0.24 GPa pressure and at temperatures shown.
3. Extrudate length vs. extrusion time for nylon 11 fibers crystallized and extruded at 0.49 GPa and at temperatures shown.
4. Extrudate length vs. extrusion time for nylon 11 fibers extruded at 194<sup>0</sup>C and at extrusion pressures shown. Crystallized at 194<sup>0</sup>C and 0.24 GPa.
5. Extrudate length vs. extrusion time for nylon 11 fiber both vacuum dried and non-dried prior to processing. Crystallized at 194<sup>0</sup>C and 0.24 GPa; extruded at 194<sup>0</sup>C and 0.49 GPa.
6. Extrudate length vs. extrusion time for a nylon 11 fiber with a 5 kg weight attached to the emerging extrudate. Crystallized at 194<sup>0</sup>C and 0.24 GPa; extruded at 194<sup>0</sup>C and 0.49 GPa.
7. Crystalline melting point vs. extrusion ratio (ER) for a nylon 11 fiber crystallized at 194<sup>0</sup>C and 0.24 GPa; extruded at 194<sup>0</sup>C and 0.49 GPa. ER = 1 is undrawn material.
8. Percent crystallinity vs. ER for a nylon 11 fiber crystallized at 194<sup>0</sup>C and 0.24 GPa; extruded at 194<sup>0</sup>C and 0.49 GPa. ER = 1 is undrawn material.

9. Entropy of fusion vs. ER for a nylon 11 fiber crystallized at  $194^{\circ}\text{C}$  and 0.24 GPa; extruded at  $194^{\circ}\text{C}$  and 0.49 GPa. ER = 1 is undrawn material.
10. Young's modulus vs. ER for a nylon 11 fiber crystallized at  $194^{\circ}\text{C}$  and 0.24 GPa; extruded at  $194^{\circ}\text{C}$  and 0.49 GPa.
11. Extrudate length vs. extrusion time for nylon 12 fibers crystallized at  $184^{\circ}\text{C}$  and 0.24 GPa; extruded at 0.49 GPa and at temperatures shown.
12. Crystalline melting point vs. crystallization/extrusion pressure for nylon 12 fibers. Crystallization/extrusion temperature:  $178^{\circ}\text{C}$ . Measurements taken at an ER = 4.
13. Percent crystallinity vs. crystallization/extrusion pressure for nylon 12 fibers. Crystallization/extrusion temperature:  $178^{\circ}\text{C}$ . Measurements taken at an ER = 4.
14. Crystalline melting point vs. crystallization/extrusion temperature for nylon 12 fibers. Crystallization/extrusion pressure: 0.24 GPa. Measurements taken at an ER = 4.
15. Percent crystallinity vs. crystallization/extrusion temperature for nylon 12 fibers. Crystallization/extrusion pressure: 0.24 GPa. Measurements taken at an ER = 4.
16. Crystalline melting point vs. ER for nylon 12 fibers crystallized and extruded at  $178^{\circ}\text{C}$  and 0.24 GPa. ER = 1 is undrawn material.
17. Percent crystallinity vs. ER for nylon 12 fibers crystallized and extruded at  $178^{\circ}\text{C}$  and 0.24 GPa. ER = 1 is undrawn material.

18. Entropy of fusion vs. ER for nylon 12 fibers crystallized and extruded at  $178^{\circ}\text{C}$  and 0.24 GPa. ER = 1 is undrawn material.
19. Linear expansion coefficients (slopes) of melt extruded and solid state extruded (ER = 5) nylon 12 fibers. Solid state extruded fiber crystallized at  $186^{\circ}\text{C}$  and 0.24 GPa; extruded at  $176^{\circ}\text{C}$  and 0.49 GPa.
20. Temperature cycling of a nylon 12 fiber in the thermomechanical analyzer. Three cycles shown: heating, cooling and reheating. Slope of the plot is the linear expansion coefficient.
21. Young's modulus vs. ER for a nylon 12 fiber crystallized at  $184^{\circ}\text{C}$  and 0.24 GPa and extruded at  $182^{\circ}\text{C}$  and 0.49 GPa.
22. SEM photographs of solid state extruded nylon 12 fibers fractured (peeled) under liquid nitrogen along draw direction which is horizontal. ER = 7. (a) magnification 300X; (b) magnification 2,000X.
23. SEM photographs of solid state extruded nylon 12 fibers at higher magnification than in Figure 22. (a) magnification 3,600X; (b) magnification 5,000X.
24. Comparison of two nylon 12 fibers photographed over print. Top, melt extruded; bottom, solid state extruded.



*a.**b.*

Figure 1

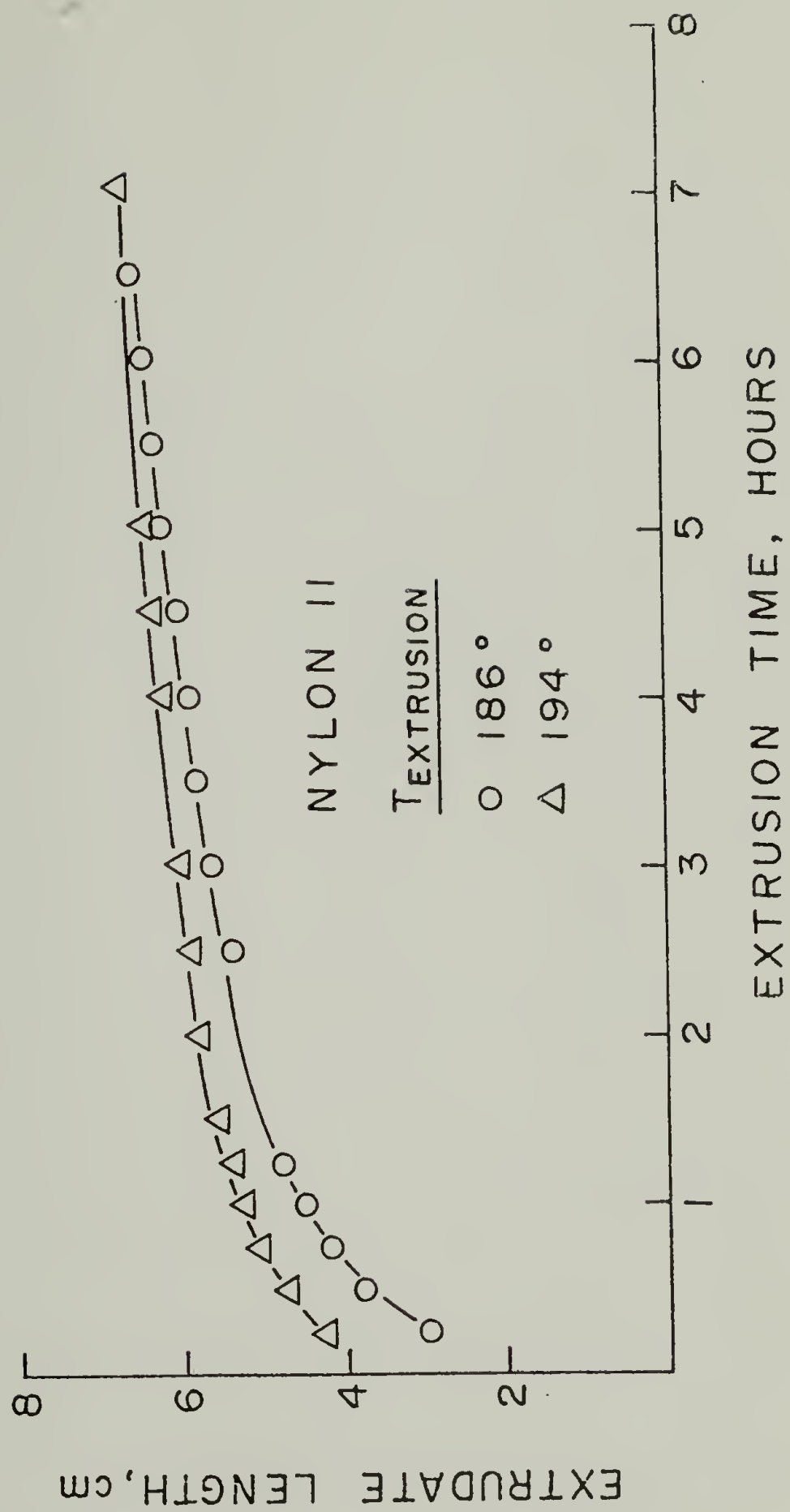


Figure 2

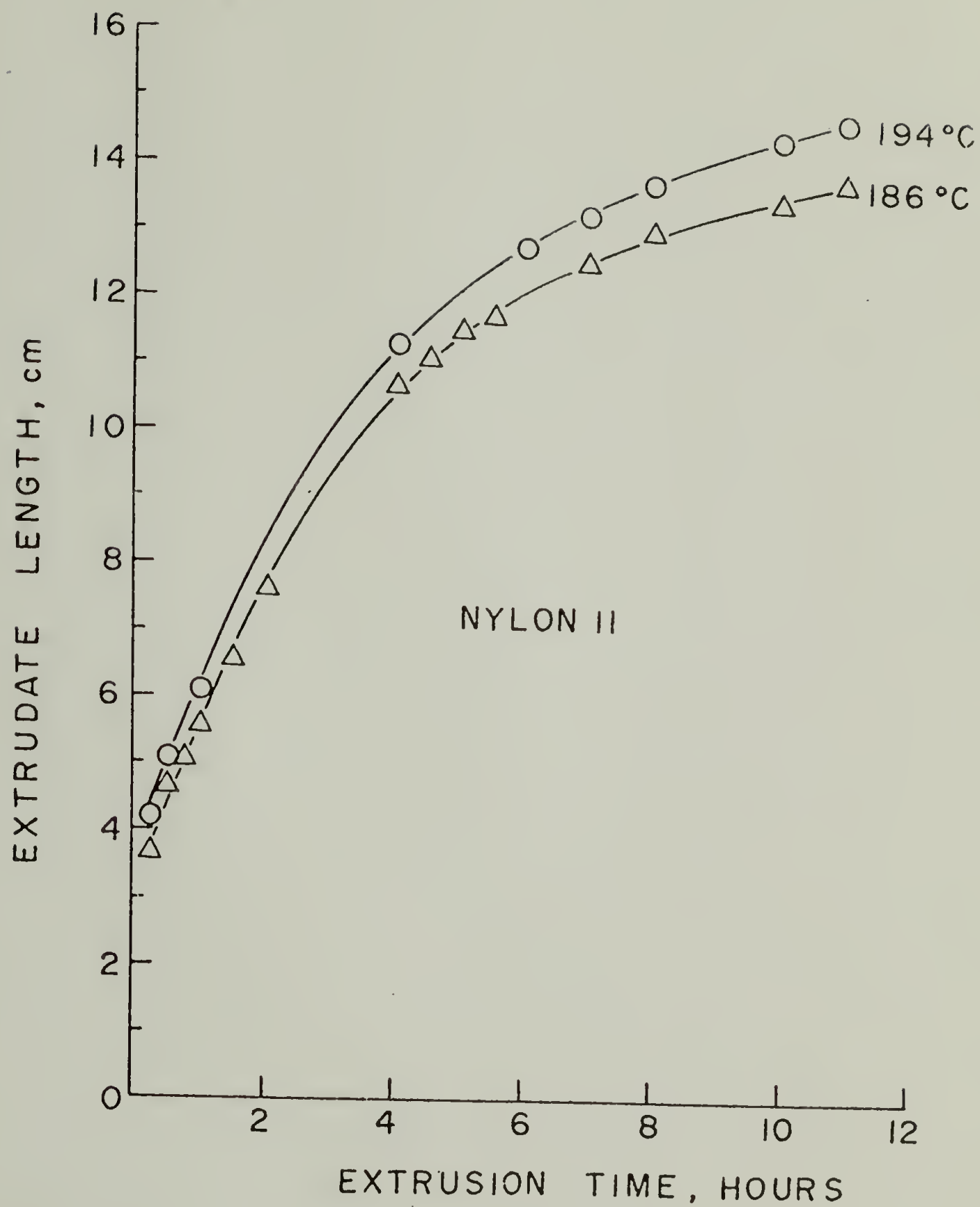


Figure 3

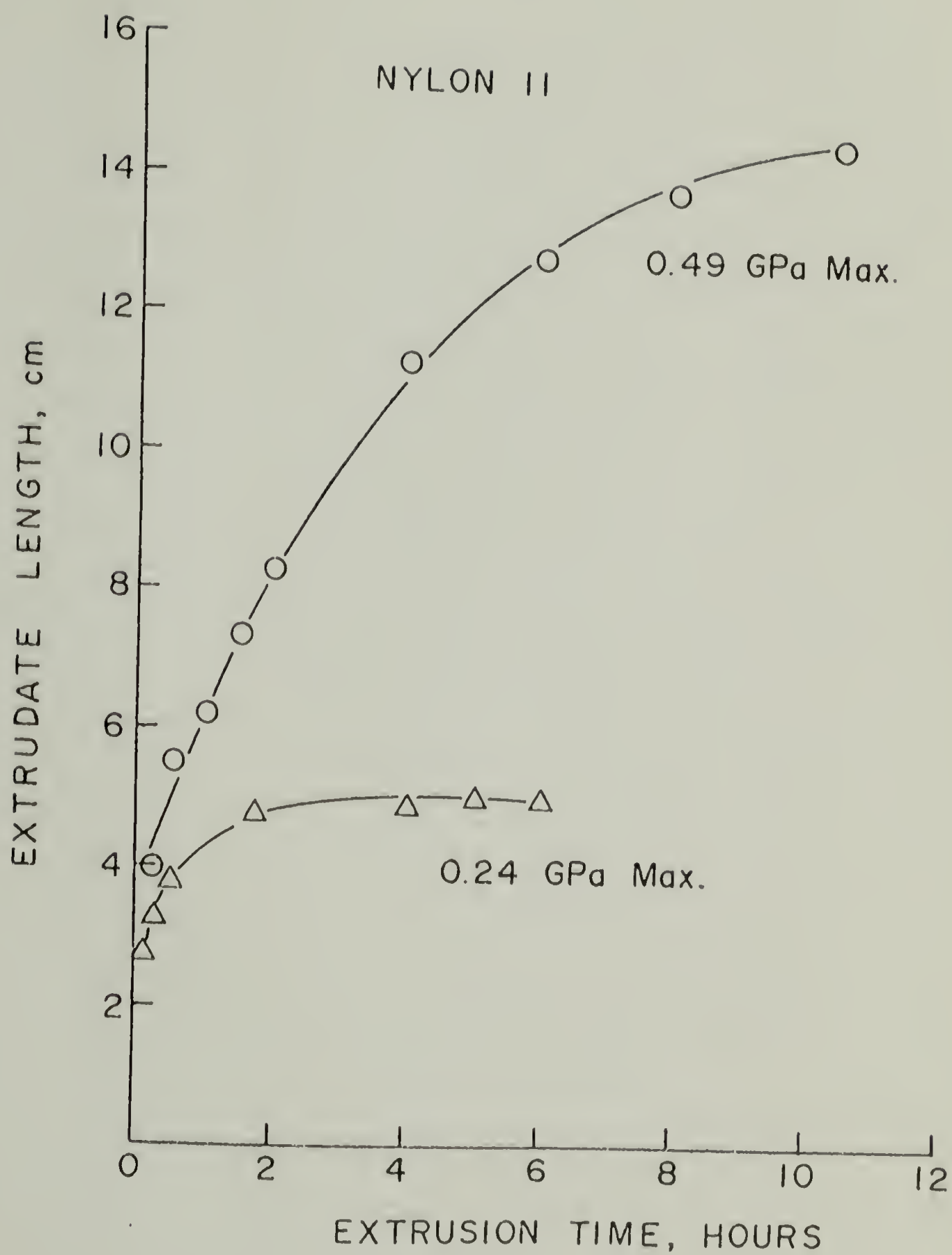


Figure 4



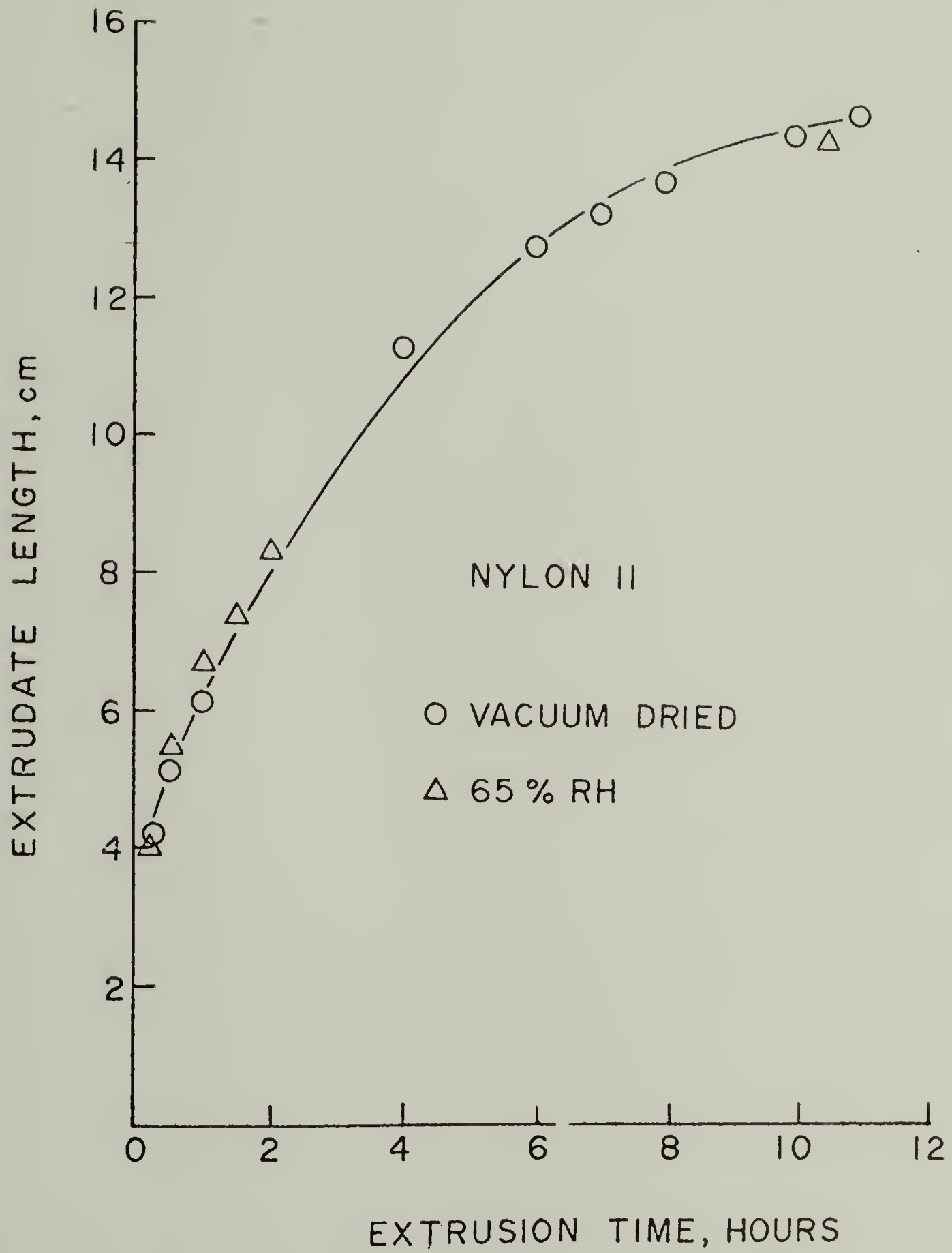


Figure 5

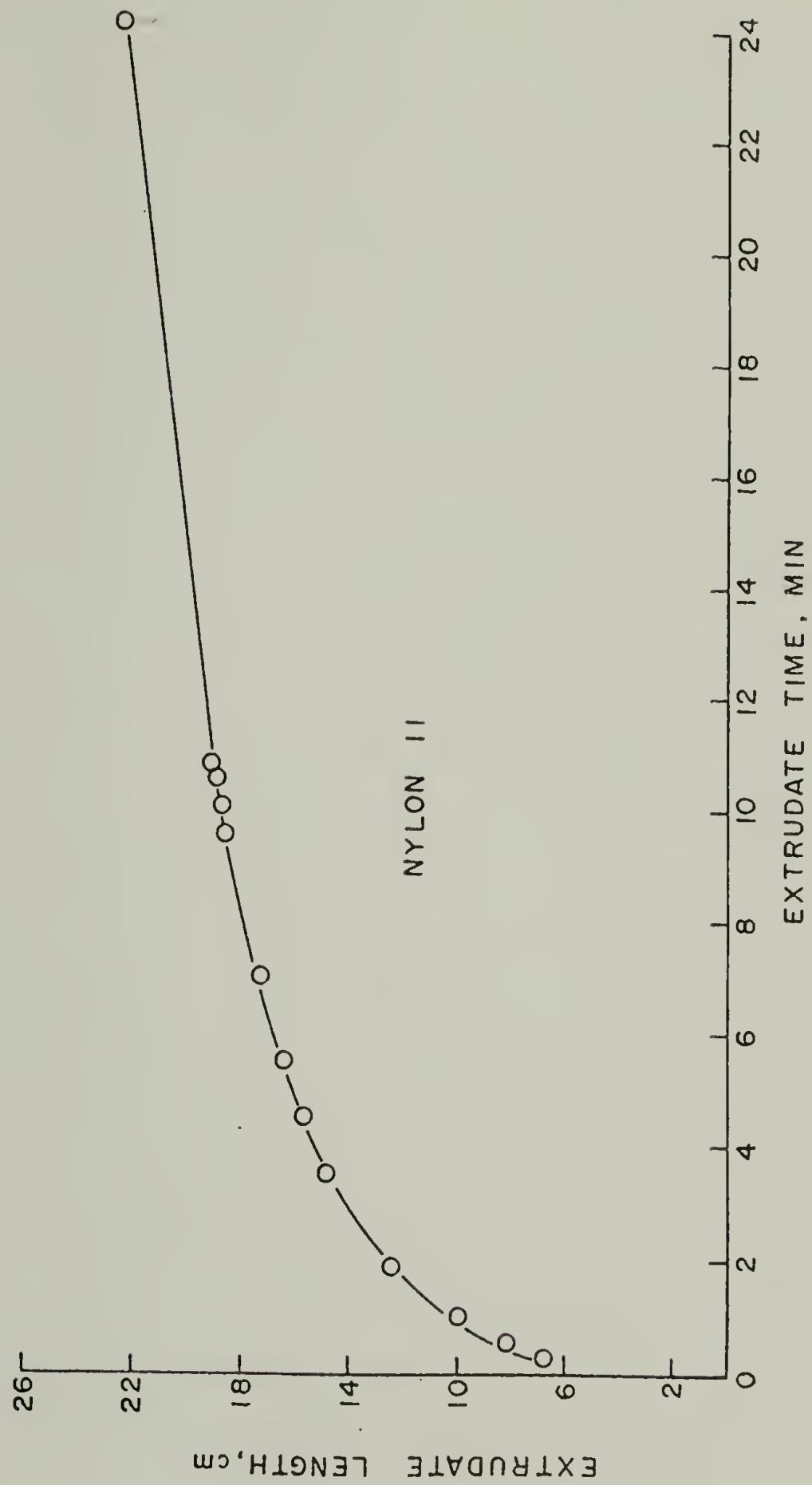


Figure 6

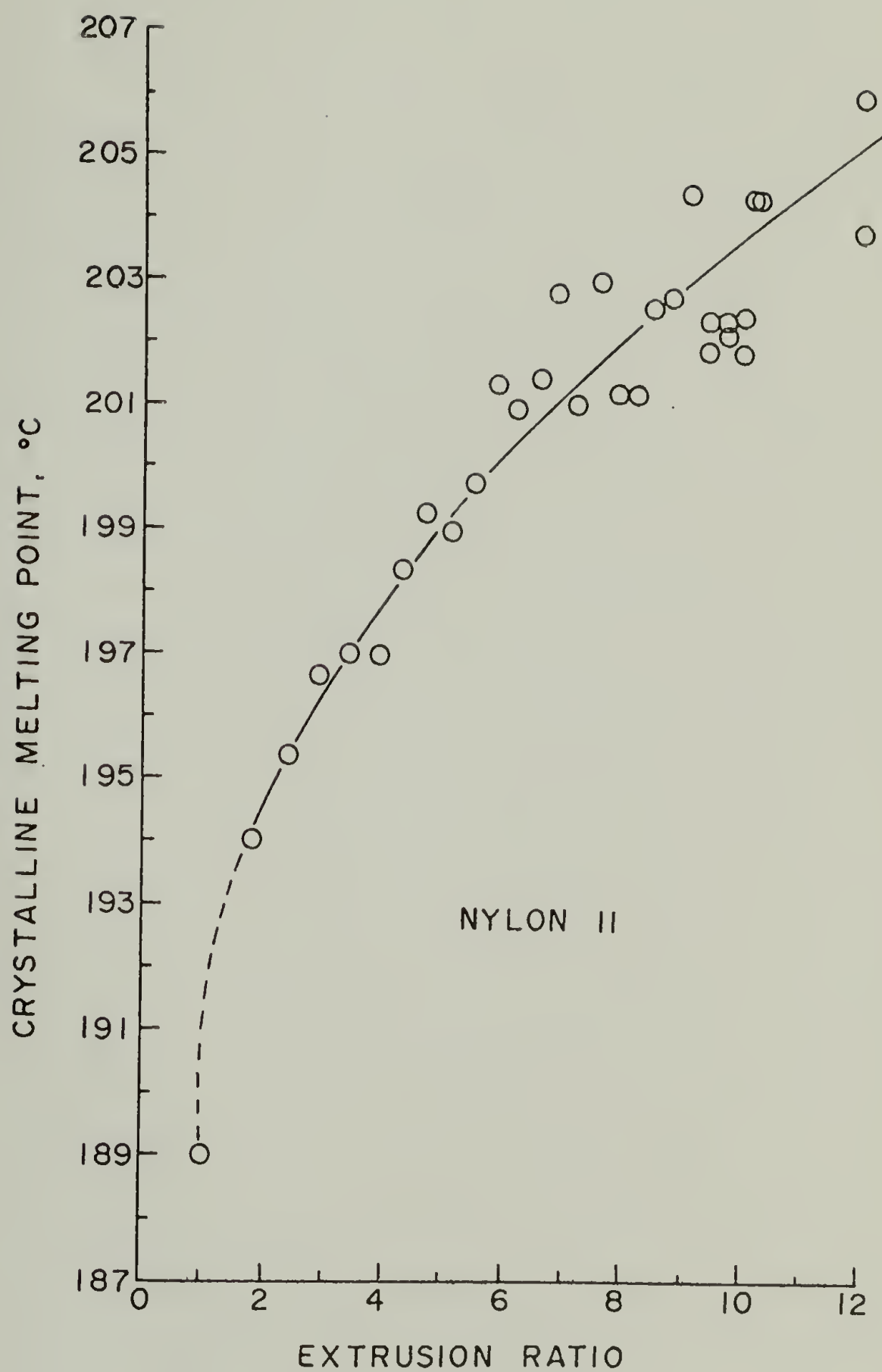


Figure 7

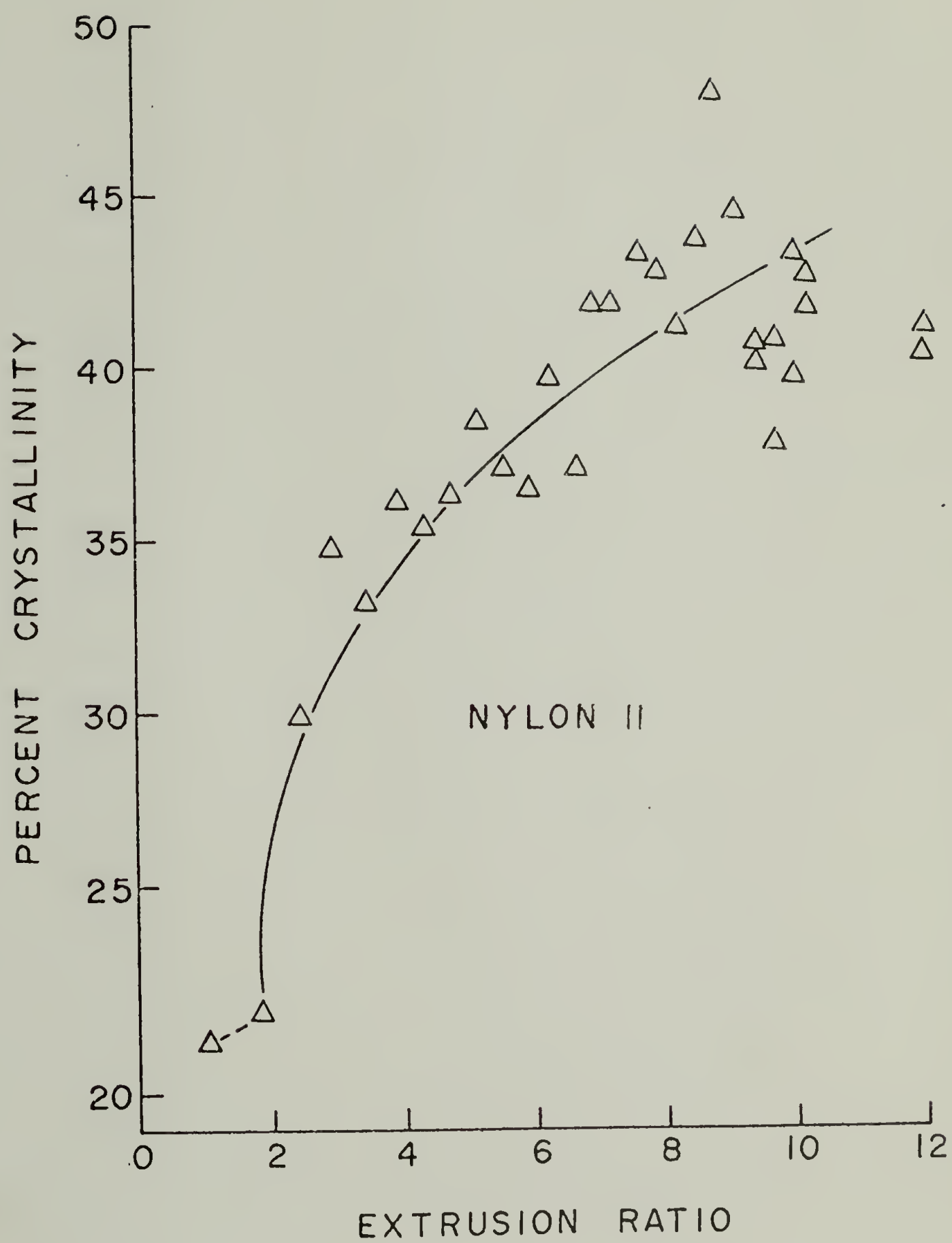


Figure 8



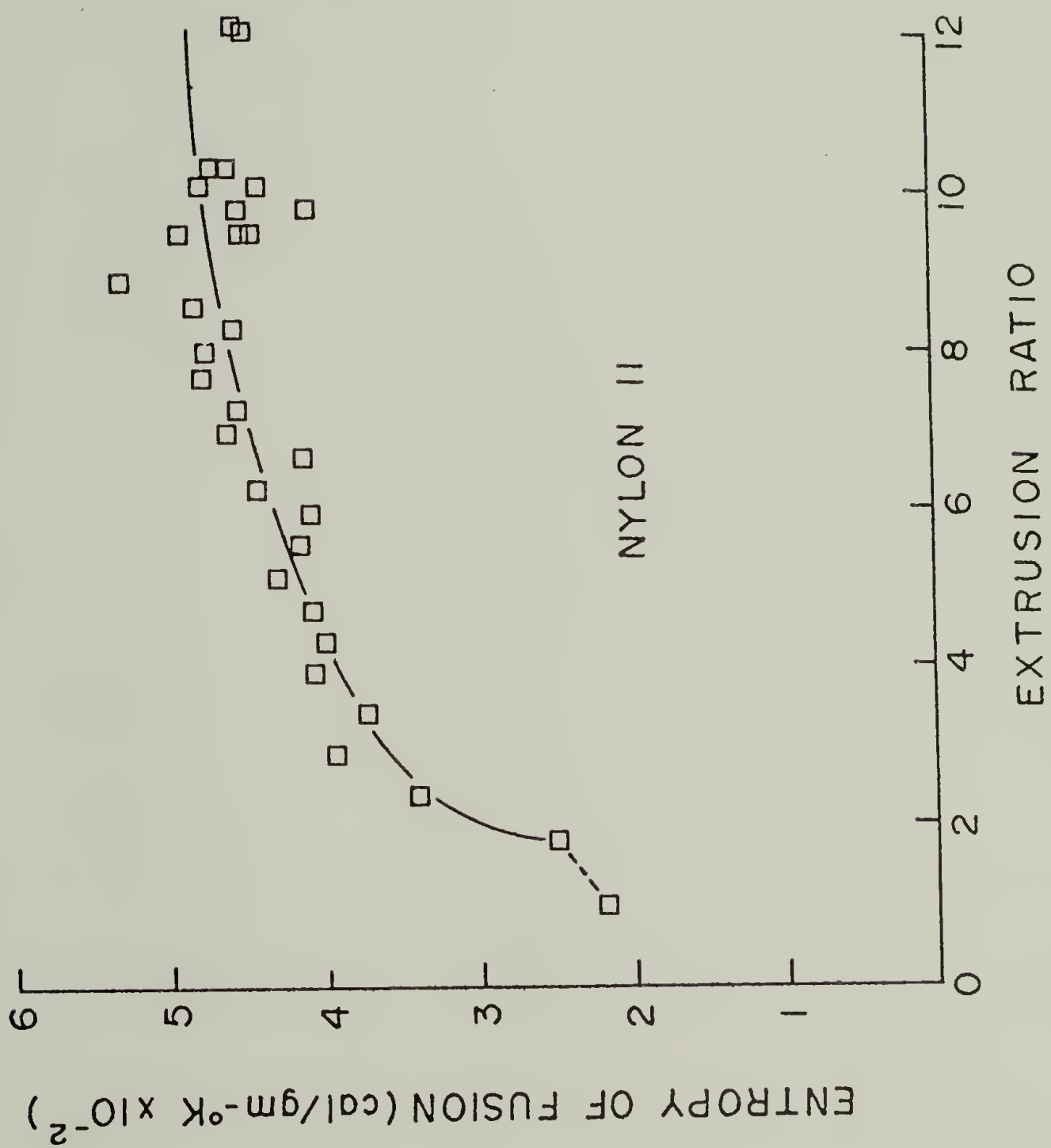


Figure 9

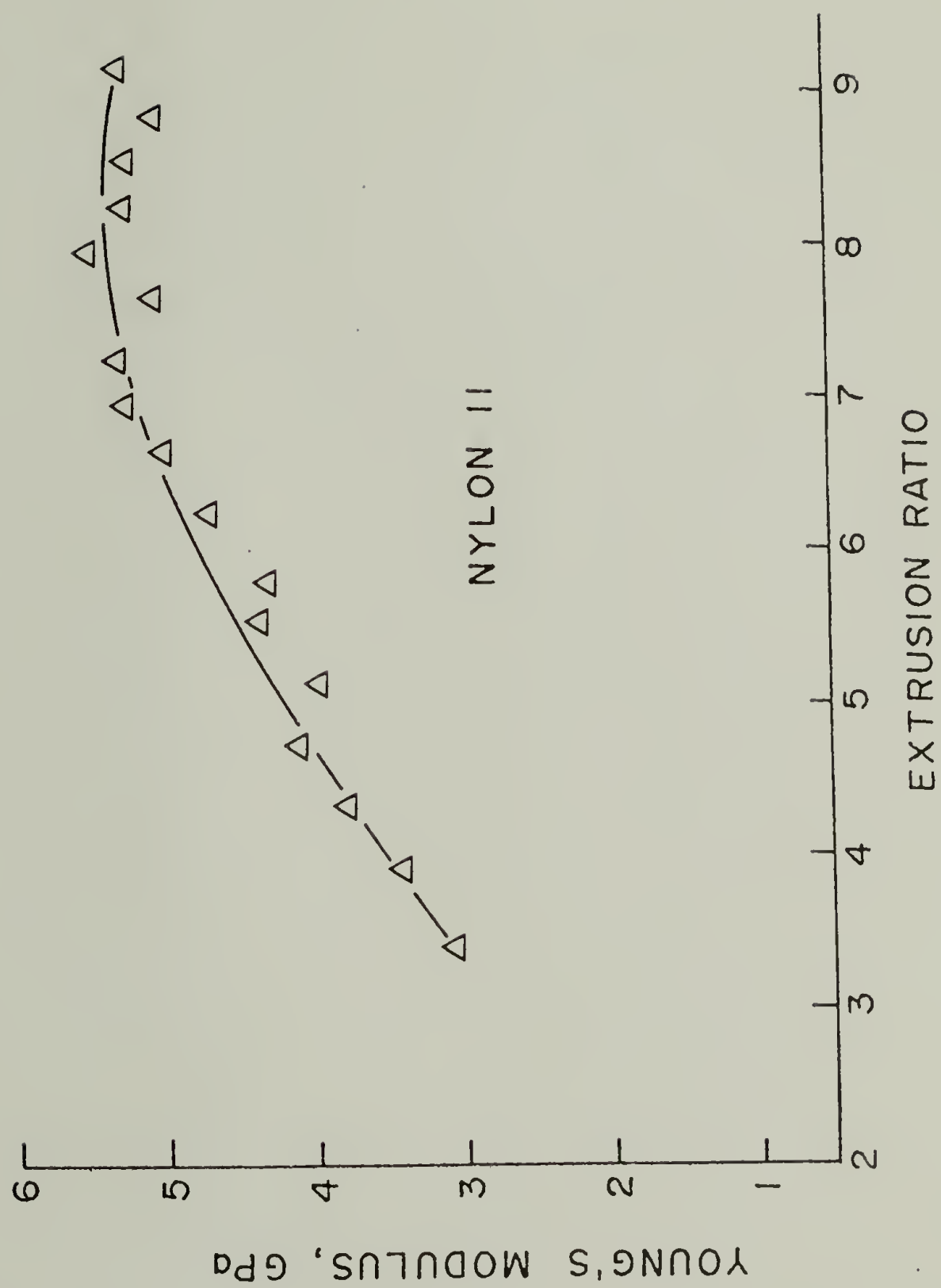


Figure 10

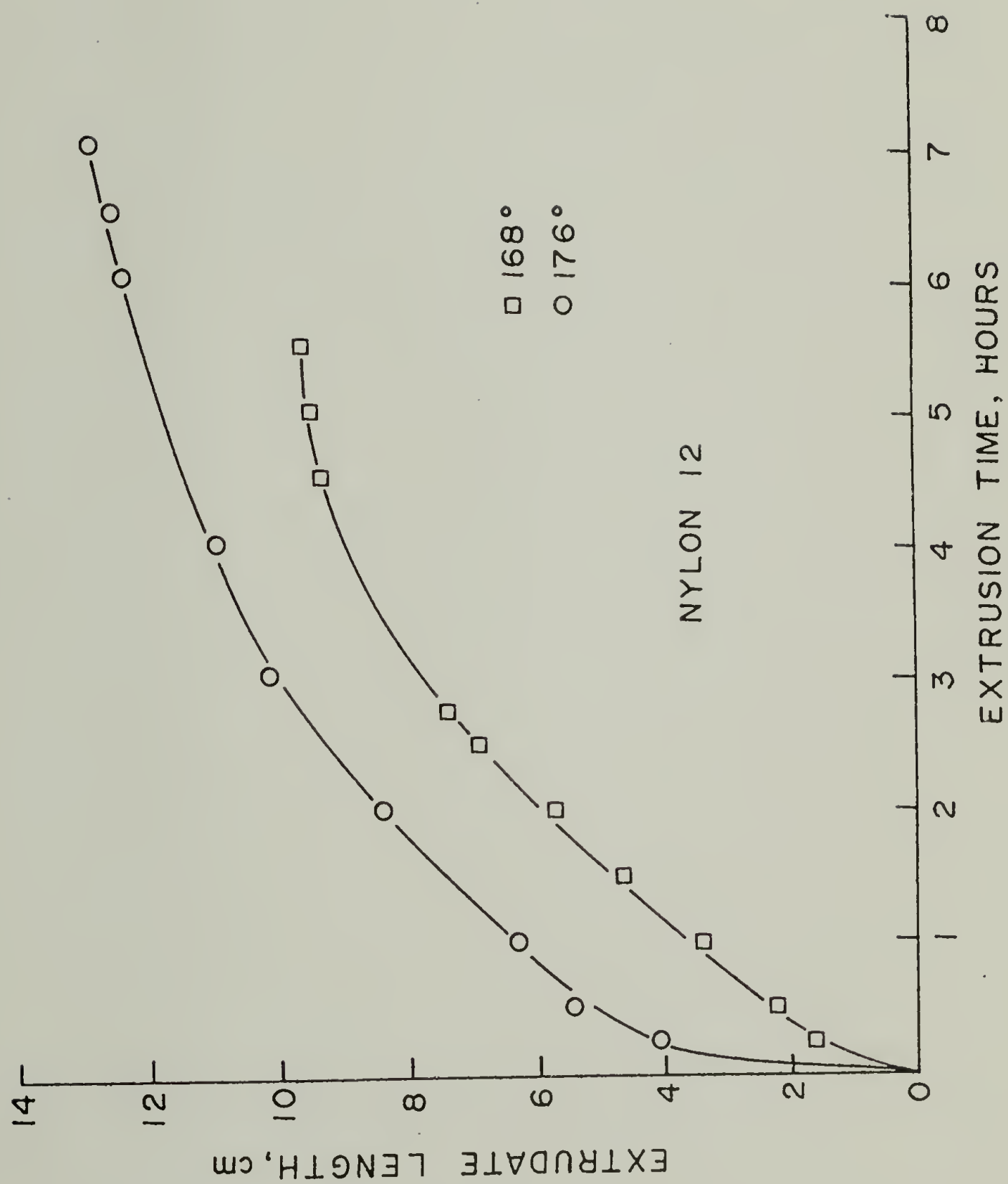


Figure 11

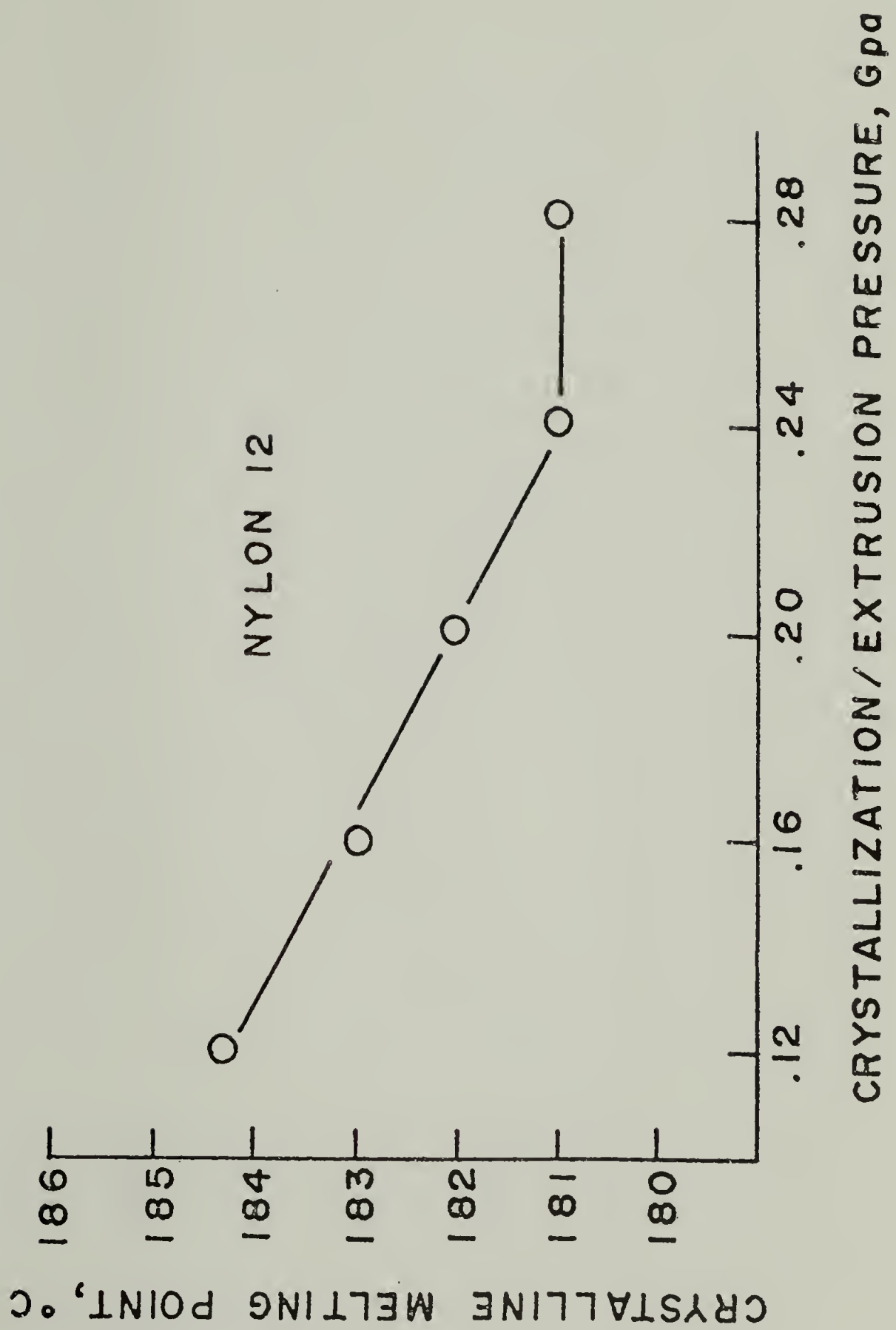


Figure 12



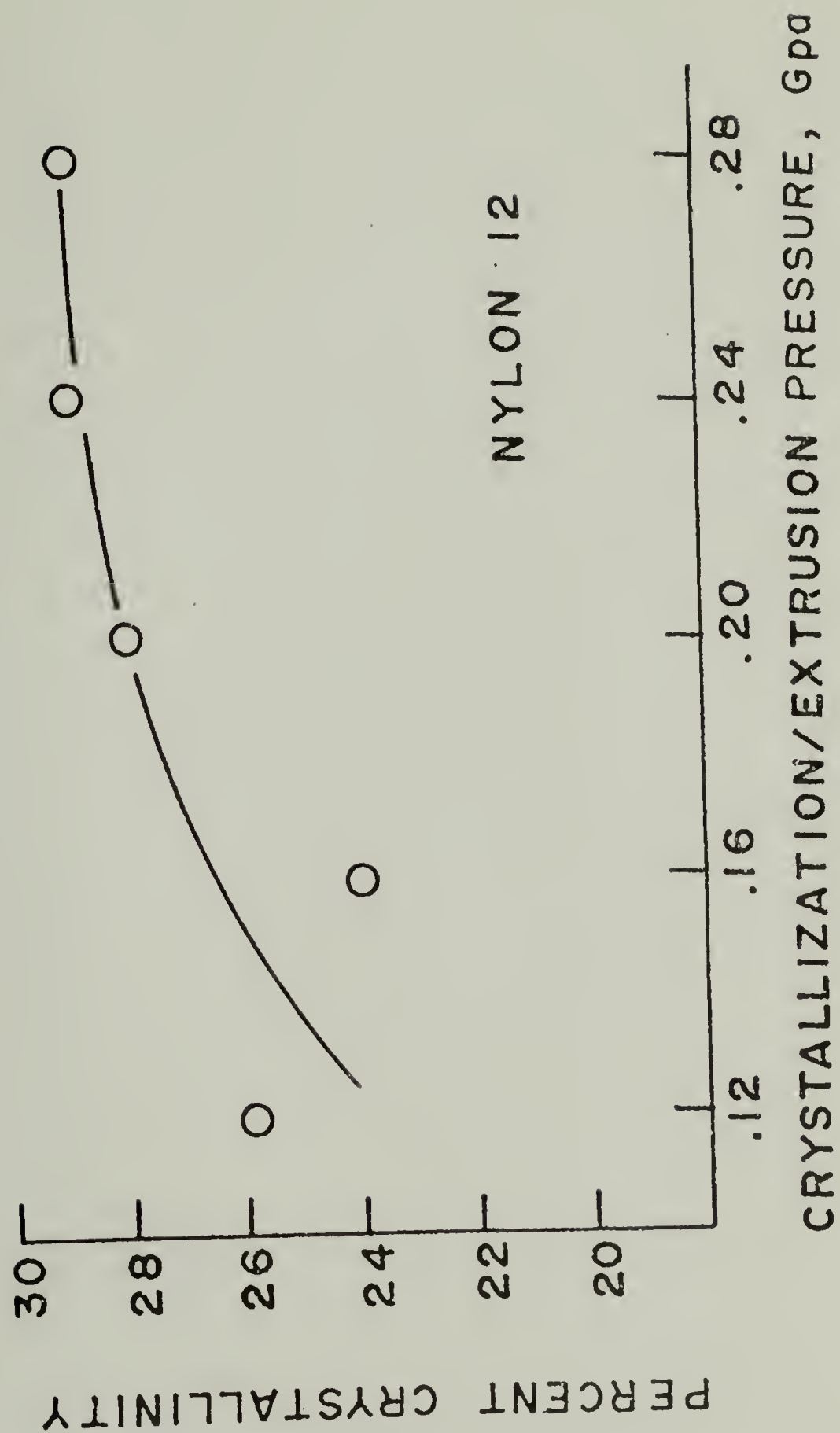


Figure 13

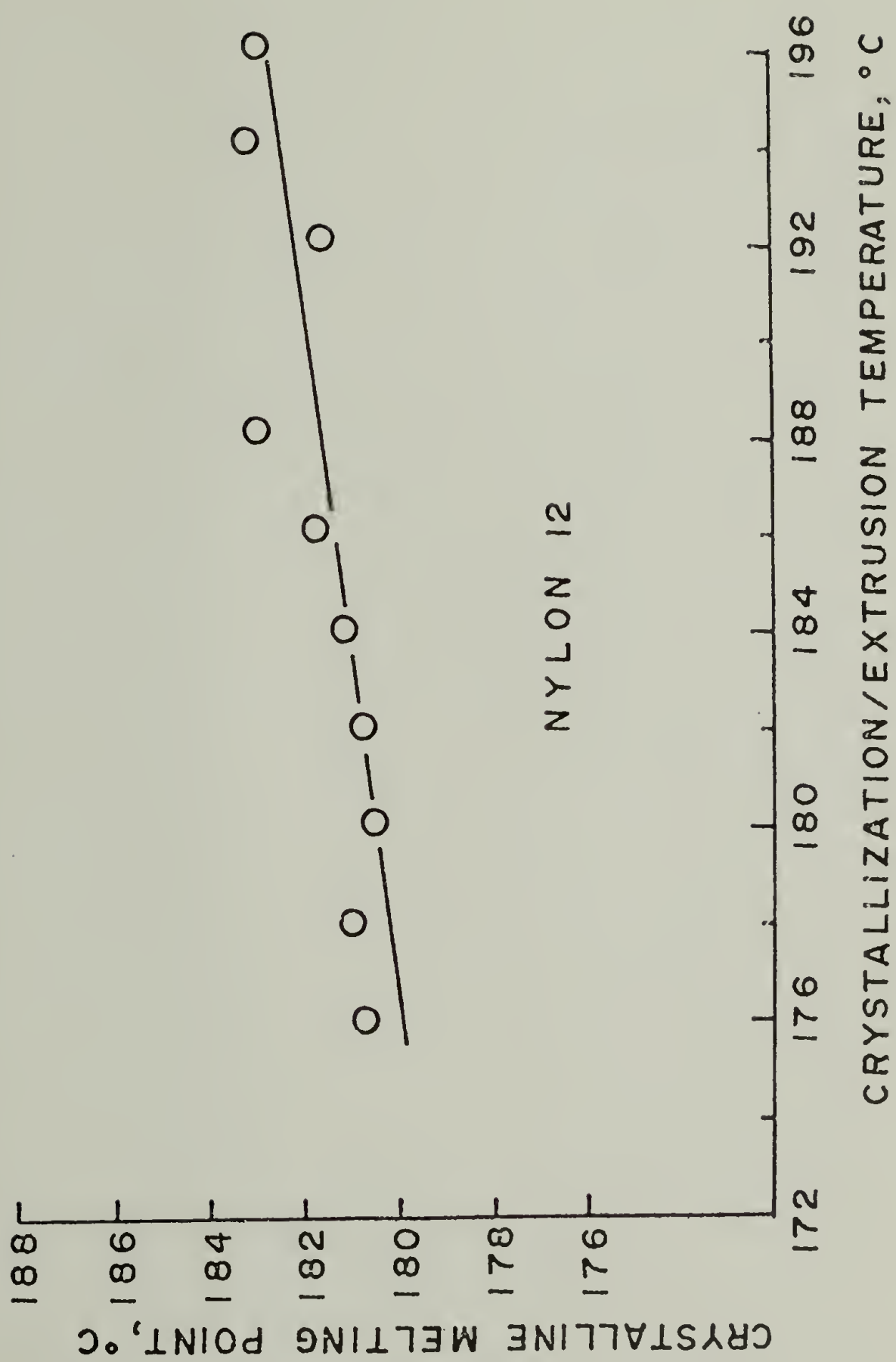


Figure 14

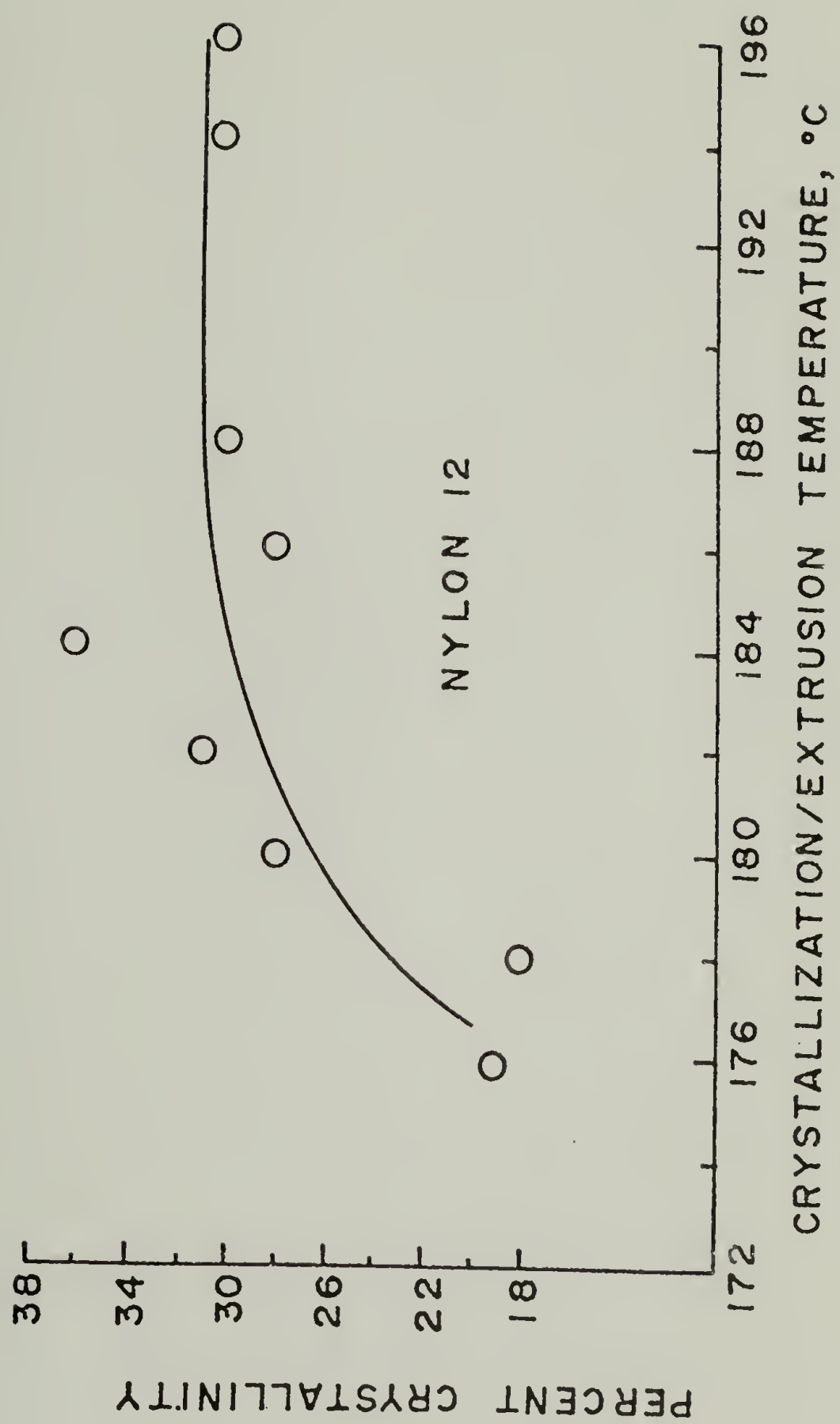


Figure 15

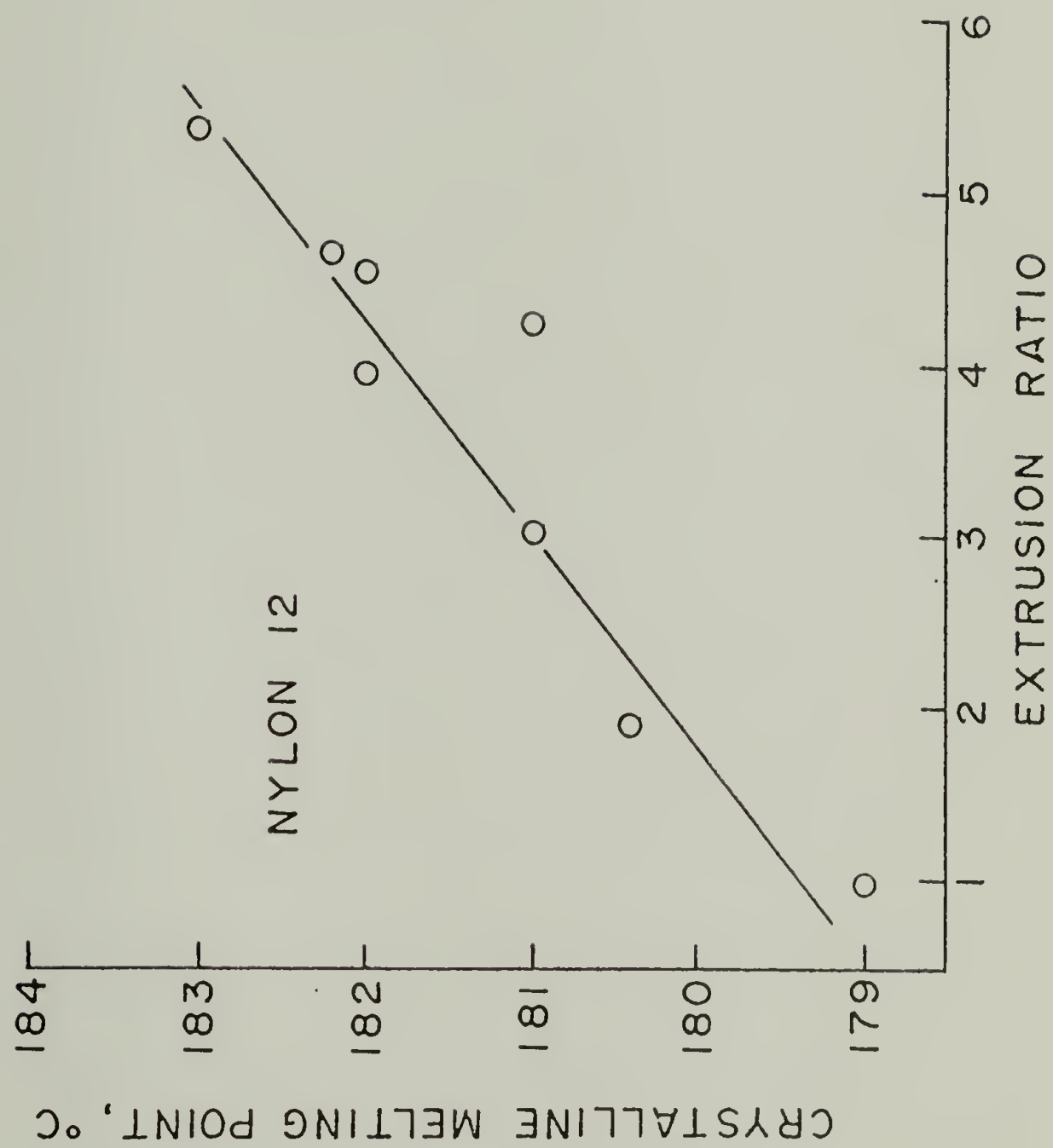


Figure 16



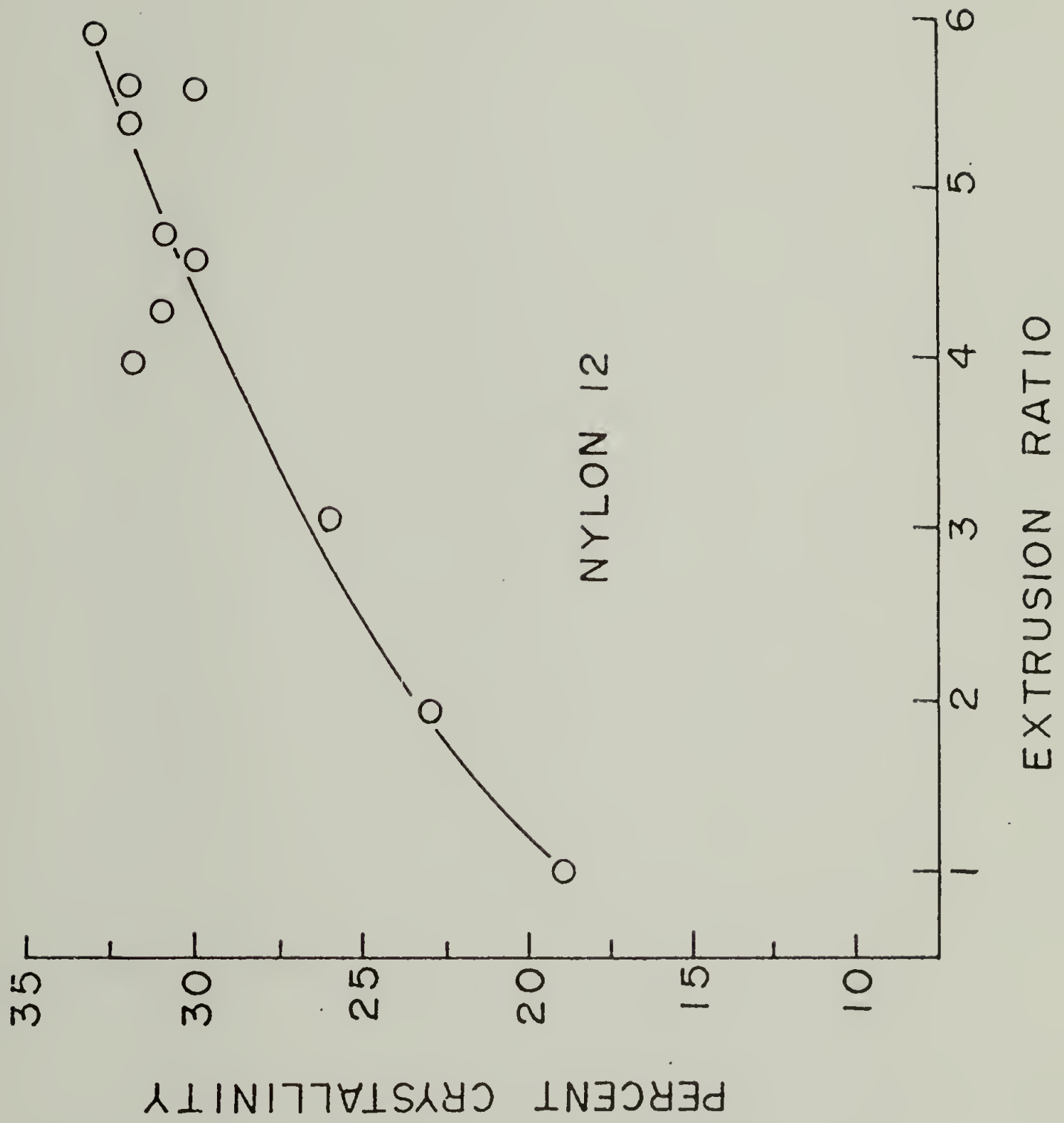


Figure 17

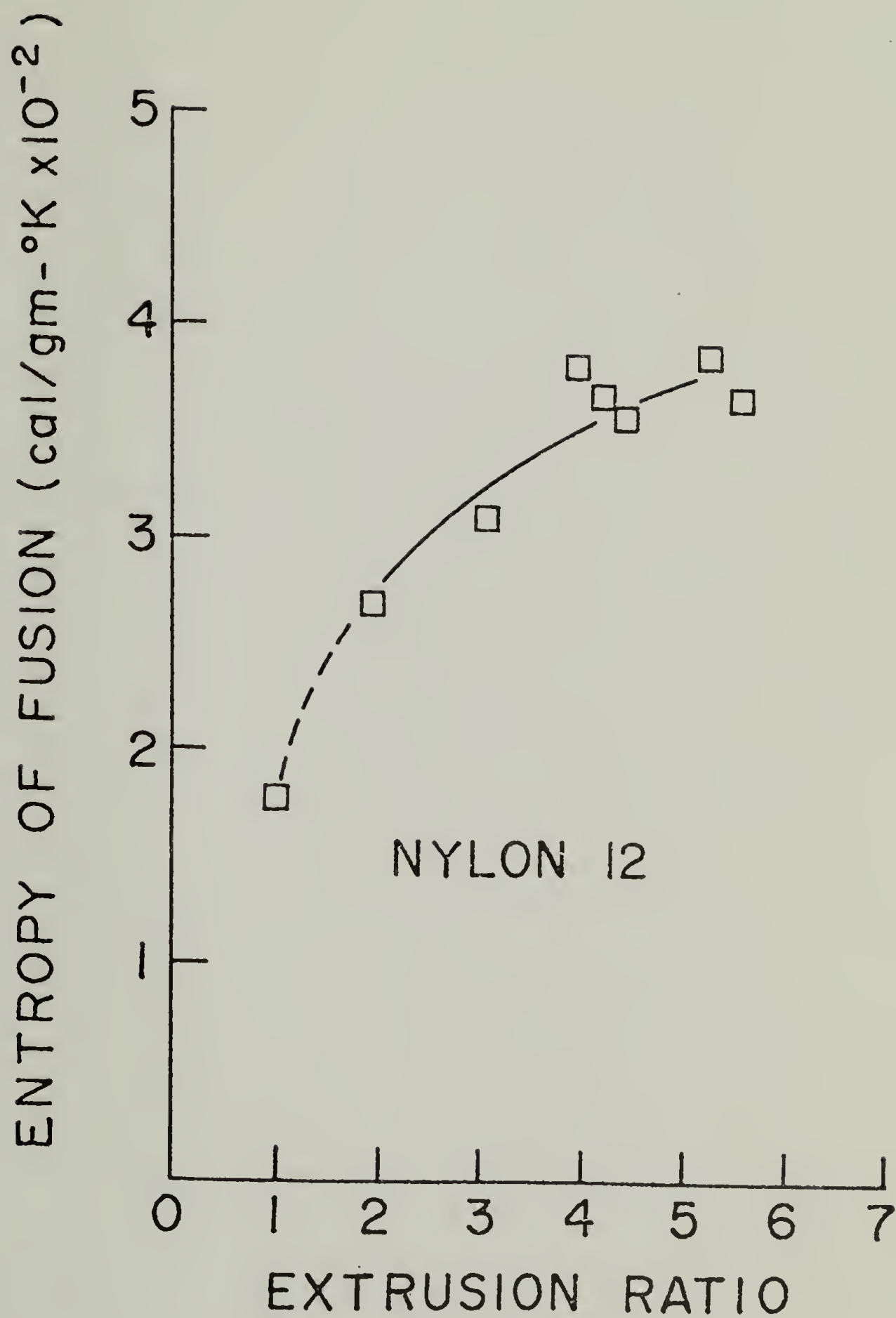


Figure 18

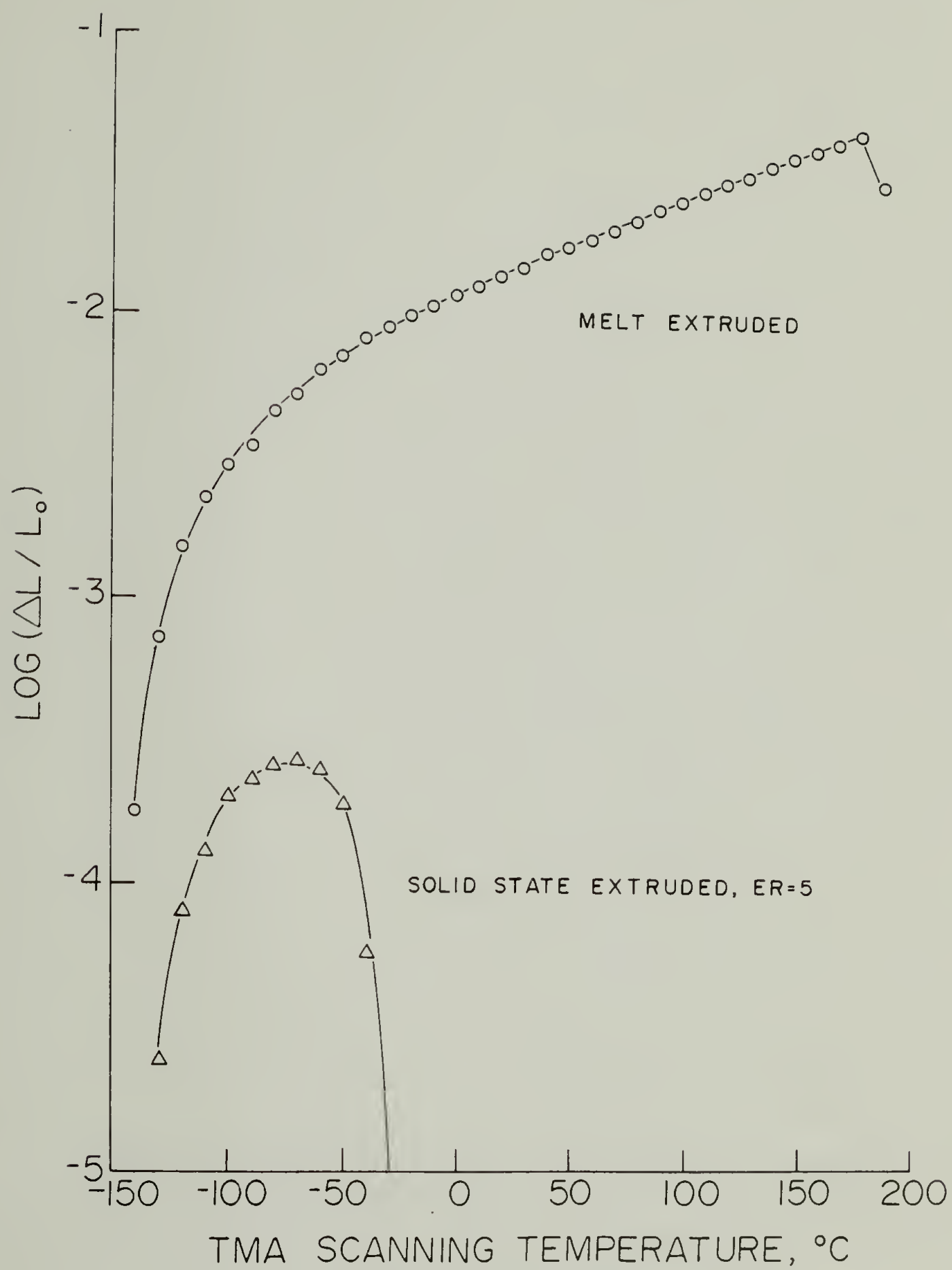


Figure 19

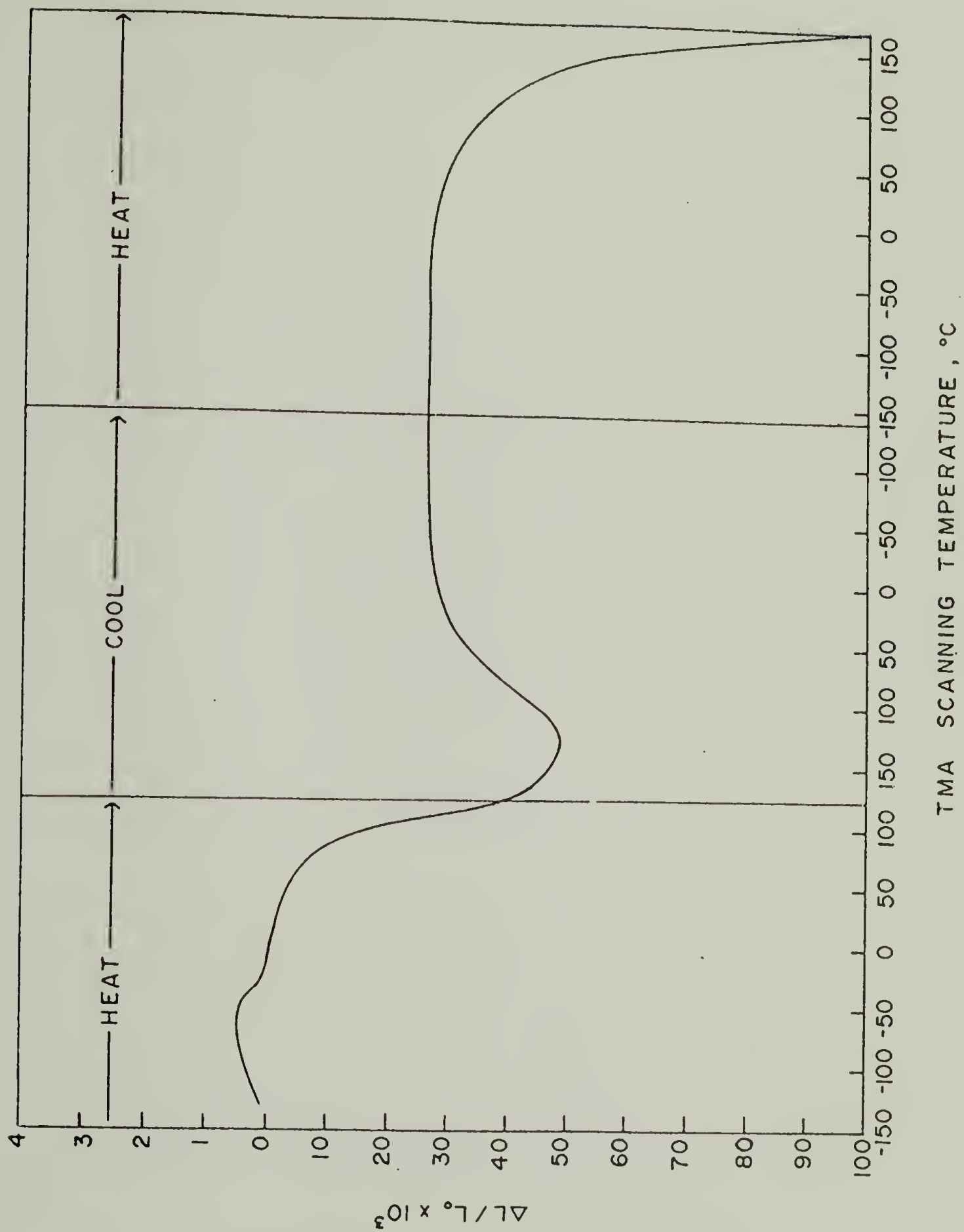


Figure 20



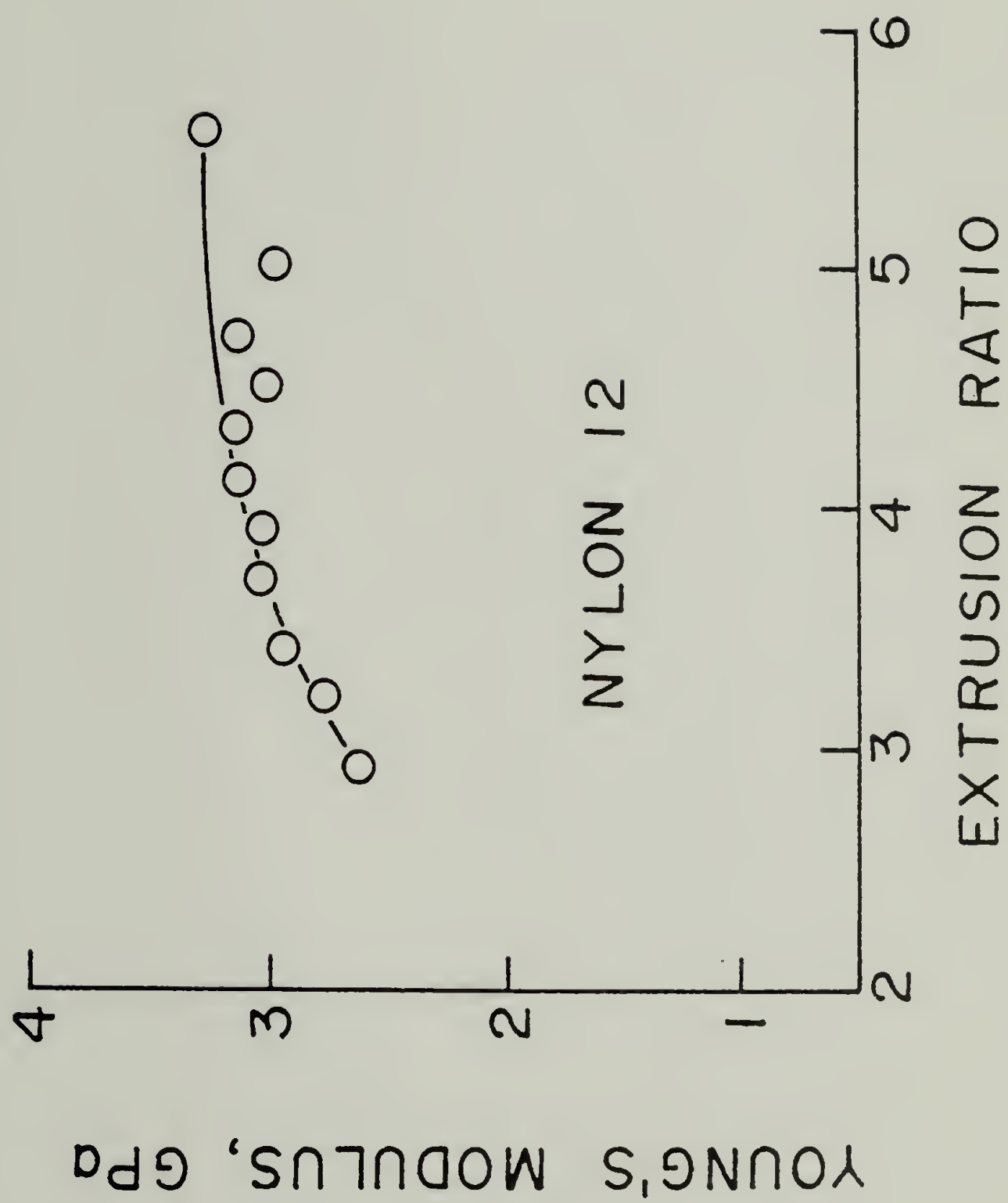



Figure 21



a.

  
10  $\mu$ 

b.


  
10  $\mu$ 

Figure 22



a.



b.

Figure 23

# U.S. Japan Seminar in Polymer Physics



## CHAPTER VII

### FUTURE WORK

#### I. Flow Patterns

Probably one of the first extensions of the work in this thesis should be the experimental determination of the type of flow occurring in capillary dies of varying entrance angles. Such determination of flow patterns of polymers through dies has been done by others in this laboratory and elsewhere with the use of flow markers. These are simply colored small-diameter rods inserted through pre-drilled holes in the side of the billet prior to extrusion. At any stage of the extrusion, the billet may be removed from the die, cut in half lengthwise, and the colored markers used as an indication of the type of deformation undergone by the polymer.

#### II. Capillary Length

A second important investigation would be the effect of capillary length on the extrusion rate, the maximum extrusion ratio attainable, and the physical properties of the extrudate. It has been qualitatively determined here that shorter lengths result in faster extrusion rates but a systematic study has not been done. Furthermore, longer capillary lengths result in longer residence time of the extrudate in a high temperature environment, caused by both slower flow times and the physically longer length itself. Such conditions are likely to cause annealing of extended chain crystals and subsequently poorer quality extrudates (1). However, this has not as yet been quantitatively investigated.



### III. Film Extrusion

The improvement of the film extrusion technique would provide samples more amenable to composite work and spectroscopic examination. Cross-ply laminates could be produced in thin sheets, cut with appropriate dies into, say, a dog-bone configuration, and tested via standard tensile testing procedures. For hydrogen-bonded polymers such as nylons, the extent and effects of hydrogen bonding could be investigated via infrared spectroscopy. This includes orientational measurements using polarized infrared spectroscopy.

### IV. Nylon 6; Nylon 66

The more strongly hydrogen-bonded nylons, -6 and -66, should prove to be interesting materials to study by solid state extrusion. Their higher melting points and greater strength due to their considerable intermolecular bonding may provide films and fibers of extremely high tensile strength. Nylon 66 has been tried to date but proved quite difficult to extrude. Newer methods of plasticizing the polymer prior to extrusion using lithium or potassium salts (2,3) and subsequent removal of these additives after extrusion may facilitate use of this polymer in our process. Other methods of temporarily disrupting hydrogen bonding and/or crystallinity in these nylons during the extrusion process can also be investigated.

### V. Split Billet

A new variation of the solid state extrusion technique has recently been developed in this laboratory (4) using a split (lengthwise) billet.

Extrusion rates are up to 10X faster than the conventional process and thin ultra-oriented films are being extruded from high density polyethylene. Application of this technique to the solid state extrusion of nylons should prove quite useful.

## VI. Drawing

Post-extrusion drawing may be a method of extending the maximum extrusion (draw) ratio beyond the present limit of ~ 40. Two methods of doing this would be: (1) pulling on the extrudate as it emerges from the extrusion die. Work on this is presently underway in this laboratory and it is thought that a relief of compressional forces on the billet may allow the material to deform further without fracturing. A second method would be to post-draw an extruded sample at elevated temperatures and slow extension rates in the Instron environmental chamber. This would obviously eliminate compressive forces while allowing great latitude in drawing temperature and rate of draw.

## VII. Morphological Characterization

More complete morphological examination of solid state extruded polymers is necessary. Probably the facet that has been least investigated is the state of the amorphous material. Nuclear magnetic resonance and infrared spectroscopy have been used to a limited extent but more widespread use of these techniques is required. Also, scanning electron microscopy has only sparingly been employed to look at fracture surfaces and crystalline/amorphous domains. The nature, size, and orientation of

lamellae could be studied. New equipment recently acquired can improve this situation considerably.

### VIII. Strain Cycling

Although mechanical testing in the form of standard stress-strain curves has been used for some time to characterize the ultra-oriented extrudates, more information from these and similar tests can be obtained. For example, changes in birefringence after strain cycling would shed light on the phenomenon of "strain hardening" which is, of course, an increase in overall orientation. A study of elastic hysteresis curves from repeated strain-cycling tests would indicate the amount of strain hardening taking place (as it invariably does) and, under optimum conditions of strain rate and amount of strain, modulus might be considerably improved.

### IX. Lubricants

Finally, a systematic study of the effect of lubricants on the solid state extrusion process is inevitable. Such a study was begun as part of this thesis but the control of variables proved extremely time-consuming. Lubricants may be oils or greases, powders applied with a bonding resin or added to the polymer prior to crystallization and extrusion, or simply low molecular weight waxes. Also, as extrusion proceeds, those lubricants which are directly applied to the die are abraded off during extrusion, so their concentration varies with extrudate length. Other lubricants are significantly affected by high

temperatures or pressures and this must also be taken into consideration. We consistently attain higher extrusion ratios by applying a Teflon film bonding grade spray to the die entrance region but other systems may yet prove to be better.

References

1. W. T. Mead and R. S. Porter, J. Appl. Phys. 47, 4278 (1976).
2. D. Acierno, E. Bianchi, A. Ciferri, B. DeCindio, C. Migliaresi and L. Nicolais, J. Polym. Sci., Part C, 54, 259 (1976).
3. D. Acierno, F. P. LaMantia, G. Polizzotti, G. C. Alfonso and A. Ciferri, J. Polym. Sci., Part B, 15, 323 (1977).
4. P. Griswold, A. E. Zachariades and R. S. Porter, to be published.



